DTIC FILE COPY

(4)

AD-A196 435

AFGL-TR-87-0303

The Determination of the Spacecraft Contamination Environment

B.D. Green
W.T. Rawlins
G.E. Caledonia
W.J. Marinelli
C. White
G.A. Simons
B. Gold
H. Miranda

Physical Sciences Inc.
Research Park, P.O. Box 3100
Andover, MA 01810

October 1987

DTIC
ELECTE
JUN 16 1988
S D
H

Final Report
12 September 1983 - 28 February 1987

Approved for public release; distribution unlimited

AIR FORCE GEOPHYSICS LABORATORY
AIR FORCE SYSTEMS COMMAND
UNITED STATES AIR FORCE
HANSCOM AIR FORCE BASE, MASSACHUSETTS 01731-5000

88 6 16 029

"This technical report has been reviewed and is approved for publication"

(Signature)
G.K. YATES
Contract Monitor

(Signature)
C.P. PIKE,
Branch Chief

FOR THE COMMANDER

(Signature)
RITA C. SAGALYN
Division Director

This report has been reviewed by the ESD Public Affairs Office (PA) and is releasable to the National Technical Information Service (NTIS).

Qualified requestors may obtain additional copies from the Defense Technical Information Center. All others should apply to the National Technical Information Services.

If your address has changed, or if you wish to be removed from the mailing list, or if the addressee is no longer employed by your organization, please notify AFGL/DAA, Hanscom AFB, MA 01731. This will assist us in maintaining a current mailing list.

Do not return copies of this report unless contractural obligations or notices on a specific document requires that it be returned.

Unclassified

SECURITY CLASSIFICATION OF THIS PAGE

REPORT DOCUMENTATION PAGE

1a. REPORT SECURITY CLASSIFICATION Unclassified	1b. RESTRICTIVE MARKINGS
2a. SECURITY CLASSIFICATION AUTHORITY	3. DISTRIBUTION/AVAILABILITY OF REPORT Approved for public release; distribution unlimited
2b. DECLASSIFICATION/DOWNGRADING SCHEDULE	
4. PERFORMING ORGANIZATION REPORT NUMBER(S) PSI-9139/TR-728	5. MONITORING ORGANIZATION REPORT NUMBER(S) AFGL-TR-87-0303
6a. NAME OF PERFORMING ORGANIZATION Physical Sciences Inc. 6b. OFFICE SYMBOL (If applicable)	7a. NAME OF MONITORING ORGANIZATION Spacecraft Interactions Branch Air Force Geophysics Laboratory
6c. ADDRESS (City, State and ZIP Code) Research Park, P.O. Box 3100 Andover, MA 01810	7b. ADDRESS (City, State and ZIP Code) Hanscom AFB 01731
8a. NAME OF FUNDING/SPONSORING ORGANIZATION AFGL 8b. OFFICE SYMBOL (If applicable) PHK	9. PROCUREMENT INSTRUMENT IDENTIFICATION NUMBER F19628-83-C-0139
8c. ADDRESS (City, State and ZIP Code) Hanscom AFB 01730	10. SOURCE OF FUNDING NOS. PROGRAM ELEMENT NO.: 62101F PROJECT NO.: 7661 TASK NO.: 11 WORK UNIT NO.: AF
11. TITLE (Include Security Classification) The Determination of the Spacecraft Contamination Environment	
12. PERSONAL AUTHOR(S) B.D. Green; W.T. Rawlins; G.E. Caledonia; W.J. Marinelli; C. White; G.A. Simons; B. Gold*; H. Miranda**	
13a. TYPE OF REPORT Final 13b. TIME COVERED FROM 9/12/83 TO 2/28/87	14. DATE OF REPORT (Yr., Mo., Day) 1987 October 15. PAGE COUNT 410
16. SUPPLEMENTARY NOTATION * EKTRON Applied Imaging; ** Miranda Laboratories (cont'd)	
17. COSATI CODES FIELD / GROUP / SUB. GR.	18. SUBJECT TERMS (Continue on reverse if necessary and identify by block number) Contamination; Optical Environment; Low Earth Orbit; Spacecraft Glow Particulates, Space Shuttle, Chemiluminescence; space environments; manned [illegible] (47)

19. ABSTRACT (Continue on reverse if necessary and identify by block number)

This report details our efforts in the determination of the on-orbit environment surrounding spacecraft. The research was performed for the Spacecraft Interactions Branch of the Space Physics Division of the Air Force Geophysics Laboratory. This report includes contributions from our subcontractors EKTRON Applied Imaging and Miranda Laboratories. The multiyear project consisted of three major tasks: a literature survey, preparation for the data of the Particle Analysis Cameras for Shuttle (PACS), and the analysis of the data to create a model of the orbital particulate environment.

During the literature search we discovered that many observations were presented with little or no insight provided. Physical Sciences Inc. (PSI) therefore undertook a critical review of the data in an attempt to reconcile seemingly contractory observations and provide needed understanding of the variety of unexpected processes

20. DISTRIBUTION/AVAILABILITY OF ABSTRACT UNCLASSIFIED/UNLIMITED ☒ SAME AS RPT. ☐ DTIC USERS ☐	21. ABSTRACT SECURITY CLASSIFICATION Unclassified
22a. NAME OF RESPONSIBLE INDIVIDUAL G. Kenneth Yates	22b. TELEPHONE NUMBER (Include Area Code) (617) 377-2931 22c. OFFICE SYMBOL AFGL/PHK

DD FORM 1473, 83 APR EDITION OF 1 JAN 73 IS OBSOLETE.

Unclassified

SECURITY CLASSIFICATION OF THIS PAGE

occurring above spacecraft surfaces in low-earth orbit. We were able to make contributions to the understanding of the neutral molecular contamination cloud; the modifications of the ionic environment; the optical contamination glow; and the earlier observations of particulates.

In order to prepare for the data to be returned by the PACS stereoscopic cameras, EKTRON, PSI, and Miranda Laboratories provided suggestions for PACS optical configuration, performed a sensitivity and error budget analysis, and developed a data reduction plan.

The PACS Cameras were aboard Shuttle Mission STS61-C (Columbia) in January 1986. We helped support AFGL during the mission at the Hitchhiker Command Center. PSI and its subcontractors provided a rapid review of the PACS data. We presented a data quality review meeting 1 month after receiving the film data (1-1/2 months after mission) and a quick-look report/briefing 4-1/2 months after receiving the data. Because only a single camera functioned properly, accurate information can be obtained only about irradiance levels, particle counts, and clearing times. These time scales are critical for the guidance of future Air Force Missions. As our final task, we developed a rough model of the Shuttle Particulate Environment which will guide future observations.

ACKNOWLEDGEMENTS

Physical Sciences Inc. was fortunate to be involved in this exciting field during a period when our knowledge and understanding were progressing so rapidly. It has been a uniformly pleasant experience interacting with the people we have met in association with this project. The researchers at the Air Force Geophysics Laboratory, in particular Drs. G.K. Yates and E. Murad and Mr. C. Pike and M. Ahmadjian, were enthusiastic, helpful, and provided excellent technical interactions. The Shuttle environment community is filled with researchers from a variety of backgrounds which produces an exciting forum for the formulation of new ideas. Although we have acknowledged the contributions of many in our papers, we would particularly like to thank L. Legner, S. Clifton, and E. Miller of NASA for many thought-provoking discussions. Participation in the Shuttle ground support was a wonderful (and exhausting) experience. The Hitchhiker personnel at NASA/Goddard (T. Goldsmith, J. Kunst, and R. Day et al.) were uniformly helpful and knowledgeable. Our ability to rapidly categorize, analyze, and isolate key data was based largely upon the wealth of information they supplied. Finally, it was a pleasure working with Dr. Bennett Gold (EKTRON) and Henry Miranda (Miranda Laboratories) throughout this project.

DTIC COPY INSPECTED 4

Accession For
NTIS GRA&I ☑
DTIC TAB ☐
Unannounced ☐
Justification
By
Distribution/
Availability Codes
Dist | Avail and/or Special
A-1

CONTENTS

			Page
Section	1.	INTRODUCTION	1
	2.	REVIEW AND GLOW SUMMARY	3
	3.	PACS DATA	13
	3.1	General Observations	13
	3.2	Particular Observations	14
APPENDICES			
	A	The Shuttle Environment Gases, Particles and Glows	29
	B	Atomic Recombination into Excited Molecular States	97
	C	Spectral Identification/Elimination of Molecular Species in Spacecraft Glow	113
	D	Chemiluminescent Processes Occurring Above Shuttle Surfaces	133
	E	Radiance Calculations for IMPS/Glow Experiments	155
	F	The Shuttle Glow as an Indicator of Material Changes in Space	163
	G	Review of the Vehicle Glow	183
	H	Chemical Interactions on High Temperature Chemistry	195
	I	Spectral Signatures of Micron-Sized Particles in the Shuttle Optical Environment	219
	J	Error Budget Calculations for Stereo Camera Pairs	261
	K	Catalogue of PACS Film Data	277
	L	EKTRON Final Report	293
	M	Briefing to CIRRIS Staff	335
	N	The Particle Environment On-Orbit: Observations, Calculations, and Implications	383
	O	The Particulate Environment Around the Shuttle as Determined by the PACS Experiment	393

FIGURES

		Page
FIGURE 1.	Shuttle ground system attitude display.	21

TABLES

		Page
TABLE 1.	*Definitive glow experiment* to distinguish plasma from chemical mechanisms	8
2.	Data analysis plan	18
3.	PACS film exposure sequence.	19
4.	Particle model (Shuttle environment)	27

1. INTRODUCTION

This report details our efforts in the determination of the on-orbit environment surrounding spacecraft. The research was performed for the Spacecraft Interactions Branch of the Space Physics Division of the Air Force Geophysics Laboratory. This report includes contributions from our subcontractors EKTRON Applied Imaging and Miranda Laboratories. The multiyear project consisted of three major tasks: a literature survey, preparation for the data of the Particle Analysis Cameras for Shuttle (PACS), and the analysis of the data to create a model of the orbital particulate environment.

During the literature search we discovered that many observations were presented with little or no insight provided. Physical Sciences Inc. (PSI) therefore untertook a critical review of the data in an attempt to reconcile seemingly contractory observations and provide needed understanding of the variety of unexpected processes occurring above spacecraft surfaces in low-earth orbit. We were able to make contributions to the understanding of the neutral molecular contamination cloud; the modifications of the ionic environment; the optical contamination glow; and the earlier observations of particulates.

In order to prepare for the data to be returned by the PACS stereoscopic cameras, EKTRON, PSI, and Miranda Laboratories provided suggestions for PACS optical configuration, performed a sensitivity and error budget analysis, and developed a data reduction plan.

The PACS Cameras were aboard Shuttle Mission STS61-C (Columbia) in January 1986. We helped support M. Ahmadjian of AFGL during the mission at the Hitchhiker Command Center. PSI and its subcontractors provided a rapid review of the PACS data. We presented a data quality review meeting 1 month after receiving the film data (1-1/2 months after mission) and a quick-look report/briefing 4-1/2 months after receiving the data. Because only a single camera functioned properly, accurate information can be obtained only about

irradiance levels, particle counts, and clearing times. These time scales are critical for the guidance of future Air Force Missions. As our final task, we developed a rough model of the Shuttle Particulate Environment which will guide future observations.

Because PSI recognized the need to draw clear conclusions and disseminate this information in a timely manner, we have been careful to document our results promptly throughout the research project and made numerous presentations at scientific/engineering meetings and published extensively. These reports are provided as appendices in this final report. They accurately summarize our work. We will provide in this section a description of the overall project and particular technical details not covered elsewhere.

2. REVIEW AND GLOW SUMMARY

Our literature search provided guidance to us about which aspects of on-orbit environment must be most clearly understood and characterized to ensure the success of Air Force future missions. In particular the molecular and ionic contamination cloud, glow and particles will all generate emissions which could interfere with observations

We became aware that most of this data was not yet published or even analyzed. Preliminary analyses and findings were presented mostly at conferences and as short notes in the literature. In order to get abreast of the latest results, one of our staff attended the AIAA Shuttle Environment and Operations Meeting in Washington, DC on 31 October-2 November 1983. That meeting provided a good overview of the current state of knowledge of the Shuttle on-orbit environment. This knowledge base was very incomplete and often inconsistent. Each experimenter had analyzed only a small portion of his data, which was not directly comparable to the data of others. Thus, broad conclusions could not be drawn without further insightful interpretation. Largely by luck, we were asked to give an invited paper reviewing the Shuttle environment at the 22nd Aerospace Sciences Meeting of the AIAA in Reno and as a seminar at AFGL. In preparing the talk we gained a greater understanding of the available data base, searched for inconsistencies between experimental observations, and identified areas of greatest concern for future Shuttle users.

The text arising from that talk is presented as Appendix A was published in J. Spacecraft 22, 500 (1985). The key conclusions drawn were:

- The large variability of the natural and Shuttle-induced environment might largely explain differences between experimental observations.

- The environment is often "benign" but thruster events can frequently and strongly perturb the entire local environment.

- Water vapor is the dominant gaseous contaminant and its desorption rate off Shuttle surfaces is not known.

- The existence of a Shuttle-induced enhancement of the plasma density is clouded by contradictory observations.

- The glow over Shuttle surfaces is the most puzzling and intriguing phenomenon observed. Several possibilities for the source of the glow exist and each may contribute under certain conditions. We proposed a new class of mechanisms relying upon the catalytic nature of the spacecraft surfaces: atomic recombination into electronically excited states after impact dissociation on Shuttle surfaces. Such a catalytic mechanism is currently believed responsible for the visible glow. A manuscript describing these processes has been published in Geophysics Research Letters 11(6), 576 (1984). A copy of the manuscript is attached as Appendix B.

- The particulate environment suffers from contradictory observations. The IECM cameras showed low particulate densities after the first day of the mission. Video and Star Camera data from STS-3 and -4, respectively, indicate the presence of a great number of large particles persisting around the Shuttle during its entire week-long mission. The AFGL PACS camera data film pairs were to provide critical data needed to resolve this issue.

- NASA was reported to be slow at providing data on Shuttle activities to experimenters, thus considerably hampering post-flight analyses. Thus experimenters were urged to accumulate much supporting data during the mission.

- NASA views the Shuttle as a clean, reliable transportation system to space and states that the users must assess the impact of its total environment of their experiments, basically - caveat emptor. Our

independent review provides a first step toward the goal of permitting Shuttle users to perform that difficult evaluation.

Throughout the remainder of the project we continued to improve our understanding of the Shuttle environment as data from additional missions became available and was analyzed.

An area of particular concern was the glow observed above surfaces exposed to impact by the residual atmosphere. Although the glow has only been studied in the visible, its source and its magnitude at UV and especially IR wavelengths could have significant impacts on detection thresholds of Air Force sensor systems. Thus throughout the rest of the project, we were active in the glow community; critically reviewing the results from each mission and proposing new theories. At the second Workshop on Spacecraft Glow at NASA/Marshall (on May 1985), we presented a paper reviewing the existing data base and confirming or eliminating proposed species via spectral identification. No one had yet surveyed the classes of mechanisms that could be occurring over the various surfaces, and no attempt had been made to estimate the magnitude of the processes or even their relative importance. The paper represented our first attempt at such a survey. Drs. Terry Rawlins and William Marinelli at PSI assisted in the analysis and computer calculations. The PSI spectral synthesis code was used to clearly show that highly vibrationally excited species could give rise to visible emission with a spectral shape and intensity matching the observed glow. We showed that the most likely excitation processes involve surface interactions. Surface bulk reactions were not considered in this draft. The text from the published proceedings of that workshop is presented in Appendix C. This concept of the application of spectral fitting to the data base and the importance of various types of processes was further refined and published in Planetary and Space Sci. 34, 839 (1986). That article is presented as Appendix D. The NASA Workshop was an intensive two-day meeting. It included talks on the existing data bases, on postulated source mechanisms, on ground-based simulation facilities, and on planned glow experiments. The three major data bases

appear to be internally self-consistent but do not support each other. Lockheed's spectrophotometer camera system looks above ram surfaces and observes a spectral continuum peaking at 670 nm with a characteristic width of 20 cm. They attribute the glow to NO_2^* exclusively. The ISO instrument (M. and D. Torr) looks out into the earth limb at 250 km. They observed limb emissions as well as underlying spectrally structured emissions which vary latitudinally and temporally. They attribute the emissions to N_2 and unknown species. Their observations may be distorted by the occurrence of thruster events during their time averaged spectra. Several of their spectra are anomolous containing many features which are broadened and have unusual shapes. The Atmospheric Explorer (AE) Satellite Sensors (Yee and Dalgarno) look outward from the satellite body through a glow layer. Radiances in six bandpasses across the visible are observed. The spectral distribution of these bands is roughly intermediate in shape to the two Shuttle observations. They attribute the glow to two constituents OH and NO_2.

PSI feels that different mechanisms (plasma, gas phase chemistry, surface catalysis, and surface reactions) are all operating over surfaces under certain conditions which occur in the extremely variable orbital environment. For example: 1) at high altitudes or perhaps during thruster events, plasma processes will give rise to emission; 2) during thruster firings the neutral gas density is high enough that gas phase reactions will give rise to chemiluminescent and collision-induced emission; 3) the thruster effluents coat surfaces due to backscattering and these species will be available for reacting with the ambient flux to give rise to chemilumiescent gas phase emission; 4) the ambient flux (including impact-dissociated N_2) will be adsorbed on surfaces and can recombine to form NO, O_2, N_2, and NO_2 in excited electronically and vibrationally excited states; and 5) the ambient flux can react with surface materials to give excited NO, CO, or OH. The consensus at the Workshop was that surface catalyzed reactions are the dominant processes responsible for glow. If such is the case, the glow in the infrared is likely to be considerably brighter than the visible as demonstrated in Appendix C.

Ground-based simulation facilities were discussed at the NASA Workshop. Cross (LANL), Arnold (Aerospace), Bareiss (MMC), and Langer (Princeton) described their experiments. None of these facilities reported producing oxygen atoms at orbital velocity kinetic energies of 5 eV. As part of a separate NASA/SBIR project, PSI has produced a high density flux of neutral-O at energies $\geq$ 5 eV.

Several glow experiments were discussed at that meeting. Not all of them will be made. M. Torr is trying to coordinate an experiment using several existing spectrometric instruments looking at surfaces suspended within the field of view. Fazio (Harvard) described the IR Telescope Experiment which was part of the Spacelab 2 mission. IR radiometers in six bandpasses (2 to 3 μm, 4.5 to 9.5 μm, 6.1 to 7.1 μm, 8.5 to 14 μm, 18 to 30 μm, and 70 to 120 μm) looked directly out of the bay. Although primarily astronomic in nature, his experiment will look across the bottom of the PDP package held just outside his field of view. M. Mumma (NASA/GSFC) is planning to fly a CVF (from Utah State University) capable of detecting wavelengths between 0.9 and 5.5 μm as part of the SKIRT experiment. This instrument will be in a gas canister looking directly out of the bay. The University of Colorado is planning to build a 1/8m Ebert-Fastie Spectrometer in a gas canister which will use a scanning mirror to look at Shuttle tail surfaces at wavelengths of 1900 to 3000 angstrom.

We participated in a preliminary experimental design meeting at AFGL on 14 May 1985 to develop an experiment on a free flying pallet which would acquire data aimed toward the identification of glow excitation mechanisms under a variety of conditions. Our suggestions for the key observations are listed in Table 1.

We attended an IMPS Workshop on 31 July 1985. The exciting glow experiment presented at that meeting prompted us to review the existing orbital observations data base to make intensity predictions for different altitudes and viewing geometries to help guide that mission. This exercise is presented

Table 1. Definitive Glow Experiment to Distinguish Plasma from Chemical Mechanisms

1. Geometric variability - look over broad, pointed, folded surfaces. Observe intensity, spatial extent, spectral distribution versus distance.

2. Vary ionic concentrations:

   a. Prevent from reaching surface using charged grid, pulsed duty cycle. Observe intensity, emitters, spectral distribution.

   b. Increase ion density using low work function surface; create or enhance plasma.

   c. Spacecraft charging effects.

3. Study surface dependence:

   a. Surfaces where glow is catalytic (both conductive and non-conductive) (MgF_2, Al, Z306 black paint)

   b. Surfaces which are degrded (Kapton, Mylar,...EOIM3).

4. Thruster plumes should be observed as a function of time, distance.

5. Surface glows should be observed as a function of time after dumps, thruster events.

ANALYSIS

5. See excitation energy required for various emitting states to isolate plasma from various chemical mechanisms (electron energies of $\leq$ 100 eV versus kinetic energy + reaction exothermicity)

INSTRUMENTAL

6. Only need resolution sufficient to discriminate overlapped branches and lines.

7. Use 2D detection array - simultaneous spatial and spectral.

8. Use radiometers:

   a. As bore sight to home in on glow regions

   b. Single wavelength to compare with Mende

   c. Multiple bandpasses to look for gross changes 500 to 800 nm.

as Appendix E of this report: Radiance Calculations for the IMPS/Glow experiment. The current AIS glow experiment grew out of these two previously proposed payloads.

The impact of glow on future space-based observations was addressed in a talk presented at the AIAA 20th Thermophysics Conference. This talk was entitled "The Nature of the Glow and its Ramifications on Space-Based Observations." Dr. Edmond Murad coauthored this work. There for the first time the role of kinetic energy in inducing endothermic reactions with bulk materials to produce chemiluminescent species was proposed. This concept was clearly outlined in an article "The Shuttle Glow as an Indicator of Material Changes in Space" coauthored by Dr. Murad of AFGL which appeared in Planetary and Space Science, 34,219 (1986), and is presented as Appendix F. The key concept here was that ram oriented surfaces could have a unique spectral signature which could affect its ability to be remotely observed.

The next major technical interchange on glow occurred at the AIAA Shuttle Environment and Operations II Conference in Houston in November 1985. Our paper "A Review of the Shuttle Glow" led off an interesting session, and is included as Appendix G. This review was updated with the new findings presented at the conference and as such it represents a complete review of the knowledge of Shuttle Glow up to 1986. Since this meeting, no further workshops on glow were held during the period of performance of this contract.

The Shuttle Glow as only one aspect of the role of kinetic energy in inducing or altering the products of chemical reactions was the topic of a talk presented at a High Temperature Chemistry Gordon Conference in 1986. Again, Dr. Murad of AFGL provided useful advice and insight. The viewgraphs of this talk are presented as Appendix H of this report. Because of our review and glow activities, we were able to provide significant insight into several environments surrounding the Shuttle.

We performed several basic calculations in order to assess the magnitude of various effects on the environment surrounding large space structures. Several interesting conclusions were reached, indicating that more accurate calculations should be performed in the future. We summarize our preliminary findings below.

1. Inside thruster exhaust columns, the pressures and densities are high enough that continuum flow relationships apply for distances up to many meters from the expansion throat. For all but the shortest burns, a sufficient number of collisions exist for the exhaust to expand and travel along the Shuttle surface and even (if the transition radius has not been reached) to travel around corners. As a result, Shuttle surfaces are frequently exposed to thruster exhausts and effects of thruster firings should be observable in the payload bay. The AFGL mass spectrometer data supports this conclusion having observed enhancements of exhaust species (H_2O, N_2/CO, and H_2) after certain thruster events that were not within the direct field of view. Thruster exhaust effects should remain a large source of concern.

2. In the absence of thruster events, outgassing within the bay has been monitored in the 10^{-6} to 10^{-4} torr range. This is a sufficiently high pressure that a contamination molecule after leaving the surface of the Shuttle has a large probability of colliding with another contamination molecule before it escapes to space. The mean free path between collisions will be 3 to 80 meters above the surface as the pressure at the surface varies from 10^{-6} to 10^{-4} torr. The above calculations assume the Shuttle is roughly spherical with a 10m radius. Under these conditions, free molecular flow or transition flow applies. This calculation implies that contamination from one site (leak or experiment) can be collisionally reflected back to another site in the bay. Again, mass spectrometers have observed such enhancements. Contamination of your

instrument by other experiments in the bay is a potentially serious problem. Quantification of the problem will be difficult and will be extremely geometry and collision interaction specific. Codes such as CONTAM appear to be largely empirical and not well documented.

3. Assuming that contaminant-contaminant collisions did not occur, the mean free paths of the outgassed molecule before it is struck by a "high velocity" ambient O or N_2 is 400m at 300 km and 80m at 240 km if its exit velocity is thermal (sonic at 300 K). Thus, collisional excitation of outgassed H_2O or CO_2 by ambient species with a relative kinetic energy 5 or 10 eV could give rise to considerable emission. Under the above assumptions, thruster exhausts at higher velocity can travel an order of magnitude further before colliding with an ambient species.

4. The density of the cloud surrounding Shuttle, has been monitored to cover the range between the limits where few incoming ambient species collide with contamination molecules and mainly interact with the surface to the other extreme where each ambient species undergoes multiple collisions with (and excitations of) contaminant species. Certainly in the thruster exhaust, the density is sufficient high that all of the directed kinetic energy of incoming O or N_2 will be lost to collisions with exhaust molecules. In fact, the mass spectrometer results indicate that a nearby thruster event can prevent ambient species from reaching Shuttle surfaces - the exhaust cloud moves the shock front (or interface between contamination and ambient species) well away from the vicinity of the surface.

5. For a representative column density of 10^{12} molecules/cm^2, collisional excitation of a state which can radiatively decay leads to calculated emission intensities of ~ 10^{-8} W/cm^2 sr within a strong

band. This intensity is comparable to the entire earth limb emission intensity within certain bandpasses. Both near-field emission and the earth limb radiances are very structured spectrally and these effects should be calculated more carefully. Nevertheless, they are of concern.

6. Absorption of light from far-field sources by the local contamination cloud is estimated to be completely negligible even for resonant absorption of H_2O and CO_2 emission. Resonant re-emission of absorbed airglow or earthshine may pose significant problems. Data from the Imaging Spectrometric Observatory should provide insight into the magnitude of the resonance fluorescence emission from near-field species.

These conclusions laid the basis for understanding the local Shuttle-induced environment in which the particles will be observed.

3. THE PACS DATA - PREPARATION, ANALYSIS, AND MODEL DEVELOPMENT

During 1985 preparations were made for the particulate data to be acquired by the PACS experiment.

The PACS payload was manifested for the December 1985 Shuttle mission. In order to prepare for analysis of that data, we visited Stu Clifton of NASA/Marshall after the Glow Workshop. Stu was kind enough to spend 2 days going through his experiences with stereo camera experiments on Shuttle, showing NASA/MSFC digitization and analysis capabilities and discussing problems we might encounter with the PACS data analysis.

The NASA pair of stereo cameras (built by Epsilon) are part of the Induced Environment Contamination Monitor (IECM) pallet which was flown on STS 2, 3, 4, and 9 (Spacelab 1) but is not currently planned to be used again. The cameras look straight out of the bay and are not scanned. They are focused at infinite distance, are separated by 0.4m, and have parallel 32-deg fields of view. Mechanical shutters are opened for 0.8s and closed for 0.2s. A white light photometer integrates emission within the field of view until an intensity limit is reached and the exposure is terminated. The mechanical shutter can open many times during the exposure and thus a particle's trajectory can be captured on a single frame. Looking to deep space, a typical exposure will take 15s. The next frame exposure starts 150s later. NASA used Kodak XX Negative Type 7222 film (400 ASA). With the aid of two stepping projectors, we looked at all 151 hr worth of data from Spacelab 1 (3700 frame pairs). This took 6 hr of elapsed time just to look at and comment upon interesting frames.

3.1 GENERAL OBSERVATIONS

Two airglow layers at 90 and 250 km were observable on many frames. They also observed an aurora (in the Southern Hemisphere South of Australia at 150W, 56S), lightning, structure in clouds, a satellite, city lights, and

particles. There were frames when the reflected particle emission was as bright as city lights or even lightning, demonstrating the serious magnitude of near-field effects on remote observations. Of the 3700 frame pairs, many were completely overexposed by sunlight or at night when no particle reflected light could be observed. Scattered light from the baffles was a problem, even cabin lights may have affected exposures. During periods when the Shuttle was in a stable trajectory and no maneuvers were attempted, the star field remained fixed and stable for up to 30 min (1/3 orbit). Only a few hundred frames showed evidence of particles. During a water dump (which could last for an hour), the film was totally overexposed. Each dump had a different appearance. Dumps often did not occur when scheduled. After a dump terminated, the particles in the field of view exponentially decay, with an e-folding time of 5 min and a return to baseline levels in 30 min. The Flash Evaporator System located near the tail operates continuously and its effluent can be reflected up over the bay for certain orientations of the wing flaps. The particle concentration in the FES effluent is not known but thought to be small.

3.2 PARTICULAR OBSERVATIONS

1. The particles are irregularly shaped as deduced from reflected light variations as they rapidly tumble in their trajectories. Up to 11 alterations in intensity (rotations?) are observed per second. This raises the issue of angular dependence of scattered intensity since the particles are obviously not spherical.

2. The particles observed were not spatially resolved. The film exposure area was the grain size or the blur circle and not the focused image of the particle. Thus, the stereo cameras were needed to determine the size/distance relationship. One exception occurred at the end of the mission. At hour 150 on-orbit, a hugh particle (on the order of cm diameter) was observed to move slowly across the

field of view. It had a visible diameter and could be used to determine particle emissivity based on its known size and distance.

3. When water dumps terminate at night, there is often a rise in particle count after the Shuttle moves into the sunlight. Particles may adhere to surfaces after a dump and be disturbed by thermal gradients upon sunrise to escape off surfaces.

4. Groups of particles are observed to move in the same general direction (as if from a common source), but there is an angular distribution around the mean direction. There is no apparent relationship of particle size and velocity. There are often two fields of particles observed in a frame. Each has a different net velocity direction. For example, there were several frames where the near set of particles was moving in one direction, while the far field set was moving at right angles to that direction.

5. Payload bay operations (such as RMS arm movements, EVAs, or bay door movements) tend to shake particles loose. These particles are very close to the cameras.

The decision to use a single camera or pair of cameras in a stereo configuration involves tradeoffs. For their IECM payload, NASA considered using a single camera to determine particle sizes, ranges, and angular velocities based on analysis. They selected the more complex (and heavier) stereo camera pair because of the limitations and assumptions which must result from the monoscopic analysis.

Stereoscopic information from a pair of coaligned cameras permits greater accuracy ranging directly from the film images. Each camera can place bounds on range based on geometric optics arguments. Triangulation provides an extremely precise (3 percent) range determination. Moreover, when larger particles with a visible disk are observed (and many have been observed), the

scattering efficiency can be found based on the stereo-determinated range and absolute irradiance. This will provide insight into particle composition.

The analysis of single camera film data can be pushed to attempt to determine particle size and range. It is always desirable to get the most information from the data, however all the uncertainties must be carefully stated. The cameras are focused at infinity, a particle at infinity would still have a blurred image on the film due to film granularity. Within the hyperfocal distance, however, even a point source particle will create a larger blur circle as its image is focused behind the film plane. However, because the particle has a physical size, it will have a finite size image adding to the blur circle size. Thus a unique solution for particle size and range is not obtained: a small particle near the camera will appear the same on film as a much larger particle farther away. There are insufficient measured quantities to specify particle size and range absolutely, a family of solutions exist. Moreover, any changes in film plane positioning and uniformity (planarity) will lead to errors in range and size calculated. Even micron size changes in the film plane position will lead to substantial errors. Basing a size determination upon irradiance value (no matter how carefully determined) relies too heavily upon assumed scattering efficiencies which are a function of shape, size, composition, and viewing/illumination geometry. A direct reflection glint from a surface irregularity could give rise to order of magnitude changes in the size determined.

The IECM investigators at NASA/Marshall found it difficult to obtain ephermeris data (mission trajectories, line of sights, attitudes, wind vectors, etc.) for some months after the mission. This could seriously hamper the PACS analysis. Selecting interesting frame sequences will be easy. Detailed analysis will be much more difficult. We planned to align frame pairs using star images, and began algorithm development.

Prior to October 1985, PSI and its subcontractors had some involvement with the PACS cameras. (Under a separate contract EPSILON had assembled the camera pair and designed, fabricated, and tested the probe assembly.) As part of this contract, we suggested the best tilt angle (5 deg) between the cameras to optimize stereo coverage in the observable near-field region; we recommended a 75 ft focal point as the best compromise between sensitivity to near-field particles and loss of the star field which is useful for pointing; we recommended against push processing the already grainy Kodak 2484 film beyond ASA2000; we recommended that additional fiduciary marks on the film be adapted to increase interframe relative position determination; and finally we mapped out the near-field threshold sizes as being (depending on lateral velocity) particles greater than 25 μm in diameter.

Dave Bunnell of Utah State University was tasked with final integration, testing and delivery, of the PACS cameras. At this request, PSI suggested a few quick tests to determine sensitivities of the cameras. It was suggested that he drop uniform size particles into his field of view - salt (300 μm diameter) and talcum power (40 μm) were suggested. Due to background brightness in his laboratory, these particles were not observable. Dave Bunnell was able to photograph several strings and objects in the laboratory. EKTRON has used these frames of film to become familiar with the future 16 mm data images in terms of image quality, fiducials, frame boundaries, image pairs, and digitization. No real calibration was performed. A post-flight calibration would have been useful in understanding the on-orbit data.

The first roundtable PACS data analysis meeting was held on 1 November 1985 at AFGL/PHK. PSI presented several viewgraphs detailing the analysis plan and key parameters. These are summarized in Table 2. The film exposure sequence is given in Table 3. Key information to assist in the analysis of the data was provided by the detailed Mie scattering calculations. The signal levels expected for different size particles as a function of illumination conditions, solar scattering angle, and particle size for H_2O particulates were calculated to assist in data analysis planning. The

TABLE 2. Data Analysis Plan

1. Preparation
   - Algorithms for fov geometry (camera, tilt, stereo coverage) (EKTRON/PSI)
   - Particle radiance predictions (r_p, λ, η, illumination (PSI))

2. Data Reduction (LS/Aerospace)
   - ASA 2000 processing
   - Ephemeris, who else on mission
   - Mission profile

3. Typical Data
   - NASA/MSFC pictures
   - Dump clearing
   - Number particles versus MET

4. Visual Inspection (PSI/EKTRON/Miranda/AFGL)
   - Identify critical/interesting frame pairs -75% no visible particles
   - Tests
     - Stars versus particles
     - Close (PLBOps) versus far limits (bright/weak)
   - Comparisons existing data
     - Decay after water dump
     - Statistics versus mission elapsed time
     - Attitude dependence
   - Interesting cases
     - Particle groups, different velocity vectors
     - Rotations/flakes
     - Evolution night/day (thermal)

5. Particulate trajectory analysis
   - (EKTRON/PSI/Miranda) X, Y, Z, V_x, V_y, V_z, brightness, r_p
   - Benefits:
     - Sources
     - Magnitude of problem
     - Size distribution
     - Emission other spectral regions
     - Acceptable mission operating conditions

6. Future Measurements
   - Chopping shutter arrangement - increase information trajectories
   - Detection wavelength refractive index (T_p)
   - Polarization shape, size
   - Radiometers

TABLE 3. PACS Film Exposure Sequence

Frame	T_{open}(s)	T_{close}(s)
1	0.0	0.3
2	1.0	1.3
3	2.0	3.0*
4	4.0	6.5
5	120.0	120.3
⋮		
· repeat 1-4, 5-9, ···		

*Strobe flash at start and end of this exposure

detailed calculations and interesting conclusions are presented in Appendix I. Predictions are also presented there for the emission intensities in other spectral bandpasses from the ultraviolet to the infrared.

As a result of this meeting, a subcontract was let to EKTRON by PSI to develop a film reduction methodology. It was decided that a quick-look report would be due at AFGL 5 months after receipt of film.

This same group met on 17 December 1985 at EKTRON. EKTRON presented their geometry model and error budget analysis. The uncertainty in the focal length was found to be the major source of error. This value should be determined in post-flight calibrations. Film plane displacement will also be a substantial source of error. (The tightly focused image requires knowledge of film location beyond lens manufacturer's specifications.) The angular orientation of the PACS experiment within the bay will also be uncertain due to Shuttle torsional motion. This error budget has proved useful in specifying

the parameters which must be most closely measured; EKTRON performed this task well. The viewgraphs they presented are given as Appendix J. We recommended that the PACS experiment should be made available to AFGL for post-flight calibration. A meeting to review the PACS film data was planned for approximately 1 month after receipt of film. At this meeting all those involved with the program were to have the opportunity to see and suggest useful tactics for analyzing the data.

Space Transportation System Mission 61C was originally scheduled for launch on 18 December 1986. Due to poor visibility, rain, and mechanical delays, it was postponed until January 1986.

Shuttle Mission STS61C lifted off at 6:55 a.m. on 12 January 1986. D. Green and M. Ahmadjian (LSP) arrived at the Hitchhiker G Command Center at Goddard Space Flight Center shortly after the payload was turned on. This occurred at 0:03:30:12 (day:hour:minute:second) Mission Elapsed Time (MET). Although downlink data was sporadic at first, there was some indication of trouble. The downlink shutter monitor on Camera 1 was observed to operate at first, but ceased to operate before 6 hr MET. There was no similar monitor on Camera 2. Current was being drawn by the experiment and the flash was visually observed by the astronauts. After considerable real-time agonizing, it was decided to shut down PACS (at 1:03:26:10), then restart it a few minutes later (at 1:03:28:58). No change in its status was observed after this procedure, the monitor indicated no shutter action, the flash was visually observed. Nothing further could be attempted, so for the rest of the mission supporting data was gathered hoping the cameras were operational. Due to poor visibility at the prime landing site (Kennedy Space Center), two additional days were gained on-orbit. PACS and the entire Hitchhiker G pallet was turned off before the payload bay doors were closed in preparation to landing each morning. The PACS experiment was off for periods of 6:38 and 7:56 on the two mornings. Even though the temperature monitors on PACS indicated 2° to 3°C temperatures, no trouble was encountered restarting the camera and strobe. Prior to the first landing attempt, a K_u band antenna was stowed in

the cargo bay. It was not deployed again. In the stowed position, it appears to have partially obscured the field of view of Camera 2. The light from the strobe was strongly reflected off the stowed antenna. The strobe was disabled (much to the crew's relief, the scattered light was bothering them). The field of view of Camera 1 was probably totally obstructed by the antenna. This was an unfortunate choice of payload positioning. Post-flight inspection revealed that the film in Camera 1 had been improperly loaded causing the camera to jam. The other camera acquired in excess of 350 ft of film during the 6-day mission.

During the mission we gathered detailed information on Shuttle attitudes, solar angles, and mission operations. NASA personnel were extremely helpful in advising and assisting in the gathering of these data. Difficulties experienced by previous investigators in getting useful ancillary data prompted us to bring back as much real-time information as possible. This information was valuable defining the exact orbital scenarios for many sets of exposures. A modified example of the Shuttle Ground System output provided by GSFC is shown in Figure 1. Three views of the Shuttle are notated with earth,

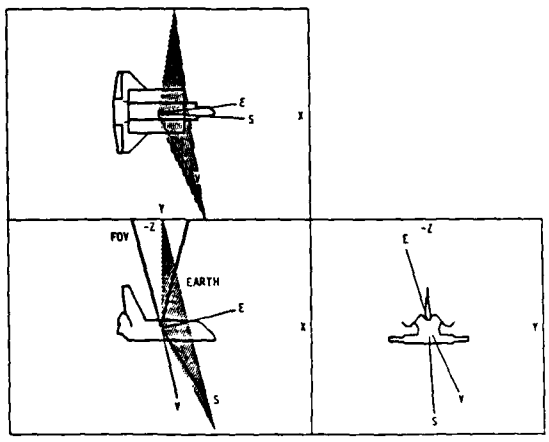

Figure 1. Shuttle ground system attitude display. V is velocity vector, S is sun sector, and E is center of earth vector. Solid angle subtended by earth is indicated as PACS field of view.

sun, and velocity vectors. This information was updated four times a minute. The angle subtended by the earth and the PACS field of view are also indicated in the figure. With this figure, viewing geometries can be more easily visualized. After the mission, Mark Ahmadjian was extremely helpful in obtaining data on fuel cell purges, ventings, and water dumps. As this was the first flight of Columbia in 2 years and there had been severe rains during the week before the flight, the particle environment around Shuttle was expected to be severe.

The original film from Camera 2 was delivered to PSI by G. Kenneth Yates on 3 February 1986. Mark Ahmadjian had taken the film from Kennedy to Aerospace Corporation for development and finally to AFGL, where he turned it over the PHK. With the assistance of Ken, we decoded the time code beside each negative film frame. The sets of four exposures comprising a 6.5s sequence were partitioned into various categories upon visual inspection. Most of the exposures showed no evidence of particles and contained either stars or the earth. Usually more than a dozen stars were visible in an extended exposure and several constellations have been identified. Earth limb views and airglow layers were frequently observed. City lights were also frequently observed and are being correlated with ground track information to increase our confidence of our understanding of the real Shuttle attitudes.

On average there were, however, several sets of exposures during each orbit which displayed particles. Subsequent analysis indicates that the near-field particles are illuminated by the sun only under certain attitude configurations, and that these are the frames in which particles are evident. Thus, particles may be present often during the orbit but are not visible due to the lack of proper illumination. This certainly will not be the case in the infrared spectral region where self-emission, not solar scattering, controls particle radiances. There are a few sets of frames which contain a large number (> 100) of particles. These have been correlated with a satellite launch (RCA K_u band satellite deployment at 0:09:31) and water dumps. Many tracks of non-spherical particles have been observed including a

large triangular mass and apparently rapidly rotating particles whose intensity oscillates more than ten periods during a 2.5s exposure. There is a general trend of fewer particles with elapsed MET, suggesting a decrease in particle ejection rate as the Shuttle surfaces free themselves of any particles they collected on the ground. Our catalogue of the entire PACS mission data base is Appendix K to this report. It categorizes 3697 sets of exposures (14788 frames of film data) and represents a considerable effort. Mission Elapsed Time, orbit, and visual observations are also listed. The sets of exposures were correlated with altitudes, solar angles, and mission events. The catalogue represents a solid foundation upon which we can build a careful detailed understanding of the STS61C Mission's environment. Some observations are quite striking such as the frames containing backlit, solar-illuminated particles rivaling the brightness of the city lights of the Florida peninsula.

A data review meeting was held at PSI on 3 March 1986. Messrs. Gold, Jumper, Miranda, Murad, Pike, and Yates were present in addition to PSI personnel. At that meeting it became apparent that significant insight can be gained into the on-orbit environment even without the Camera 1 film data. Particle positions, velocity, and hence size will be difficult (if not impossible) to extract from the data. Radiant intensity, track foreshortening and blur circle size comparisons, however, will permit estimates to be made in the future of the magnitude of the contamination source and its impact on remote sensing from the Shuttle. The gross characterization of the particle densities will be useful in defining exposure sequences on future missions.

Priorities were defined at the 3 March meeting.

- Quick-look data report for CIRRIS mission needs: A description of general findings and highlighted interesting frames was presented on 27 June 1986. Specifically, observations during the requested deep space viewing and gravity gradient orbits during hours 50-53 MET were examined in detail.

- These observations were placed in the context of relevant scenarios as part of that briefing.

- The lessons learned and what can be extracted from the data were summarized there also.

- A consideration of how to improve future data such as more frames per set of exposures, a different focal point, better fiducial marks, or a better film plane definition was formulated.

- We recommended actions to improve our chances of success in future missions.

Responsibilities for the continuing data analysis were also assigned at the March 1986 meeting. EKTRON was provided with the original film data. They established a gray scale for the film so that particle exposures can be quantitatively compared to stars. Also, they developed background subtraction algorithms to extract particles from the strongly exposed (nearly black) film frames. Particle scattering is peaked in the forward lobe, so this geometry permitted smaller particles to be detected. EKTRON also digitized a few selected densely populated frames to estimate the number of particles present. They demonstrated that filter operations could extract particles from over-exposed frames and enhance detection limits by a factor of two to five. Their excellent final report is attached at Appendix L. Considerably more information can be extracted from the existing PACS data base by future analysis efforts. PSI continued with the mission timeline development correlating PACS data with mission attitude, solar angles, and events. We also determined the temporal dependence of the particle densities during selected time sequences such as solar inertial or for CIRRIS relevant observations.

The quick-look data briefing report to the CIRRIS mission staff occurred on 27 June 1986. That presentation is included as Appendix N. The key points

are summarized here. The PACS film data clearly indicates that the solar illumination angle is the key parameter. We suspect particles were often present but we were able to observe them only under proper illumination conditions. At terminator crossings (when illumination conditions were reasonably good), particles were observed about one-third of the time within the 17 x 24 deg field of view of the PACS cameras. Particles were observed: when all activity was suppressed, after maneuvering, after payload bay door operations, during the preparations for a satellite launch, during and after water dumps, and after sunrise. During active events such as dumps and the satellite launch, the particle trajectories observed extrapolated back to the vicinity to the source. Atmospheric drag accelerations only slightly perturb the trajectories of detected particles during these events. Only a few particles were detected by the strobe illumination. This indicates that the particles were nearly always beyond 2m from the cameras. It also appears that particles are often very asymmetric offering different geometrical areas to the cameras at an angular rate of up to 20 per second. Particles with trajectories from every direction were observed. The PACS results are encouraging in that there may be quiescent times when the optical environment it quite clean. Unfortunately there are many times when it is not.

The larger IECM data base shows many of the same trends observed in the PACS data. The PACS data was more carefully analyzed to determine the time evolution of events such as sunrises and water dumps. The partial analysis of the PACS data has shown that the camera equipment and experiment philosophy were excellent and that additional data taken with the same instrument with stereoscopic imagery would provide useful trajectory and size data of particulates surrounding the Shuttle bay associated with events. For example, during a water dump when particles are known to be mainly H_2O in composition, we can use the stereo camera to obtain absolute sizes and distances using particle emissivities/scattering efficiencies taken from our Mie calculations. For particles exhibiting finite size on the film, accurate verification of the scattering efficiency can be made from the known size and distance.

In order to place the PACS data in perspective, the orbital particulate data base was reviewed at the end of the contractual effort. Our summary of the pre-PACS state of knowledge is summarized in Appendix N: The Particle Environment On Orbit - Observations, Calculations, and Implications. Our current understanding of the orbital particulate data base based on all orbital data but highlighting the important findings of the PACS Mission are described in Appendix O: The Particulate Environment Around the Shuttle as Determined by the PACS Experiment.

The findings of the orbital data bases were used to develop a particulate model for the Shuttle environment. This model is presented in Table 4. It is meant to guide the development of future mission/scenario specific models for Air Force missions.

Although further analysis of the PACS data will yield much additional information and insight into the induced environment on-orbit, a number of significant insights into the sunrise generation of particles, irradiance levels, particle occurrence and clearing times have come from the PACS data. This data was analyzed in a timely manner with its conclusions reaching sponsors and the scientific community before camera data from missions flow years earlier.

Finally, it should be stressed that IECM, PACS, and previous camera observations only provide information during sunlit portions of the orbit in the visible spectral region where scattering dominates. Observations of infrared particle emissions through the entire orbital period are needed to assess the impact of particles on Air Force systems. A re-flight should be aimed at addressing these uncertainties not merely repeating previous observations.

TABLE 4. Particle Model (Shuttle Environment)

Clearing Time: Decay (e-fold)		
- Quiescent	(constant solar angle) (total mission after day 1)	4.8 hr 11 days
- Dump	(altitude dependent)	2 to 10 min
Density:		
- Quiescent	($r > 40$ μm, distance < 100m) (CRDG -1.5×10^{-5} sr fov)	8 particles/sr-s 2/3 particles/orbit
- Dump	optical attenuation	~ 1
Composition:	unknown (source dependent)	Suggest H_2O, SiO_2, NaCl
Size:	unknown (source dependent)	Suggest $r^{-3/2}$ (r = 2-40 μm) r^{-1} (r = 40 μm - 1 cm)
Velocity:	observed	0.3 to 3 m/s range
- Quiescent	unknown	Suggest proportional to distance from shuttle (drag)
- Event	unknown (source dependent)	Suggest initial velocity plus drag
Additional Effects:		
- Rotations		0 to 20 rps
- Solar-induced component		100 particles/sr 10 min duration

APPENDIX A

The Shuttle Environment Gases, Particles and Glows

J. Spacecraft 22, 500 (1985)

PSI SR-171R is reproduced in its entirety.

A7647 REVISED
PSI SR-171R

The Shuttle Environment: Gases, Particulates and Glow

Byron David Green* and George E. Caledonia†

Physical Sciences Inc.

Research Park, P.O. Box 3100

Andover, MA 01810

and

Thomas D. Wilkerson††

University of Maryland

College Park, MD 20742

*Manager of Atmospheric Sciences Group
†Vice President Research
††President, Environmental Science Communications, Inc., Member, AIAA

ABSTRACT

This review covers selected Shuttle-environment phenomena that will impact planning for future observations from the Shuttle platform: the gas/plasma and particulate local concentrations and the Shuttle glow processes. The gaseous envelope which surrounds Shuttle is dominantly water vapor. Neutral and ionic concentrations exhibit extreme variability with factors such as angle of attack, thruster events, and water dumps. At a minimum, part of the differences between various experimenters' observations can be attributed to instrumental differences and atmospheric variabilities. Although some observations indicate the presence of very large particulates around the Shuttle, that environment appears to be clean enough for many applications, but may compromise the most sensitive instruments. Several possible mechanisms for vehicle glows are considered. It is clear that a full evaluation of the nature and impact of the glows must await more quantitative experiments. The Shuttle environment is hospitable for many applications, and the ultimate limitations on our ability to probe from this orbital platform remain to be tested.

INTRODUCTION

The growing number of Space Shuttle missions has presented the aerospace community with an unprecedented body of data on the Shuttle environment itself, as well as new data - on astrophysical domains far from earth. This paper focuses attention on selected Shuttle-environmental phenomena that may impact plans for future observations from the Shuttle platform. In this review we will compare and contrast data from STS 2-4 which have recently become available. These data have all been presented previously although largely not in the open literature.

Among the many environmental factors that will interest users of the Shuttle, we have selected three that must be reckoned with for a broad range of instruments and measurements:

- Gases
- Particulates
- Vehicle glows

We leave aside other issues such as mechanical structure, vibroacoustics, thermal excursions, electromagnetic interference, and materials degradation; the first three of these appear to be well understood at this time, and the last two are active research areas.

Gases, such as H_2O, surrounding the Shuttle can potentially absorb light from astronomical sources giving false, partially attenuated spectra (UV, visible, IR), and can contaminate those types of particle/optical detectors that are open to the vacuum. Particulate matter can settle out on optical surfaces, reducing their transmission, and can scatter unwanted light from the sun or the earth into the line of sight of a telescope. Vehicle glows may stand in the way of a telescopic line of sight, adding spurious signals and limiting the sensitivity of astronomical or earth observations.

While a great deal of attention[1] has been given to the Shuttle environmental parameters as potential problems for Shuttle users, we wish to stress that so many of the original requirements on the Shuttle have been met that perhaps undue emphasis can now be seen to have been given to these "problem areas". This emphasis may have been strong enough as to make it hard for users to know, a priori, that the Shuttle is in fact a working spaceship ready to convey many successful instruments into space over the years ahead.

What is important now for users of the Shuttle is (1) to have a candid and complete description of the environment in the payload bay on-orbit, controversies notwithstanding, and (2) to make sure that the Shuttle environment is not only consistent with any given set of measuring instruments but also steadily improves with successive launches. In an effort in this direction Scialdone has recently[2] presented a baseline model for the gaseous and particulate environment of the Shuttle bay. The developing Shuttle bay data base provides both a test bed for such models and a means for extending them.

In this paper we concentrate on the data (and interpretation thereof) from various early STS flights, as regards the gaseous envelope surrounding the Shuttle, the particle populations in orbit with the Shuttle, and the optical interferences from local (rather than astronomical) sources. It seems that many design goals for the on-orbit environment have been met. On the other hand, the environment is very variable, depending on angle of attack, thruster events, water dumps, solar angle, and payload bay activities. We will attempt to highlight the role of these effects whenever possible.

GASEOUS/PLASMA ENVIRONMENT AROUND THE SPACE SHUTTLE

Several different instruments have been used to sample the on-orbit neutral/ionic gas composition in the Shuttle payload bay. These include: a neutral mass spectrometer[3], which was part of the Induced Environment Contamination Monitor (IECM); a Bennett RF ion mass spectrometer,[4] which was part of the Plasma Diagnostics Package (PDP) on STS-3; and a fast sampling quadrupole mass spectrometer[5] used in both ion and neutral sampling modes on STS-4. These devices were backed up with additional diagnostics such as pressure monitors and electron density probes (see for example Ref. 6). In general the Shuttle contaminants were apparently no more severe than anticipated[1]; however, very large variations in species/densities are observed during the course of flight, most of which can be related to either orbital considerations, i.e. angle of attack, solar attitude, spin (etc.) or Shuttle events such as engine firings, water dumps and bay door operation. While a sampling of the available data base has appeared in Refs. 3-5, no detailed comparison or interpretation of the results has yet been presented. A brief overview of these results is provided below.

The Natural Atmosphere

These composition measurements must be interpreted in light of the natural atmospheric constituents in order to separate the Shuttle-induced component. Shuttle missions 2, 3 and 4 which we consider here had on-orbit altitudes of 240-300 km. Both higher and lower altitude orbits have been achieved during later missions. At these altitudes atmospheric densities are on the order of 10^9 particles/cm^3. Representative atmospheric compositions[7] at altitudes of 240 and 305 km are given in Table 1. Atomic oxygen is the dominant constituent, although N_2, O_2 and He are present in significant quantities. At these

Table 1

ATMOSPHERIC COMPOSITION (from Ref. 7)

Molecules/cm^3 [1.7×10^9 = 1.7(9)] / Fractional Composition

Altitude (km)	O	N_2	O_2	He	A	H
240	1.7(9)/70.1%	6.8(8)/28.0%	3.7(7)/1.5%	1.0(7)/0.4%	2.5(5)/0.01%	1.3(5)/0.005
305	5.0(8)/84.2%	8.3(7)/13.9%	3.3(6)/0.6%	7.4(6)/1.25%	1.3(4)/0.002%	1.0(5)/0.02%

altitudes the atmospheric kinetic temperature is comparable to the exospheric value and ranges between 800-2000 K. This tenuous atmosphere has a collisional mean free path of about a kilometer. The dominant characteristic of the atmosphere at these altitudes is its variability. Even the most simplistic treatment of the atmosphere must consider its dependence on diurnal, latitudinal and solar activity effects. The ionosphere is a multiconstituent plasma whose behavior is linked with that of the neutral atmosphere through solar ionizing radiations, and with electrodynamic influences of the magnetosphere. Shuttle missions occur in the midst of the F2 region, which is the ionospheric layer having the highest plasma density, up to 10^6 ions/cm^3. The dominant ion is O^+ produced from absorption of solar UV ionizing radiation; on the order of 0.1% of the O-atoms are ionized. The ionosphere exhibits even more extreme variability than the neutral atmosphere, with the F2 peak generally being at lower altitudes during the day, higher at night. It is within this very variable natural environment that the Shuttle operates. Thus it is obvious that care must be taken in generalizing any specific observational finding.

The Shuttle will perturb this natural environment both by its flow field and its emissions: leakage, evaporation, outgassing, desorption, and orbital control thrusters.

The orbiter carries a vernier thruster system of six rockets which provide 1.1×10^7 Newtons of thrust and a reaction control system consisting of 38 main thrusters which can produce up to 3.8×10^8 Newtons each. All these hypergolic engines utilize monomethylhydrazine (MMH) as fuel and N_2O_4 as oxidizer. The exhaust products are modeled to be dominantly H_2O, N_2, H_2, and CO with traces of CO_2, H, unburned fuel and O_2 (see Table 2). The mean exhaust velocity is 3.5×10^5 cm/s.

TABLE 2

MODELED THRUSTER EXHAUST PRODUCTS (from Ref. 8)

Species	Mole Fraction
H_2O	0.328
N_2	0.306
H_2	0.17
CO	0.134
CO_2	0.036
H	0.015
O_2	0.0004
$MMH\text{-}NO_3$	0.002

Neutral Measurements

Carignan and Miller[3] have reported neutral species observations taken on STS-2, -3, and -4. Their device spanned the mass range from 2 to 150 amu and used a three-stage skimmer pumped by zirconium oxide getters to limit the instrument field of view to 0.1 sr.

Both ambient atmospheric and contaminant species were observed by the mass spectrometers. Species identified from the measurements include He, H_2O, N_2/CO (mass 28), NO (presumably), O_2, Ar, CO_2, Freon 12 and 21, trichloroethylene and other heavy hydrocarbons (cleaning agents). Statistically significant quantities of masses 11, 19 and 36 were also observed but not identified. (Note that mass 19 could be H_3O^+ produced from a reaction between H_2O^+ and H_2O). Although O_2, N_2, He and Ar are ambient molecules, the latter three were also found to be significant contaminants. The heavier species, with the exception of Freon 21 which is used in the thermal control systems, were typically in low concentrations and the CO_2 was primarily at instrument background levels, although some contribution from the Shuttle environment was observed. Interestingly enough, methane was also seen, with its presence correlated with thruster

activity. It has been suggested that this observation reflects the presence of unburnt monomethyl hydrazine which is catalyzed to methane by the zirconium oxide getters.[3] An alternate mechanism, proposed by a reviewer, is that methane is released from the getters in the presence of increased water vapor during RCS firings. In any event Narcisi et al.[5] observed no evidence of CH_4 in their measurements.

The absolute concentrations of contaminants in the Shuttle bay are not yet well evaluated. For most of the measurements the mass spectrometer was pointed upwards out of the bay; thus, contaminants originating from Shuttle surfaces must scatter off of ambient gases into the instrument. Accounting for this effect is both complicated and uncertain, and self-calibration techniques have been employed. These calibrations have only been partially successful to date, and the results are not yet fully analyzed. Suffice it to say that ambient pressures are $\sim 10^{-7}$ Torr, and bay pressures between 10^{-7} to 10^{-4} Torr have been observed[6] during various Shuttle activities with the higher pressures correlating with ram observations and thruster firings. The principal contaminants observed were H_2O and He, and much of the mission was dedicated to the study of H_2O. The envelope of H_2O flux into the spectrometer during the STS-4 flight is shown in Fig. 1. The values within the envelope are strongly modulated by the instrument angle of attack. The large spikes have been correlated to specific RCS firings[3], although the vast majority of such firings do not lead to such large excursions in H_2O concentration.

The initial decay time for H_2O after launch is about ten hours, corresponding to outgassing from surfaces conditioned by the pre-launch environment. Interestingly enough later spikes in the H_2O count rate apparently exhibit similarly long decays, in contradiction with the observations of Narcisi et al.[5]

described below. These long decay times may be an instrumental artifact, for example reflecting vapor histories over the zirconium oxide getters. Alternately these measurements may reflect outgassing over Shuttle surfaces.[9] Additional testing with the instrument would be required to resolve this issue.

Estimates of the H_2O column density for the three flights are provided in Table 3. The maximum limits correspond to observations at early times. Note the large variations from flight to flight. STS-2 and STS-4 were subjected to heavy rains prior to launch, and this may account for the higher observed column densities in the early orbits.

TABLE 3

H_2O CONTAMINANT COLUMN DENSITY (from Ref. 3)

	Max[a]	Final
STS-2[b]	2.0×10^{13}	2.7×10^{12}
STS-3	1.5×10^{11}	4.0×10^{10}
STS-4	3.2×10^{13}	1.0×10^{12}

[a] Except for RCS firings and payload bay door closings.
[b] The STS-2 values are considered upper limits.

It is expected that ambient species will behave quite differently than contaminants as the spectrometer angle of attack is varied. This is borne out in Fig. 2 where the He and Ar count rates vs. time are shown for a particular STS-3 orbit. (These species are not collimated by the getters). The system angle of attack varies from 170 to 10 degrees over the time shown, and the He and Ar concentrations are seen to be largest in the near-ram position, in keeping with the presence of these species in the ambient gas. (The bump in the Ar trace is due to flow interference from the Remote Manipulator System (RMS)[3]). These observations along with many others not shown are in good agreement with model atmosphere expectations.

On STS-4 the IECM was picked up by the RMS and moved around so as to look down at the Shuttle bay and adjacent surfaces. Measurements were performed for fifteen different orientations as shown in Fig. 3a; each had a 10° half angle field of view. The corresponding average count rates for H_2O are shown in Fig. 3b, the spikes represent changes due to RCS thruster firings. Measurements for helium were quite similar; however, Freon 21 exhibited a distinct signature, reflecting perhaps the position of specific leaks. With the exception of freon the contaminants appear to be well distributed throughout the bay, peaking slightly in the aft section.

Narcisi et al.[5] also report Shuttle contaminant species measurements acquired using a quadrupole mass spectrometer. This instrument was positioned to look horizontally over the right wing of the Shuttle, although pitched slightly upwards, and had a 2π field of view for neutrals. Measurements were made in both ram and non-ram modes. During the ram mode, measurements are made with and without a grid retarding potential of 2.5 volts (R and NR modes respectively) so as to distinguish between ambient and contaminant species. Ambient species, having no directed kinetic energy, cannot penetrate beyond the retarding barrier.

Typical observations during vernier and OMS burns are shown in Fig. 4a. Note that the H_2O and N_2 histories follow the total pressure, with signals decaying back to steady levels within seconds, quite unlike the bay observations by Carignan and Miller.[3] It is to be remembered that Narcisi's instrument has a significantly different look configuration and a much broader field of view. Narcisi's data will observe species scattered off wing structures and thus it will be susceptible to surface-induced effects, but may more closely represent

the actual bay environment. H_2, an exhaust species not observed in the IECM measurements, was found by Narcisi to behave in a manner similar to N_2 and H_2O during thruster firings (see Fig. 4b). These species are the three major components expected in thruster exhaust. (See Table 2).

One of the more intriguing measurements reported by Narcisi et al.[5] is shown in Fig. 5. Here the average H_2O signal for a given scan is plotted versus mean MET (mission elapsed time) and compared with the spectrometer sensor temperature measurements. There is a remarkable correlation between these two histories. Although the local variation in temperature is small, thermistors placed throughout the pallet exhibit significant variations, of order 100°C, while maintaining a temporal structure similar to that shown in Fig. 5. Since the instrument has a large field of view it can sample the outgassing from a wide surface area. Indeed, Narcisi[5] concludes that the spacecraft surface temperatures seem to be a significant controlling factor in the water vapor environment. Note that measurements made in the more confined inter-payload areas within the bay may exhibit different dependencies. Additional measurements on future flights should resolve this issue. Again, unfortunately, absolute calibrations are difficult because of the scattering problem. As discussed below, Narcisi et al.[5] have suggested that absolute H_2O concentrations may be more appropriately deduced from ionic observations.

Helium was once again found to be an important species. Approximate helium pressures were found to vary between 4×10^{-9} to 2×10^{-7} torr. Since typical ambient ram He pressures were $\sim 6\times10^{-9}$ torr and the observations were primarily made in non-ram operation, substantial helium leaks, apparently from payloads, were evident. Higher molecular weight species, > 50 amu, were also observed, and the total "heavy" pressures were estimated to be $< 10^{-9}$ torr. In

these latter measurements contamination by ion source outgassing cannot be excluded, particularly since no mass discrimination was attempted.

Positive Ion Measurements

Narcisi et al.[5] also operated their instrument in the ion mode; instrument field of view in this case was 20°, and a typical scan time for amu 1-67 and TI (total ions) > 50 amu was less than one second. Species observed include O^+, H_2O^+, H_3O^+, N^+, N_2^+, NO^+, O_2^+ and OH^+.

A typical scan of H_2O^+, O^+ and N^+ vs. time is shown, contrasted to the density monitor, in Fig. 6. These measurements were performed during daytime, at an altitude of 298.5 km, and with an instrument angle of attack ranging between 33 and 38°. The O^+ and N^+ are ambient species, and H_2O^+ is a contaminant species most likely formed via

$$O^+ + H_2O \rightarrow H_2O^+ + O. \qquad (1)$$

Note that the O^+/H_2O^+ ratio typically is of order unity (factor of two). This ratio is sensitive to angle of attack and was found to be ~ 10 with the instrument looking in the ram direction in an earlier orbit. Nighttime concentrations of H_2O^+ were found to be lower, reflecting lower ambient O^+ densities.

The H_3O^+ current falls about one order of magnitude below that of H_2O^+ for the conditions of Fig. 6. This species is most likely produced via the reaction.

$$H_2O^+ + H_2O \rightarrow H_3O^+ + OH \qquad (2)$$

It has been suggested[5] that these data may be used to estimate neutral H_2O concentrations via a kinetic analysis.

The spikes seen in Fig. 6 in the vicinity of 23,210 and 23,270 seconds (MET) correspond to VCS firings. At these times, positive ion depletions of an order of magnitude are observed in the total density monitor and reflected in

the O^+, N^+ observations. Thus the thruster exhaust gases tend to displace or "blow away" the ambient atmosphere. Enhancements in the N_2^+, NO^+ and OH^+ concentrations were noted at these times. These species correspond to anticipated products of reactions between O^+ and the thruster exhaust gases N_2 and H_2. The decrease in H_2O^+ concentrations is attributable to the decrease in O^+, its precursor. The H_2O concentration is already large and the thruster event does not alter the H_2O concentration sufficiently to overcome the O^+ depletion.[5]

We note that ion measurements during thruster firings may be complicated by concomitant changes in vehicle potential.[10] Narcisi et al.[5] have performed measurements on O^+ and NO^+ where their retarding potential was swept over ranges of 12 and 19 V respectively, although this data has for the most part not yet been analyzed. They have demonstrated the ability to measure spacecraft potential in this manner, however.

Grebowsky et al.[4] have performed thermal ion measurements in the Shuttle bay on STS-3 using a Bennett ion mass spectrometer which was part of the Plasma Diagnostic Package. The STS-3 mission was in a trans-equatorial orbit (inclination of 38°) with a mean altitude of 244 km, and the ion measurements reported were specific to a nose-to-sun attitude orbit. The spectrometer was positioned within the PDP in the bay so that it faced the interior port bulkhead. The instrument scanned 1-64 amu in 2.4 seconds.

Ions observed include O^+, H_2O^+, H_3O^+, NO^+, O_2^+ and CO_2^+. A typical observation is shown in Figs. 7a, b. Note that signal is only shown for 50 minutes out of the 1-1/2 hr. orbit; no thermal ions were observed during the unplotted portion of the orbit.

As can be seen the ion concentrations all increase sharply as the Shuttle proceeds through the dawn terminator. On other orbits a brief (~ 10

minute) precursor enhancement of the ion currents is observed followed by a decrease just prior to sunrise. These observations are quite different from those of Narcisi et al.,[5] and more difficult to interpret because of the positioning of the instrument and possible interference from other payloads. In particular, for most of the orbit the majority of ambient ions would scatter off of the Shuttle outgassing layer or Shuttle/payload surfaces prior to entering the spectrometer. Surface scattering would most likely result in ion neutralization. The observed daytime dropoff in ion concentrations can be correlated with a similar drop in bay pressure, occurring as the bay faces the Shuttle wake. It would be expected that the wake would exhibit depleted ion concentrations.

The day/night ion variation does not scale with PDP pressure and is not well understood although it may also be due to ram-wake variations. Grebowsky et al.[4] originally suggested that the variation may result from photo-ionization of the Shuttle cloud. This appears unlikely given anticipated photo-ionization rates at Shuttle altitudes. Indeed one would anticipate that the contaminant ions would be produced via reaction with ambient species. Perhaps geometric effects preclude such reactive events within the instrument field of view during specific portions of the orbit. On the other hand the day/night behavior is reminiscent of F_1 region collapse which can occur at Shuttle altitudes in the equatorial region. Nonetheless, Grebowsky et al.[4] argue that the observed pre-dawn precursor ion currents result from ambient ions entering the instrument, further confusing the issue. It is clear that these observations require further investigation.

Variations in ion concentrations were also correlated with Shuttle activities such as water dumps and thruster firings. For example enhancements in

H_2O^+, H_3O^+ and NO^+ have been observed in thruster firings. Narcisi, et al.[5] observed similar enhancements in exhaust related species, although reporting a concomitant drop in total plasma density. Such a drop is not reported by Grebowsky et al.,[4] perhaps because their scan time was considerably larger than typical burn times. In any event, the interpretation of the measurements of Ref. 4 in terms of ambient ions is complicated by surface scattering effects.

It appears that during thruster events significant increases in contamination levels occur which largely dissipate on time scales of one second. If this is indeed the case, thruster firings may be viewed by Shuttle experimenters as a short-term inconvenience whose effects may be removed by appropriate filtering. On the other hand, because thruster events are so frequent (approximately once every 15 seconds on average), a cooperative arrangement between experimenters and Shuttle crew may be required for sensitive observations.

There have been several measurements of the electron densities and energies which we have not addressed here. Murphy et al.[6,10] have reported factors of 2-10 increases over ambient in the thermal electron concentrations as compared to the nearly parallel observations of the Dynamics Explorer satellite.[11] Indeed unusual electron energy distributions have been observed[11,12] and interpreted to indicate the presence of a Shuttle-induced plasma above vehicle surfaces in the velocity vector.

In summary, it is apparent that the Shuttle neutral/plasma environment is very sensitive to both the ambient atmosphere and Shuttle activity, and that the species observations strongly reflect both instrument positioning and angle of attack. Very few of the data have been analyzed to date, and most of the published results which have been highlighted here are presented as particle fluxes rather than concentrations. A number of interesting, and in some

instances unexplained, observations have been provided. It seems likely that at least some of these differences can be attributed to atmospheric variability between missions or even during a mission. Further analysis and additional careful measurements should aim to provide a sound basis for comparison so that agreements are believable, and explanations can be found for real differences. Then, finally, we will be able to increase our understanding of the dynamic Shuttle environment.

PARTICULATES

In this section we summarize data[3,13,14] from the IECM for the flights of STS-2, -3, and -4. Also we include data from a different source,[15] namely video tapes of the field of view looking aft of the forward cargo bay on STS-3. Figure 8 shows components of the IECM. We will first briefly discuss IECM data from the Passive Sample Array, Cascade Impactor, and Camera/Photometer.

The Passive Sample Array is a series of witness plates which present time integrated exposures. Size-distributions of particulates deposited on the Passive Sample Array at various times are shown in Fig. 9. These are averaged over the three flights in question. Exchanging the sample trays and using control samples makes it possible to distinguish the amounts and distribution of particulates for (1) the preflight environment (OPF) at Kennedy Space Center, (2) the ferry flight that returns the Shuttle from the landing site, and (3) the orbital mission *per se*. Note that the OPF and ferry flight distribution are quite similar, and that the mission distribution displays three principal peaks near 5, 13, and 22 μm. The OPF and Ferry distributions are not representative of a natural dusty environment, but are more smoke-like in character.

The absolute degree of cleanliness can be estimated by comparison of the size distributions with MIL-STD-1246A for product cleanliness. This is shown in Fig. 10 for STS-4 where, to state the worst case, all the points are seen to be below the standard line whose intercept represents the obscuration equivalent to one particle of 750 μm size per square foot. (A 300 μm normalized distribution was the goal set by the Contamination Requirements Design Group). Below 100 μm particle size, the distributions are more consistent with the 300 μm clean air standard.

The Cascade Impactor data for periods during the ascent and descent of STS-2, -3, and -4 are shown in Table 4. This is a differential volumetric sampling of airborne particulates separated into three size ranges for the Shuttle altitude range 0-23 km, and is also compared here with the requirements for class 100K clean air which was the CRDG goal. (We realize that relating cascade impactor particulate measurements in the bay during liftoff to a class 100K clean air environment can be inexact. For example collection efficiency can be a function of particle size). The concentrations of the largest particles were well below those goals for all three missions. The intermediate and smallest particle concentrations are low for missions with dry prelaunch and takeoff weather, and seem to be greatly enhanced under wet conditions. The rationale for this apparent correlation is unclear.

TABLE 4

CASCADE IMPACTOR PARTICULATE MEASUREMENTS (Taken from Ref. 13)

Particle Size (μm)	Class 100K Air ($\mu g/m^3$)	Flight Results ($\mu g/m^3$)		
>5	<375 (assuming $\bar{d}$ = 25 μm, ρ = 2 g/cm^3)	STS-2	Ascent	30
			Descent	10[a]
		STS-3	Ascent	10
			Descent	10
		STS-4	Ascent	Non-functional
			Descent	20
1-5	<100 (assuming $\bar{d}$ = 5 μm, ρ = 2 g/cm^3)	STS-2	Ascent	500
			Descent	250
		STS-3	Ascent	10
			Descent	10
		STS-4	Ascent	300
			Descent	10
0.3-1	<10 (assuming $\bar{d}$ = 1 μm, ρ = 2 g/cm^3)	STS-2	Ascent	250
			Descent	115
		STS-3	Ascent	10
			Descent	10
		STS-4	Ascent	90
			Descent	Non-functional

[a] Descent values should be considered upper limits due to errors introduced by thermal effects.

The on-orbit environment was probed by a Camera/Photometer experiment. Data from the IECM provide time-resolved information on the particulates orbiting with the Shuttle in the payload bay. The Camera/Photometer is actually a stereo pair of devices taking 32° FOV films of contaminant particulates as small as 25 μm, as they are illuminated by the sun against a dark sky or earth background. The photometers also provide data on the background levels of brightness not only when the illuminated particles are being photographed, but also during orbital nighttime when only the star field is observed.

Figure 11 presents curves reflecting the time histories of particle concentrations. During the first hours of Shuttle flights, the frequency diminishes for seeing many particles per frame while the likelihood of seeing no particles per frame increases to virtually 100%. These data specifically do not include the time periods of water dumps which are the major source of photographed particulates on-orbit (count rates > 100 per frame). The decay of water dump particles is very rapid, however, and is characterized by an e-folding time constant of 5 minutes, so that return to pre-dump levels takes 15-25 minutes.

After about 15 hours MET, the background sky brightness due to molecular and particulate scattering is not measurable (below threshold) with the Camera/Photometer system in the IECM. Again we emphasize that this does not include the times of water dumps or RCS/VCS thruster firings. With the scattering so low that there is no discernible day/night (orbital) difference in the sky background, tenth magnitude stars are readily seen, and it is integrated starlight that then controls the exposure time of the Camera/Photometer films.

Thus, the particulate environment on these Shuttle flights seems to be quite manageable after about 15 hours MET, with the exception of $\lesssim$ 1/2 hour periods immediately following water dumps. In the clean periods, the observable

particulate abundances, according to the IECM, are approximately equivalent to one 25 μm particle event every two orbits (~ 3 hours), per 1° FOV. Recently photometric data from STS 4 have become available from D. Smith, et al.[16] Their preliminary analysis indicated that particulate concentrations remained higher during the mission and that particulates were larger than the IECM data indicates.

A different observation[15] on STS-3 has caused some concern about populations of large particles that may orbit with the Shuttle once they are created by an unexpected or accidental event. Such an event might be, for example, RCS plume impingement on the Shuttle body flap that was suggested by L. Leger during NASA's Shuttle Environment Workshop.[1] During the second day of the STS-3 flight, a television camera looking aft from the cargo bay recorded many frames showing large particles (1 mm - 7 mm diameter) suspended well forward of the tail assembly and having velocities in the range 1/2 - 4 cm/s. For one of the episodes studied, a typical number of particles larger than 5 mm, in a 4° half-angle about the long axis of the Shuttle, was about 60. There were many more smaller particles that could not be reliably resolved and counted. Possibly larger particles were also seen, but this is not completely certain owing to assumptions that had to be made in the data reduction.[15]

Though particulates have often been observed around spacecraft (Voyager, Viking, Mariner-Venus-Mercury, Skylab), the STS-3 episode is particularly striking in appearance. We do not have further such information at this time on this or other Shuttle flights. This phenomenon could prove troublesome if left unexplained and unfixed. Further analysis or additional observations to resolve this issue would be valuable for assessing the local environment and particle production mechanisms.

In summary, the level of scattered light from particles fell below the natural background levels and detectability limits after the first day on orbit. Changes in procedures in the OPF are scheduled and will hopefully improve the preflight environment. Nevertheless, apertured doors or purging, are recommended to protect very sensitive instruments.

Generally the particulate environment looks acceptable on the basis of the IECM data, while the other STS-3 and STS-4 data raise doubts about a totally optimistic conclusion. The particulate question is extremely important for infrared observations from the Shuttle, since very demanding IR applications have been proposed that could be compromised by fluctuating intensities of scattered terrestrial or solar IR radiation. Models have been developed which either describe these early measurements[2] or try to predict on orbit particulate release rates.[17] Further measurements will be required to validate these models.

THE OPTICAL ENVIRONMENT

Thruster Glow

The optical environment surrounding the STS was recognized as a potential problem area and was the subject of extensive modeling years before any launch.[8,18] These models mainly considered attenuation and self emission by the gaseous and particulate effluents arising from thrusters, dumps, and outgassing. Perhaps the most fascinating observations from the early Shuttle missions was the appearance of the continuous glow over Shuttle surfaces during passive operation conditions, and the spatial extent and brightness of the thruster firings. Both of these glow mechanisms raise important questions about the integrity of optical measurements performed from the STS Orbiter.

The observations of the SIA experiment as reported by Weinberg[19] indicate that brightness resulting from thruster firings and associated photochemical reactions can be up to 2.5 times as bright as the brightest part of the Milky Way. (Additionally, solar radiance reflected from orbiter/payload-induced particulates can be of comparable brightness.) The SIA telescope had an instantaneous field of view of 6° but could scan azimuthally from viewing just over the engine pods through zenith to 30° past zenith toward the cabin One-color scans consistently showed an enhanced radiance peaking just above the tail. Periodically, a large brightness feature was observed near zenith and could always be directly correlated with a thruster firing. The SIA experiment also observed radiance associated with a series of thruster firings while scanning the sky at 420 nm. They indicate a widely spread glow--the entire sky flashes brightly immediately following vernier thruster firings. Observations of the glow on STS-4 by Mende[20] indicate that the thruster glow near the tail

is strongest in the red end of the spectrum, stretching from 720 nm to the system cutoff at 800 nm. Near the tail, thermal emission from the hot exhaust products (such as CO(v), H_2O(v)) may dominate, while farther from the nozzle photochemical or energetic collisions with the ambient atmosphere may give rise to molecular electronic transitions in the blue (such as NO_2 A → X). Yet another glow in the violet has been observed after thruster firings. Temporal behavior suggests its relation to re-encroachment of the ambient atmosphere into the thruster exhaust plume. Obviously better measurements of the spectral and spatial characteristics of these thruster related glows are required to quantify these fascinating observations.

Surface Glow - Observations

Even more surprising, however, was the presence of a glow above the surfaces of the Shuttle during passive operational periods. This phenomenon was observed on STS-3 by Banks and co-workers.[21] A series of observations on later Shuttle missions have been performed by Mende[20,22,23] in an attempt to quantify its nature. A visible glow has also been observed by the Atmospheric Explorer (AE) C and E satellites,[24] and by the Dynamics Explorer (DE) B satellite.[25,26] The large satellite data base has permitted a fairly convincing assignment of OH emission as the source of that glow, the vibrationally excited OH being formed by the chemical reaction of energetic atmospheric O-atoms with H on the surface. It is not at all clear that the source of the glow above Shuttle surfaces is also OH. In fact the limited Shuttle data indicate that it probably is not OH(v) emission.

Both Shuttle and satellite glows are seen on surfaces undergoing energetic collisions with the ambient atmosphere, i.e., in the ram direction. Data from STS-4[22] clearly showed a dependence of intensity with respect to the angle

of attack. No glow was observed from surfaces in the wake or shadowed by Shuttle structures. Surfaces exposed to the velocity vector exhibit substantial intensity even at large angles of attack. Atmospheric Explorer data on the other hand exhibits a sharp $\cos^3\phi$ dependence of intensity on angle of attack[24]. Yee and Abreu[24] reported the altitude dependence of the AE glow to track with the atomic oxygen profile between 190 km and 280 km. Between 140-180 K the AE glow tracks with neither N_2 nor O concentration profiles, increasing more rapidly than either concentration. Shuttle observations of absolute intensity are difficult, and a definitive altitude scaling with the O or N_2 profile can not be determined.

The photographic data on Shuttle has permitted the spatial distribution of the glow to be quantified. Preliminary estimates[21] of an extent of 5-10 cm above the surface have been revised to 20 cm in a careful analysis by Yee and Dalgarno.[27] This distance represents the region over which excited species (atoms or molecules) are emitting. The extent of the glow has been interpreted to represent the product of the emitter velocity and radiative lifetime of the excited state. If radiators leave the surface at thermal velocities, then the corresponding radiative lifetimes are less than a millisecond. If their exit velocity is faster, the lifetime becomes shorter still, approaching 50 μs if the atmosphere/surface interaction is elastic and the reflected velocity is comparable to the incident velocity. The various chemical processes which could give rise to this emission are considered below. If a plasma process is responsible for the glow, its extent represents the perpendicular relaxation length of the plasma.[28] The likely emissions resulting from a plasma over the Shuttle surface has been considered.[29]

The spectral distribution of the glow has also been measured. Mende[20,22] has reported that the glow is a nearly continuous spectrum (for a

resolution of ~ 15 nm) and increases in intensity to the red out to a 800 nm detection limit. (The Shuttle glow seems to have a spectral distribution which does not vary appreciably with distance from the surface.[27] Witteborn[30] has observed the 1-3 μm infrared emission of the entire Shuttle from the earth's surface. He concludes that the glow intensity is 2-3 times brighter in that spectral region than in the 500-800 nm region.

Surface Glow-Possible Mechanisms

Atomic oxygen is by far the dominant atmospheric component at orbital altitude. It has thus been widely considered to be the reactive source of the Shuttle glow. Molecular nitrogen is present in significant concentrations also (see Table 1). The Shuttle orbital velocity is 8×10^5 cm/s. Thus as the Shuttle sweeps through the tenuous atmosphere, the atmospheric species energetically impact the surface. For oxygen atoms, the energy of the collision is 5 eV on average, but the atomic oxygen velocity vector ($\bar{c} = 10^5$ cm/s) will provide a distribution of collision energies (3.8-6.3 eV). These energetic O-atoms could react with Shuttle surfaces to produce new chemical species which could give rise to the glow. Nitrogen molecules will have a collisional energy of 9.3 ± 2 eV, comparable with their dissociation energy of 9.8 eV, and thus may dissociate upon impact, with the atoms remaining adsorbed to the surface. Let us now consider the interactions of atoms and surfaces.

The energy partitioning in the interaction of gases with adsorbed atoms has been studied for many years. Two different types of processes are possible. In the first, the Langmuir-Henshelwood (LH) process, both atoms are adsorbed on the surface after collision. They then migrate over the surface, react, and escape into the gas phase. The level of excitation of the escaped molecule depends both on reaction exothermicity and the nature of the surface adsorption.[31-33] When surface coverage by adsorbed atoms is great, an incident

gas-phase atom is likely to strike an adsorbed atom and form a molecule which escapes into the gas phase. This is called a Rideal process. Here the interaction time is short (10^{-12} s) and little energy partitioning with the surface can occur. Consequently, the newly formed molecule can possess a large fraction of the bonding energy. The gas phase molecular products are observed to have highly non-statistical, non-Boltzmann energy distributions.

Surface catalyzed emissions have been the subject of several laboratory studies. In particular, O-atom bombardment of surfaces is observed to give rise to $O_2(b \rightarrow X)$ and $(A \rightarrow X)$ bands.[34] It is suspected that a gas-phase atom reacted with an adsorbed atom (bound to the surface by only 0.5 eV) to give rise to this emission. However, even LH processes have been observed to give rise to electronically excited molecules, such as N_2, over a variety of surfaces including glass[35] and metals.[36] The creation of these recombined molecules into electronically excited states suggests a very short surface residence time for the newly formed species, and indicates that recombination and desorption are part of a single physical process.[37] In those laboratory studies the N-atoms recombine to form the $A^3\Sigma_u^+$ state at high vibrational levels. The molecules then collisionally transfer into the $B(^3\Pi_u)$ state. Strong $B \rightarrow A$ (First Positive) emission is then observed above the surfaces. A detailed investigation of the energy accommodated by N-atoms has been studied by Halpern and Rosner.[38] They found that both Rideal and LH processes occur over a single surface under different physical conditions. The level of product excitation will thus depend on the nature of the surface and of surface coverage and temperature.

Recently laboratory experiments have begun to examine the reaction of energetic oxygen atoms and ions with solid materials. Experiments are ongoing

to measure the interaction of ~ 1 eV O-atoms with carbon by G. Arnold and D. R. Peplinski.[39] Ferguson[40] has observed the degradation of Kapton by energetic (0-1 keV) oxygen ions. Kapton is a long chain polyimide composed of substituted benzene rings linked by O and N-atoms. In Ferguson's experiments, samples of Kapton bombarded by O^+ ions changed in appearance and microscopically resembled orbitally exposed Kapton from STS-2. Hydrogen was not detectable in these experiments, and the major detectable change in composition was a severe loss of carbon. The weakest bonds are the C-N (3.2 eV) and C-O (3.7 eV) bonds which may have suffered preferential attack by the 5 eV O^+ ions resulting in chain breakage and materials properties degradation. A variety of species, including CO and OH, can be products of this bombardment. The interactions of the ambient atmospheric O-atoms with other STS materials has been studied in some detail by L. Leger.[41] Mass loss was found to be very variable from material to material. For the worst case (Mylars, graphites) 10% of the O-atoms collisions led to mass loss.

With these observations as background, we will now consider the possible emitting species resulting from chemical reactions of energetic atmospheric components on Shuttle surfaces. Specifically, vibrationally excited OH, CO and electronically excited N_2, O_2, and NO. We will also briefly consider the plasma process. Slanger[42] has postulated hydroxyl radicals above Shuttle surfaces as a glow source. Vibrationally excited OH would be created in the reaction of 5 eV O-atoms with atmospheric H or Shuttle produced H_2O adsorbed on surfaces or by direct attack on hydrogen-containing surface materials. Vibrational states emitting in the red ($v' = 6-8$, $\Delta v = 5$) have radiative lifetimes of between 4 and 10 ms.[26,43] Although spectral analyses support OH as a good candidate for the glow source above AE and DE satellites, a careful radiative

lifetime analysis of the Shuttle glow by Yee and Dalgarno[27] yielded a lifetime of 0.67 ms for thermal velocity emitters, suggesting that OH is not the Shuttle glow source unless the Shuttle environment provides an unexpectedly large degree of collisional de-excitation. Specifically, even for a gas kinetic rate coefficient, densities in excess of $10^{12}/cm^3$ would be required to quench OH in a millisecond. The OH Meinel bands (vibrational overtones) do have the proper coarse spectral distribution to match both satellite and Shuttle glow observations. On the other hand they exhibit considerable spectral structure which should have been at least partially resolved in Mende's[23] spectral observations. Thus OH seems to be precluded as the source of the Shuttle glow due to radiative lifetime and spectral structures.

Carbon monoxide is another molecular species which could give rise to the glow. Surface materials containing carbon have been shown by Leger[41] to undergo appreciable mass loss on-orbit. Vibrationally excited CO has been observed in the reaction of O-atoms with carbon adsorbed on platinum.[33] Thus vibrationally excited CO could arise from the interaction of energetic O-atoms with carbon-containing Shuttle surfaces. Vibrational transitions with $\Delta v = 6-8$ would fall in the 600-850 nm region, and should rise in intensity to the red as the transition probability increases with decreasing Δv. These overtones are not likely to be as strong as the corresponding transitions in OH. The radiative lifetimes for vibrational levels 5-11 are 4-7 ms, comparable to those for OH, and thus perhaps too long to explain the Shuttle observations. Unlike OH, however, the CO spectral distribution would be more continuous, because the bandwidths are comparable to their separations. Thus, CO emission could be a constituent of Shuttle glow over surfaces which undergo appreciable mass loss. The glow, however, is observed even over surfaces not containing carbon (such

as aluminum) and which do not suffer significant mass loss (painted surfaces), as shown by Mende.[23]

We have recently[44] suggested another possible source for the glow: atomic recombination into electronically excited molecular states. Atmospheric N_2 can dissociate upon its energetic collision with Shuttle surfaces. The N-atoms then may recombine to form highly vibrationally excited $N_2(A)$ molecules. The surface will incompletely accommodate the 9.8 eV reaction exothermicity and the molecule will leave highly excited. The degree of energy accommodation, and thus residual excitation, will depend on the nature of the surface. Some fraction of the exciting molecules will leave in the $A^3\Sigma_u^+$ state. Recombination into the ground state and other electronic states is possible (see below). The gas phase emissions observed by Mannella et al.[36] were the result of collisional processes quenching high lying A vibrational states to form vibrationally excited B state molecules (see energy levels in Fig. 12). The molecules then rapidly radiate (First Positive transitions) back to lower levels of the A state manifold. (These radiative lifetimes of the vibrational levels of the $B(^3\Pi_u)$ state are in the 6-8 μs range).

Collisional processes probably will not be significant above Shuttle surfaces. At Shuttle altitudes, the mean ambient free path between collisions is kilometers. The effect of surface reflections and thermalized velocities may decrease this pathlength by an order of magnitude.[45] In the absence of collisions, highly excited A state molecules can still radiatively decay to lower levels of the B state as indicated in Fig. 12. These reverse First Positive (A → B) transitions have not been observed, but have been estimated to occur and to be important in auroras.[46,47,48] These transitions are less strongly allowed than B-A and radiative lifetimes are estimated to be a few

orders of magnitude slower, in the 10^{-2} - 10^{-4} s range. Thus the postulated mechanism is that the N-atoms recombine on the Shuttle surfaces with varying degrees of energy accommodation. The newly formed N_2 molecule then leaves the surface in the A state with a considerable portion of the reaction exothermicity. These highly vibrationally excited A state molecules slowly radiate (in the infrared between 2 and 6 μm) into vibrationally excited B states. These, in turn, rapidly radiatively decay giving rise to First Positive band radiation. Nearly all of the 9.8 eV reaction exothermicity may be available in the N_2 product. Some small (< 1 eV) energy will be lost to overcome bonding to surface.

A spectrum of N_2 B → A emission with 5 nm resolution is presented in Fig. 13. This spectrum was obtained by electron irradiating an N_2/O_2 mixture of total density 1 x10^{13} molecules/cm^3 (0.25 mtorr).[49] The spectral intensity in each band reflects both the transition probability and the excited state populations. Thus, this particular spectrum is not meant to accurately represent the N_2 recombination glow above the Shuttle surfaces, but merely to demonstrate the possibility that this process may play a role.

In addition to N_2 B → A features, various ionic bands are present in the laboratory spectrum due to energetic electron impact. These molecular states would not be created in molecule/Shuttle collisions because of energetic constraints. If plasma processes play a role in the Shuttle glow, these transitions may be expected.[29]

The intensity onset in the red and the rise to longer wavelengths agree with Shuttle glow spectral observations.[23] The observed structure in the laboratory spectrum will decrease as resolution becomes poorer, and as rotational and vibrational temperatures increase, as would be the case for the Shuttle.

M. Torr and D. Torr[50] recently presented some preliminary findings of emissions which were observed by their Imaging Spectrometric Observatory during the Spacelab mission. The bright glow they observed was above surfaces of their experiment and not the Shuttle surfaces per se, but they tentatively assigned a number of N_2 First Positive transitions in their spectrum. Indeed N_2 First Positive Bands are the dominant contributor to their spectrum in the red/near infrared region. This fascinating observation may indicate that the postulated collisional excitation mechanism plays a role over Shuttle surfaces.

Because of the many difficulties associated with absolute intensity measurements, this aspect of the Shuttle glow is perhaps the hardest to quantify. Mende,[22] has stated that the glow on the STS-5 rear engine pod was several hundred kilorayleighs within the bandpass of his instrument.

Based on this observation, the efficiency required to produce N_2^* from collisions of ambient N_2 with the Shuttle surface has been estimated.[44] The observed radiances correspond to fluxes off the surfaces on the order of 10^{10} emitters/cm^2-s. It was shown[44] that only a small fraction of the energetically allowed dissociative collisions must result in vibrationally excited metastable state formation to give rise to the above emitter flux.

Other possible emissions could arise from recombination of O and/or N atoms on adsorbed Shuttle surfaces. It is assumed that the adsorbed atoms are not electronically excited due to rapid quenching by the surface. In N-N recombination, the A, the ground X $^1\Sigma_g^+$ and a $^5\Sigma_g^+$ state correlate to N(^{4}S) atoms. Although recombination has been the subject of much study [see Ref. 51 and references therein], it is not yet understood. N_2(A) formation seems to be the preferred excited state channel. In the absence of collisions the $^5\Sigma_g^+$

state can not populate any other molecular states (no allowed transitions), and under collisionless conditions surrounding the Shuttle only emissions arising from the A state should be expected.

If energy partitioning between the accessible electronic states occurs as the newly formed molecule leaves the surface, numerous other allowed transitions would result from population of the W $^3\Delta_u$, a' $^1\Sigma_u$, and a $^1\Pi_g$ states. These states are populated in laboratory studies where collisional redistribution occurs.[51] The most notable emissions from these states are: the Lyman-Birge-Hopfield bands (a → X) which peak at 140 nm; the Wu-Benesch (W → B) bands in the infrared; and the McFarlane infrared bands (a → a').[52] Based on their lifetimes all these transitions would have the same spatial extent. The larger the role of the surface in the reaction, the less likely the molecule is to leave the surface electronically excited. Thus the collisional mechanism forming N_2 (A, high v) would be the favored source for N_2 emissions in the Shuttle glow. The presence of other electronic states as detected by VUV-IR emissions observed in future measurements will provide insight into the nature of the different surface-molecule interactions.

Oxygen atoms from the ambient flux will also be adsorbed on Shuttle surfaces. Unlike N_2, all six O_2 electronic states lying below the dissociation energy (5.2 eV) correlate with ground state atoms, and thus could be directly populated by O atom recombination. Unfortunately, no allowed radiative transitions connect these states. The A → X is the most prompt (τ_A = 0.2 s) and has been observed weakly in the upper atmosphere and in the laboratory.[34] The radiative lifetimes of the other states are thought to be 10-100 s so that they are not likely sources of the 20 cm glow layer. The c, A', A → X bands lie in the UV-blue spectral region. The b → X transition at 762 nm was observed by

Mende[20] in the earth's airglow layer. It is difficult to assess if it is a component of the Shuttle glow layer. The b state radiative lifetime is ~ 13 s which would give rise to a much more extended glow. Thus O_2* emission does not seem a likely source of the observed Shuttle glow due to spectral distribution and radiative lifetimes, and susceptibility to collisional dissociation by energetic atmospheric species. Nonetheless, if these states are created, they could pose a serious optical problem because their lower intensity glow layer could extend many tens of meters, thus potentially interfering with measurements from any Shuttle location.

Heterogeneous recombination of N and O atoms can form NO in the excited a $^4\Pi_i$ state as well as the ground state, although several other electronic states lie below the dissociation energy.[53] The a state only has allowed transitions in the infrared to the b $^4\Sigma^-$. If electronic energy partitioning occurs near the surface then the A $^2\Sigma^+$, B $^2\Pi_r$ and the C $^2\Pi_r$ states which rapidly radiate in the UV to the ground state,[53] could also be formed. The C → A band at 1.22 μm has also been observed in the laboratory. Thus neither the spectral distributions nor lifetimes of NO* fit the observed glow. Moreover, if the surface does not play a role in partitioning the energy, we would expect to see only emission in the infrared. It must be stressed that the glow may depend on the nature of the surface and that NO emission may appear brightly in a thin layer over certain surfaces.

Plasma processes have also been suggested as a source for the Shuttle glow.[28] The physical mechanism involves the atmospheric ions being reflected off the Shuttle surfaces, creating an unstable ion distribution which then interacts collectively to heat the electrons. The more energetic electrons then can collisionally ionize more of the background gas resulting in more ions to

propagate the unstable cycle. The net effect is to enhance the number of electrons in the energetic tail of the distribution. This mechanism is appealing because it fits many of the observations. It predicts the perpendicular relaxation length of the electrons (the extent of the excitation) to be 10-20 cm. It also agrees with observations of Murphy and Shawhan[10,54] in which enhanced electron densities were observed in the ram direction, and with the number of energetic electrons enhanced.[12] Papadopoulos[28] predicts that the electron concentration, however, should depend linearly on the ambient plasma and on the total pressure. The enhanced glow intensities associated with thruster firings are a direct consequence of total pressure enhancement, according to this mechanism. The predicted altitude scaling of the surface glow is more complex. Although total pressure is decreased with altitude, the ion density could be constant or even increasing over the 240-300 km Shuttle altitude range, depending on atmospheric conditions. Altitude scaling of the plasma mechanism is not inconsistent with the sparse Shuttle data base. The spectral character of the plasma glow should reflect the excited species, dominantly O and N_2. In a thorough review, Kofsky[29] found no spectral evidence to support this mechanism. Laboratory studies of beam plasma discharges[55] in N_2 and air reveal structured First Positive bands as described above, but also exhibit the presence of higher electronic state emissions (C → B) and ionic bands of N_2 (and O_2) such as shown in Fig. 13, and which extend considerably to the blue. Indeed, Papadopoulos suggest monitoring 391.4 nm (N_2 $^+B \rightarrow X$) and 337.1 nm (N_2 C → B) emissions as a sensitive test for this theory.

In summary, it is likely that several mechanisms involving O or N_2 are simultaneously occurring over various Shuttle surfaces and that any one may dominate under certain conditions. The key to our understanding the glow phe-

nomenon lies in an extended data base which includes improved spatial, spectral and surface specific observations. It is clear that a number of processes, including those discussed above as well as chemical/erosive mechanisms, can provide for unique glows of differing characteristics under the wide range of on-orbit conditions. Atomic recombination as a source of the glow depends on the interaction of the Shuttle with the ambient atmosphere and unlike contamination-induced glow cannot be overcome by simple preventative measures. Consequently, the glow could have a significant impact over a wide range of altitudes on the instruments which hope to use Shuttle as a remote optical observatory.

CONCLUSIONS

In this paper we have singled out for special attention the Shuttle-environmental issues of gases, particulate matter and vehicle-induced glow phenomena. We now have an elementary understanding of the gaseous atmosphere which surrounds the Shuttle. It appears to be acceptable for most measurement functions envisioned for the Shuttle. Nonetheless, much remains to be understood. For example even with several observations taken, the total rate of water vapor desorption and the cause(s) of its variability remain to be defined. The existence of a Shuttle-induced enhancement of the plasma density is still unclear. The vehicle glow is the most puzzling and intriguing phenomenon observed, and several possibilities have been put forth as an explanation. A full evaluation of the glow as an interference to optical measurements is not available and is very important. Much more comprehensive spectroscopy and spatial photometry will be needed just for the empirical documentation of the glow and definition of its potential for interference with other work. The particulate environment looks promising, as regards cleanliness for most optical applications, yet there are disturbing hints from the video data on STS-3 and camera data of STS-4 that the particulates may pose a problem for some experiments or after certain on-orbit procedures.

It appears that the large variabilities in the natural and Shuttle induced environment in these early missions have created additional complications in correlating the measurements of different observers. Thus, many questions remain. Nevertheless, it is clear that the Shuttle environment is a hospitable one for many applications, and it still remains to be clarified how far one can go with the most environmentally demanding Shuttle payloads.

Note added in proof:

Discussions of several aspects of the Shuttle Environment during the early missions are now appearing in the literature. These include:

Pickett, J.S., Murphy, G.B., Kurth, W.S., Goertz, C.K., and Shawhan, S.D., "Effects of Chemical Releases by the STS 3 Orbiter on the Ionosphere," Journal of Geophysical Research, Vol. 90, Apr. 1985, pp. 3487-3497

Siskind, D.E., Raitt, W.J., Banks, P.M., and Williamson, P.R., "Interactions Between the Orbiting Shuttle and the Ionsosphere," Planetary and Space Science, Vol. 32, July 1984, pp. 881-896

Ehlers, H.K.F., Jacobs, S., Leger, L.J., and Miller, E., "Space Shuttle Contamination Measurements from Flights STS-1 through STS-4," Journal of Spacecraft and Rockets, Vol., 21, May-June 1984, pp. 301-308

Torr, M.R., and Torr, D.G., "A Preliminary Spectroscopic Assessment of the Spacelab 1/Shuttle Optical Environment," Journal of Geophysical Research, Vol. 90, Feb. 1985, pp. 1683-1690.

Recent observations of the Glow above Shuttle tile surfaces indicate a broad spectral emission. Excited nitrogen dioxide (NO_2) catalytically formed upon Ram surfaces has been suggested as a potential source of the gas phase emission by Swenson, G.R., Mende, S.B., and Clifton, K.S., "Ram Vehicle Glow Spectrum; Implication of NO_2 Recombination Continuum," Geophysical Research Letters, Vol. 12, Feb. 1985, pp. 97-100.

ACKNOWLEDGEMENTS

The authors express their thanks to the following individuals for many helpful discussions: G. R. Carignan, D. C. Ferguson, J. M. Grebowsky, L. Leger, E. R. Miller, G. B. Murphy, S. B. Mende, and J. L. Weinberg, and acknowledge many useful discussions with the late R. S. Narcisi. This work was funded partly by Physical Sciences Inc. internal research funds and partly by Air Force Geophysics Laboratory.

REFERENCES

[1]Proceedings of The Shuttle Environment Workshop, Lehmann, J. (Organizer), Tanner, S. G. and Wilkerson, T. (eds.), workshop sponsored by the NASA Office of Space Sciences and Applications, (October 1982).

[2]Scialdone, J. J., "Shuttle Measured Contaminant Environment and Modeling for Payloads," AIAA Paper 83-2583CP, Shuttle Environment and Operations Meeting, October 31-November 2, 1983, Washington, D.C.

[3]Carignan, G. and Miller, E. R. in "STS-2, -3, -4 Induced Environment Contamination Monitor (IECM) Summary Report", Miller, E. R., (ed.), NASA EM-82524 (Feb. 1983); pp. 87-101.

[4]Grebowsky, J. M., Pharo, M. W., III, Taylor, H. A., Jr., Eberstein, J. J. "Measured Thermal Ion Environmental of STS-3", AIAA 83-2597 Proceedings of the AIAA Shuttle Environment and Operations Meeting, October 31 - November 2, 1983, Washington, D.C., pp. 47-51.

[5]Narcisi, R. Trzcinski, E. Federico, G. Wlodyka, L. and Delorey, D., "The Gaseous and Plasma Environment Around Space Shuttle," AIAA 83-2659 Proceedings of the AIAA Shuttle Environment and Operations Meeting, op cit., pp. 183-190.

[6]Shawhan, S. D., Murphy, G. B. and Pickett, J. S., "Plasma Diagnostics Package Assessment of the Orbiter Plasma Environment," Journal of Spacecraft and Rockets Vol. 21 #4, July-August 1984, pp. 387-391.

[7]U. S. Standard Atmosphere 1976 (NOAA/NASA/USAF), U.S. Government Printing Office, Washington, D.C. October 1976.

[8]Bareiss, L. E., et al. "User's Manual Shuttle/Payload Contamination Evaluation (SPACE) Program," Martin Marietta Aerospace, Denver Division, MCR-77-104, April 1977 and Version II MCR-81-509, February 1981.

References (Continued)

[9]Carignan, G. R., private communication, (1983).

[10]Murphy, G. B., Shawhan, S. D., Pickett, J., and Leger, L., "Perturbations of the Plasma Environment Induced by the Orbiters Maneuvering Thrusters," AIAA-83-2599-CP Proceedings of the Shuttle Environment and Operations Meeting, op. cit., pp. 59-65.

[11]Murphy, G.B., private communication 1984.

[12]McMahon, W. J., and Salter, R. H., Mills, R. S., and Delory, D., "Measured Electron Contribution to Shuttle Plasma Environment," AIAA-83-2598-CP Proceedings of the Shuttle Environment and Operations Meeting, op. cit., pp. 52-58.

[13]Miller, E. R., "Update of IECM Results," AIAA 83-2582-CP presented at Shuttle Environment and Operations Meeting, op cit., and entire report of Ref. 3.

[14]Linton, R. C. and Wilkes, D. R., in "STS -2,-3,-4 Induced Environment Contamination Monitor (IECM) Summary Report," Miller, E. R. (ed.), NASA EM-82524 (Feb. 1983); pp. 21-41.

[15]Barengolz, J., Kuykendall, F., and Maag, C., "The Particulate Environment of STS-3 as Observed by the Cargo Bay TV System," JPL Final Report (October 1982). See also Maag, C., Barengolz, J., and Kuykendall, F., "STS-3 Snowflake Study," Proceedings of the Shuttle Environment Workshop, op cit., pp. A289-294.

[16]Smith D, Ahmadjian, M., McInerney, R.E., Trowbridge, C.A., Burt, D.A., Jenson, L.L. and Pound, E.F., "Optical/Particulate Contamination During On-Orbit Space Shuttle Operations," AIAA-83-2626CP, presented at the Shuttle Environment and Operations Meeting, op cit., (1983).

[17]Barengolz, J., "Particulate Release Rates from Shuttle Orbiter Surfaces due to Meteroid Impact," J. Spacecraft and Rockets Vol. 17 #1, Jan. 1980, pp. 58-62.

References (Continued)

[18]Simpson, J. P., and Witteborn, E. C., "Effect of the Shuttle Contaminant Environment on a Sensitive Infrared Telescope," Applied Optics Vol. 16, Aug. 1977, pp. 2051-2065.

[19]Weinberg, J. L., "The Shuttle Optical Environment: Local and Astronomical," paper no. AIAA 83-2610-CP, presented at Shuttle Environment and Operations Meeting, op cit.

[20]Mende, S. B., Garriott, O. K., and Banks, P. M., "Observations of Optical Emissions on STS-4," Geophysics Research Letters, Vol. 10, Feb. 1983, pp. 122-125.

[21]Banks, P. M., Williamson, P. R., and Raitt, W. J., "Space Shuttle Glow Observations," Geophysics Research Letters, Vol. 10, Feb. 1983, pp. 118-121.

[22]Mende, S. B., "Vehicle Glow," AIAA-83-2607-CP, Proceedings of the Shuttle Environment and Operations Meeting, op. cit, pp. 79-86.

[23]Mende, S. B., "Experimental Measurement of Shuttle Glow," AIAA-84-0550 presented at AIAA 22nd Aerospace Sciences Meeting, Reno, January 1984.

[24]Yee, J. H., and Abreu, V. J., "Visible Glow Induced by Spacecraft - Environment Interaction," Geophysics Research Letters, Vol. 10, Feb. 1983, pp. 126-129. Also, "Optical Contamination on the Atmospheric Explorer-E Satellite," Proceedings of the Spacecraft Contamination Environment Meeting, SPIE, Vol. 338, May 1982, pp. 120-128.

[25]Abreu, V. J., Skinner, W. R., Hays, P. B., and Yee, J. H., "Optical Effects of Spacecraft-Environment Interaction: Spectrometric Observations by the DE-B Satellite," AIAA-83-2657-CP Proceedings of the Shuttle Environment and Operations Meeting, op. cit, pp. 178-182.

References (Continued)

[26]Langhoff, S. R., Jaffe, R. L., Yee, J. H., and Dalgarno, A., "The Surface Glow of the Atmospheric Explorer C and E Satellites," Geophysics Research Letters, Vol. 10, Sept. 1983, pp. 896-899.

[27]Yee, J. H., and Dalgarno, A., "Radiative Lifetime Analysis of the Spacecraft Optical Glow," AIAA-83-2660-CP Proceedings of the Shuttle Environment and Operations Meeting, op. cit., pp. 191-197.

[28]Papadopoulos, K., "On the Shuttle Glow (the Plasma Alternative)" Radio Science, Vol. 19, Mar-Apr 1984, pp. 571-577.

[29]Kofsky, I. L., and Barrett, J. L., "Optical Emissions Resulting from Plasma Interactions Near Windward Directed Spacecraft Surfaces," AIAA-83-2661-CP Proceedings of the Shuttle Environment and Operations Meeting, op. cit., pp. 198-203.

[30]Witteborn, F., "Ground based IR photometry of STS 9," presented at the Physics of Spacecraft and Glow Workshop, Huntsville, Alabama, Jan 1984.

[31]Talley, L. D., Sanders, W. A., Bogan, D. J., and Lin, M. C., "Internal Energy of Hydroxoyl Radicals Desorbing from Polycrystalline Pt Surfaces," Chemical Physics Letters, Vol. 78, March 1981, pp. 500-503.

[32]Wong, C., Yang, R. T., and Halpern, B. L., "The Mode of Attack of Oxygen Atoms on the Basal Plane of Graphite," Journal of Chemical Physics, Vol. 78, 15 March 1983, pp. 3325-3328.

[33]Kori, M., and Halpern, B. L., "Vibrational Energy Distribution of CO in the Oxidation of C on Pt," Chemical Physics Letters, Vol. 98, 10 June 1983, pp. 32-36.

[34]Mannella, G., and Harteck, P., "Surface-Catalyzed Excitations in the Oxygen System," Journal of Chemical Physics, Vol. 34, June 1961, pp. 2177-2180.

[35]Evenson, K.M., and Burch, D.S., "Atomic-Nitrogen Recombination, in Journal of Chemical Physics, Vol. 45, Oct. 1966, pp. 2450-2460.

[36]Mannella, G. G., Reeves, R. R., and Harteck, P., "Surface Catalyzed Excitation with O and N atoms," Journal of Chemical Physics, Vol. 33, Aug. 1960, pp. 636-637.

[37]Thorman, R. P., Anderson, D., and Bernasek, S. L., "Internal Energy of Heterogeneous Reaction Products: Nitrogen Atom Recombination on Iron," Physical Review Letters, Vol. 44, 17 March 1980, pp. 743-746.

[38]Halpern, B., and Rosner, D. E., "Incomplete Energy Accommodation in Surface-Catalyzed Reactions," in Heterogeneous Atmospheric Chemistry, Geophysical Monograph Series, Americal Geophysical Union, Vol. 26, (1982), pp. 167-172.

[39]Arnold, G. S., and Peplinski, D. R., "Reactions of High Velocity Atomic Oxygen with Carbon," AIAA-84-0549 presented at AIAA 22nd Aerospace Sciences Meeting, op. cit., (1984).

[40]Ferguson, D. C., "Laboratory Degradation of Kapton in a Low Energy Oxygen Ion Beam," AIAA-83-2658-CP presented at Shuttle Environment and Opera-tions Meeting, op. cit.

[41]L.J. Leger, "Atomic Oxygen Interactions with Materials," AIAA-84-0548 presented at AIAA 22nd Aerospace Sciences Meeting, op cit., January 1984.

[42]Slanger, T. G., "Conjectures on the Origin of the Surface Glow of Space Vehicles," Geophysics Research Letter, Vol. 10, Feb. 1983, pp. 130-133.

[43]Mies, F. H., "Calculated Vibrational Transition Probabilities of OH ($X\ ^2\pi$)," Journal of Molecular Spectroscopy, Vol. 53, 1974, pp. 150-188.

[44]Green, B.D., "Atomic Recombination into Excited Molecular States - A Possible Mechanism for Shuttle Glow," Geophysics Research Letters, Vol. 11, June 1984, pp. 576-579.

[45]Scialdone, J. J., "Self-Contamination and Environment of an Orbiting Spacecraft," NASA TN D-6645 (May 1972).

[46]Gilmore, F. R., Comment on paper, "Semi-Empirical Electron Impact Cross Sections for Atmospheric Gases," Canadian Journal of Chemistry, Vol. 47, 1969, p. 1779.

[47]Mulliken, R. S., "The Energy Levels of the Nitrogen Molecule," in The Threshold of Space, Zelikoff, M. (ed.), Pergamon Press, New York, 1958, pp. 169-179.

[48]Cartwright, D. C., "Vibrational Populations of the Excited States of N_2 under Auroral Conditions," Journal of Geophysical Research, Vol. 83, Feb. 1, 1978, pp. 517-531.

[49]Green, B.D., Piper, L.G., Caldeonia, G.E., Murphy, H.C., Krech, R.H., and Pugh, E.R., "LABCEDE Fluorescence Studies," Physical Sciences Inc., Technical Report TR-356, (Feb. 1983). Available from the author upon request.

[50]Torr, M.R., and Torr, D., "Preliminary Results of the Imaging Spectrometric Observatory on Spacelab 1," AIAA-84-0044 presented at AIAA 22nd Aerospace Sciences Meeting, Reno (1984).

[51]Golde, M.F., and Thrush, B.A., "Afterglows," Reports on Progress in Physics, Vol. 36, Oct. 1973, pp. 1285-1364.

[52]Huber, K.P., and Herzberg, G., Molecular Spectra and Molecular Structure, Vol. IV, Van Nostrand, New York, 1979.

[53]Loftus, A., and Krupenie, P.H., "The Spectrum of Molecular Nitrogen,"

Journal of Physical and Chemical Reference Data, Vol. 6, No. 1, 1977, pp. 113-307.

[54]Murphy, G. B., Kurth, W. S., Pickett, J. S., Shawhan, S. D., and Papadopoulos, K., "Broadband Orbiter Generated Electrostatic Noise," presented at Fall AGU Meeting 1983, op. cit., EOS, Transactions American Geophysical Union, Vol. 64, Nov. 1983, p. 805.

[55]Piper, L. G., Green, B. D., Pugh, E. R., and Blumberg, W. A. M., "Laboratory Studies of Beam Plasma Discharges," presented at Fall AGU Meeting (1983), op. cit., EOS, Transactions of American Geophysical Union, Vol. 64, Nov. 1983, p. 808.

FIGURE CAPTIONS

Figure 1 Envelope of H_2O count rate over the duration of the flight of STS-4. (Ref. 3.)

Figure 2 Variation in measured helium and argon as instrument angle of attack varies from 170 deg to 10 deg. (Ref. 3.)

Figure 3a STS-4 geometry of some contamination survey positions.

Figure 3b STS-4 H_2O counts during contamination survey. (Ref. 3.)

Figure 4a Orbit 4.6 measurements of N_2, H_2O and the pressure monitor exhibiting effects of the Vernier and OMS burns. (Ref. 5.)

Figure 4b Orbit 4.6 measurements of hydrogen showing clear increases due to engine firings. (Ref. 5.)

Figure 5 The average H_2O currents and sensor temperature measurements throughout flight. (Ref. 5.)

Figure 6 Orbit 5.4 daytime measurements of O^+,N^+ and H_2O^+, and the density monitor. (Ref. 5.)

Figure 7a The collected ion currents in the bay for the ion species with atomic masses of 16 and 18 for orbit 34. (Ref. 4.)

Figure 7b The heavy mass ions measured on orbit 34. The ions with masses 18 (H_2O^+) and 44 (CO_2^+) are STS-3 borne contaminants. (Ref. 4.)

Figure 8 Induced environment contamination monitor OFT/DFI and Spacelab VFI unit. (Ref. 18.) TQCM and CQCM are temperature-controlled and cryogenic quartz crystal microbalances respectively.

Figure 9 Passive sample array particle distributions. (Ref. 13.)

Figure 10 Passive sample array: particle size distributions for STS-4, combined mission operations. (Ref. 14.)

Figure 11 A summary of the contamination observed during the first 48 hr combined from the STS-2, -3, and -4 missions. (Ref. 13.)

Figure 12 Potential energy diagram for X, A, and B electronic states involved in nitrogen recombination glow mechanism.

Figure 13 The emission from electron-irradiated air at 1/4 m torr pressure. (Ref. 47.)

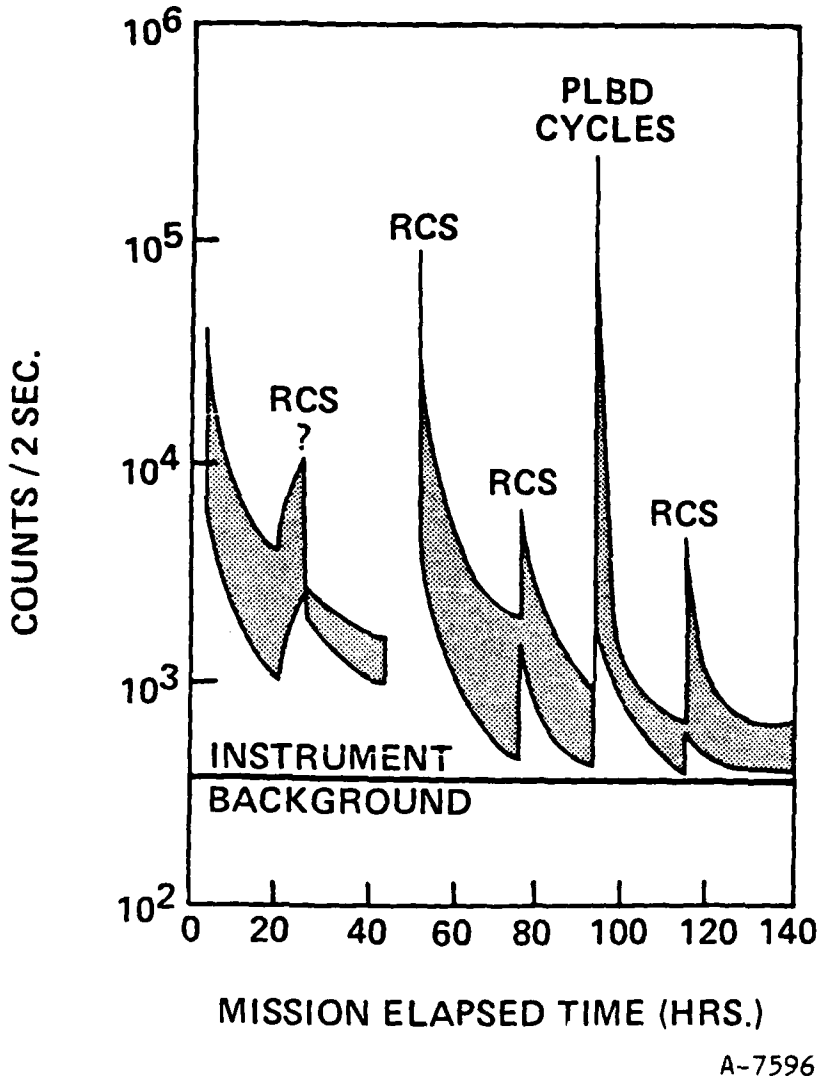
10^6
10^5
10^4
10^3
10^2
COUNTS / 2 SEC.
PLBD
CYCLES
RCS
RCS
?
RCS
RCS
INSTRUMENT
BACKGROUND
0
20
40
60
80
100
120
140
MISSION ELAPSED TIME (HRS.)
A-7596

FIGURE 1

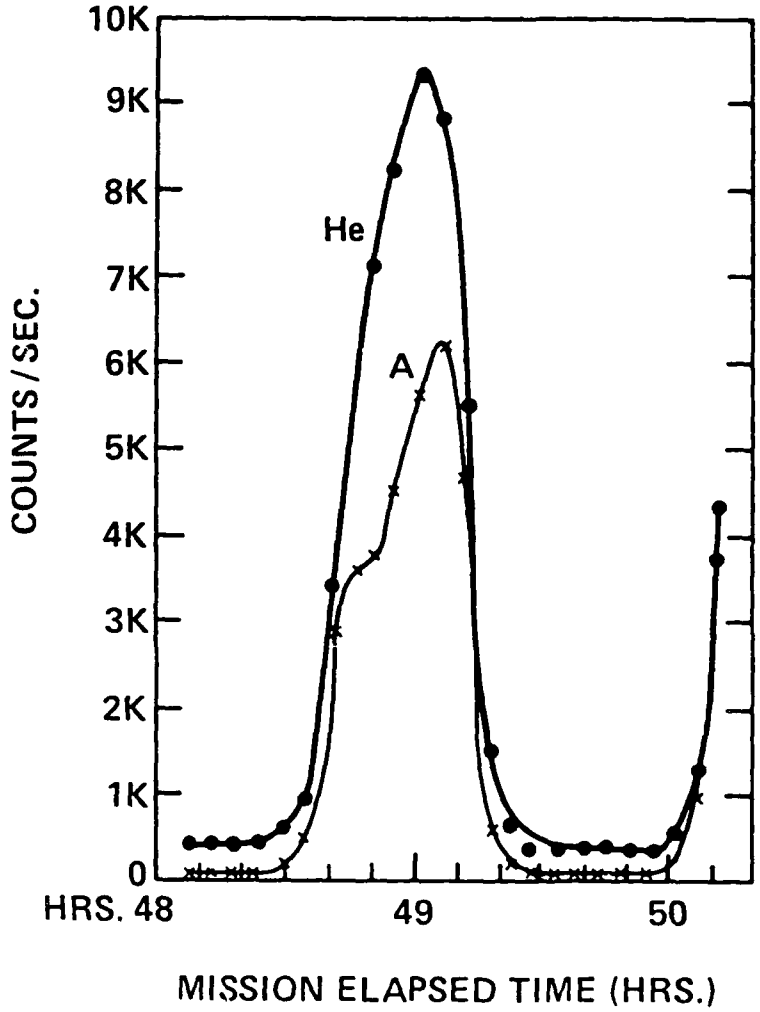
10K
9K
8K
7K
6K
5K
4K
3K
2K
1K
0
COUNTS/SEC.
He
A
HRS. 48
49
50
MISSION ELAPSED TIME (HRS.)
A-7597

FIGURE 2

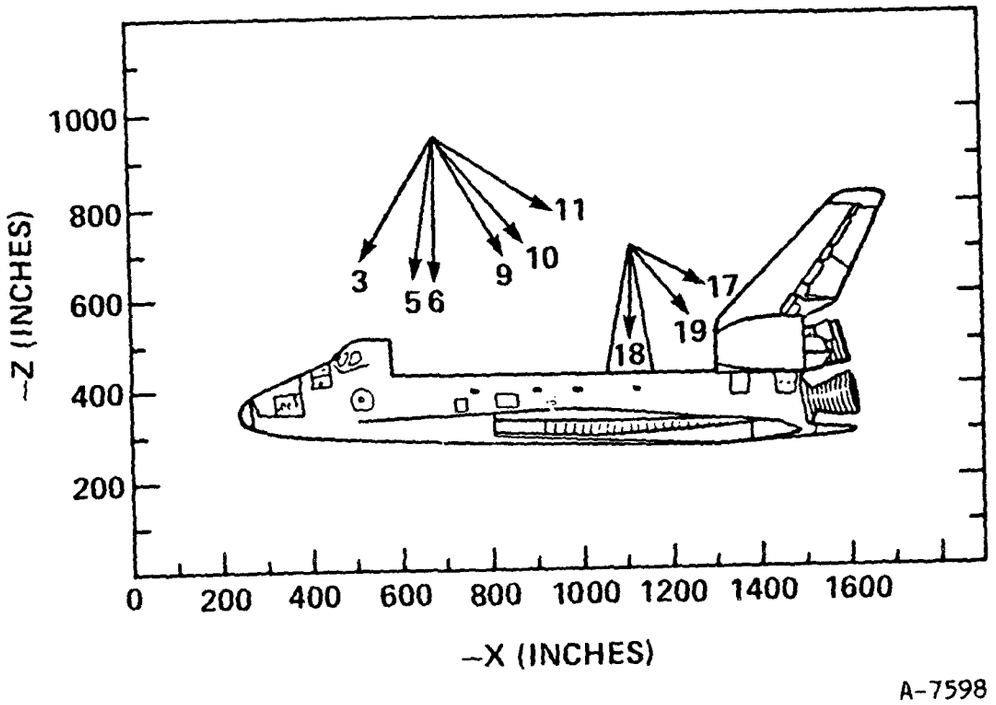
1000
800
600
400
200
-Z (INCHES)
0
200
400
600
800
1000
1200
1400
1600
-X (INCHES)
3
5 6
9
10
11
17
18
19
A-7598

FIGURE 3a

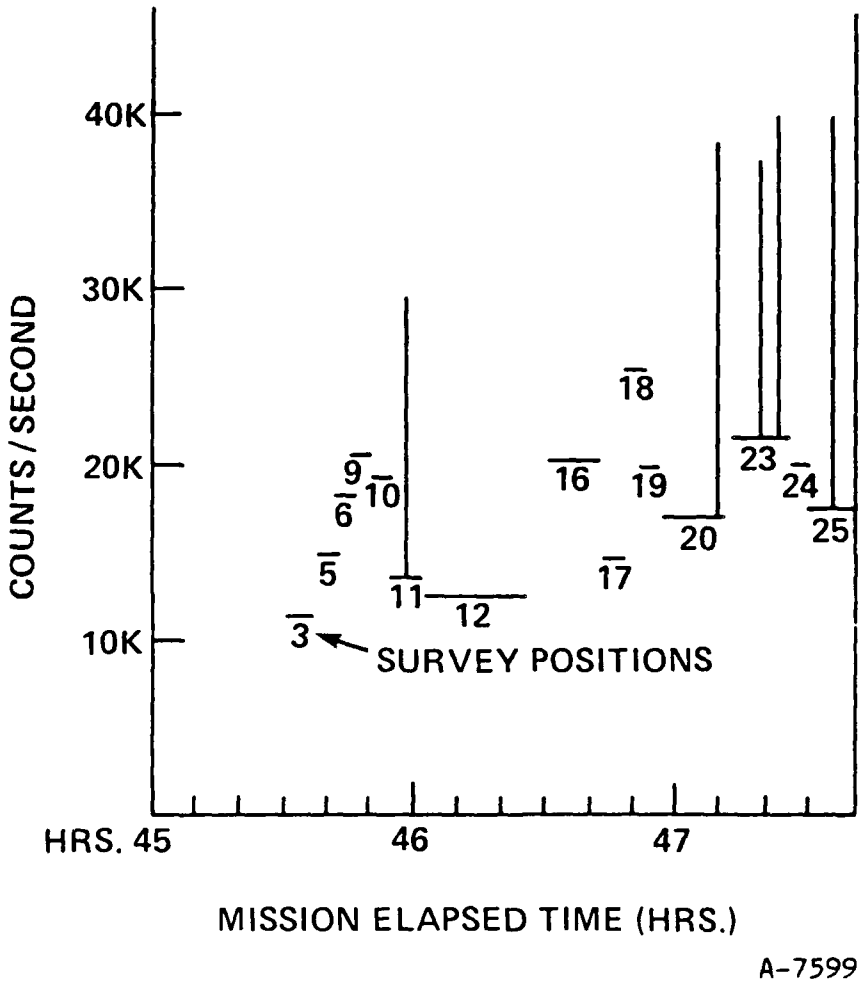
40K
30K
20K
10K
COUNTS/SECOND
3
5
6
9
10
11
12
16
17
18
19
20
23
24
25
SURVEY POSITIONS
HRS. 45
46
47
MISSION ELAPSED TIME (HRS.)
A-7599

FIGURE 3b

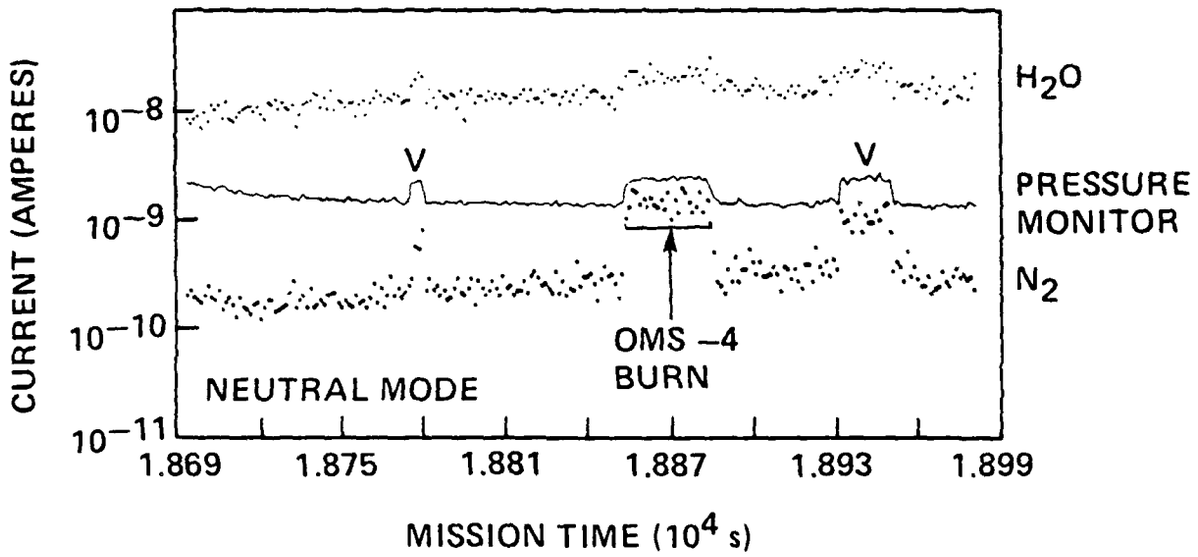

A-7600

FIGURE 4a

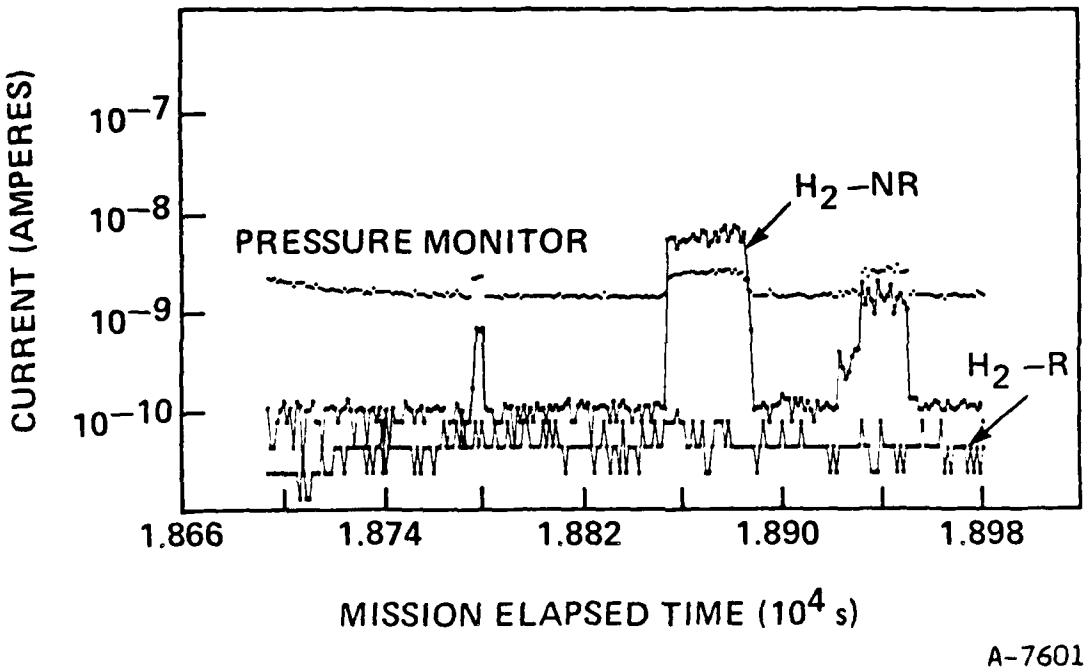
CURRENT (AMPERES)
10^{-7}
10^{-8}
10^{-9}
10^{-10}
PRESSURE MONITOR
H_2 –NR
H_2 –R
1.866
1.874
1.882
1.890
1.898
MISSION ELAPSED TIME (10^4 s)
A-7601

FIGURE 4b

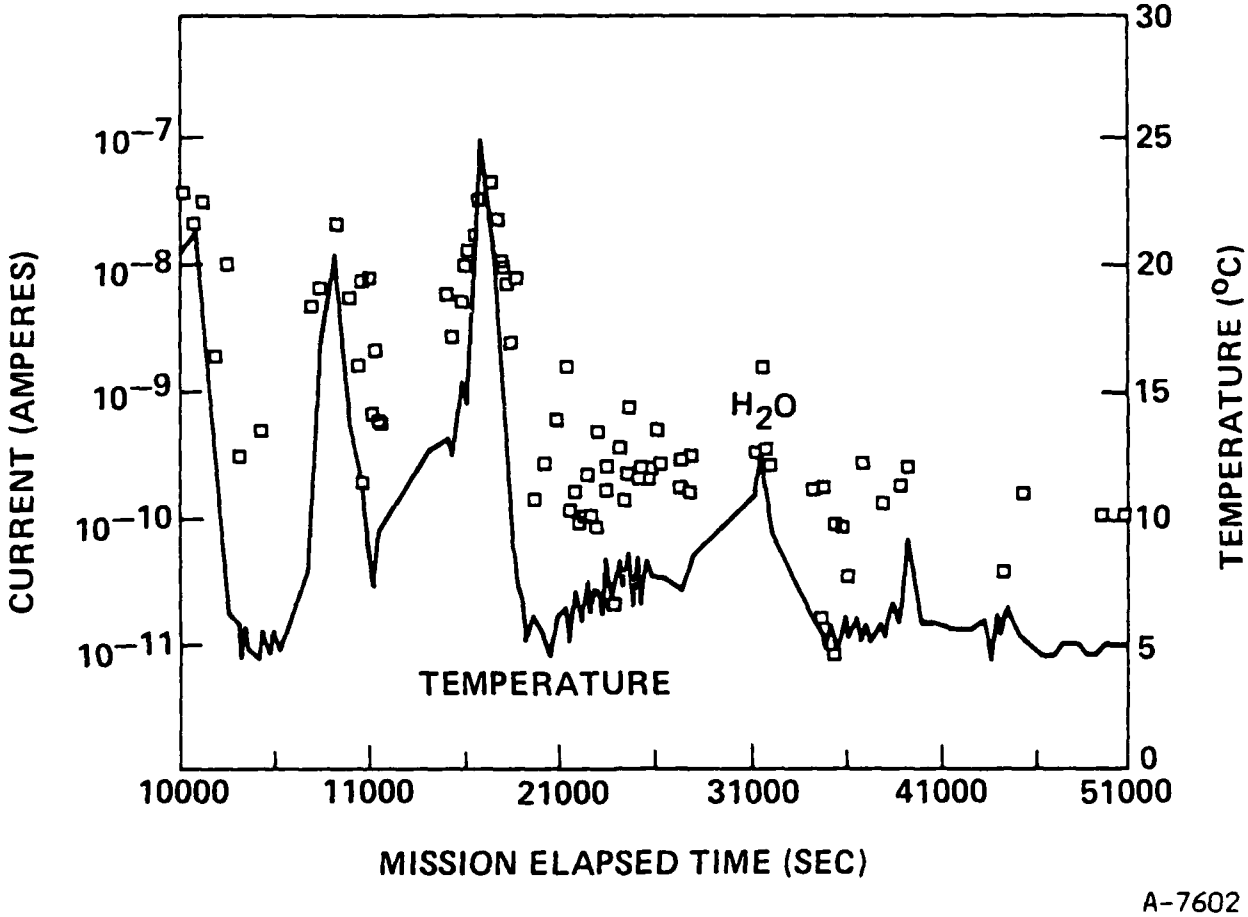
CURRENT (AMPERES)
10^{-7}
10^{-8}
10^{-9}
10^{-10}
10^{-11}
TEMPERATURE (^{o}C)
30
25
20
15
10
5
0
H_2O
TEMPERATURE
10000
11000
21000
31000
41000
51000
MISSION ELAPSED TIME (SEC)
A-7602

FIGURE 5

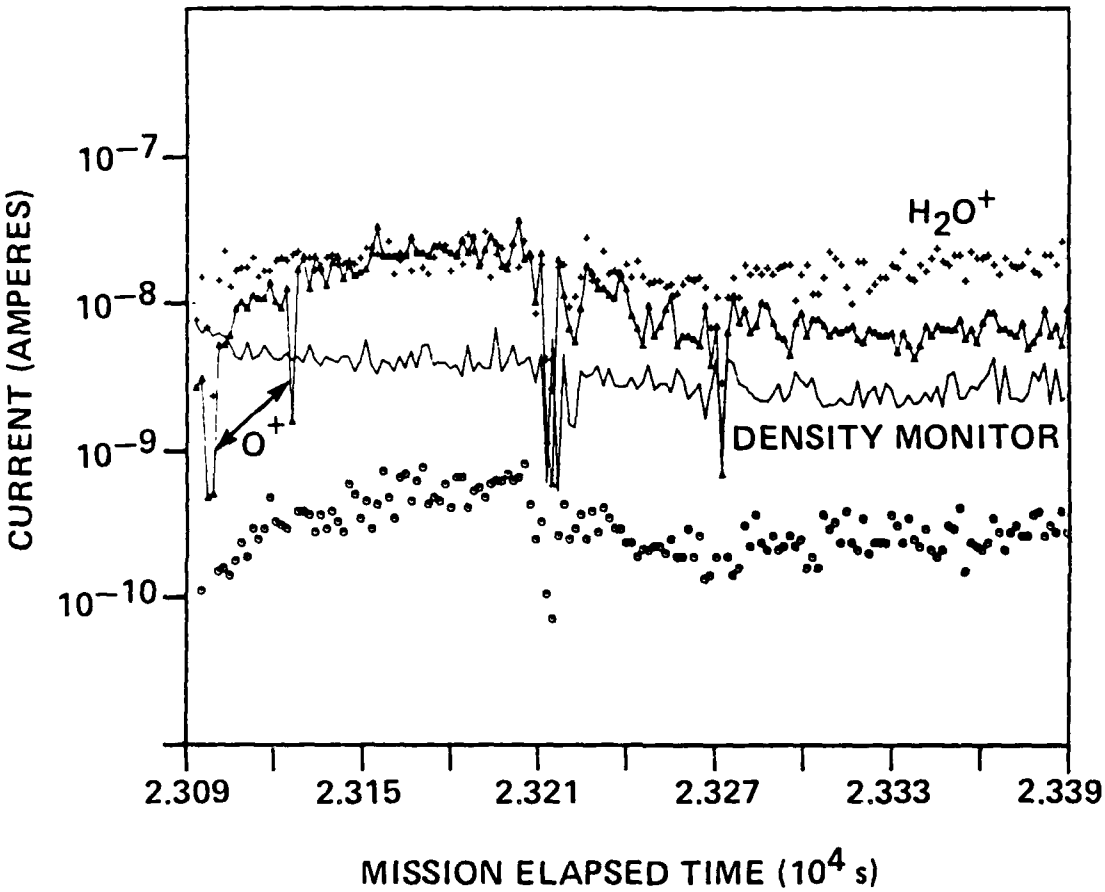

A-7603

FIGURE 6

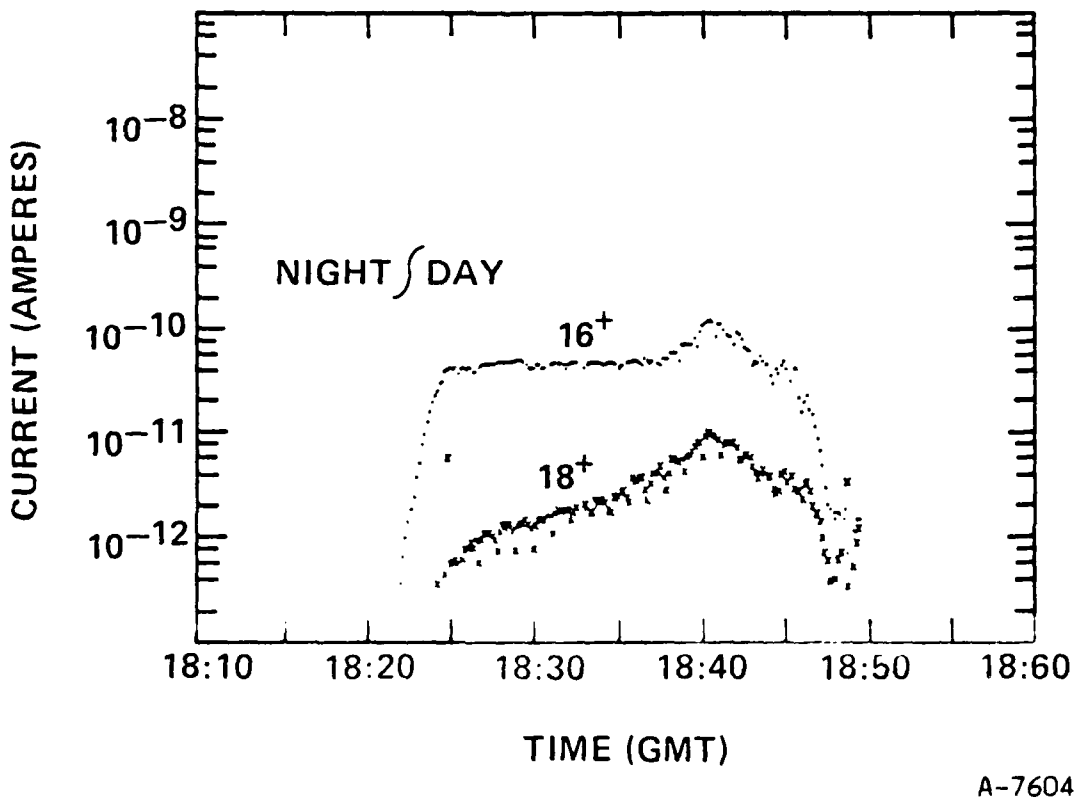
CURRENT (AMPERES)
10^{-8}
10^{-9}
10^{-10}
10^{-11}
10^{-12}
NIGHT ∫ DAY
16^+
18^+
18:10
18:20
18:30
18:40
18:50
18:60
TIME (GMT)
A-7604

FIGURE 7a

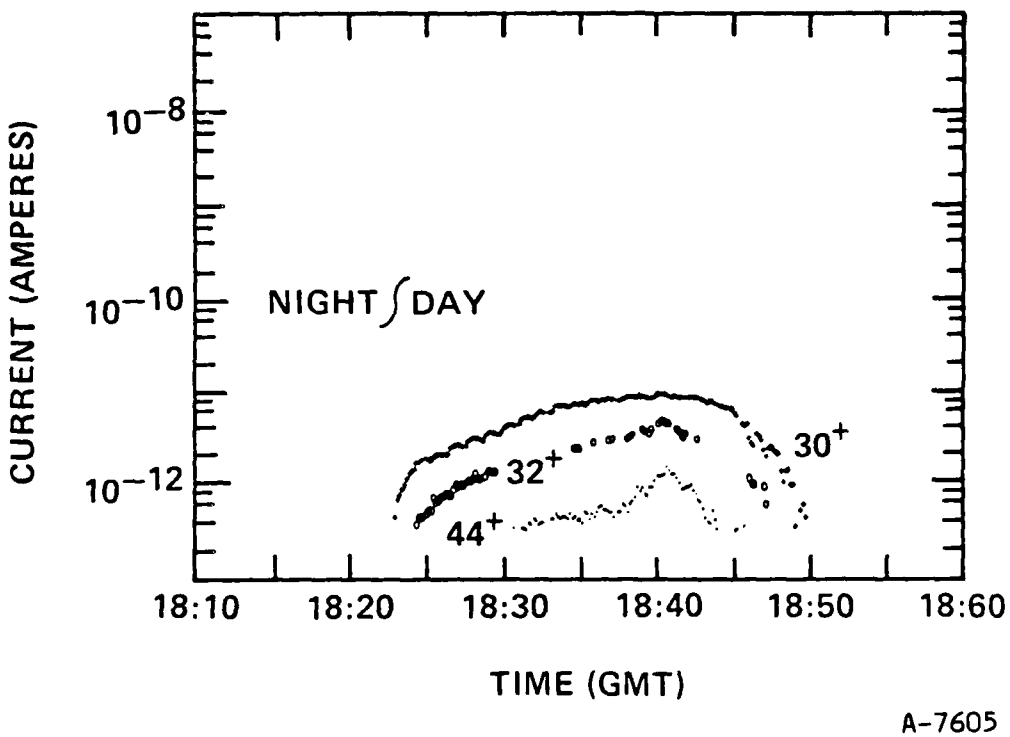
CURRENT (AMPERES)
10^{-8}
10^{-10}
10^{-12}
NIGHT ∫ DAY
30^+
32^+
44^+
18:10
18:20
18:30
18:40
18:50
18:60
TIME (GMT)
A-7605

FIGURE 7b

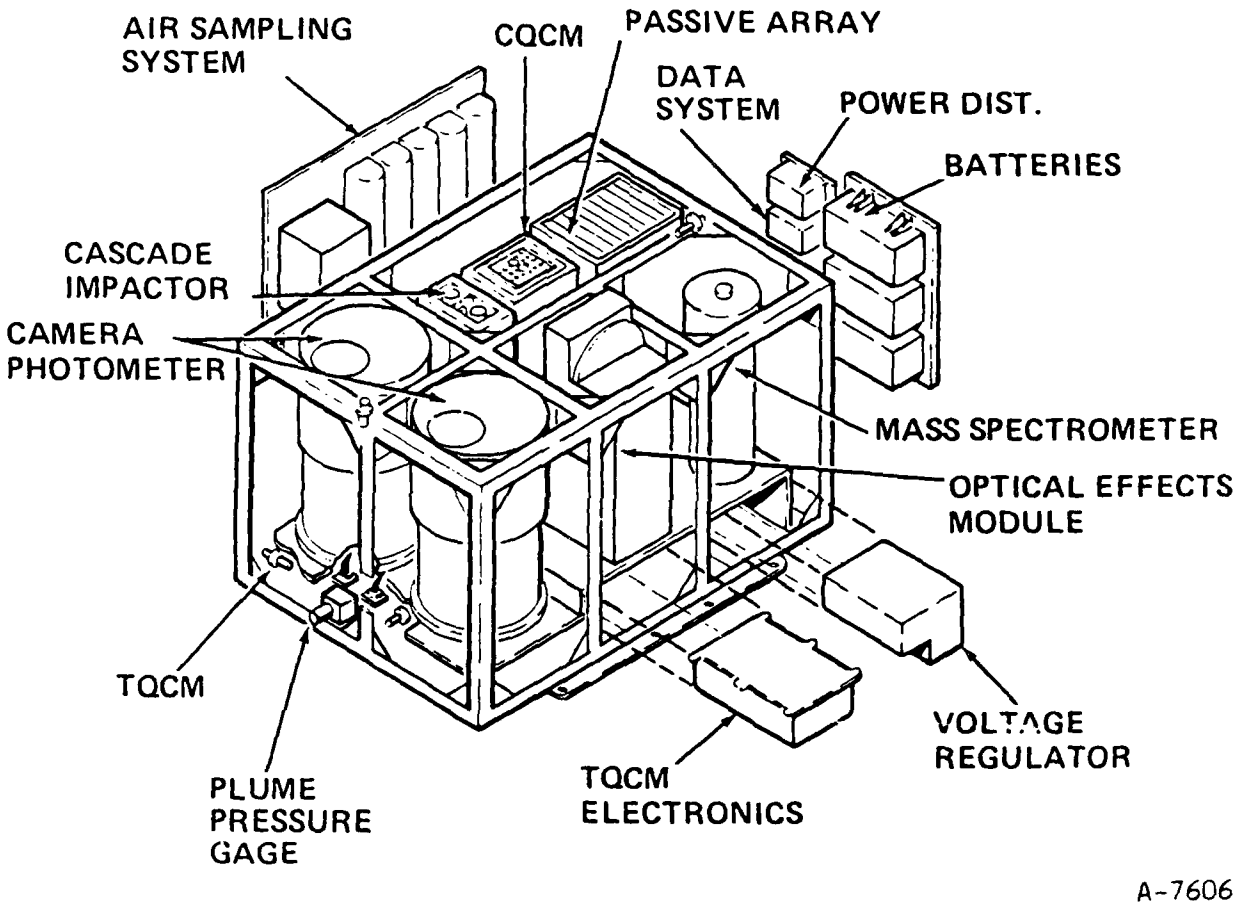
AIR SAMPLING SYSTEM
CQCM
PASSIVE ARRAY
DATA SYSTEM
POWER DIST.
BATTERIES
CASCADE IMPACTOR
CAMERA
PHOTOMETER
MASS SPECTROMETER
OPTICAL EFFECTS MODULE
TQCM
VOLTAGE REGULATOR
PLUME PRESSURE GAGE
TQCM ELECTRONICS
A-7606

FIGURE 8

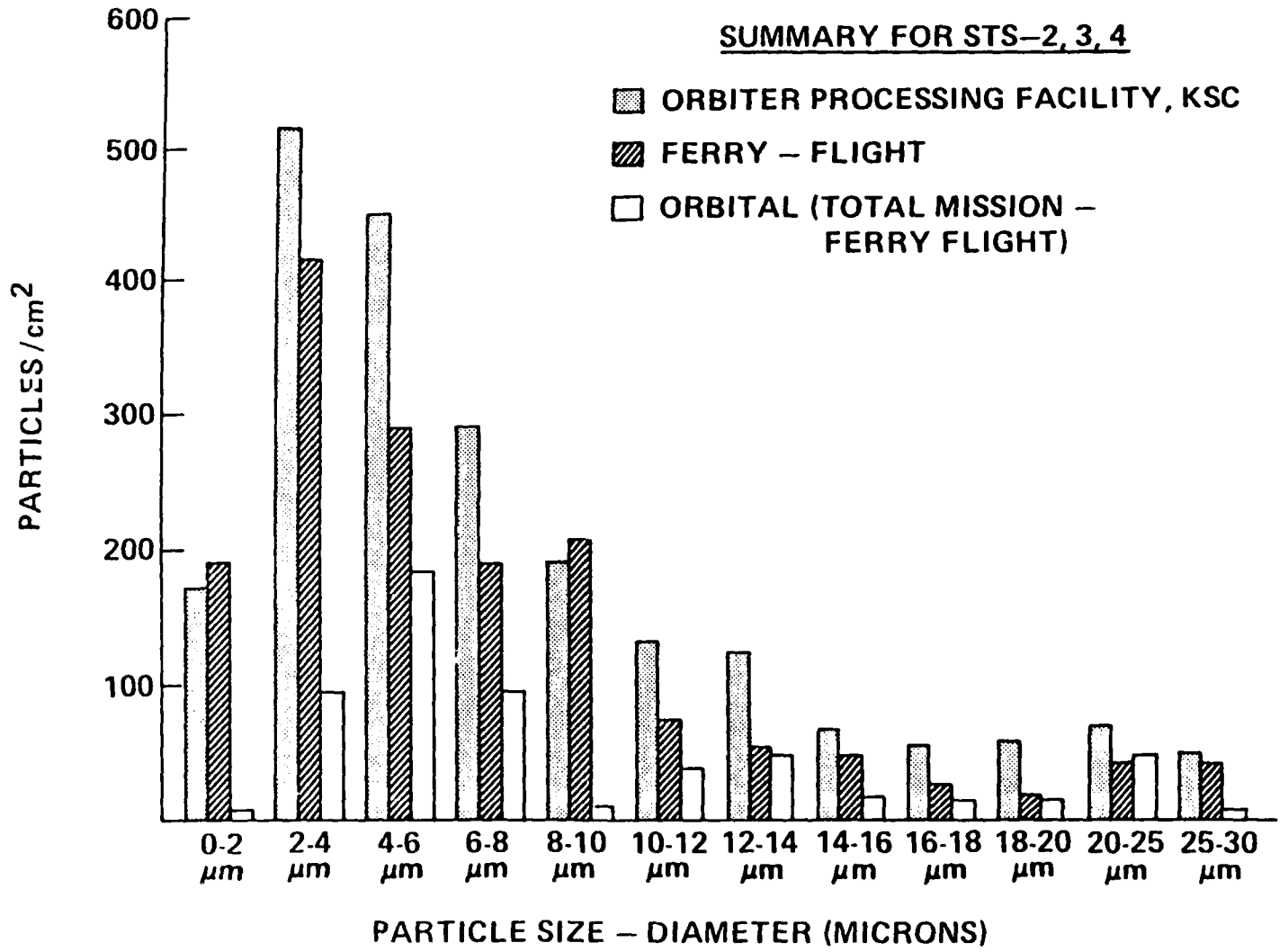
SUMMARY FOR STS–2, 3, 4
ORBITER PROCESSING FACILITY, KSC
FERRY – FLIGHT
ORBITAL (TOTAL MISSION – FERRY FLIGHT)
PARTICLES/cm²
600
500
400
300
200
100
0-2 μm
2-4 μm
4-6 μm
6-8 μm
8-10 μm
10-12 μm
12-14 μm
14-16 μm
16-18 μm
18-20 μm
20-25 μm
25-30 μm
PARTICLE SIZE – DIAMETER (MICRONS)
A-7607

FIGURE 9

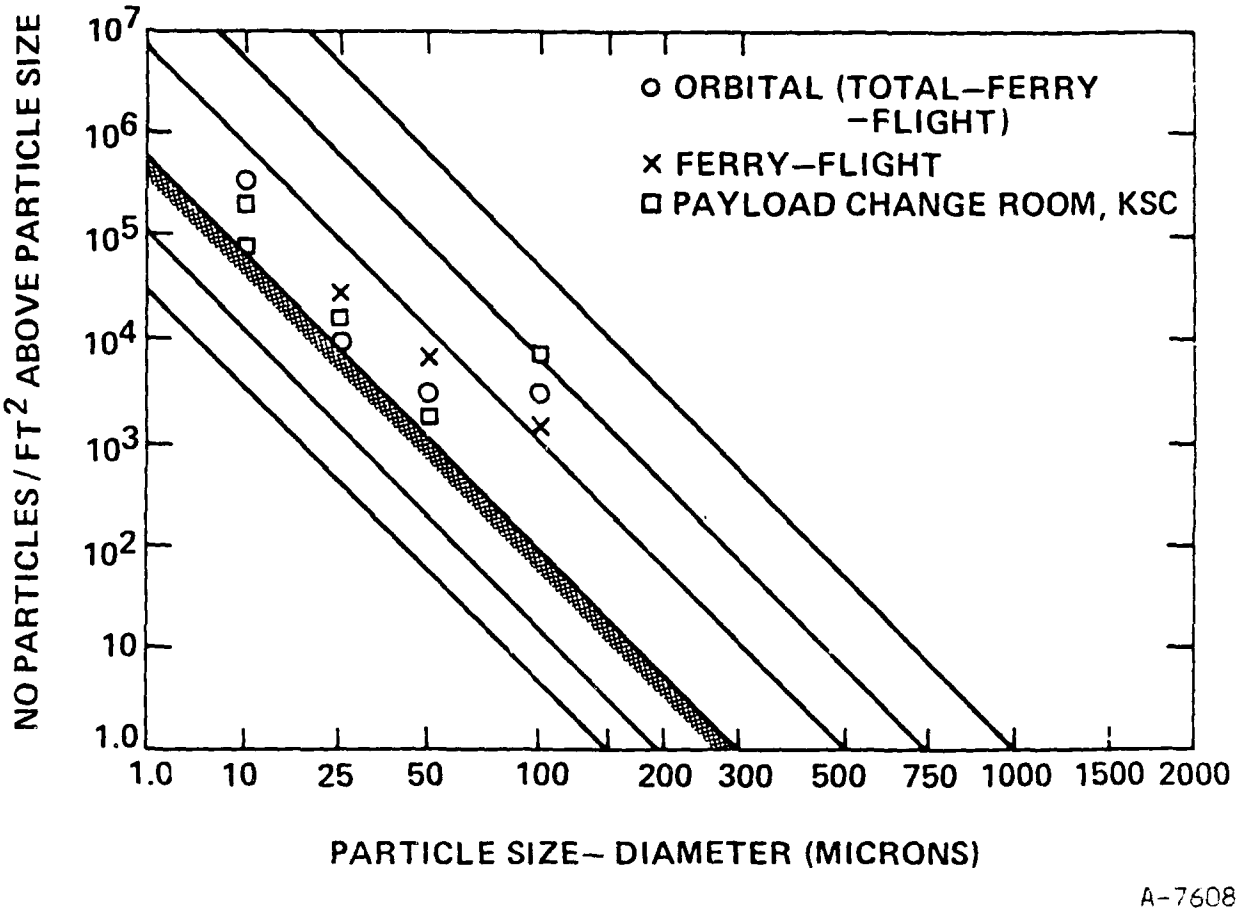
NO PARTICLES / FT^2 ABOVE PARTICLE SIZE
10^7
10^6
10^5
10^4
10^3
10^2
10
1.0
o ORBITAL (TOTAL–FERRY –FLIGHT)
× FERRY–FLIGHT
□ PAYLOAD CHANGE ROOM, KSC
1.0
10
25
50
100
200
300
500
750
1000
1500
2000
PARTICLE SIZE– DIAMETER (MICRONS)
A-7608

FIGURE 10

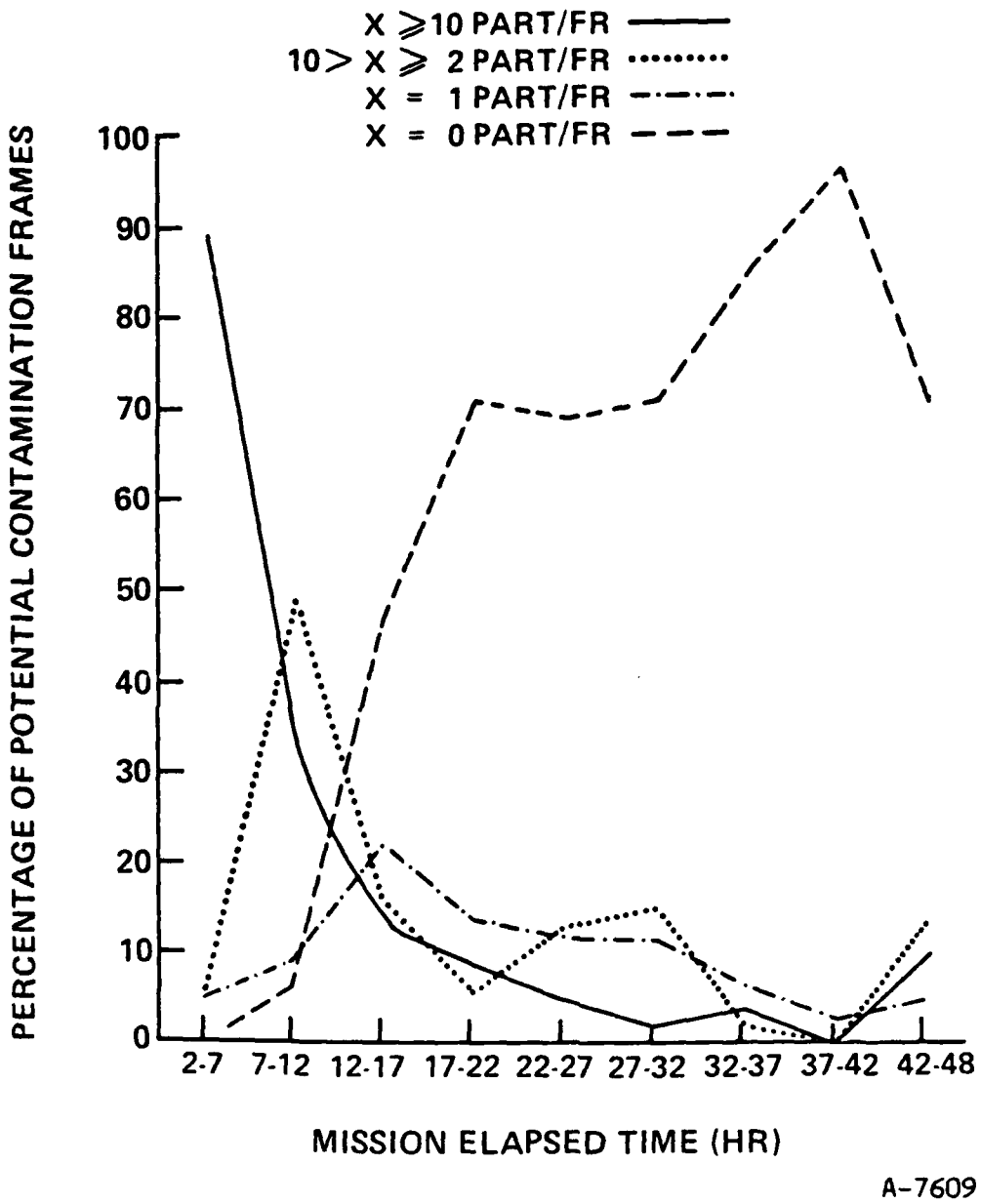
X ≥10 PART/FR
10> X ≥ 2 PART/FR
X = 1 PART/FR
X = 0 PART/FR
PERCENTAGE OF POTENTIAL CONTAMINATION FRAMES
100
90
80
70
60
50
40
30
20
10
0
2-7
7-12
12-17
17-22
22-27
27-32
32-37
37-42
42-48
MISSION ELAPSED TIME (HR)
A-7609

FIGURE 11

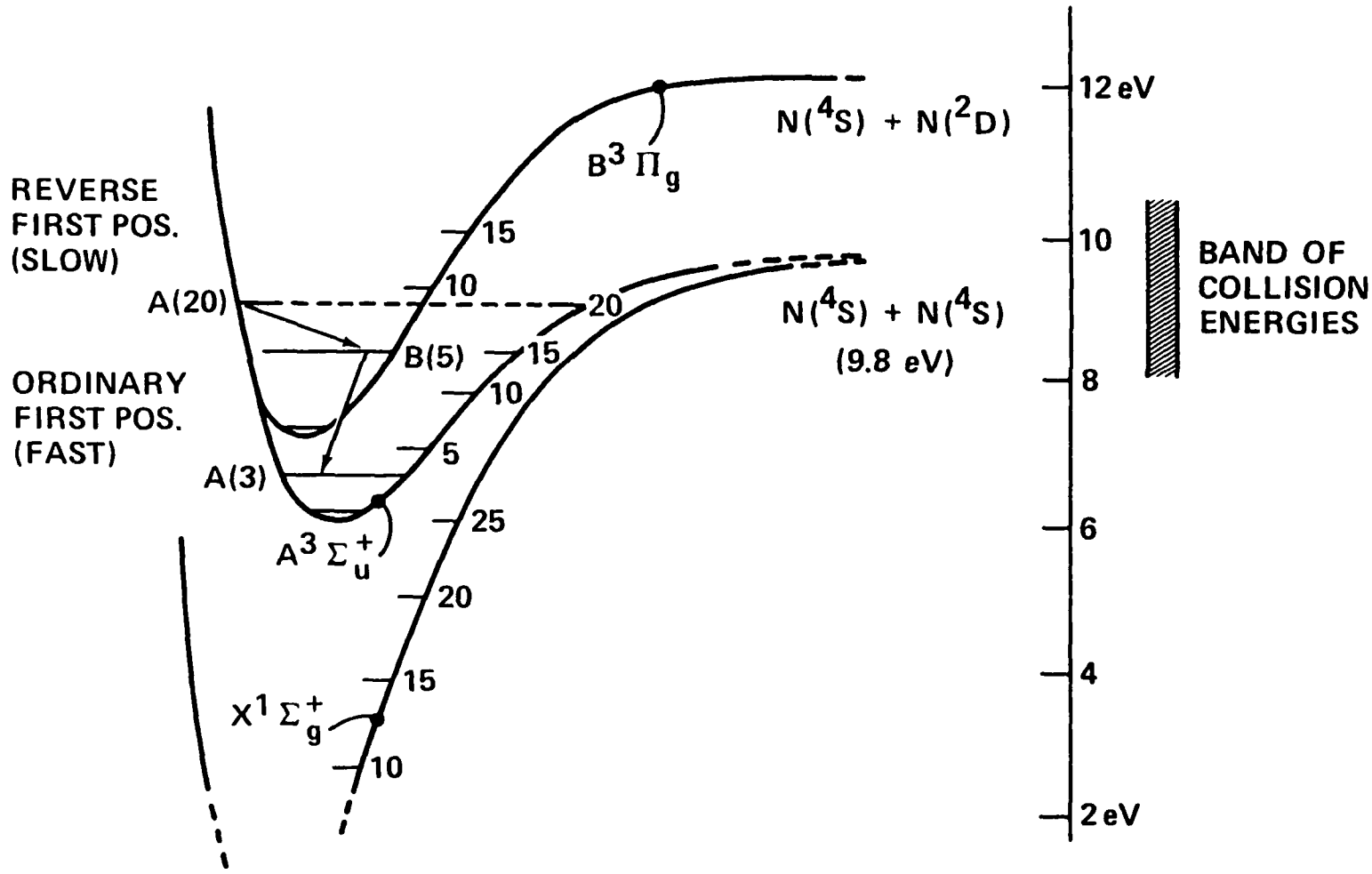

A-7610

FIGURE 12

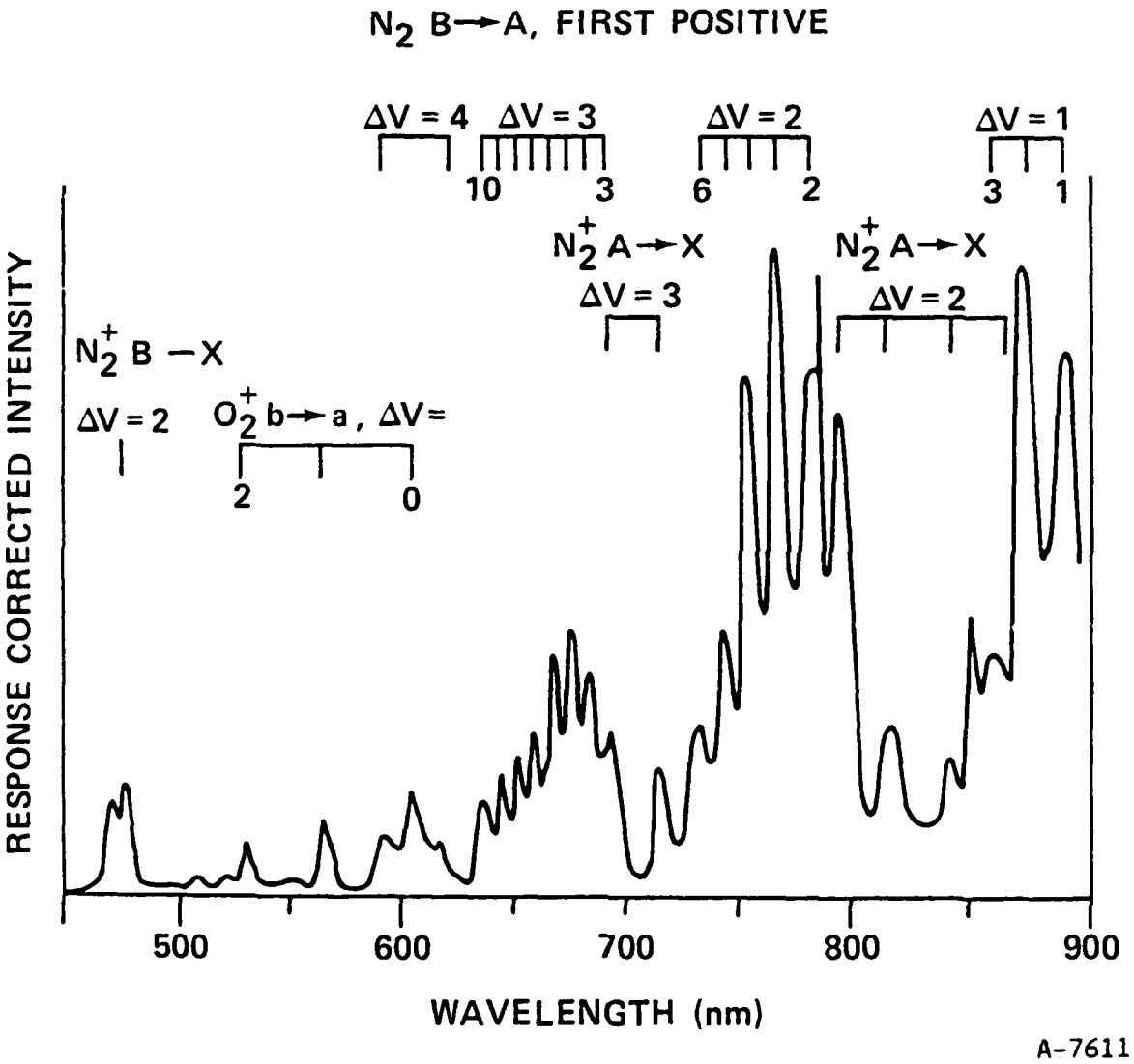
N2 B→A, FIRST POSITIVE
ΔV = 4
ΔV = 3
10
3
ΔV = 2
6
2
ΔV = 1
3
1
N2+ A→X
ΔV = 3
N2+ A→X
ΔV = 2
N2+ B −X
ΔV = 2
O2+ b→a, ΔV=
2
0
RESPONSE CORRECTED INTENSITY
500
600
700
800
900
WAVELENGTH (nm)
A-7611

FIGURE 13

APPENDIX B

Atomic Recombination into Excited Molecular States

Geophys. Res. Lett. 11,576 (1984)

PSI SR-174R is reproduced in its entirety.

PSI SR-174R

ATOMIC RECOMBINATION INTO EXCITED MOLECULAR STATES - A POSSIBLE MECHANISM FOR SHUTTLE GLOW

Byron David Green

Physical Sciences Inc.
Research Park, P.O. Box 3100
Andover, MA 01810

ATOMIC RECOMBINATION INTO EXCITED MOLECULAR - A POSSIBLE MECHANISM FOR SHUTTLE GLOW

Byron David Green

Physical Sciences Inc.

Abstract. A class of mechanisms is presented which could give rise to the observed glow above Shuttle surfaces exposed to energetic collisions with ambient atmospheric constituents as the Shuttle sweeps through its orbit. The collisional energies involved are sufficient to dissociate atmospheric N_2 upon impact with the Shuttle surfaces. The N-atoms formed can recombine on or over the surfaces to produce high vibrational levels of the N_2 $A(^3\Sigma_u^+)$ electronic state. At Shuttle altitudes, collisional quenching is negligible and the metastable N_2(A, high v) molecules slowly radiatively decay to form N_2 $B(^3\Pi_g)$ molecules on a millisecond time scale. The B state molecules then rapidly radiate to the A state producing the red N_2 First Positive Bands. This mechanism can explain both the spatial and spectral distributions of the observed glow.

Glow Observations

One of the most surprising observations on the early missions of the Space Transportation System (STS) was the presence of a glow above the surfaces of the Shuttle during passive operational periods. This phenomenon was observed on STS-3 by Banks and co-workers [1983]. Observations on later Shuttle missions have been performed by Mende [1983a,b, 1984] to quantify its nature. A visible glow has also been observed by the Atmospheric Explorer (AE) C and E satellites [Yee and Abreu, 1982, 1983], and by the Dynamics Explorer (DE) B satellite [Langhoff et al., 1983; Abreu et al., 1983]. The large satellite data base has permitted assignment of OH emission as the source of that glow. The limited Shuttle data base indicates that OH(v) emission probably is not the the source of the glow above Shuttle surfaces.

The Shuttle glow is seen on surfaces undergoing energetic collisions with the ambient atmosphere, i.e., in the ram direction. Data from STS-4 [Mende, 1983b] clearly showed a dependence of intensity with respect to the angle of attack.

No glow was observed when observed surfaces were in the wake or shadowed by Shuttle structures. Photographic data on Shuttle has quantified the spatial distribution of the glow. Preliminary estimates [Banks et al., 1983] of 5-10 cm extent above the surface have been revised to 20 cm in a careful analysis by Yee and Dalgarno [1983]. The extent of the glow has been interpreted to represent the region over which excited species are emitting--the product of the emitter velocity and radiative lifetime of the excited state. If radiators leave the surface at thermal velocities, then the corresponding radiative lifetimes are less than a millisecond. If their exit velocity is faster, the lifetime is shorter still, approaching 50 μs if the atmosphere/surface interaction is elastic. The spectral distribution of the glow has also been measured. Mende [1983a,b] has reported that the glow is a nearly continuous spectrum (for a resolution of ~ 15 nm) and increases in intensity to the red out to a 800 nm detection limit.

Possible Mechanisms

Atomic oxygen is the dominant atmospheric component at orbital altitudes. It has thus been widely considered as the reactive source of the Shuttle glow. Molecular nitrogen is present also, comprising 28% of the atmosphere at 240 km and 14% at 305 km. (These are the average altitudes of STS-3 and -5, respectively). The corresponding N_2 number densities from the U.S. Standard Atmosphere [1976] are 7×10^8 and 8×10^7 molecules/cm^3. The Shuttle orbital velocity is 8×10^5 cm/s. Thus as the Shuttle sweeps through the tenuous atmosphere, the atmospheric species energetically impact its surface. For oxygen atoms, the energy of the collision is 5 eV on average, but the atomic oxygen velocity vector ($\bar{c} = 10^5$ cm/s) will provide a distribution of collision energies (3.8-6.3 eV). These energetic O-atoms can react with Shuttle surfaces to produce new chemical species which could give rise to the glow. Nitrogen molecules will have a collisional energy of 9.3 ± 2 eV, comparable with their dissociation energy of 9.8 eV, and thus may dissociate upon impact, with the atoms remaining adsorbed to the surface. Let us now consider the interactions of atoms and surfaces.

The energy partitioning in the interaction of gases with adsorbed atoms has been studied for many years. In the Langmuir-Henshelwood (LH) type process, both atoms are adsorbed on the surface after collision. They then migrate over the surface, react, and escape into the gas phase. The level of excitation in the escaped molecule depends on reaction exothermicity and the nature of the surface adsorption. When surface coverage by adsorbed atoms is great, an incident gas-phase atom is likely to strike an adsorbed atom and form a molecule which escapes into the gas phase. This is called a Rideal process. This interaction time is short (10^{-12} s) and little energy partitioning with the surface can occur. The newly formed molecule can possess a large fraction of its bonding energy.

Both Rideal and LH processes have been observed to give rise to electronically excited molecules, such as N_2 and O_2 [Mannella and Harteck, 1961], over a variety of surfaces including glass [Evenson and Burch, 1960] and metals [Mannella et al., 1960]. The creation of these recombined molecules into electronically excited states suggests a very short surface residence time for the newly formed species, and indicates that recombination and desorption are part of a single physical process [Thorman et al., 1980]. A detailed investigation of the energy accommodated by N-atoms has been studied by Halpern and Rosner [1982]. They found that both Rideal and LH processes occur over a single surface under different physical conditions. The level of product excitation will thus depend on the nature of the surface and of surface coverage and temperature.

The most likely emitting species resulting from chemical reactions of energetic atmospheric components on Shuttle surfaces are vibrationally excited OH, CO and electronically excited N_2.

Hydroxyl radicals were postulated as a glow source for the Shuttle by Slanger [1983]. Vibrational states emitting in the red ($v' = 6-8$, $\Delta v = 5$) have radiative lifetimes of between 4 and 10 ms [Mies, 1974; Langhoff, et. al., 1983]. The careful analysis of the Shuttle glow by Yee and Dalgarno [1983] yielded a lifetime of 0.67 ms for thermal velocity emitters, suggesting that OH is not the Shuttle glow source. Although the OH Meinel vibrational bands do have the proper coarse spectral distribution to match both satellite and Shuttle glow observations, they exhibit

spectral structure which should have been partially resolved in Mende's [1984] spectral observations. Thus OH seems to be precluded as the source of the Shuttle glow due to radiative lifetime and spectral structure.

Carbon monoxide is another species which could give rise to the glow. Surface materials containing carbon have been shown by Leger [1983] to undergo appreciable mass loss on-orbit. Vibrationally excited CO could arise from the interaction of energetic O-atoms with carbon-containing Shuttle surfaces. Vibrational transitions with $\Delta v = 6-8$ would fall in the 600-850 nm region, and should rise in intensity to the red as the transition probability increases with decreasing Δv. These overtones are not as strong as the corresponding transitions in OH. The radiative lifetimes are comparable to those for OH, and thus perhaps too long to explain the Shuttle observations. Unlike OH, however, the CO spectral distribution would be more continuous, because bandwidths are comparable to their separations. Thus, CO emission could be a constituent of shuttle glow over surfaces which undergo appreciable mass loss. The glow, however, is observed even over surfaces not containing carbon (such as aluminum) and which do not suffer significant mass loss (painted surfaces) [Mende, 1984].

We suggest here another source for the glow: atomic recombination into electronically excited molecular states. Atmospheric N_2 can dissociate upon its collision with Shuttle surfaces. The N-atoms then may recombine to form highly vibrationally excited $N_2(A)$ molecules. The surface will incompletely accommodate the 9.8 eV reaction exothermicity and the molecule will leave highly excited. The degree of energy accommodation, and thus residual excitation, will depend on the nature of the surface. Some fraction of the exciting molecules will leave in the $A^3\Sigma_u^+$ state. Gas phase emissions observed in the laboratory [See Golde and Thrush, 1973] are the result of collisional processes quenching high lying A vibrational states to form vibrationally excited B state molecules (see levels in Figure 1).

Collisional processes probably will not be significant above shuttle surfaces. At Shuttle altitudes, the ambient mean free path between collisions is kilometers. Surface reflections and thermalized velocities may decrease this pathlength by an order of magnitude. In the

absence of collisions, however, highly excited A state molecules can still radiatively decay to lower levels of the B state as indicated in Figure 1. These reverse First Positive (A → B) transitions have not been observed, but have been estimated to occur and to be important in auroras [Gilmore, 1969; Mulliken, 1957; Cartwright, 1978]. These transitions are less strongly allowed than B-A and radiative lifetimes are estimated to be a few orders of magnitude slower, in the 10^{-2} - 10^{-4} s range. Thus the postulated mechanism for glow above Shuttle surfaces is that the N-atoms recombine on the Shuttle surfaces with varying degrees of energy accommodation. The newly formed N_2 molecule then leaves the surface in the A state with a considerable portion of the reaction exothermicity. These highly vibrationally excited A state molecules slowly radiate (in the infrared between 2 and 6 μm) into vibrationally excited B states. These, in turn, rapidly radiatively decay (6-8 μs) giving rise to First Positive band radiation. Nearly all of the 9.8 eV reaction exothermicity may be available in the N_2 product. Some small (< 1 eV) energy will be lost to overcome bonding to surface.

A spectrum of N_2 B → A emission with 5 nm resolution is presented in Figure 2. This spectrum was obtained by electron irradiating an N_2/O_2 mixture of total density 1 x 10^{13} molecules/cm^3 (0.3 mtorr) [Green, et al., 1983]. This particular spectrum is not meant to accurately represent the N_2 recombination glow above the Shuttle surfaces, but merely to demonstrate the possibility that this process may play a role.

In addition to N_2 B → A features, various ionic bands are present in the laboratory spectrum due to energetic electron impact. These ionic states would not be created in molecule/Shuttle collisions because of energetic constraints. The intensity onset in the red and the rise to longer wavelengths agree with Shuttle glow spectral observations [Mende, 1984]. The observed structure in the laboratory spectrum will decrease under poorer resolution and as rotational and vibrational temperatures increase, as would be the case for the Shuttle.

M. Torr and D. Torr [1984] have presented a preliminary analysis of emissions which were observed by their Imaging Spectrometric Observatory during the Spacelab mission. They observed a bright glow above surfaces of their experiment

(not the Shuttle surfaces per se). They tentatively assigned N_2 First Positive Bands as the dominant contributor to their spectrum in the red/near infrared region. This observation may indicate that collisional excitation mechanisms play a role over surfaces exposed to the atmospheric velocity vector. The satellite observations of AE and DE do not support this recombination mechanism, however.

Mende [1983b] has stated that the glow on the STS-5 rear engine pod was several hundred kilorayleighs within the bandpass of his instrument. Based on this observation we can crudely estimate the efficiency required for production of N_2^* from collisions of ambient N_2 with the Shuttle surface. Three hundred kilorayleighs (3×10^{11} photons/ cm^2 s) are emitted in a column about 10 m long when looking along the Shuttle tail, giving a volume emission rate of 3×10^8 photons/cm^3 s. If excited state species are radiatively decaying to produce this glow over a 20 cm layer, then the emitter flux off the surface would be greater than 6×10^9 emitters/cm^2 s, where the inequality results from the possibility of emission occurring outside of the instrumental bandpass. The total emitter flux may be as high as $1\text{-}2 \times 10^{10}$ emitters/cm^2 s.

At 305 km altitude where this emission intensity was observed, the atmospheric nitrogen flux is 6×10^{13} molecules/cm^2 s. These ambient molecules have a random thermal velocity distribution. Depending on the atmospheric temperature only a certain fraction (12-18%) of the molecules will undergo sufficiently energetic collisions with the Shuttle surfaces to dissociate the molecule. The molecules impinging on the Shuttle surface with enough energy to dissociate must eventually give rise to an exit flux of $1\text{-}2 \times 10^{10}$ N_2 (A, high v) molecules/cm^2 s. Thus, only one collision in 500-1000 must eventually result in metastable formation.

The collisional mechanism forming N_2 (A, high v) would be the most likely source for N_2 emissions in the Shuttle glow. If energy partitioning between the accessible electronic states occurs as the newly formed N_2 leaves the surface, other allowed transitions could result from population of the W, a', and a states. Emissions from other electronic states as detected by future VUV-IR observations will provide insight into the different surface-molecule interactions.

Oxygen atoms from the ambient flux will also be adsorbed on Shuttle surfaces. Unlike N_2, all O_2 electronic states lying below the dissociation energy can be created in recombination. Unfortunately, no allowed radiative transitions connect these states. O_2* emission is not a likely source of the observed Shuttle glow due to long radiative lifetimes, spectral distribution, and susceptibility to collisional dissociation by energetic atmospheric species. If these states are created, they could pose a serious optical problem because their lower intensity glow layer could extend tens of meters, potentially interfering with measurements from any shuttle location.

Heterogeneous recombination of N and O atoms can form electronically excited NO. Neither the spectral distributions nor lifetimes of NO* fit the observed glow. If the surface does not play a role in partitioning the energy, only emission in the infrared would be observed. If electronic energy partitioning occurs near the surface then the A, B, and C states which emit in the UV could also be formed. The glow then would depend on the nature of the surface and NO emission could appear as a bright thin layer over certain surfaces.

Conclusions

We have identified a class of mechanisms which can produce emission which matches the observed Shuttle glow characteristics. Nitrogen First Positive ($B \rightarrow A$) fluorescence is proposed as the most prominent emission from recombination of N-atoms under Shuttle conditions. Other emissions (such as N_2 $a \rightarrow X$, W-B; NO δ, β bands) are possible contributors depending on the nature of the surface-(recombining molecule) interaction. Only 1 collision in 500 of atmospheric N_2 with the shuttle surfaces must produce N_2 (A) in order to explain the observed intensities. This mechanism would exhibit an intensity variability dependent on the nature of the surface material.

It is likely that several mechanisms involving O or N_2 are simultaneously occurring over various Shuttle surfaces and that any one may dominate under certain conditions. The key to our understanding the glow phenomenon lies in an extended data base which includes improved spatial, spectral and surface specific observations. Atomic recombination as a source of the glow depends on the interaction of the shuttle with the ambient

atmosphere and unlike contamination-induced glow can not be overcome by simple preventative measures. Consequently, the glow could have a significant impact over a wide range of altitudes on the instruments which hope to use Shuttle as a remote optical observatory.

Acknowledgements. The author expresses his thanks to the following individuals for many helpful discussions: G. E. Caledonia, W. T. Rawlins, A. Gelb, T. D. Wilkerson L. Leger and L. Piper. This work was funded in part by Physical Sciences Inc. internal research funds and by the Air Force Geophysics Laboratory. This work was originally presented at AIAA 22nd Aerospace Sciences Meeting in January 1984.

References

Abreu, V. J., W. R. Skinner, P. B. Hays, and J. H. Yee, Optical effects of spacecraft-environment interaction: spectrometric observations by the DE-B satellite, AIAA-83-2657-CP presented at Shuttle Environment and Operations Meeting, Washington, D.C. Oct. 31-Nov. 2, 1983.

Banks, P. M., P. R. Williamson, and W. J. Raitt, Space Shuttle glow observations, Geophys. Res. Lett., 10, 118-121, 1983.

Cartwright, D. C., Vibrational populations of the excited states of N_2 under auroral conditions, J. Geophys. Res., 83, 517-531, 1978.

Evenson, K. M. and D. S. Burch, Atomic-nitrogen recombination, J. Chem. Phys., 45, 2450-2460, 1960.

Gilmore, F. R., Comment on paper, Semi-empirical electron impact cross sections for atmospheric gases, Can. J. Chem., 47, 1779, 1969.

Golde, M. F., and B. A. Thrush, Afterglows, Reports on Prog in Physics, 36, 1285-1364, 1973.

Green, B. D., L. G. Piper, G. E. Caledonia, H. C. Murphy, R. H. Krech, and E. R. Pugh, LABCEDE fluorescence studies, Rep. TR-356, 95 pp., Physical Sciences Inc., Andover, MA, 1983.

Halpern, B., and D. E. Rosner, Incomplete energy accommodation in surface-catalyzed reactions, in Heterogeneous Atmospheric Chemistry, 26, 167-172, 1982, Geophysical Monograph Series, American Geophysical Union, 1982.

Langhoff, S. R., R. L. Jaffe, J. H. Yee, and A. Dalgarno, The surface glow of the atmospheric explorer C and E satellites, Geophys. Res. Lett., 10, 896-899, 1983.

Leger, L., Shuttle payload bay environment, AIAA-83-2576-CP presented at Shuttle Environment and Operations Meeting, 1983.

Mannella, G., and P. Harteck, Surface-catalyzed excitations on the oxygen system, J. Chem. Phys., 34, 2177-2180, 1961.

Mannella, G. G., R. R. Reeves, and P. Harteck, Surface catalyzed excitation with O and N atoms, J. Chem. Phys., 33, 636-637, 1960.

Mende, S. B., O. K. Garriott, and P. M. Banks, Observations of optical emissions on STS-4, Geophys. Res. Lett., 10, 122-125, 1983a.

Mende, S. B., "Vehicle Glow," AIAA-83-2607-CP, presented at Shuttle Environment and Operations Meeting, 1983b.

Mende, S. B., Experimental measurement of Shuttle glow, AIAA-84-0550 presented at AIAA 22nd Aerospace Sciences Meeting, Reno, Jan. 12, 1984

Mies, F. H., Calculated vibrational transition probabilities of OH (X $^2\pi$), J. Mol. Spec., 53, 150-188, 1974.

Mulliken, R. S., The energy levels of the nitrogen molecule, in The Threshold of Space, edited by M. Zelikoff, pp. 169-179, Pergamon Press, New York, 1957.

Slanger, T. G., Conjectures on the origin of the surface glow of space vehicles, Geophys. Res. Lett., 10, 130-132, 1983.

Thorman, R. P., D. Anderson, and S. L. Bernasek, Internal energy of heterogeneous reaction products: nitrogen atom recombination on iron, Phys. Rev. Lett., 44, 743-746, 1980.

Torr, M. R. and D. Torr, Preliminary results of the imaging spectrometric observatory on Spacelab 1, AIAA-84-0044 presented at AIAA 22nd Aerospace Sciences Meeting, Reno, 1984.

U. S. Standard Atmosphere 1976, 227 pp., U. S. Government Printing Office, Washington, D.C. (October 1976).

Yee, J. H., and V. J. Abreu, Optical contamination on the Atmospheric Explorer-E satellite, Proc. SPIE-Soc. Opt. Eng., 338, 120-128, 1982.

Yee, J. H., and V. J. Abreu, Visible glow induced by spacecraft - environment interaction, Geophys. Res. Lett., 10, 126-129, 1983.

Yee, J. H., and A. Dalgarno, Radiative lifetime analysis of the spacecraft optical glow, AIAA-83-2660-CP presented at Shuttle Environment and Operations Meeting, 1983.

B. D. Green, Physical Sciences Inc., P.O. Box 3100, Andover, MA 01810.

(Received 03/09/84;
revised 04/13/84;
accepted 04/13/94)

Copyright 1984 by the American Geophysical Union.

Paper number 4L6075
0094-8276/84/004L-6075$03.00

Green: Atomic Recombination

Green: Atomic Recombination

Fig. 1. The N_2 recombination glow mechanism. N atoms are formed by N_2 impact with shuttle surfaces at collisional energies shown on right. A fraction of the atoms recombine into the A state at high vibrational levels. These slowly radiate to the B state. The molecules in the B state then rapidly radiate back to low levels of the A state giving First Positive emission.

Fig. 2. The emission from electron-irradiated air at 0.3 mtorr pressure is dominated by N_2 First Positive emission which rises to the red. Data taken on LABCEDE facility at Air Force Geophysics Lab [Green et al., 1983].

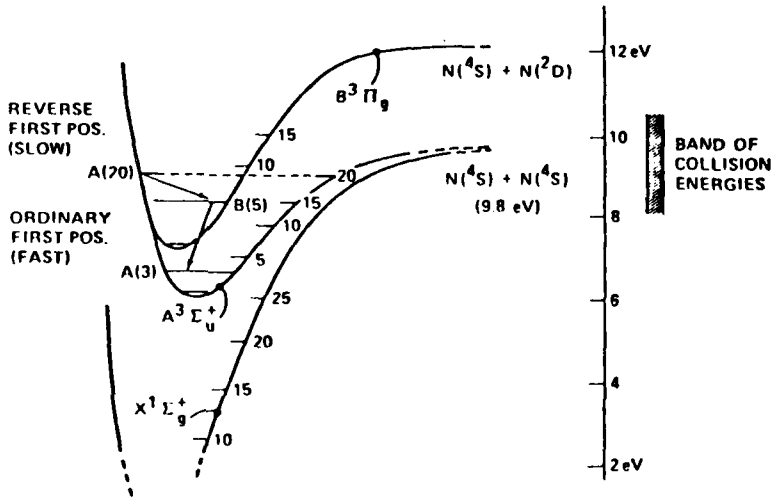

4L6075
GREEN: Atomic Recombination
Figure 1

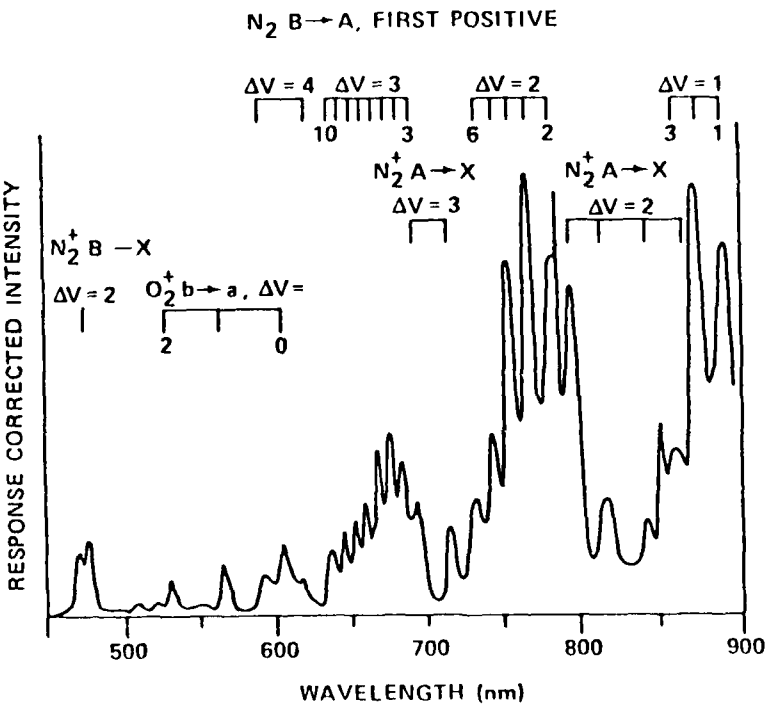

4L6075
GREEN: Atomic Recombination
Figure 2

APPENDIX C

Spectral Identification/Elimination of Molecular Species in Spacecraft Glow

Second Workshop on Spacecraft Glow

NASA Conference Publication 2391

SR-216 is reproduced in its entirety.

SPECTRAL IDENTIFICATION/ELIMINATION OF MOLECULAR SPECIES IN SPACECRAFT GLOW

B. D. Green, W. J. Marinelli, and W. T. Rawlins

Atmospheric Sciences Group, Physical Sciences Inc.

Abstract. We have developed computer models of molecular electronic and vibrational emission intensities. Known radiative emission rates (Einstein coefficients) permit the determination of relative excited state densities from spectral intensities. These codes have been applied to the published spectra of glow above shuttle surfaces [Swenson et al., 1985] and to the Spacelab 1 results of Torr and Torr [1985]. The theoretical high-resolution spectra have been convolved with the appropriate instrumental slit functions to allow accurate comparison with data. The published spacelab spectrum is complex but N_2^+ Meinel (A→X) emission can be clearly identified in the ram spectrum. N_2 First Positive emission does not correlate well with observed features, nor does the CN Red System. Spectral overlay comparisons are presented. The spectrum of glow above shuttle surfaces, in contrast to the ISO data, is not highly structured. Diatomic molecular emission has been matched to the observed spectral shape. Source excitation mechanisms such as (oxygen atom)-(surface species) reaction product chemiluminescence, surface recombination, or resonance fluorescent re-emission will be discussed for each tentative assignment. These assignments are the necessary first analytical step toward mechanism identification. Different glow mechanisms will occur above surfaces under different orbital conditions. Effective remedial actions can only be planned once the glows have been characterized.

Introduction

While it is clear that a more extensive database is required in order to characterize spacecraft glows, considerable insight into potential mechanisms can be gained by careful analysis of existing data to extract all the information contained therein. We present here our preliminary spectral analyses of the published ISO data on Spacelab 1 [Torr and Torr, 1985] and the spectrum from Lockheed's hand-held spectrophotometer on STS 41-D [Swenson et al., 1985]. Spectral predictions are made for various molecular electronic and vibrational emission bands and compared with the data. The particular emitters were chosen as likely candidates in a kinetic review of the shuttle local environment. This review considered various classes of mechanisms that could occur both above and on shuttle surfaces. Because glows have been observed over a variety of surfaces, chemical reactions with the surface materials were not highlighted in this review. They will be considered in a future paper [Green et al., 1985a]. Our comparison of spectral predictions with observations clearly eliminates many potential radiators (such as N_2 First Positive and CN Red Systems), clearly identifies other features as far-field

atmospheric emissions (such as N_2^+ Meinel and First Negative), and suggests other potential radiators (such as vibrational overtones of CO and NO in addition to OH). We will present these comparisons after our kinetic review.

Potential Chemical Excitation Mechanisms

The variety of chemical processes that could be occurring in the local shuttle environment is shown schematically in Figure 1. As the ambient atmospheric O and N_2 enter the local shuttle cloud (at a relative velocity 8 km/s), they can strike gas-phase contaminants and react with or collisionally excite them. A major portion of the atmospheric flux reaches the surface where it can excite or react with adsorbed species on shuttle surfaces. If the atmospheric N_2 strikes a bare surface site it can dissociate on impact [Green, 1984]. Atomic oxygen, if slowed by gas-phase collisions, can also be adsorbed. Surface recombination and desorption could then give rise to emissions. Finally, the ambient atmospheric species can react with surface materials. In the gaseous contaminant cloud, the prevalent species have been measured to be H_2O and CO_2 [Miller, 1983; Narcisi et al., 1983], although He, O_2, Ar, freons, cleaning agents and other species have also been detected in trace amounts. H_2O is dominantly attributable to outgassing and the flash evaporator system releases. The most likely gas phase reactions are

$$H_2O + O \rightarrow OH(v) + OH(v) \qquad \Delta H_{298} = +\ 0.7\ \text{eV} \tag{1}$$

$$CO_2 + O \rightarrow CO(v) + O_2 \qquad \Delta H_{298} = +\ 0.35\ \text{eV} \tag{2}$$

and in the reflected atmospheric shocklayer:

$$N_2 + O \rightarrow NO(v) + N \qquad \Delta H_{298} = +\ 3.2\ \text{eV}\ . \tag{3}$$

Even though all these processes are endothermic, in the ram velocity vector the kinetic energies involved in the collisions are sufficient (5.2 ± 1 eV) to permit the reactions to proceed. In particular, the reverse reaction (1) is reasonably fast ($k_{-1} = 1.8 \times 10^{-12}$ cm^3/s), while the forward reaction involving O^* is extremely rapid ($k_4 = 9.9 \times 10^{-11}$ cm^3/s):

$$O(^1D) + H_2O \rightarrow OH + OH \quad \Delta H_{298} = -\ 1.2\ \text{eV}\ . \tag{4}$$

Thus, the possibility exists for creating vibrationally excited CO and OH from these gas-phase reactions. In addition to reaction, processes 1 and 2 could simply lead to vibrationally excited H_2O and CO_2 (resulting in infrared emission). These vibrational excitation cross sections have been measured to be large [Dunn et al., 1975] at somewhat lower translational energies (4-6 km/s). Radiance levels can be estimated from these cross sections, contaminant levels, and atmospheric fluences to be less than 100 kR in the infrared. Overtone emission in the visible will be much weaker and should make negligible contributions to visible glow spectra. Gas-phase chemical reactions do not occur at a sufficient rate to generate significant glow

intensities. For contaminant column densities of 2×10^{12} cm^{-2} and assuming (1) rate constants 0.01 gas kinetic and (2) that 1% of the product molecules are excited and emit in the visible, total glow intensities of hundreds of Rayleighs are predicted. Stated in another manner, only 1% of the incoming ambient flux undergoes collisions with the H_2O contaminant cloud. However, if the column densities were considerably higher due to ram pressure build up, then gas-phase chemical reactions could contribute to the glow. The spatial extent of the glow for these processes would reflect the contamination concentration gradients above the surfaces.

An additional gas-phase glow has been observed during/after thruster firings. The thruster equilibrium exhaust concentrations are calculated as 33% H_2O, 31% N_2, 17% H_2, 13% CO, and 4% CO_2, with traces of H, O_2, and monomethylhydrazine-NO_3. However, radicals will be produced in high concentrations during the thruster firing and will persist in this environment. Likely candidates are OH and NH_2. NH_2 has a structured emission spectrum in the yellow region of the visible. During thruster firings exhaust species leave the nozzle at an average velocity of 3.5×10^5 cm/s. If the thruster exhaust is directed into the ram, large collisional energies can result. For example, the reaction

$$N_2 \text{ (thruster)} + O \rightarrow NO(v) + O \qquad \Delta H_{298} = +\ 3.2 \text{ eV} \tag{3}$$

could occur at collisional energies of up to 6.5 eV. Under these conditions up to 15 quanta of vibrational energy in NO could be excited. Additional processes such as

$$O + H_2 \rightarrow OH + H \qquad \Delta H_{298} = +\ 0.1 \text{ eV (exothermic)} \tag{5}$$

$$N_2 + H_2 \rightarrow NH + N + H \qquad \Delta H_{298} = +\ 10.7 \text{ eV} \tag{6}$$

$$N_2 + H_2 \rightarrow NH_2 + N \qquad \Delta H_{298} = +\ 6.9 \text{ eV} \tag{7}$$

can occur. Due to the high concentrations of neutrals released in a typical RCS thruster firing (10^{25} molecules in 80 ms), hundreds of kilorayleighs of radiance could easily arise, even assuming only one collision in 10^6 leads to a visible photon. In summary, gas-phase chemiluminescent reactions can easily account for observed bright flashes associated with thruster events. If thruster effluents are trapped above ram surfaces, these concentration enhancements could give rise to detectable chemiluminescent glows. Outgassing/offgassing contamination levels appear to be sufficiently small so that gas-phase reactions of these species cannot explain observed radiance levels in the visible. The relative importance of various processes contributing to the glow may change in other spectral regions.

All of these gas-phase species will be adsorbed to some extent on shuttle surfaces. Self-contamination has long been recognized as a problem [Scialdone, 1972] because the mean-free-path between collisions is large enough for molecules from localized contamination sources to be collisionally backscattered over large areas of the shuttle. Mass spectrometric observations in the cargo bay detect remote thruster firings, refrigerant, and He leaks. The degree of adsorption of a given species is surface-specific. However, H_2O, the

most prevalent gas-phase contaminant, is notorious for being easily physisorbed on a host of surfaces. Carbon dioxide, carbon monoxide, nitrogen, and hydrogen are also likely to be present in order of decreasing concentration. These physisorbed species are dynamically moving over surface sites, creating a surface consisting of both occupied and bare bonding sites. The molecules in the ambient flux continuously strike the shuttle surface sites. For a polished surface, there are 10^{15} sites/cm^2 and at 250 km; an ambient oxygen atom will strike a surface site once a second on average. For rougher surfaces, the number of surface sites can be much greater. Ambient O or N_2 may not react or collisionally desorb these species with unit efficiency. Thus, if contaminant/effluent molecules are adsorbed on tile surfaces, it may take minutes or even hours for the ambient flux to "clean" the surface. Contaminant mobility on the surface will allow "creep" from non-ram surfaces to replenish the physisorbed species concentration on ram surfaces. In analogy with the gas phase, reactions 1-3 and 5-7 may occur. The energy of physisorption will also have to be overcome, making the reactions slightly more endothermic. Nevertheless, there is still sufficient kinetic energy in collision that chemiluminescent reactions or collisional excitation could occur.

If N_2 in the atmospheric flux strikes a bare surface site, there is often enough energy in the collision to dissociate the N_2 with the product N atoms remaining physisorbed on the surface. Atomic oxygen in the ram flux may not be adsorbed as readily since the energy of the collision is not channeled into potential energy and must be dissipated through other channels. If reflected oxygen atoms undergo numerous collisions with contaminant species, they may remain in the vicinity of the surface and be adsorbed. Thus, the relative concentration of O and N on the surfaces is not obvious. The nitrogen and oxygen atoms on the surface can then recombine to excited molecular states. This class of mechanisms was first suggested by Green [1984] and reviewed thoroughly by Green et al. [1985b]. Recombination can give rise to N_2, O_2, and NO. All these species have been observed in heterogeneous recombination in the laboratory by varying mole fractions of N and O [Halstead, 1985]. There appears to be no obvious preference for recombination partner; i.e., N_2 recombination is not excluded in the presence of O atoms.

The above chemical mechanisms can produce chemiluminescent excitation up to the level of reactant kinetic energies (as modified by reaction exo/endothermicities). Plasma excitation mechanisms, on the other hand, involve energetic (~100 eV) electrons which could excite higher molecular electronic states and even dissociate or ionize species. Thus, significant spectral differences are expected (as demonstrated below).

Spectral Comparisons

In order to quantify emission levels, we have developed at PSI spectral synthesis codes which predict very high-resolution molecular electronic and vibrational spectra for a host of molecules and band systems. These "basis functions" are then convolved with the appropriate slit function for each application. The emission from various states and species can be combined to give a composite spectrum.

Least-squares fitting is used to adjust the individual state populations to achieve a "best" fit. The relative emitting state populations are the end product of this analysis.

As an example of the code's capability, the 220-400 nm section of the ISO ram spectrum [Torr and Torr, 1985] is plotted in Figure 2, along with synthetic spectral prediction for N_2^+ First Negative bands. The best fit was achieved for a rotational temperature of 2000 K and 18 Å resolution. This resolution is lower than quoted, yet spectra at the nominal 6 Å resolution do not match the observed fluorescence signature. The relative shapes and intensities of the $\Delta v = 0$ and 1 series (and even the marginal intensity of the $\Delta v = 2$ series) all agree well with the data. Five vibrational levels ($v' = 0-4$) were included in the fit, and the vibrational distribution derived is quite similar to the distribution expected for solar resonance fluorescence excitation of $N_2^+(X)$ as suggested by Torr and Torr, although the populations of levels 2-4 had to be increased somewhat above the resonance fluorescence distribution, and may indicate vibrational excitation in $N_2^+(X)$. There is no evidence for chemical glow processes such as NO(B) emission. Certainly, the $N_2^+(B)$ could not arise from a chemical source. A plasma process, on the other hand, would excite considerable N_2 Second Positive (C→B) emission. A laboratory UV spectrum of a beam plasma discharge is plotted in Figure 3. The discharge was conducted in pure N_2 at 4×10^{13} molecules/cm^3 density. Strong Second Positive emission is evident and in fact, dominates the spectrum. Lyman-Birge-Hopfield and Fourth Positive bands are also observed weakly in the laboratory spectrum. Since these features are absent in the ISO spectrum, we conclude that the UV portion of the ISO spectrum is dominated by far-field atmospheric emission.

The complex visible portion of the published ISO ram spectrum is reproduced in Figure 4a. Assignment of features in this spectrum is more difficult but various atomic lines and N_2^+ Meinel (A→X) transitions are clearly identified (again presumably from resonance fluorescence excitation in the far-field atmosphere). Synthetic Meinel band predictions are shown in Figure 4b, as are the First Positive features. Agreement of the synthetic spectrum with the data is marginal--Meinel bands match observed spectral features but First Positive emission is clearly not a major component of the ISO spectrum. CN Red bands (A→X) were also synthesized and did not match the observed features. These features are in the correct spectral region but have the wrong shape. In light of the above kinetic discussion, overtone vibrational transitions for CO and NO were created. A synthetic spectrum of these transitions is shown in Figure 5. Because the molecular dipole moment functions are not well known, there are large uncertainties in the spectral intensities. The band positions are quite accurately known and the relative spectral shape should be accurate enough to provide insight. Hydroxyl, the most probable radiator, is not included at present. We are incorporating recent spectroscopic constants into our code at present [Langhoff, 1985]. A laboratory visible spectrum of an N_2/O_2 mixture during a beam plasma discharge is displayed in Figure 6. Much structured emission including O_2^+ First Negative, N_2 First Positive, and N_2^+ Meinel bands, is observed along with several atomic lines. The overlap with the ISO spectrum is again poor; no broad spectral features rise to the red as a result of plasma processes.

The Swenson et al. [1985] data are presented in Figure 7. Upon inspection of this broad spectrum, there are several striking features. The "noise" level is not constant but is much larger where there is spectral intentity. The "noise" spikes are often several resolution elements wide. Both these observations suggest that the "noise" features are real structure. Finally, the strongest "noise" spike falls at 520.0 nm, exactly where $N(^2D)$ atmospheric emission line occurs. Prompted by these observations, we felt that structure possibly existed in the broad continuum--that Mende's data were perhaps less noisy than they appeared. Nitrogen electronic spectra (including First Positive) were unable to match the broad spectral features for any vibrational or rotational distribution. However, in response to our kinetic analysis, we performed a least-squares fit of NO overtone vibrational bands to the observed spectrum. The NO emission series are more structured than the data; nevertheless, several spectral features are reproduced. The present calculations extend only to $v' = 19$; inclusion of higher vibrational levels of NO would tend to fill in the gaps in the computed spectrum. Inclusion of additional radiators such as OH may also improve the comparison. We feel that vibrational emissions are present at some level in this spectrum. The highly structured laboratory BPD spectrum of Figure 6 clearly does not agree with the Lockheed data.

Using a 20,000 K rotational temperature, together with the vibrational distribution for NO(v) obtained from our best fit to the Swenson et al. [1985] spectrum, we calculated the infrared emission spectrum. This spectrum is presented in Figure 8. If indeed NO (and CO or OH) is present in spacecraft glow, the infrared emission spectrum will be very bright. It will significantly interfere with remote observations of deep space or the Earth's atmosphere where infrared radiances are in the MegaRayleigh range.

Summary

Although this work is preliminary, spectral fitting analysis has suggested that chemical processes will play a role in observed glows. The two glow observations considered were quite different in spectral distribution. The alarming aspect of the ISO data is that even looking out of the payload bay and not observing any shuttle surfaces, a glow spectrum was obtained underlying far-field atmospheric emissions. A number of chemiluminescent mechanisms have been suggested as giving rise to vibrationally excited OH, CO, and NO dominantly, in addition to previously suggested surface recombination mechanisms. Vibrational overtone emissions may well be present in the glow data. Due to the variability of the shuttle's environment, it is likely that there will be conditions on-orbit when different chemical plasma mechanisms will dominate glow emission. Given this, it is not really surprising that the two spectra do not agree. Extension of the data base will allow the various physical regimes to be quantified, allow the key mechanisms to be identified, and permit meaningful remedial actions to be taken.

Acknowledgements. This work has supported by the Air Force Geophysics Laboratory and by Physical Sciences Inc. internal research funds.

References

Dunn, M. G., G. T. Skinner, and C. E. Treanor, Infrared radiation from H_2O, CO_2, or NH_3 collisionally excited by N_2, O, or Ar, AIAA J. 13, 803-812, 1975.

Green, B. D., Atomic recombination into excited molecular states -A possible mechanism for Shuttle glow, Geophys. Res. Lett. 11, 576-579, 1984.

Green, B. D., E. Murad, and W. T. Rawlins, The nature of the glow and its ramifications on space based observations, to be presented at AIAA 20th Thermophysics Conference, VA (June), AIAA-85-0910, 1985a.

Green, B. D., G. E. Caledonia, and T. D. Wilkerson, The shuttle ervironment - Gases, particles and glows, J. Space. Rockets (September), 1985b.

Halstead, J., private communication, 1985.

Langhoff, S., private communication, 1985.

Miller, E., STS-2, -3, -4 Induced Environment Contamination Monitor (IECM) summary report, NASA TM-82524, February 1983.

Narcisi, R. S., E. Trzcinski, G. Frederico, and L. Wlodyka, The gaseous environment around space shuttle, AIAA-83-2659-CP, Presented at shuttle Environment and Operations Meeting, Washington, D.C., 1983.

Scialdone, J. J., Self-contamination and environment of an orbiting spacecraft, NASA-TN D-6645, May 1972.

Swenson, G. R., S. B. Mende, and K. S. Clifton, Ram vehicle glow spectrum: Implication of NO_2 recombination continuum, Geophys. Res. Lett., 12, 97-100, 1985.

Torr, M. R. and D. G. Torr, A preliminary spectroscopic assessment of the Spacelab 1/Shuttle optical environment, J. Geophys. Res., 90, 1683-1960, 1985.

Figure Captions

Figure 1. Conceptual drawing of gas-phase/adsorbed species above shuttle surfaces

Figure 2. Comparison of ISO ultraviolet data (solid line) from Spacelab 1 (Torr and Torr) with theoretical N_2^+ first negative spectrum (dashed); v' = 0-4, rotational temperature 2000K, 1.8 nm resolution

Figure 3. Laboratory UV spectrum of a beam plasma discharge in N_2. This spectrum does not resemble ISO data, second positive features are clearly present.

Figure 4a. Visible data from ISO under near-ram conditions

Figure 4b. Synthetic spectrum of N_2 containing Meinel and first-positive transitions. This spectrum represents a best fit to the data of Fig. 4a, but clearly does not reproduce all the spectral features.

Figure 5. Overtone emission from highly vibrationally and rotationally excited NO showing visible emission features

Figure 6. Laboratory visible spectrum of a beam plasma discharge in N_2 and O_2 showing O_2 ionic, atomic line and N_2 electronic transitions

Figure 7. Comparison of NO vibrational overtone transitions with response corrected Lockheed glow data

Figure 8. Plot of NO vibrational emission between wavelengths 0.5 and 6.5 μm. NO emission is much stronger in the infrared

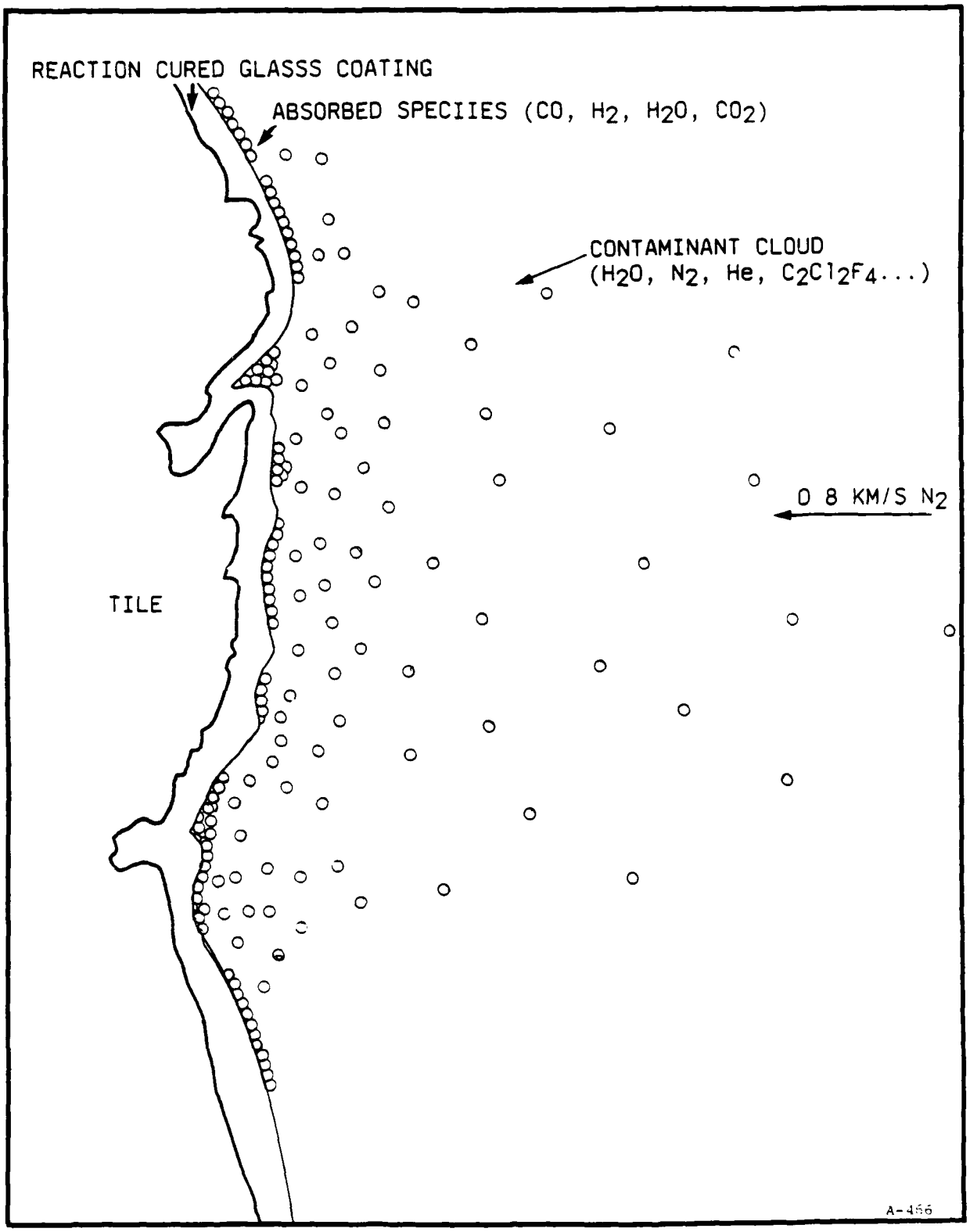
REACTION CURED GLASSS COATING
ABSORBED SPECIIES (CO, H_2, H_2O, CO_2)
CONTAMINANT CLOUD
(H_2O, N_2, He, $C_2Cl_2F_4$...)
0 8 KM/S N_2
TILE
A-466

FIGURE 1

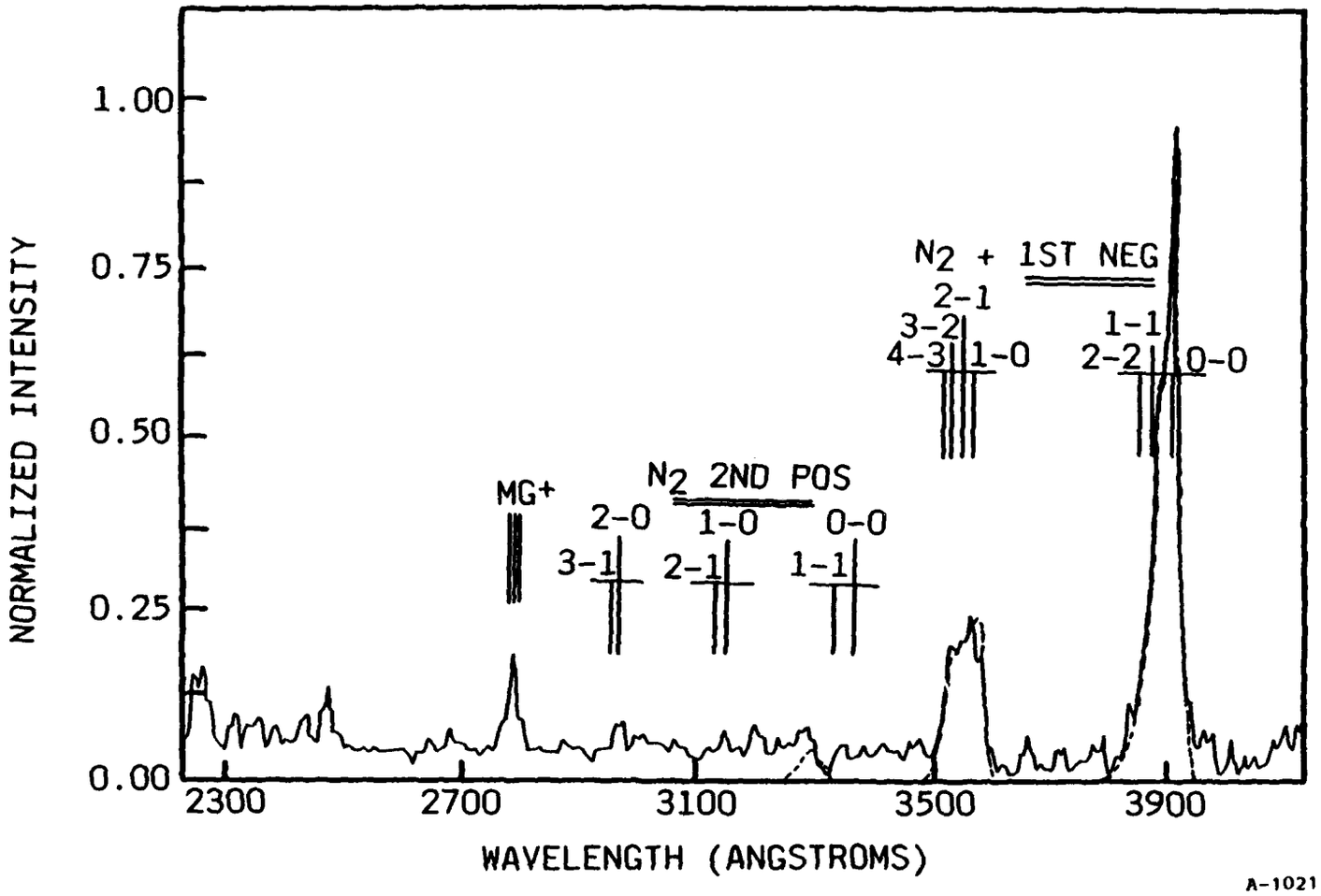
NORMALIZED INTENSITY
1.00
0.75
0.50
0.25
0.00
2300
2700
3100
3500
3900
WAVELENGTH (ANGSTROMS)
MG+
N2 2ND POS
2-0
3-1
1-0
2-1
0-0
1-1
N2 + 1ST NEG
2-1
3-2
4-3
1-0
1-1
2-2
0-0
A-1021

FIGURE 2

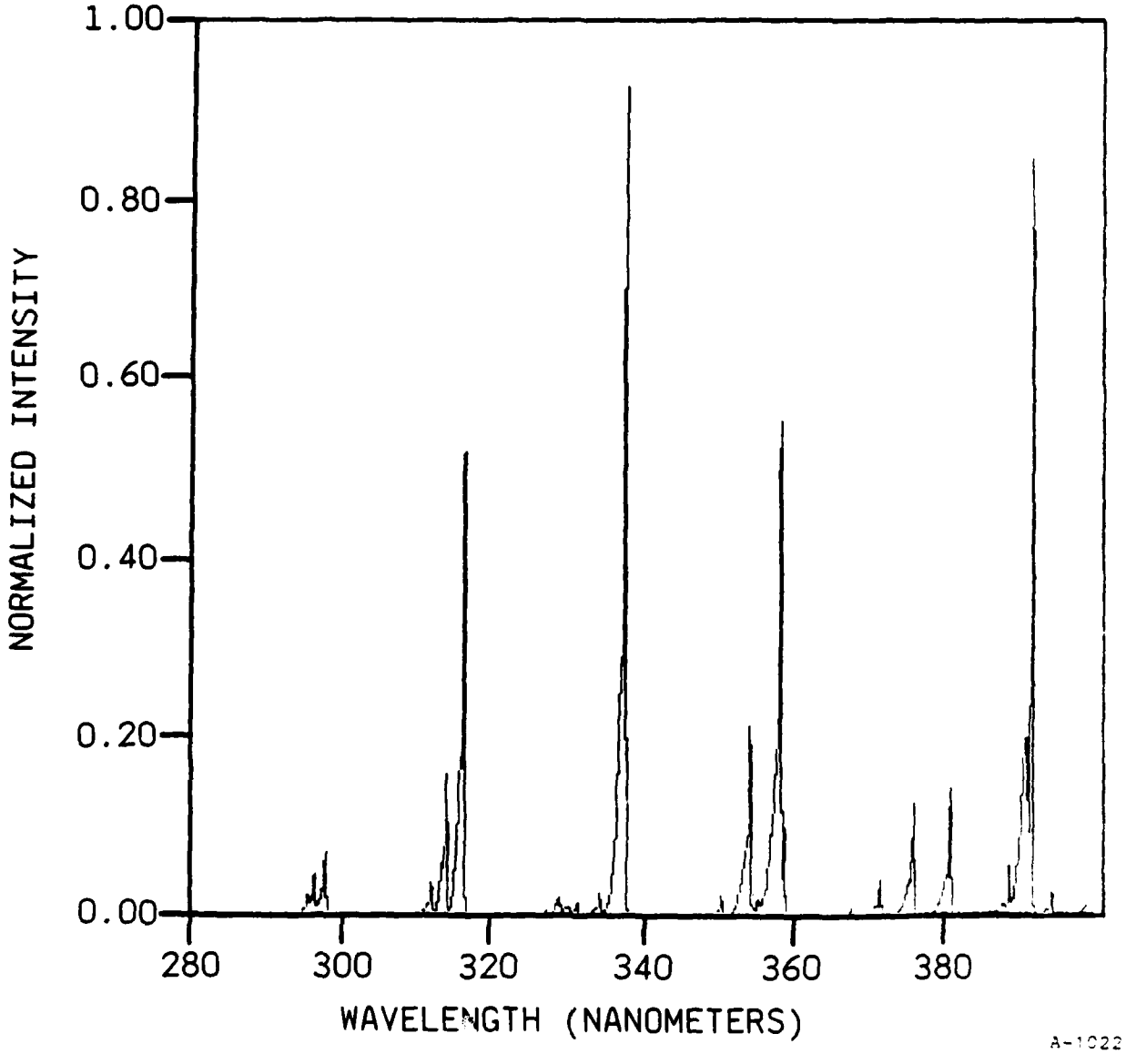
1.00
0.80
0.60
0.40
0.20
0.00
NORMALIZED INTENSITY
280
300
320
340
360
380
WAVELENGTH (NANOMETERS)
A-1022

FIGURE 3

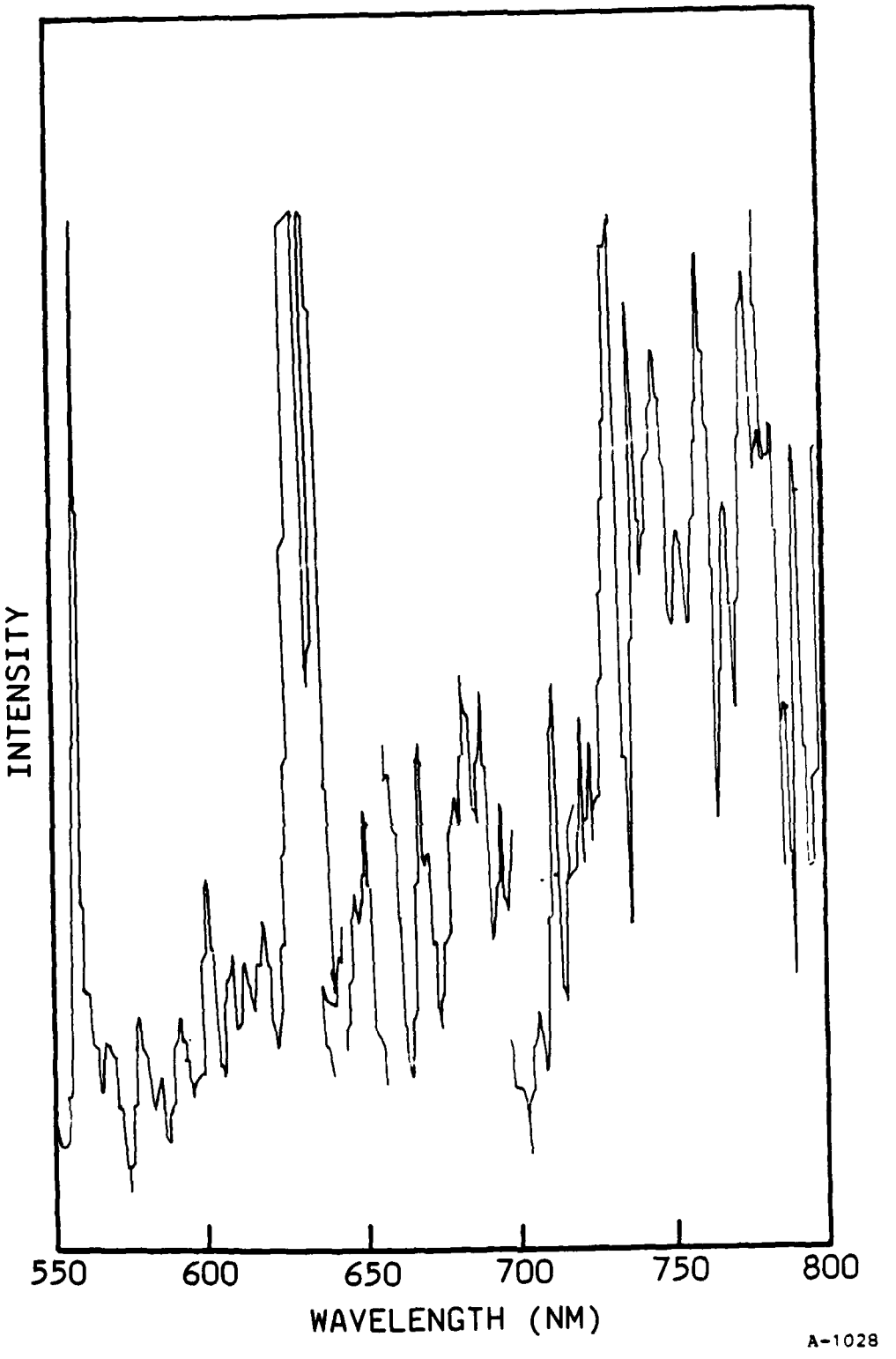

FIGURE 4a

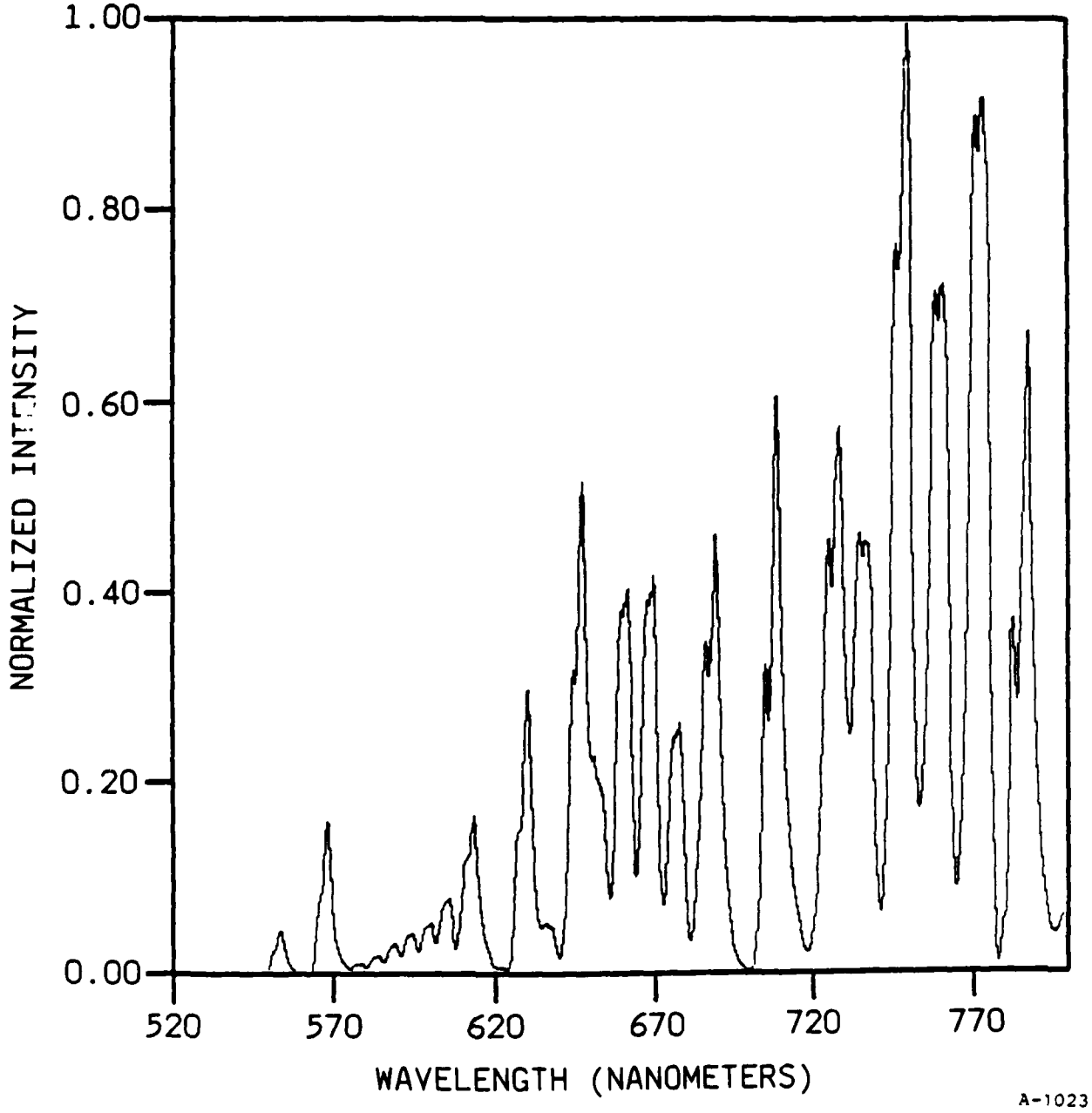
1.00
0.80
0.60
0.40
0.20
0.00
NORMALIZED INTENSITY
520
570
620
670
720
770
WAVELENGTH (NANOMETERS)
A-1023

FIGURE 4b

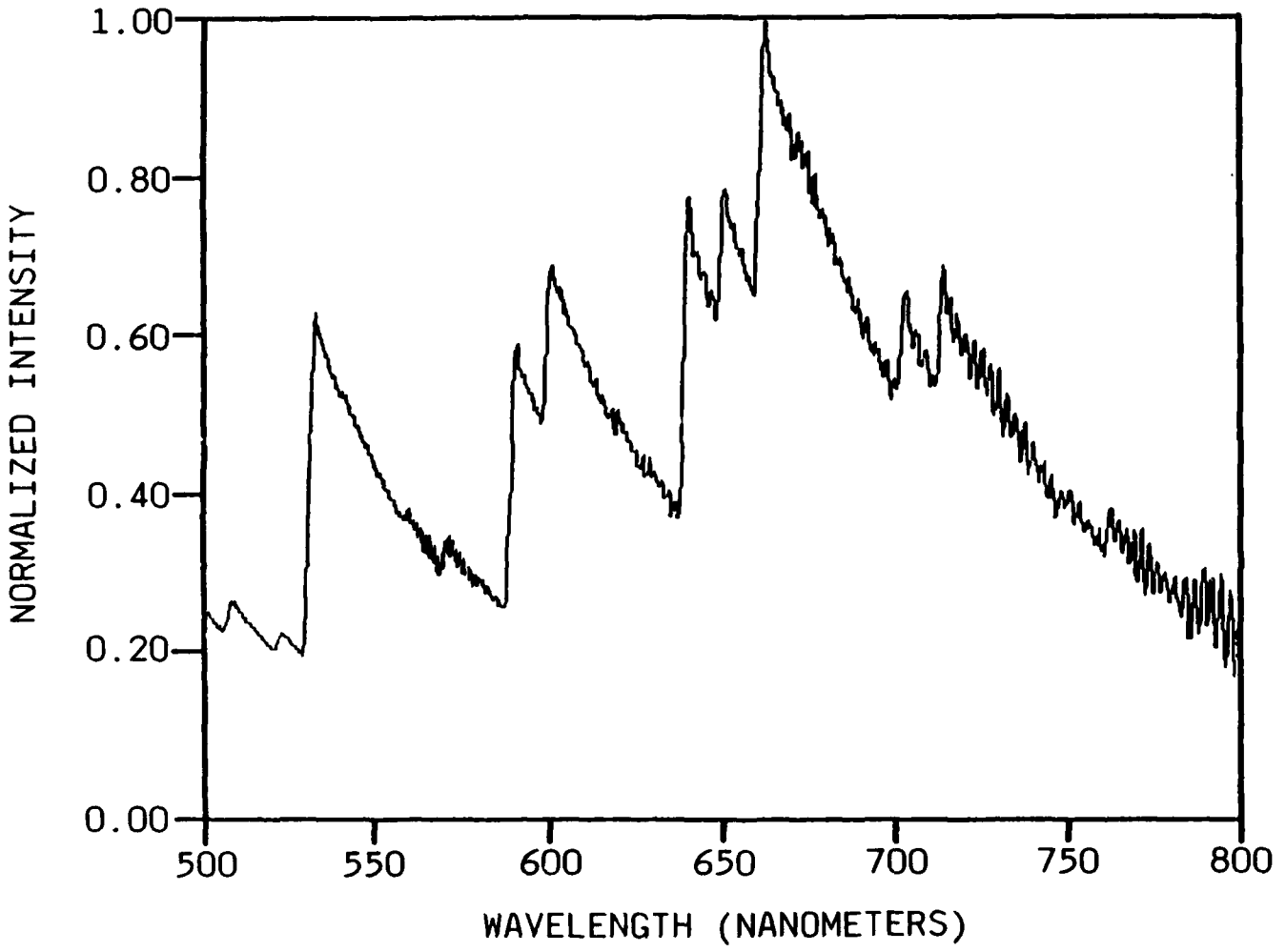

A-1024

FIGURE 5

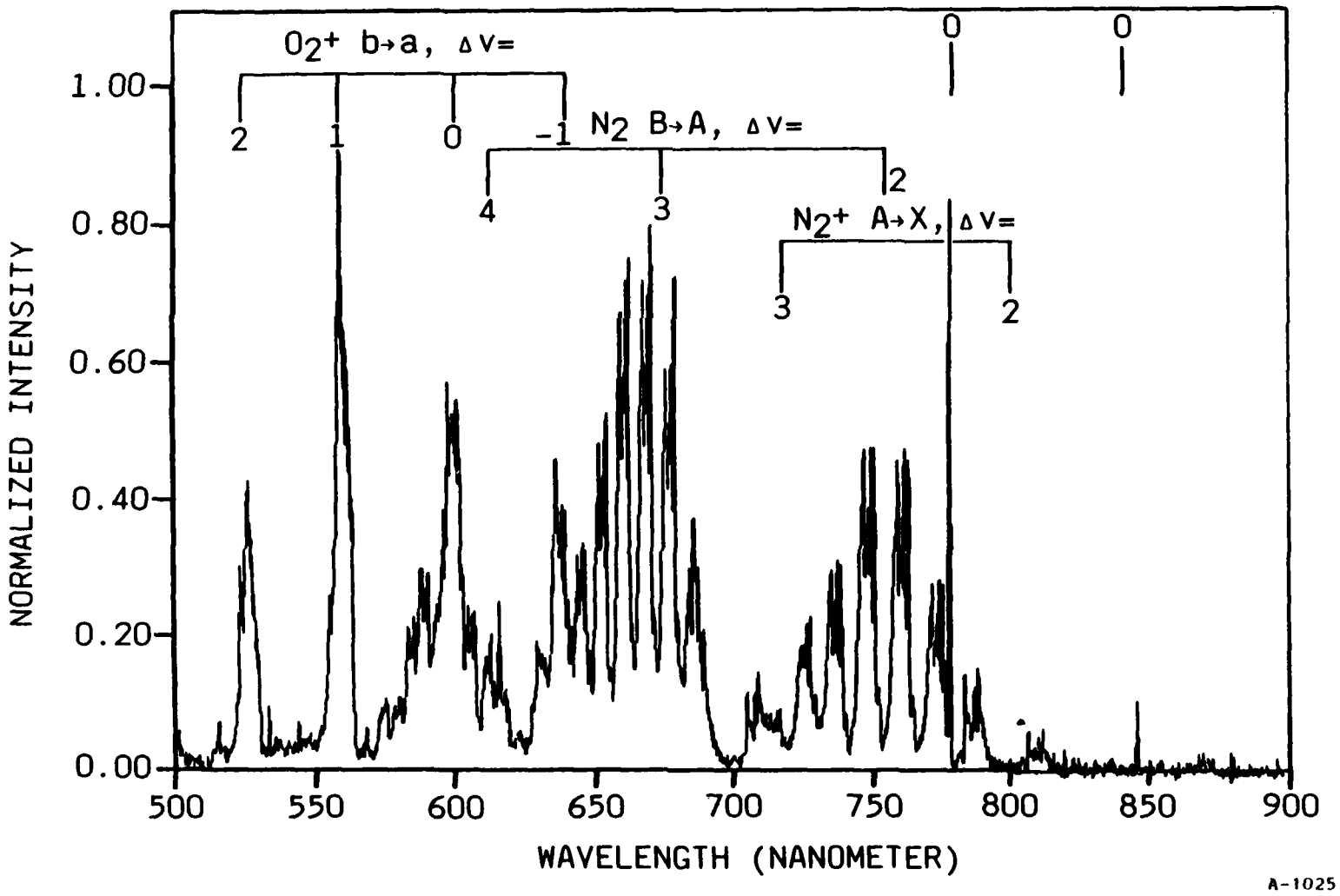
O_2^+ b→a, Δv=
2
1
0
-1
N_2 B→A, Δv=
4
3
2
N_2^+ A→X, Δv=
3
2
0
0
1.00
0.80
0.60
0.40
0.20
0.00
NORMALIZED INTENSITY
500
550
600
650
700
750
800
850
900
WAVELENGTH (NANOMETER)
A-1025

FIGURE 6

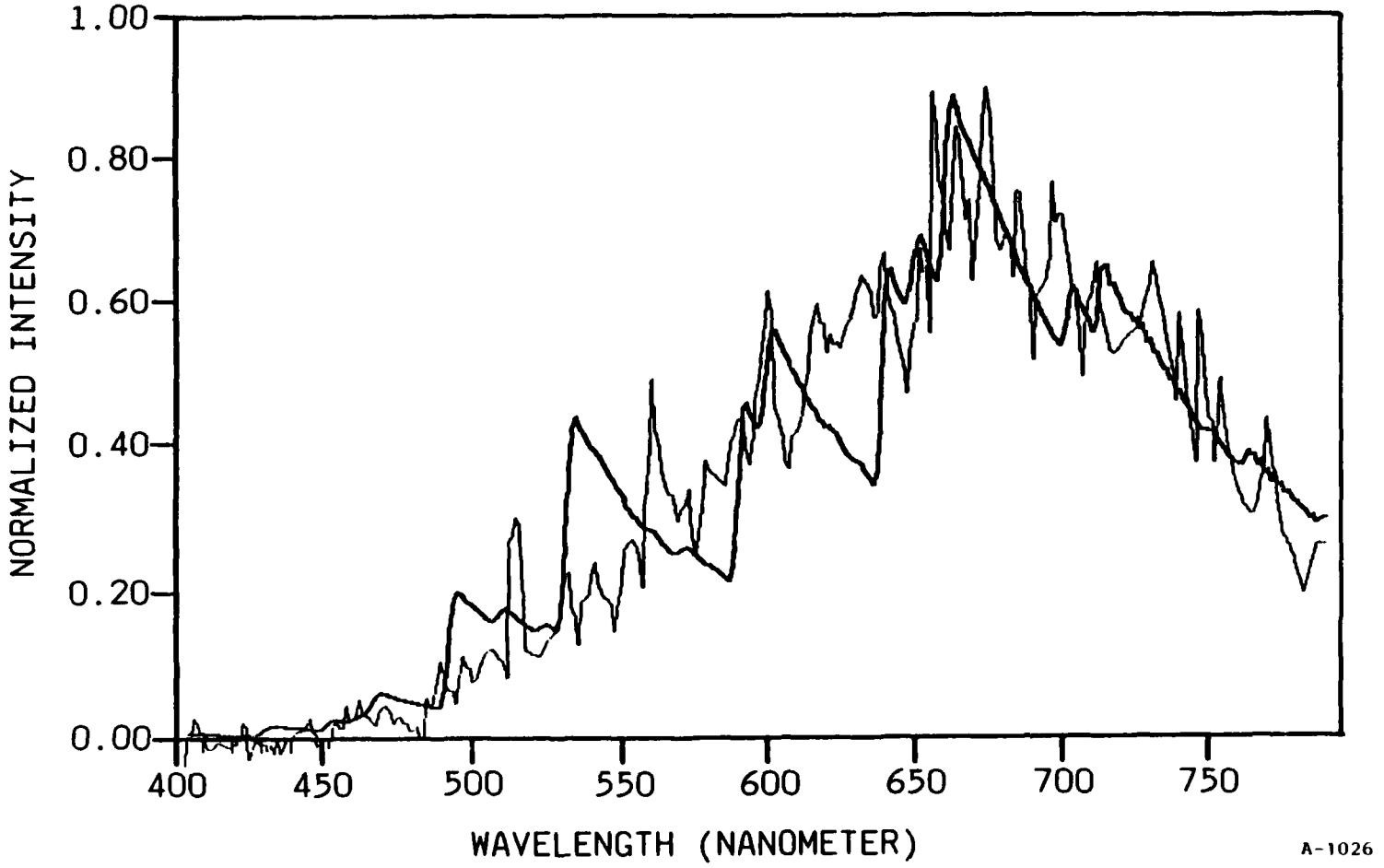
1.00
0.80
0.60
0.40
0.20
0.00
NORMALIZED INTENSITY
400
450
500
550
600
650
700
750
WAVELENGTH (NANOMETER)
A-1026

FIGURE 7

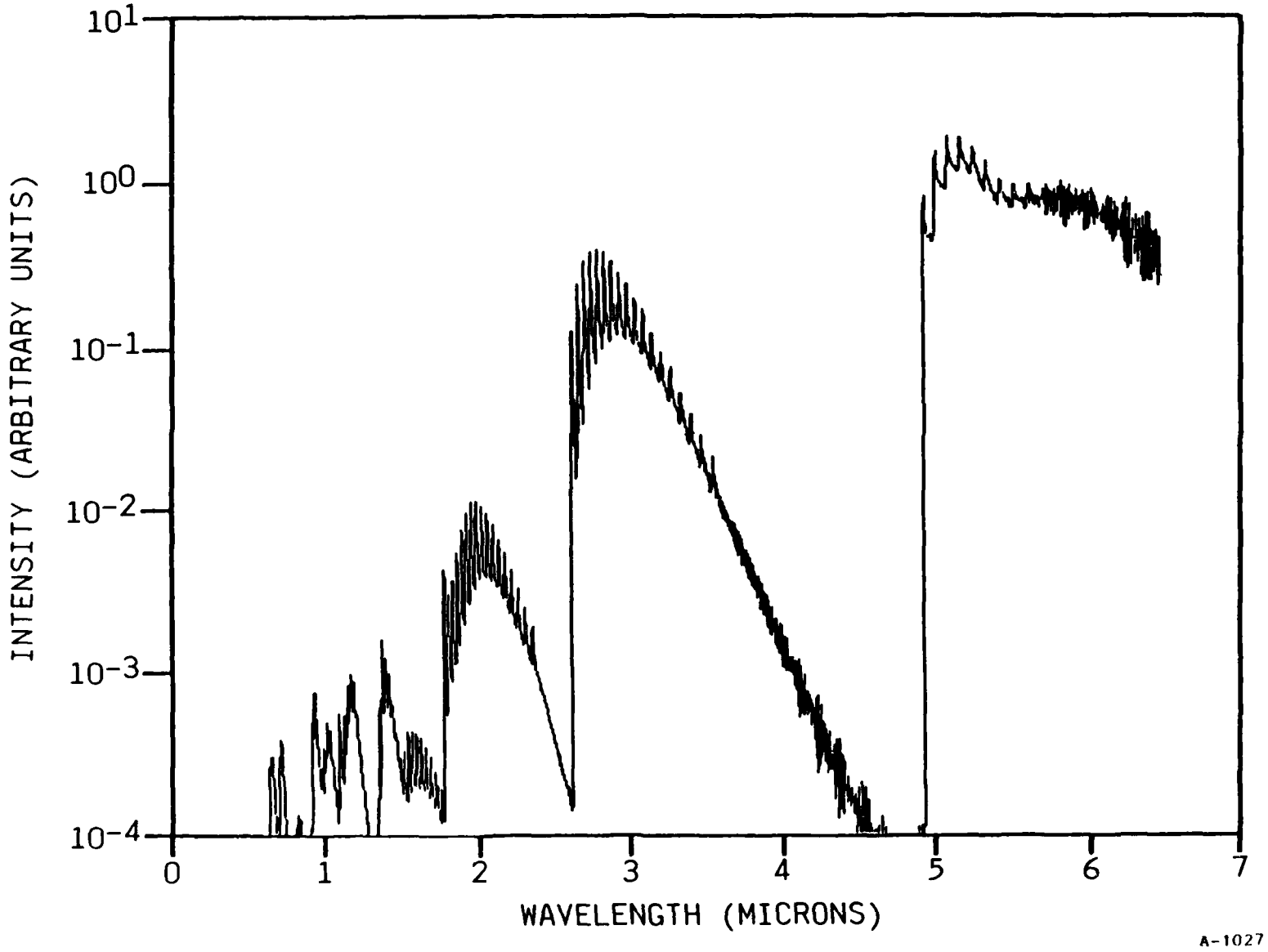
INTENSITY (ARBITRARY UNITS)
10^1
10^0
10^{-1}
10^{-2}
10^{-3}
10^{-4}
0
1
2
3
4
5
6
7
WAVELENGTH (MICRONS)
A-1027

FIGURE 8

APPENDIX D

Chemiluminescent Processes Occurring Above Shuttle Surfaces

Planetary and Space Science 34, 879 (1986)

SR-232 is reproduced in its entirety.

Chemiluminescent Processes Occurring Above Shuttle Surfaces

B.D. Green, W.J. Marinelli, and W.T. Rawlins

Physical Sciences Inc., Andover, MA

to be submitted to

The Journal of Geophysical Research
JGR-Space Physics

Abstract

The diffuse glow which occurs above surfaces exposed to the ambient atmosphere in low-earth orbit has become a source of both interest and concern for potential users of space-based observation platforms. In this paper we will consider the various chemical mechanisms which could be the source of this glow, including gas-phase and surface-catalyzed chemical reactions. The relevant species concentrations, necessary excitation rates and possible radiant intensities are calculated. We predict the spectral distributions of the emission from one of these species using a theoretical spectral model (NO(v)) and compare it with the observed spectrum of the glow. This model is also used to predict the emission shapes in the infrared other spectral region. Different glow mechanisms are likely to occur above various surfaces under different orbital conditions. Our aim is to distinguish between the various mechanisms so that remedial steps can be taken in future missions. At present the available data cannot be explained by a single mechanism although surface-catalytic processes are likely to play a dominant role in low earth orbit. These calculations provide the necessary first analytical step toward mechanism identification.

Introduction

One of the most surprising observations on the early missions of the Space Transportation System (STS) was the presence of a glow above the windward surfaces of the Shuttle during passive operational periods. This phenomenon was observed on STS-3 by Banks and co-workers [1983]. Observations on several later Shuttle missions have been performed to quantify its nature [Mende, 1983; Mende et al., 1983, 1984a,b, 1985; Swenson et al., 1985]. This glow was observed from the Shuttle cabin using a hand-held camera/ spectrometer. A visible glow has also been observed by the Atmospheric Explorer (AE) C and E satellites (Yee and Abreu [1982, 1983], and by the Dynamics Explorer (DE) B satellite (Langhoff et al. [1983; Abreu et al. [1985]). Torr and Torr [1983] have observed strong emission features not associated with the remote earth atmosphere during Spacelab 1 using their Imaging Spectral Observatory. These latter observations were from instruments exposed to the ambient atmospheric flux observing deep space, not surfaces per

se. Although the total observational data base is continuously growing observations are still sparse and apparently occasionally contradictory. No single mechanism has yet emerged as the obvious source of the glow.

The Shuttle glow is seen only over surfaces undergoing energetic collisions with the ambient atmosphere, i.e., exposed in the ram direction. Emission from surfaces in the wake are at least 10^2 weaker. Data from STS-4 clearly showed a dependence of intensity with respect to the angle of attack. No glow was observed over surfaces which were in the wake or shadowed by Shuttle structures. Photographic data has shown the spatial intensity of the glow above Shuttle tile surfaces decays exponentially with a characteristic distance of 20 cm [Yee and Dalgarno, 1983]. The meaning of the extent of the glow is subject to interpretation, either representing the spatial distance a molecule travels until it radiatively decays, the thickness of a higher density gas layer where collisional excitation or deexcitation or ionization occurs. This extent has been measured to be the same over several different surfaces on the Remote Manipulator arm [Mende and Swenson, 1985]. The glow layer thickness above the arm is smaller than the layer on the tail. The glow intensity did depend on the surface material. The glow observed in a 10m column along the surface above the rear engine pods during the STS-5 mission has been estimated to have a total visible intensity of ~300 kiloRayleighs (3×10^{11} photons/cm^2 s) [Mende, 1983]. The spectral distribution of the glow has also been measured. Based on observations from mission STS-41D, [Swenson et al., 1985] the glow is a broad spectrum (at a resolution of ~3 nm) spanning the 500 to 800 nm region and peaks in intensity in the red at 670 nm. There may be weak spectral features on this broad continuum. Infrared (1 to 3 μm) observations by Witteborn et al. [1985] indicate a substantial glow with bandpass intensities exceeding the visible by a factor of two or three. The satellite data has been analyzed to indicate a greater spatial extent in its visible bandpasses. Only coarse spectral distributions can be determined from the bandpass filters of the AE satellite. The intensity distribution observed by the satellite [Yee and Dalgarno, 1983] does not match the distribution observed above Shuttle surfaces. The ISO data [Torr and Torr, 1985] is quite spectrally structured and seems to contain emissions from many nitrogen electronically excited states as well as several as yet unidentified features. The gas-phase luminosity associated with thruster firings has also been

studied. The temporal behavior of the total (visible) luminosity has been measured; however, the spectral distribution of this glow has not been obtained to date.

Potential Chemical Excitation Mechanisms

The potential chemical mechanisms for producing Shuttle glow involve the excitation of resonant molecular emissions as a result of collisions of species in the tenuous atmosphere with the rapidly moving orbital vehicle and its surrounding effluent cloud. The dominant atmospheric constituent at orbital attitudes is atomic oxygen. Molecular nitrogen is also present. A number of other species are present in trace concentrations including NO, H, and Ar. The Shuttle orbital velocity is 8×10^5 cm/s. Thus as the Shuttle sweeps through the atmosphere, the atmospheric species energetically impact its surface. For oxygen atoms, the energy of the collision is 5 eV on average, but the atomic oxygen velocity vector ($\bar{c} = 10^5$ cm/s) will provide a distribution of collision energies (4.5 to 6.1 eV). Nitrogen molecules will have a collisional energy of 9.3 ± 1 eV.

The variety of chemical processes that could be occurring in the local Shuttle environment is shown schematically in Figure 1. As the ambient atmospheric O and N_2 enter the local Shuttle cloud, they can strike gas-phase contaminants and react with or collisionally excite them. A major portion of the atmospheric flux reaches the surface where it can excite or react with adsorbed species on shuttle surfaces. If the atmospheric N_2 strikes a surface site it can dissociate on impact or transfer energy to an adsorbed species. Atomic oxygen, if slowed by gas-phase collisions, can also be adsorbed. Surface recombination and desorption could then give rise to emissions. Finally, the ambient atmospheric species can react with surface materials. In the gaseous contaminant cloud, the prevalent species have been measured to be H_2O and CO_2 [Miller, 1983, 1984; Narcisi et al., 1983], although He, O_2, Ar, freons, cleaning agents and other species have also been detected in trace amounts. H_2O is dominantly attributable to outgassing and the flash evaporator system releases. The most likely gas phase reactions are indicated as reactions (1-3) of Table 1. Reactions (1) and (2) involve incoming O-atoms

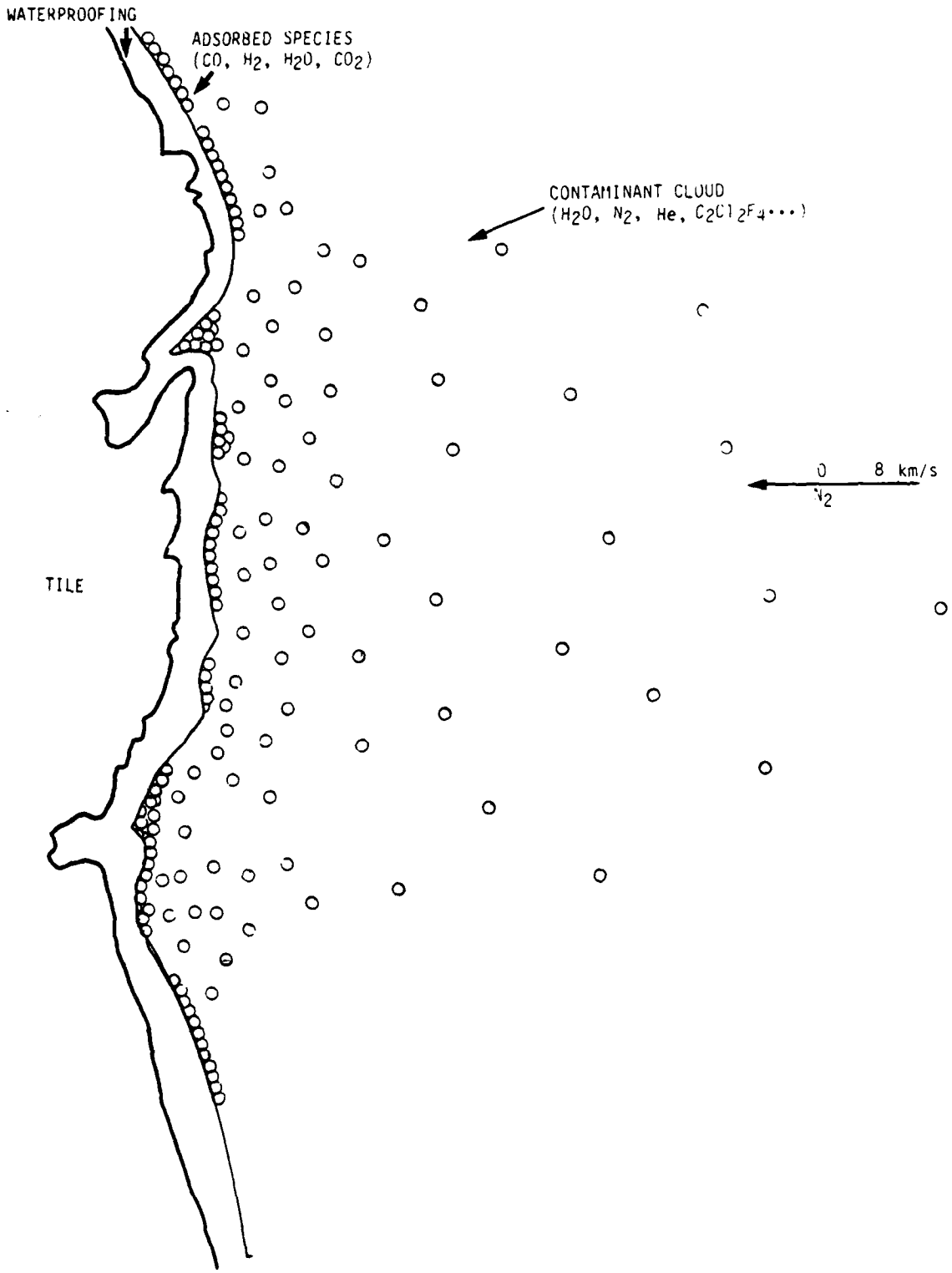

Figure 1. Conceptual Drawing of Gas-Phase/Adsorbed Species Above Shuttle Surfaces

TABLE 1

CHEMICAL REACTORS NEAR ORBITER SURFACES

	Reaction	* $4H_{298}$(eV)	* E_A(eV)/ mole	Orbital Kinetic Energy (eV)
R1	$H_2O + O \rightarrow OH(v) + OH(v)$	+0.7	0.8	5.2
R2	$CO_2 + O \rightarrow CO(v) + O_2(v)$	+0.35	2.3	5.2
R3	$N_2 + O \rightarrow NO(v) + N$	+3.2	3.3	5.2 - 14.5
R3A	N_2 (thruster) $+ O \rightarrow NO(v) + N$	+3.2	3.3	7.0
R4	$O('D) + H_2O \rightarrow OH + OH$	-1.2	0.0	-
R5	$O + H_2 \rightarrow OH + H$	+0.1	0.39	5.2
R6	$CO + M \rightarrow CO(v) + M$	+0.26*V	-	5.2 - 9.3

*At thermal energies

colliding with contamination cloud constituants. Reaction (3) involves the reflected atmospheric shock layer. In Table 1, ΔH_{298} is the enthalpy of reaction for thermal reagents at 298K, and E_A is the apparent activation energy in the Arrhenius expression for the thermal rate coefficient: $k(T) = A \exp[-E_A/kT]$. Even though all these processes are endothermic and have substantial energy barriers, in the ram velocity vector the kinetic energies involved in the collisions are sufficient (5.2 ± 1 eV) to permit the reactions to proceed. In particular, the reverse of reaction (1) is reasonably fast ($k_{-1} = 1.8 \times 10^{-12}$ cm^3/s) [NASA, 1981], while the forward reaction involving $O(^1D)$ is extremely rapid ($k_4 = 9.9 \times 10^{-11}$ cm^3/s):

$$O(^1D) + H_2O \rightarrow OH + OH \qquad \Delta H_{298} = -1.2 \text{ eV} . \tag{1}$$

Thus, the possibility exists for creating vibrationally excited CO and OH directly from these gas-phase reactions. In addition to reaction, processes 1 and 2 could simply lead to vibrationally excited H_2O and CO_2 (resulting in infrared emission). These vibrational excitation cross sections have been measured to be large [Dunn et al., 1975] at somewhat lower translational

velocities (4 to 6 km/s). Radiance levels estimated from these cross sections, contaminant levels, and atmospheric fluences are significantly les than the observed glow intensities ~ 100 kR in the infrared and much lower in the visible overtone transitions, assuming contaminant column densities of 2×10^{12} cm^{-2} and assuming: 1) rate constants 0.01 gas kinetic; and 2) that 1 percent of the product molecules are excited and emit in the visible. Gas-phase chemical reactions do not occur at a sufficient rate to generate significant glow intensities, since only 1 percent of the incoming ambient flux undergoes collisions with the H_2O contaminant cloud. However, if the column densities were considerably higher due to ram pressure build up, then gas-phase chemical reactions could contribute to the glow. The spatial extent of the glow for these processes would reflect the contamination concentration gradients above the surfaces.

A diffuse gas-phase glow has been observed during/after thruster firings. The thruster equilibrium exhaust concentrations are calculated as 33 percent H_2O, 31 percent N_2, 17 percent H_2, 13 percent CO, and 4 percent CO_2, with traces of H, O_2, and monomethylhydrazine-NO_3. However, radicals will be produced in high concentrations during the thruster firing and will persist in this environment. Likely candidates are OH and NH_2. NH_2 has a structured emission spectrum in the 550 to 600 nm region of the visible. During thruster firings exhaust species leave the nozzle at an average velocity of 3.5×10^5 cm/s. If the thruster exhaust is directed into the ram, large collisional energies can result. For example, the reaction (3a) could occur at collisional energies of up to 7 eV. Under these conditions over 15 quanta of vibrational energy in NO could be excited. Additional processes such as reactions 5 and 6c can occur where M can be any gas phase ambient species. Due to the high concentrations of neutrals released in a typical RCS thruster firing (10^{25} molecules in 80 ms), hundreds of kilorayleighs of radiance could easily arise, even assuming only one collision in 10^6 leads to a visible photon. In summary, gas-phase chemiluminescent reactions can easily account for observed bright flashes associated with thruster events. If thruster effluents are trapped above ram surfaces, these concentration enhancements could give rise to detectable chemiluminescent glows. Outgassing/offgassing contamination levels appear to be sufficiently small so that gas-phase reactions of these species cannot explain observed radiance levels in the visible. The relative

importance of various processes contributing to the glow may change in other spectral regions.

All of these gas-phase species will be adsorbed to some extent on shuttle surfaces. Self-contamination has long been recognized as a problem [Scialdone; 1972, 1985] because the mean-free-path between collisions is large enough for molecules from localized contamination sources to be collisionally backscattered over large areas of the shuttle. Mass spectrometric observations in the cargo bay detect remote thruster firings, refrigerant, and He leaks. The degree of adsorption of a given species is surface-specific. However, H_2O, the most prevalent gas-phase contaminant, is notorious for being easily physisorbed on a host of surfaces. Carbon dioxide, carbon monoxide, nitrogen, and hydrogen are also likely to be present in order of decreasing concentration. These physisorbed species are dynamically moving over surface sites, creating a surface consisting of both occupied and bare bonding sites. The molecules in the ambient flux continuously strike the shuttle surface sites. For a polished surface, there are 10^{15} sites/cm^2 and at 250 km, an ambient oxygen atom will strike a surface site once a second on average. For rougher surfaces, the number of surface sites can be much greater. Ambient O or N_2 may not react or collisionally desorb these species with unit efficiency. Thus, if contaminant/effluent molecules are adsorbed on tile surfaces, it may take minutes or even hours for the ambient flux to "clean" the surface. Contaminant mobility on the surface will allow "creep" from non-ram surfaces to replenish the physisorbed species concentration on ram surfaces. In analogy with the gas phase, reactions 1-3 and 5-7 may occur. The energy of physisorption will also have to be overcome, making the reactions slightly more endothermic. Nevertheless, there is still sufficient kinetic energy in collision that chemiluminescent reactions or collisional excitation could occur. Mende and Swenson [1985] have observed an enhanced glow above surfaces after thruster events. This enhanced luminescence persists over the range of a few through tens of seconds in rough accord with these calculations.

If N_2 in the atmospheric flux strikes a bare surface site, there is often enough energy in the collision to dissociate the N_2 with the product N atoms remaining physisorbed on the surface. Prince [1985] argues there is no experimental evidence supporting this hypothesis. Ambient N and NO (which should

dissociate on impact) will provide N on the surface. The atomic oxygen and nitrogen in the ram flux may not be readily adsorbed since the energy of the collision is not channeled into potential energy and must be dissipated through other channels. If reflected oxygen atoms undergo numerous collisions with contaminant species, they may remain in the vicinity of the surface and be adsorbed. Thus, the relative concentration of O and N on the surfaces is unknown. The nitrogen and oxygen atoms on the surface can then recombine to excited molecular states. This class of mechanisms has been considered previously [Green, 1984 and Green et al., 1985]. Recombination can give rise to N_2, O_2, NO, and NO_2. All these species have been observed in heterogeneous recombination in the laboratory by varying mole fractions of N and O [Chu, et al, 1985]. There appears to be no strong preference for recombination partner; i.e., N_2 recombination is not excluded in the presence of O atoms.

In this mechanism, the atmospheric species are adsorbed on spacecraft surfaces upon collision, then recombine into excited molecular states as they leave the surface. Thus the surface acts as a catalytic substrate for recombination. The most prevalent adsorbed atoms will be N and O which may recombine to give: N_2 electronically excited which fluoreses in the visible and in the infrared O_2 electronically excited into many states giving rise to a much more long lived glow; and NO vibrationally and electronically excited. The molecular states populated will depend on the nature of the interaction between excited species and the particular surface material. The same molecular species could give rise to different glow intensities and even different spectral distributions over various surfaces. Spectrally resolved emissions can thus provide insight into the dynamics of the creation process. For these surface-catalyzed recombinations (and for the surface reactions considered next) the extent of the glow has been interpreted to represent the region over which excited species are emitting -- the product of the emitter velocity and radiative lifetime of the excited state. If radiators leave the surface at thermal velocities, then the corresponding radiative lifetimes are less than a millisecond. If their exit velocity is faster, the lifetime is shorter still, approaching 50 μs if the atmosphere/surface interaction is elastic.

Evidence for this surface recombination is found in mass spectrometer data from satellites. Engebretson [1985] has observed both NO and NO_2 at

enhanced levels in a semi-open source M.S. on AE-C and D and in a closed source spectrometer on DE-B. NO is formed by a fast process and is observed initially. NO_2 is observed at later times. The observed concentrations were dependent on surface temperature.

A recent study of the Shuttle glow led Swenson et al. [1985] to conclude that the emission is due to NO_2 which is formed on the surface of the Shuttle. They postulate that recombination of N and O atoms forms an NO molecule which sticks to the surface long enough to react with another O atom to give an excited NO_2. Consequently, the glow should depend on $[O]^2$ and on [N]. The observations by Yee and Abreu [1983] on AE indicate that the intensity of the glow varies linearly with [O] in two wavelength bands: 6563 nm and 7320 nm. Thus, NO_2 may not be the major constituent of the satellite glow, or the satellite and Shuttle glows arise from different mechanisms.

The above chemical mechanisms can produce chemiluminescent excitation up to the level of reactant kinetic energies (as modified by reaction exo- or endothermicities). Plasma excitation mechanisms, as suggested by Papadopoulos [1984], involve energetic (~100 eV) electrons which could excite higher molecular electronic states and even dissociate or ionize species. Thus, significant spectral differences are expected as described by Kofsky [1984], and Green et al [1985].

In addition to the gas-phase and surface interactions, a fraction of the ambient flux will penetrate through the cloud, reach Shuttle surfaces and possibly undergo reactions there which lead to the formation of new species. If these reaction products are released into the gas phase, they could potentially contribute to glow intensities. Slanger [1983] was the first to suggest that these reactions could contribute to spacecraft glow. A dependence of the intensity of the glow on surface material has been observed by Mende, et al. [1984b, 1985]. Since the Shuttle glow is observed only on surfaces in the ram direction, either a density effect or the kinetic energy of the incoming atmospheric species is likely required for reactions to occur and thus this kinetic energy can be added to the reaction enthalpy so that reactions which are endothermic at thermal energy become exothermic and proceed rapidly when on-orbit. Reactions of this nature are the subject of a separate paper [Green and Murad, 1985].

Spectral Comparisons with Orbital Observations

Of the three sets of spectrally resolved observations described in the introduction, only the Lockheed data [Swenson et al., 1985] provides a spectrum of the glow above surfaces. The ISO data contains emissions from N_2^+ (at least partially of atmospheric origin) as well as a complex spectrally structured emission in the red. Similarly, the satellite measurements looked radially outward from the spacecraft and observed only a portion of the glow layer. Spectral content of the AE data is limited to six filter bandpasses (~20Å) between 280 and 732 nm [Yee and Abreu, 1982].

In order to quantify emission levels, we have developed at PSI spectral synthesis codes which predict very high-resolution molecular electronic and vibrational spectra for a host of molecules and band systems. These "basis functions" are then convolved with the appropriate slit function for each application. The emission from various states and species can be combined to give a composite spectrum. Least squares fitting is used to adjust the individual state populations to achieve a "best" fit. The relative emitting state populations are the end product of the analysis.

In light of the above kinetic discussion, overtone vibrational transitions for OH, CO, and NO were created. A synthetic spectrum of NO overtone transitions is shown in Figure 2. These transitions involve high vibrational levels of the ground electronic state NO($v < 19$) undergoing transitions with Δv = 6-9 between 500 and 800 nm. Because the molecular dipole moment functions are not well known, there are large uncertainties in the spectral intensities. The band positions are quite accurately known and the relative spectral shape should be accurate enough to provide insight.

The Swenson et al. [1985] data is also presented in Figure 2. Upon inspection of this broad spectrum, there are several striking features. The "noise" level is not constant but is much larger where there is spectral intensity. The "noise" spikes are often several resolution elements wide. Both these observations suggest that the "noise" features may be real structure. Finally, the strongest "noise" spike falls at 520.0 nm, exactly where $N(^2D)$ atmospheric emission line occurs. Prompted by these observations, we felt

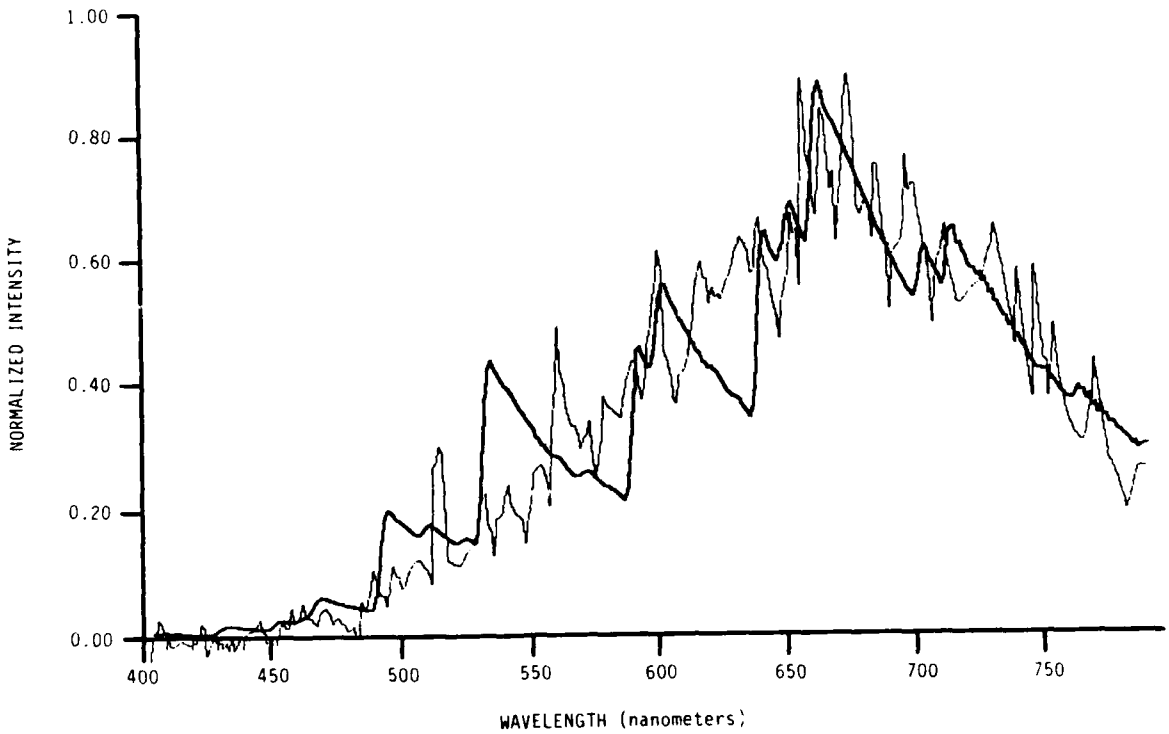

Figure 2. Comparison of NO Vibrational Overtone Transitions with Response-Corrected Lockheed Glow Data

that structure possibly existed in the broad continuum--that Mende's data were perhaps less noisy than they appeared. Nitrogen electronic spectra (including First Positive) were unable to match the broad spectral features for any vibrational or rotational distribution. However, in response to our kinetic analysis, we performed a least-squares fit of NO overtone vibrational bands to the observed spectrum. The NO emission series are more structured than the data; nevertheless, several spectral features are reproduced. The present calculations extend only to v' = 19; inclusion of higher vibrational levels of NO would tend to fill in the gaps in the computed spectrum. Inclusion of additional radiators such as OH may also improve the comparison. We feel that the presence of vibrational emissions at some level in this spectrum cannot be excluded. The radiative lifetime of high vibrational levels of NO is several milliseconds. In order to match the observed extent of the glow, the excited molecules would be constrained to travel at less than thermal velocities. This is quite possible since reaction energy partitioning on the surface may

leave little kinetic energy in the desorbed molecule. Alternatively, if there exists a high density gas layer above ram surfaces, collisional scattering of the excited species will give it an effectively smaller velocity outward from the surface. The accuracy of our prediction is compromised by lack of knowledge of the dipole moment function of NO in its ground state. Vibrational levels greater than v = 19 can certainly be populated in the surface recombination process. We felt uncertain of our predictions above this level and limited our code accordingly.

The above example is meant to illustrate that diatomic emission could be the source of the visible glow above surfaces. This approach was also applied to overtone vibrational bands of CO and OH, both of which are (along with NO) ubiquitous products of the chemical mechanisms outlined above. While CO overtone transitions ($\Delta v=6-9$) appear not to have the same intensity distribution as the observed glow spectrum, the overtones of OH also bear a striking resemblance to the distribution and structure of the data at high rotational temperatures (~5000K). Unfortunately, it is difficult to make conclusive arguments about OH due to the inadequacy of the spectroscopic data base describing the transition probabilities and branching ratios in this wavelength range. Surface catalytic recombination would be likely to give rise to these vibrationally excited species as well as NO_2. The dominant radiator will certainly depend on the orbital environment, the viewing geometry (and distance above surfaces) and spectral region. Indeed, estimation of the significance of the glow in other spectral regions must await a better understanding of the mechanisms responsible. Kofsky and Barrett [1985] recently estimated that NO_2 would not be an extremely bright radiator in the infrared above Shuttle surfaces. On the other hand, if NO were a significant contributor in the visible region, then the glow intensity in the infrared would be orders of magnitude brighter than the visible. (The spectral distribution of the intensity would obviously depend on the initial vibrational distribution.) NO favors single or double vibrational quantum loss by radiation and thus many photons can be emitted by a single highly vibrationally excited molecule. As an illustration, the visible-infrared vibrational emission spectrum of NO with a 5000K Boltzmann vibrational distribution is plotted in Figure 3. The intensity axis is in photons and is logarithmic. The infrared fundamental and

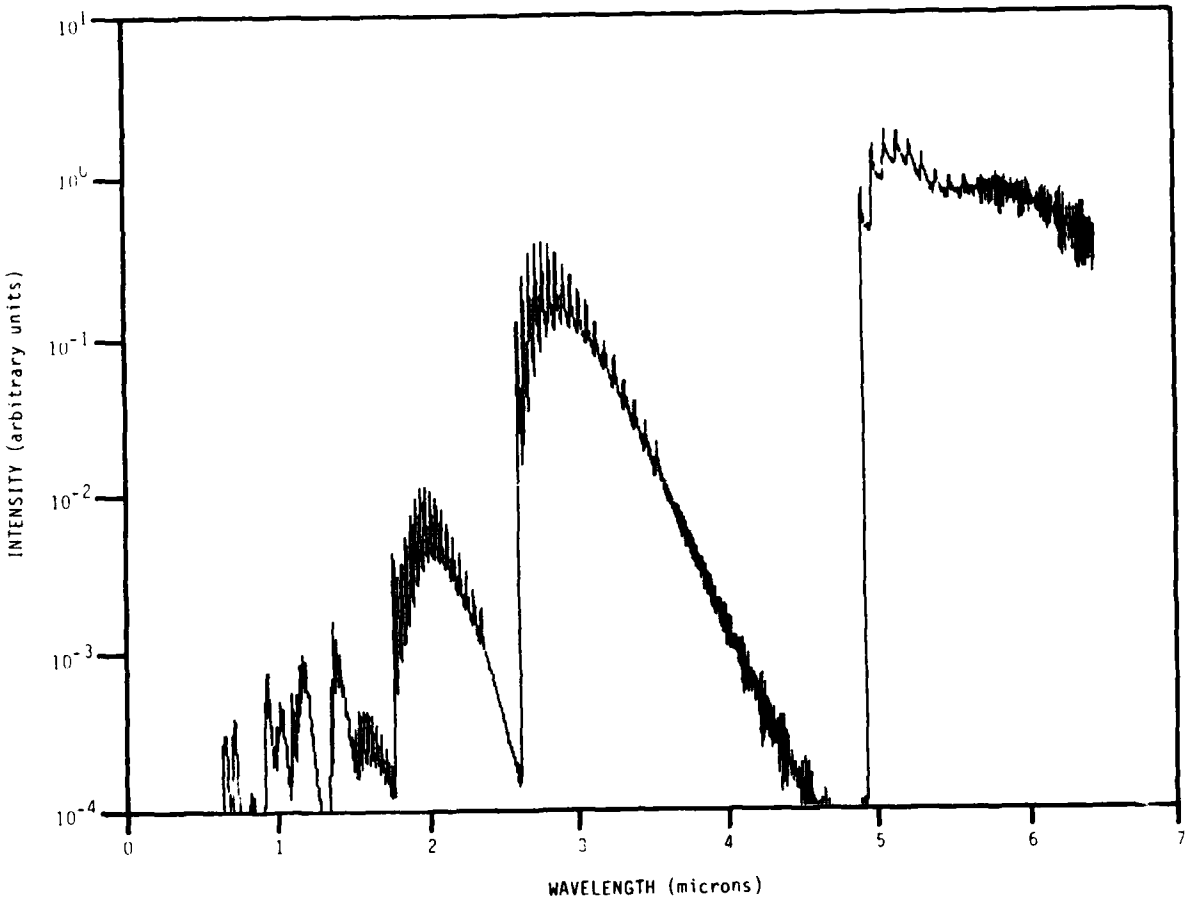

Figure 3. Plot of NO Vibrational Emission Between Wavelengths 0.5 and 6.5 μm. NO emission is much stronger in the infrared.

first overtone bands are orders of magnitude more intense than the visible emissions. This suggests potential problems for IR space-borne observations of deep space or the Earth's atmosphere if NO contributes to the glow since atmospheric radiances are in the MegaRayleigh range. Similar calculations have been performed for OH by Langhoff et al., [1983].

Summary

A review of some of the types of chemical reactions that could occur above Shuttle surfaces has indicated reactions of thruster effluents or outgassing adsorbed on surfaces with the ramming ambient flux could easily account for observed radiance levels. Reactions of ambient species on surfaces to form $N_xO_y^*$ are also likely. Gas-phase reactions over the inactive

Shuttle are too infrequent to explain the observed luminescence unless a substantial pressure buildup above ram surfaces is occurring. Gas-phase reactions in the thruster exhaust plume are also capable of generating mega-Rayleigh intensities. Plasma processes may be occurring with these dense thruster plumes as well.

A spectral fitting analysis has suggested that chemical processes will play a role in observed glows. A number of chemiluminescent mechanisms have been suggested as giving rise to vibrationally excited OH, CO, and NO, in addition to previously suggested surface recombination mechanisms such as NO_2 or N_2^*. Vibrational overtone emissions may well be present in the glow data.

Due to the variability of the shuttle's environment, it is likely that there will be conditions on-orbit when different chemical and plasma mechanisms will dominate glow emission. An alarming aspect of the ISO data is that even looking out of the payload bay and not observing any Shuttle surfaces, a glow spectrum is obtained underlying far-field atmospheric emissions. The key to our understanding the glow phenomenon lies in an extended data base which includes improved spatial, spectral, and surface specific observations. It appears that a number of processes can provide for unique glows of different characteristics under the wide range of on-orbit conditions. Thus, although several ingenious detection systems have been flown to characterize the glow, we have not been able to assign the mechanism(s) responsible over the variety of operational conditions and locales. We suggest that a series of complementary experiments be assembled to systematically observe the glow with an aim to discriminate between the various classes of mechanisms and even to identify the dominant radiant species for a given on-orbit scenario. This extension of the data base will allow the various physical regimes to be quantified, allow the key mechanisms to be identified, and permit meaningful remedial actions to be taken by future mission planners.

Acknowledgements

The authors acknowledge several useful discussions with E. Murad (AFGL) and G. Caledonia (PSI). This work was supported by the Air Force Geophysics Laboratory.

References

Abreu, V.J., Skinner, W.R., Hays, P.B., and Yee, J.H., Optical Effects of Spacecraft-Environment Interaction: Spectrometric Observations by the DE-2 Satellite, J. Spacecraft Rockets 22, 177, 1985.

Banks, P.M., Williamson, P.R., and Raitt, W.J., Space Shuttle Glow Observations, Geophys. Res. Lett., 10, 118, 1983.

Chu, A.L., Reeves, R.R., and Halstead, J.A., Surface Catalyzed Formation of Electronically Excited Nitrogen Dioxide and Oxygen, submitted to J. Phys. Chem., 1985.

Dunn, M.G., Skinner, G.T., and Treanor, C.E., Infrared Radiation from H_2O, CO_2, or NH_3 Collisionally Excited by N_2, O, or Ar, AIAA J., 13, 803, 1975.

Engebretson, M.J., AE and DE Mass Spectrometer Observations Relevant to the Shuttle Glow, Proceedings of the Second Workshop on Shuttle Glow, NASA/MSFC, May 1985 (In press).

Green, B.D., Atomic Recombination into Excited Molecular States - A Possible Mechanism for Shuttle Glow, Geophys. Res. Lett., 11, 576, 1984.

Green, B.D., Caledonia, G.E., and Wilkerson, T.D., The Shuttle Environment: Gases, Particles, and Glow, J. Spacecraft and Rockets, 22, September 1985.

Green, B.D. and Murad, E., The Shuttle Glow as an Indicator of Material Changes in Space, accepted by Planetary Space Sci., 1985.

Kofsky, I.L., Spectroscopic Consequences of Papadopoulos' Discharge Model in Spacecraft Ram Glows, Radio Sci., 19, 578, 1984.

Kofsky, I.L. and Barrett, J.L., Infrared Emission from NO_2^* and NO^* Desorbed from LEO Spacecraft Surfaces, submitted to J. Spacecraft and Rockets, June 1985.

Langhoff, S.R., Jaffe, R.L., Yee, J.H., and Dalgarno, A., The Surface Glow of the Atmospheric Explorer C and E Satellites, Geophys. Res. Lett., 10, 896, 1983.

Mende, S.B., "Vehicle Glow," AIAA-83-2607-CP, presented at Shuttle Environment and Operations Meeting, Washington, DC, 1983.

Mende, S.B., Garriott, O.K., and Banks, P.M., Observations of Optical Emissions on STS-4, Geophys. Res. Lett., 10, 122, 1983.

Mende, S.B., Nobles, R., Banks, P.M., Garriott, D.K., and Hoffman J., Measurement of Vehicle Glow and Space Shuttle, J. Spacecraft Rockets, 21, 374, 1984.

Mende, S.B., Banks, P.M., and Klingelsmith, III, D. A. Observation of Orbiting Vehicle Induced Luminosites on the STS-8 Mission, Geophys. Res. Lett., 11, 527, 1984b.

Mende, S.B. and Swenson, G.R., Vehicle Glow Measurements on the Space Shuttle, AIAA-85-0909, presented at AIAA 20th Thermophysics Conference, Virginia, 1985, submitted to J. Spacecraft.

Miller, E., STS-2, -3, -4 Induced Environment Contamination Monitor (IECM) Summary Report, private communication.

Miller, E., ed, Induced Environment Contamination Monitor - Preliminary Reports from the Spacelab 1 Flight, private communication.

Narcisi, R.S., Trzcinski, E, Frederico, G., and Wlodyka, L., The Gaseous Environment Around Space Shuttle, AIAA-83-2659-CP, Presented at Shuttle Environment and Operations Meeting, Washington, D.C., 1983.

NASA Panel for Data Evaluations, Chemical Kinetic and Photochemical Data for Use in Stratospheric Modeling, JPL Publication 81-3, 1981.

Papadopoulos, K., On the Shuttle Glow (The Plasma Alternative), Radio Science, 19, 571, 1984.

Prince, R.H., On Spacecraft-Induced Optical Emission: A Proposed Second Surface Luminescent Continuum Component, Geophys. Res. Lett. 12, 453, 1985.

Scialdone, J.J., Self-contamination and Environment of an Orbiting Spacecraft, NASA-TN D-6645, May 1972.

Scialdone, J.J., An Estimate of the Outgassing of Space Payloads, AIAA-85-0957, presented at AIAA 20th Thermophysics Conference, Virginia, 1985.

Shawhan, S.D., Murphy, G.B., and Pickett, J.S., Plasma Diagnostics Package Initial Assessment of the Shuttle Orbiter Plasma Environment, J. Spacecraft, 21, 389, 1984.

Slanger, T.G., Conjectures on the Origin of the Surface Glow of Space Vehicles, Geophys. Res. Lett., 10, 130, 1983.

Swenson, G.R., S.B. Mende, and K.S. Clifton, Ram Vehicle Glow Spectrum: Implication of NO_2 Recombination Continuum, Geophys. Res. Lett., 12, 97, 1985.

Torr, M.R. and D.G. Torr, A Preliminary Spectroscopic Assessment of the Spacelab 1/Shuttle Optical Environment, J. Geophys. Res., 90, 1683, 1985.

U.S. Standard Atmosphere 1976, 227 pp., U.S. Government Printing Office, Washington, DC, October 1976.

Witteborn, F.C., O'Brient, K., and Caroff, L., Measurements of the Nighttime Infrared Luminosity of Spacelab 1 in the H- and K-bands, private communication.

Yee, J.H. and Abreu, V.J., Optical Contamination on the Atmospheric Explorer-E Satellite, Proc. SPIE-Soc. Opt. Eng., 338, 120, 1982.

Yee, J.H and Abreu, V.J., Visible Glow Induced by Spacecraft - Environment Interaction, Geophys. Res. Lett., 10, 126, 1983.

Yee, J.H. and Dalgarno, A., Radiative Lifetime Analysis of the Spacecraft Optical Glow, AIAA-83-2660-CP presented at Shuttle Environment and Operations Meeting, 1983.

APPENDIX E

Radiance Calculations for IMPS/Glow Experiments

We had the pleasure of attending an IMPS Workshop on 31 July 1985. A wide variety of exciting experiments are being incorporated into this pallet to be flown on the Space Shuttle. That mission is planned to be at 350 km in a polar orbit. One experiment in particular, IMPS/GLOW, was described by L. Broadfoot and E. Murad (P.I.). It is designed to gather data which will provide a much better understanding of the chemical and plasma mechanisms occurring above surfaces in space. Glow is but one manifestation of these processes. The IMPS/GLOW experiment will cover the broad spectral range of 1150-9000Å. During pallet free flight it will observe a variety of surfaces and materials over a range of orbital conditions and viewing geometries. It has a quoted sensitivity of 1 R-s; i.e., a signal of 1R $(10^6$ photons/cm^2-s$)$ in its 3Å resolution element will have a signal-to-noise (S/N) of 1 if a 1s integration time is used. In order to assist in defining useful and successful measurements for that experiment, PSI has estimated the expected radiance levels based solely on previous orbital glow observations neglecting mechanisms and variabilities such as surface material. These orbital observations include Mende's data from STS 3, 5,[1] and 41D[2], the Atmospheric Explorer satellite data as analyzed by Yee and coworkers,[3,4] and data from the Imaging Spectrometer Observatory (ISO) as analyzed by M. and D. Torr.[5]

S. Mende based on film data from a hand held camera-spectrophotometer estimated glow radiance levels as being 300 kR at 305 km and about 1 MR at 240 km. Attempts to observe glows at 400-500 km have not been successful. The glow is below the sensitivity of this instrument at those altitudes.

The above radiances were for a specific viewing geometry - along the surface of the rear stabilizer fin, a 10m long path. The spectral

distribution of this glow has also been published and is reproduced in Figure 1. The integrated radiance (300 kR) was partitioned into 50 nm bandpasses based on this spectral distribution. The resulting intensities are presented in Table 1. The next column converts these radiances to R/Å. In order to estimate the glow intensities expected at IMPS altitudes (350 km) the glow intensity was scaled as atomic oxygen density. The AE satellite data supports this scaling at high altitudes.[4] This will result in an upper bound estimate of the glow because the other major atmospheric constituents fall off more rapidly with altitude. Since the US Standard Atmosphere 1976 was used, no latitudinal variability was assumed. The expected radiances from a 10m column along a ram surface at 350 km are given in the next column of the table. The column of glow observed by the IMPS experiment will vary considerably - 20 cm for a radial view, 10m along the tail fin, up to 37.5m along the bottom of the shuttle. Thus, the normalized radiances R/Å-m of glow column observed are given in the table also. Finally, the S/N per meter path for a 1s integration time is given for each bandpass in the last column of the table based on a 1/3 R/Å radiance giving a S/N of 1 at 1s integration time. For example, for a 1s observation time, a 1m surface path would exhibit a glow at 6800Å which would have a S/N of 10. The expected S/N levels are plotted as a function of wavelength for several integration times in Figure 2, assuming S/N scales as (integration time)$^{1/2}$. From this figure we observe that we would have to integrate for 100s to attain a S/N of 10 for the glow levels expected at 4900Å.

The AE satellite data is acquired using filtered bandpass (20Å) radiometers looking radially outward from the satellite surface through a telescoped baffle. This baffle extends 8 cm beyond the surface of the satellite so that a portion of the glow layer is missed. Thus, this data provides a lower bound on expected radiance levels. The 656.3 and 732 nm channels exhibited the strongest glow radiances. Both these bands have signal levels of about 1R within their bandpass at 350 km altitude. This corresponds to a S/N of 0.15 for a radial view with 1s observation (integration time); i.e., an observation time of 45s would be required to exceed a S/N of 1.

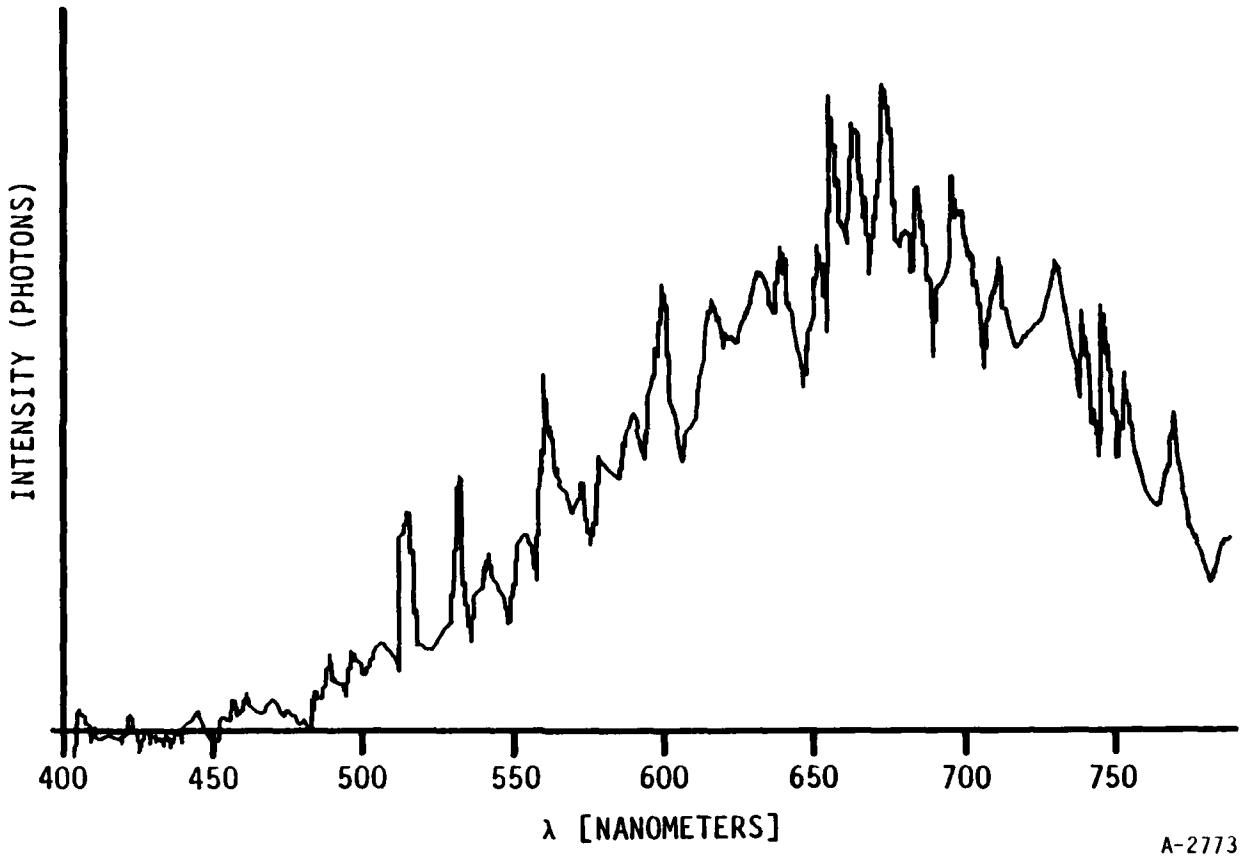

Figure 1. Glow Above Shuttle Stabilizer Fin (Ref.2)

Table 1. Glow Radiance Estimates

Shuttle Data (Ref. 2) in Bandpass (nm)	Intensity in Bandpass at 305 km (kR)	R/Å at 305 km	R/Å* at 305 km	R/Å-m Path at 305 km	S/N Per m Path** (τ=1s)
400-450	0.8	1.6	0.3	0.03	0.1
450-500	5	10	2	0.2	0.7
500-550	18	36	7	0.7	2
550-600	39	78	16	1.6	5
600-650	60	120	24	2.4	8
650-700	78	156	31	3.1	10
700-750	60	120	24	2.4	8
750-800	39	78	16	1.6	5
Sum	299.8 kR	300 kR			

*Equatorial O profile assumed

**S/N = 1 for radiance of 1/3 R/Å with 1s integration time

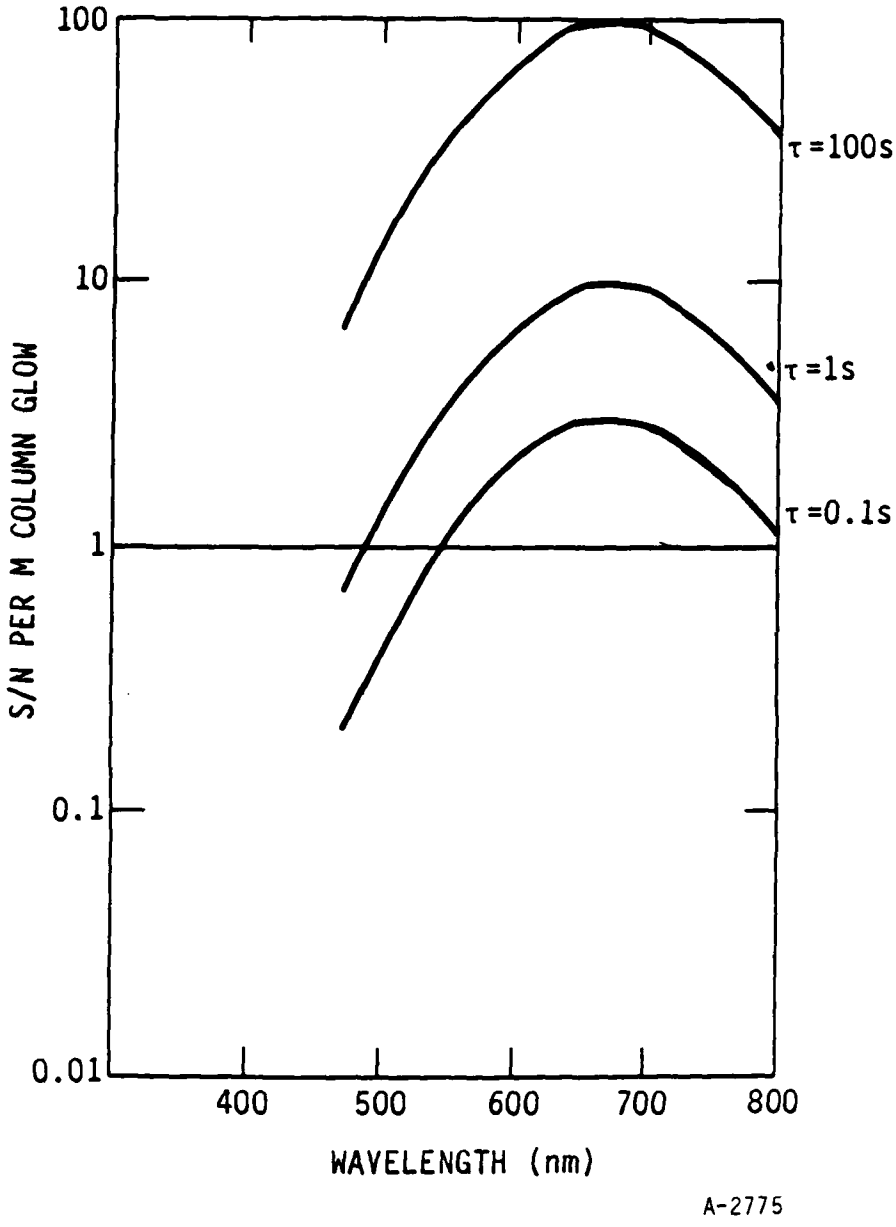

Figure 2. IMPS Glow Predicted Signal-to-Noise Levels Per Meter Column Above (and Along) Surfaces for Several Integration Times (τ). Assumed 350 km Altitude, Scaling of Mende Data as [O] Concentration, Sensitivity of 1 R-s and $\tau^{1/2}$ Sensitivity Scaling.

The ISO experiment was on STS-9 (Spacelab 1). It looked radially outward from the bay. This data exhibited a complex spectrum spanning the UV through near IR. The interaction surface/source of the glow has not been determined for these data. The UV intensities have been attributed in part to earth airglow.[6] The residual intensities have been used as an upper bound of any surface glow between 115 and 415 nm. At 250 km this glow is less than 7.5 R/Å between 1150 and 2300Å and is less than 5 R/Å between 2300 and 4150Å. At 350 km (again scaling as 0) these radiances become <0.5 R/Å respectively for a radial view.

All three sets of data are presented in Figure 3 for a radial view (such as would be seen by the IMPS/GLOW experiment when looking into ram). Surprisingly the three sets of observations agree to within an order of magnitude. Considering that large assumptions have been made and that two sets are bounds, the agreement is quite good. The AE data observed glow above insulation blankets; ISO perhaps above painted surfaces; and Mende above Shuttle reaction cured glass tiles. Because the spatial extent of the glow is measured only for Mende's data it can be most readily transformed into a radial geometry for comparison with the other data sets. Transforming the radially viewing data into radiances in a path along a surface is hampered by ignorance of its spatial distribution. To adjust the S/N levels in Figure 3 for surface path length viewing, the values should be multiplied by the ratio of (path length along surface observed)/(assumed spatial extent of glow). The AE data has been analyzed to have a 10m spatial extent.

Figure 3 is meant to be a guide in IMPS/GLOW experiment definition. The actual viewing geometries and mission objectives must be coupled with Figure 3 to define measurement times. Further analysis needs to be performed once surfaces, timescales and sample sizes are determined.

Conclusions

The IMPS/GLOW experiment may require observation of large surface paths with long integration times to observe UV glows (based on ISO mission upper

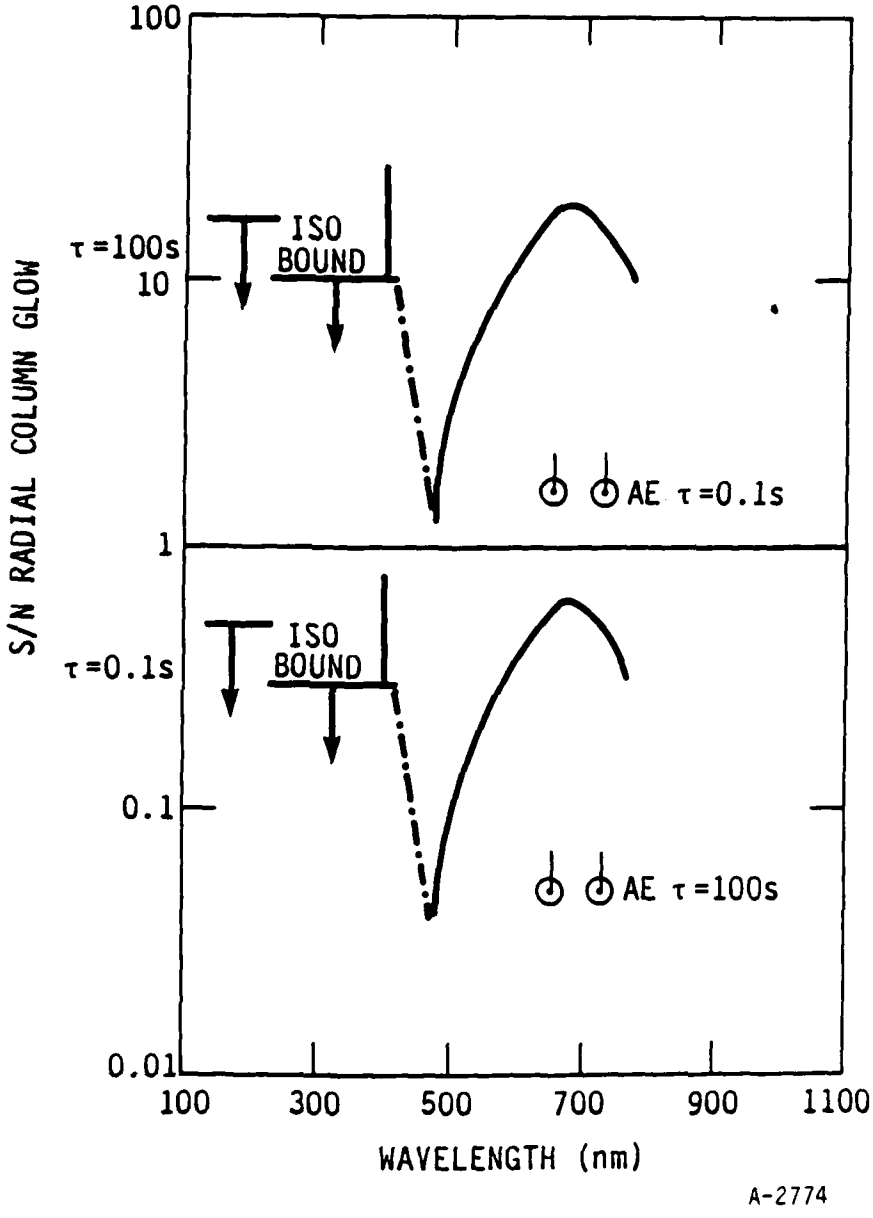

Figure 3. IMPS Pallet Glow Radial Viewing Signal-to-Noise Levels Based on Scaling of Previous Observations

bounds). The mission being at high altitude severely compromises the measurement program. Thruster events should be easily observable and should contain a great deal of new information about energetic atmospheric interactions with spacecraft effluents. Of course IMPS pallet thrusters should be disabled during observations and the glow experiment should not unintentionally look into the ram since self glow will easily obscure the more remote glow above shuttle surfaces. The altitude scaling is uncertain. The weakest scaling (as [O]) was chosen. Thus these radiance estimates may be too intense. The instrument has excellent spectral resolution. Tradeoffs between lower resolution and increased S/N should be considered. Emissions observed over short surface paths or surfaces which create less intense glows will be difficult to observe. The spectral distributions of particles may be observable in the imaged system.

REFERENCES

1. Mende, S.B., Nobles, R., Banks, P.M., Garriott, O.K. and Hoffman J., "Measurements of Vehicle Glow on the Space Shuttle," J. Spacecraft 21(4) 374-381 (1984).

2. Swenson, G.R., Mende, S.B., and Clifton, K.S., "Ram Vehicle Glow Spectrum: Implication of NO_2 Recombination Continuum," Geophys. Res. Lett. 12, 97-100 (1985).

3. Yee, J-H, Abreu, V.J., and Dalgarno, A., "Characteristics of the Spacecraft Optical Glow," Geophys. Res. Lett. 11, 1192-1194 (1984).

4. Yee, J-H, Abreu, V.J., and Dalgarno, A. "The Atmospheric Explorer Optical Glow Near Perigee Altitudes," Geophys. Res. Lett. 12, 651-654 (1985).

5. Torr, M.R., and Torr, D.G., "A Preliminary Spectroscopic Assessment of the Spacelab 1/Shuttle Optical Environment," J. Geophys. Res. 90, 1683-1690 (1985).

6. Green, B.D., Marinelli, W.J., and Rawlins, W.T., "Spectral Identification/Elimination of Molecular Species in Spacecraft Glow," Proceedings of the Second Workshop on Spacecraft Glow, NASA/MSFC Conf. Pub. 2391.

APPENDIX F

The Shuttle Glow as an Indicator of

Material Changes in Space

Planetary and Space Science 34, 219 (1986)

SR-230 is reproduced in its entirely.

PSI-39/
SR-230

THE SHUTTLE GLOW AS AN INDICATOR OF MATERIAL CHANGES IN SPACE

by

Byron David Green
(Physical Sciences Inc., Andover, MA 01810)

and

Edmond Murad
(Air Force Geophysics Laboratory, Hanscom AFB, MA 01731)

ABSTRACT

We present here a summary of the relevant observations of the glow occurring above spacecraft surfaces in low-earth orbit and a discussion of the possible reactions of the atmospheric constituents with spacecraft surfaces. The importance of these reactions is not just as a source of the glow which has deleterious effects on our ability to make remote observations from spacecraft, or as the cause of material erosion, which have been considered previously. These reactions can change surface composition and properties altering spacecraft thermal, structural, or electrical characteristics. In addition to the normal reaction exothermicities, these processes have available the large kinetic energy of the atmospheric precursor impacting Shuttle surfaces. We consider the spectral emissions which could arise from evolved surface reaction products will give rise to a variety of surface specific glows.

Short Title: Shuttle Glow as an Indicator of Material Changes

INTRODUCTION

One of the most surprising observations on the early missions of the Space Shuttle was the presence of a glow above the surfaces on the windward direction of the Shuttle during passive operational periods. This phenomenon was observed on STS-3 (Space Transportation System, or Space Shuttle, Flight Number 3) by Banks et al. (1983). Although these observations have been extended, information about this phenomenon is fragmentary: there are still few observations, the spectral resolution of measured emission is still not sufficient for unique identification, and the observations are sometimes contradictory. A number of theories have been put forward to explain this phenomenon, although a single theory which explains all the observations has not emerged to date. The Space Shuttle and other spacecraft in low-earth orbit travel at a speed of ~8 km s^{-1}. Thus the ambient molecules and atoms collide with the Shuttle surfaces and with the contaminant gas cloud surrounding the Shuttle at fairly high energies (the relative kinetic energies are 4.6 eV for N, 5.2 eV for O, 9.3 eV for N_2, and 10.6 eV for O_2). Consequently, a discussion of possible mechanisms need not only consider reactions which occur at thermal energies, but should also consider reactions which can occur at these increased interaction energies. In this paper we present an abbreviated summary of the observations, of the theories that have been put forward to date, and then a discussion of possible reactions involving collisions of the ambient gases with the surfaces of the Shuttle or other solids in space.

SUMMARY OF RESULTS AND EXPLANATIONS

Briefly, the observations are as follows:

a. The Shuttle glow is observed only in the ram direction, within the dynamic range of the observations, which is a factor of about 20 (Banks et al., 1983);

b. The Shuttle glow has been observed only in the visible, 400 to 800 nm (Banks et al., 1983; Mende et al., 1983; 1984a; Swenson et al., 1985);

c. The Atmospheric Explorer satellites, AE-C and AE-E, seem to exhibit extraneous emission, which is thought to be due to the glow (Yee and Abreu, 1982; 1983);

d. The Dynamic Explorer satellite, DE-B, also exhibits extraneous emission (Langhoff et al., 1983; Abreu et al., 1983);

e. Data from STS-4 clearly show a small but real dependence of intensity on angle of attack (Mende et al., 1983; 1984b); the AE-C data exhibits a much stronger (Cos^3) dependence on the angle of attack (Yee and Abreu, 1983);

f. The glow seems to extend about 20 cm beyond the Shuttle tail stabilizer surfaces (Yee and Dalgarno, 1983); the spatial extent is smaller over the curved Remote Manipulator System (RMS) arm (Mende and Swenson, 1985);

g. The spatial extent of the glow is independent of material, but the intensity depends on the material (Mende et al., 1984b);

h. At an altitude of 305 km, the glow intensity is about 300 kR (3×10^{11} cm^{-2} s^{-1}) above the rear engine pods, as estimated on STS-5 (Mende et al., 1983);

i. A coarse spectroscopic measurement in the region 420 to 800 nm at a resolution of 3 nm shows a broad spectrum with a maximum at about 670 nm (Swenson et al., 1985);

j. A high resolution spectrum obtained with a telescope on Spacelab 1 pointing towards deep space indicates the presence of many lines, some of which resemble N_2 electronic transitions (Torr and Torr, 1985). These measurements were not made near a Shuttle surface, however;

k. The glow intensity of the AE-satellites seems to scale with [O] at altitudes >180 km and with $[N_2]^2$ or $[O_2]^2$ at altitudes <160 km (Yee and Dalgarno, 1983; Yee et al., in press);

l. An extraneous emission due to the Lyman-α line of H has been observed on a satellite (STP78-1) at an altitude of 600 km (Chakrabarti and Sasseen, 1985);

m. Both NO and NO_2 have been observed at enhanced levels by a semi-open source mass spectrometer on AE-C and D and by a closed source mass spectrometer on DE-B. NO is formed by a fast process and is observed initially. NO_2 is observed at later times. The observed concentrations were dependent on surface temperature (Engebretson, 1985);

n. Concentrations of non-ionospheric alkali ions, NO^+ and O_2^+ have been observed above surfaces of the AE-D satellite. The altitude scaling of the alkali ions is similar to O^+ at high altitudes. At lower altitudes the alkali ions and O_2^+ scale as N_2 and O_2. NO^+ ions appeared to be formed by O collisions with the surfaces. The released ions have a characteristic energy of 1 eV (Hanson et al., 1981).

The theories which have been offered to explain this phenomenon are:

a. Simple gas-phase or gas-solid reactions giving rise to excited neutrals, such as OH^* (Slanger, 1983);

b. Surface-induced decomposition of molecules followed by recombination into excited electronic and vibrational states (Green, 1984); (Green, et al., 1985);

c. A plasma interaction arising from the critical ionization phenomenon (Papadopoulos, 1984);

d. Adsorption of O and O_2 on surfaces (Prince, 1985); and

e. Surface recombination of [O] and [N] to yield [NO], followed by recombination of [NO] with [O] on the surfaces to yield [NO_2^*] (Swenson et al., 1985).

The observations referred to above do not provide enough information to choose among the hypotheses offered thus far. The explanations are also incomplete in that objections can and have been raised to each (see, for example, the review of the plasma hypothesis by Kofsky (1984)). It is most likely that several different processes are occurring at various times over the surfaces of the Shuttle as the orbital environment changes. The effects of outgassing, thruster firings, and dumps on glow are only beginning to be investigated (see, for example, the review by Mende and Swenson (1985)).

REACTIONS ABOVE SHUTTLE SURFACES

A number of interactions between the energetic ambient flux and the Shuttle near-field environment are possible. These include gas-phase collisions between the ambient flux and 1) the reflected ambient flux, 2) the outgassed and offgassed contamination cloud, and 3) the thruster plume effluents. In addition all of the above species will be adsorbed to some extent on the Shuttle surfaces where they are subjected to the raming atmospheric flux. The magnitudes of these processes which can occur on and above Shuttle surfaces and the resulting spectral signatures are treated in a separate paper (Green et al., 1985). The most likely radiators resulting from these interactions are vibrationally excited diatomic molecules notably NO, CO, and OH. High vibrational overtones of NO were shown to resemble the observed visible glow emission spectrum.

Another recent study of the Shuttle glow led Swenson et al. (1985) to conclude that the emission is due to NO_2 which is formed on the surface of the Shuttle. In this process N and O atoms recombine to form an NO molecule which sticks to the surface long enough to react with another O atom to give an

exited NO_2. Consequently, the glow should depend on $[O]^2$ and on [N]. Alternately, if the atmospheric NO concentration is comparable to the N atom concentration, a simpler two-step process may be occurring: adsorption of ambient NO followed by a Rideal mechanism attack by O-atoms to form gas-phase NO_2^*. Here the glow would scale as [NO][O]. The observations by Yee and Abreu (1983) indicate that the intensity of the glow at high altitudes varies linearly with [O] in two wavelength bands 656.3 and 732 nm. Thus, NO_2 may not be a major constituent of the satellite glow or the satellite and Shuttle glows arise from different mechanisms. Recent analysis by Yee et al. (in press) suggests that the AE data can be interpreted in terms of a dependence on [O] at altitudes above 180 km, and on $[N_2]^2$ or $[O_2]^2$ at altitudes below 160 km.

If future higher resolution measurements of the glow above surfaces substantiate the identification of the origin of the glow as being NO_2, then an alternative class of mechanisms may be occurring as well. For example, water adsorbed on the surface could react with ambient N atoms, according to Reaction (1) in Table 2, which is exothermic by 33.9 kcal/mol (1.47 eV) in the gas phase for even thermal energy reactants. The product NO can then recombine with atomic oxygen or energetic O_2 to form NO_2.

GAS-SOLID REACTIONS

In addition to the above processes, the ambient flux can interact with the spacecraft surfaces directly. In this section we consider some possible reactions of energetic (5 to 10 eV) ambient ions and neutrals with Shuttle surfaces which can lead to the formation of excited species which can produce glow in several spectral regions. We will also consider briefly the interaction of the ambient with advanced materials being considered for long-term use in space. The importance of these reactions is not just the production of the glow or even material erosion, but that the composition and properties of the surface will change altering their thermal, structural, or electrical characteristics. For example, changing a insulator into a semiconductor or altering spectral emissivity (see below). These insidious effects can have a

significant impact on long-term space structures in Low Earth Orbit (LEO). The fact that gas-surface reactions often occur was demonstrated by mass spectrometric observations of Von Zahn (1985) on the Shuttle where non-atmospheric CO was created inside that instrument by ambient O reacting with carbon impurities in the stainless steel instrument walls.

Since the Shuttle glow has been observed only on surfaces in the ram direction, the composition of the surface material and the interaction of this material with the ambient at orbital velocities appears to be responsible for the observed emission. The thermal protection system (TPS) of the Space Shuttle consists of silica fiber tiles (Korb et al., 1981) which have high strength and thermal stability at the same time as low weight. The exact composition of the outer layers of the tiles depends on their location and on the function they serve. On the bottom of the Shuttle, black tiles are used for high emittance properties (emittance >0.8), whereas on the top of the Shuttle the tiles are white and have emittance of 0.2 to 0.4 (Korb et al., 1981). The surfaces which have been observed to glow are composed of silica tiles coated with borosilicate glass doped with small amounts of other compounds. Other surfaces and other materials glow as well but the intensity (and perhaps the spectral distribution) varies (see, for example, Mende et al., 1984a). All of the successful spectroscopic studies have been made looking at the glow near the tail surface.

The materials doped into the borosilicate glasses of the tiles include alumina, SiB_4, SiC, and other minor constituents which are used for specialized applications. It may be that the glow arises from the reaction of these minor constituents with the ambient. For example, silicon carbide, which is a constituent of the tiles, can react with fast O_2 to yield either SiO or CO, via Reaction (2), which is exothermic by about 34 kcal/mol. When the orbital velocity is taken into account, the reaction becomes exothermic by >11 eV, enough to form SiO and CO in excited electronic states. There are numerous possibilities. Table 1 lists the heats of formation of some compounds (possible reactants and products). Table 2 lists the heats of reaction for a few possible reactions of the type discussed here based on the heats of formation

TABLE 1

Thermodynamic Properties of Selected Materials*

Species	ΔH_{f_o} (kcal/mol)
$A\ell N(c)$	-74.9
$A\ell_2O_3(c)$	-390.4
CO(g)	-27.2
CN(g)	+103.8
N(g)	+112.8
NO(g)	+21.6
O(g)	+59.0
SiC(c)	-15.5
SiN(g)	+116.0
$Si_3N_4(c)$	-177.8**
SiO(g)	-24.1
$SiO_2(c)$	-217.3
$TiO_2(c)$	-223.5
TiO(c)	-123.4

*Data were taken from Wagman et al. (1982)

**$\Delta H_{f_{298}}$

TABLE 2

Heats of Some Reactions*

A.	**Exothermic Reactions at Thermal Energies**		
(1)	$N + H_2O = NO + H_2$	-33.9 kcal/mol	(~1.5 eV)
(2)	$SiC(c) + O_2 = SiO(g) + CO$	-34 kcal/mol	(~1.5 eV)
(3)	$(1/5)\ S_3N_4(c) + O_2 = 3/5\ SiO_2(c) + (4/5)\ NO$	-78.4 kcal/mol	(~3.4 eV)
(10)	$SiC(c) + O = Si(c) + CO$	-71 kcal/mol	(~3 eV)
(11)	$2/3\ SiC(c) + O_2 = 2/3\ SiO_2(c) + 2/3\ CO$	-153 kcal/mol	(~6.7 eV)
B.	**Reactions Endothermic at Thermal Energies but Exothermic at Orbital Energy**		
(12)	$SiC(c) + N = Si(c) + CN$	+6.9 kcal/mol	(0.3 eV)
(13)	$SiO_2(c) + 2N = Si(c) + 2\ NO$	+34.9 kcal/mol	(~1.5 eV)
(9)	$TiO_2(s) + O = TiO(s) + O_2$	+41 kcal/mol	(~1.8 eV)
(5)	$6/7\ SiC(c) + N_2 = 2/7\ Si_3N_4(c) + 6/7\ CN$	+51.5 kcal/mol	(2.2 eV)
(8)	$SiO_2(c) + N = SiO(g) + NO$	+102 kcal/mol	(~4.4 eV)
(6)	$2/5\ A\ell_2O_3(c) + N_2 = 4/3\ A\ell N(c) + 5\ NO$	+122 kcal/mol	(5.3 eV)
C.	**Reactions Slightly Endothermic at Orbital Velocities**		
(4)	$3/2\ SiO_2(c) + N_2 = 1/2\ Si_3N_4(c) + 3/2\ O_2$	+237.5 kcal/mol	(~10.3 eV)
(7)	$SiC(c) + N_2 = SiN(g) + CN$	+234 kcal/mol	(10.2 eV)

*Negative heats indicate the reaction is exothermic, while positive heats indicate the reaction is endothermic.

of Table 1. Due to its reactive nature, atomic oxygen is a strong candidate to undergo reactions of this type. It should be emphasized, however, that the equilibria listed above are thermodynamic processes. The actual path to a given equilibrium may involve tens of intermediate steps. As a result there may be several rate-limiting steps causing the reactions to proceed slowly.

In surfaces containing hydrocarbons, excited OH, and CO may be created, as documented by various laboratory observations (see, for example, the review by Green et al., 1985). Infrared and even visible emissions can result from these interactions.

An example of another possible class of reactions is the catalytic reaction of N_2 and O_2 to form NO via a nitridation cycle consisting of Reaction (3) followed by Reaction (4). Reaction (4), which is endothermic by 10.3 eV at thermal energies, becomes endothermic by ~1 eV when the energy of N_2 arising from the relative velocities of the Shuttle and the atmosphere are considered. However, the ambient N_2 molecules have a random thermal velocity distribution which alters the kinetic energy of impact on surfaces. Although the average kinetic energy for N_2 is 9.3 eV, approximately 10 percent of the molecules will strike the surfaces with 10.3 eV or greater energy (in the absence of gas-phase collisions which slow the incoming ambient molecules). A few percent of the collisions will even occur with kinetic energies of greater than 11 eV. (Correspondingly 10 percent of the collisions will have an energy of less than 8.3 eV.) Consequently even the endothermic processes listed in Table 2 have a finite probability for reaction. The catalytic formation of NO via a nitride intermediate becomes possible for N_2^+ impact on a silica surface (similar to Reaction (2) above), since the ionization energy of N_2 is released in collision. Experiments by Shamir et al. (1978) and by Taylor et al. (1982) show that nitridation of SiO_2, Aℓ, Cu, Mo, and Ni can take place quite easily at collision energies varying between 0 and 500 eV. Surface nitridation (Reactions (5) - (7)) can change the surface properties enhancing reaction rates (erosion), changing thermal or electrical properties. A further example of this is given by the transformation of an insulator SiO_2(c) into a semiconductor, Si(c). This process can be conceptually viewed as an N atom attack

on $SiO_2(c)$ to form SiO dissolved in the solid SiO_2 followed by two SiO molecules reacting to form Si(c). Both NO and O_2 are generated in this process. Although the thermochemistry of dissolved SiO is not known, the gas-phase products could have in excess of 4 eV internal energy (based on Reaction (8)).

Another possibility is that the surface material may extract oxygen atoms from adsorbed H_2O. Porter and Smith (1962) observed that $CF_3C\ell_3$ reacts with graphite at temperatures varying between 500 and 1000K in such a way that $CF_2C\ell_2$ is released in the gas phase and one atom each of $C\ell$ and F is retained in the graphite in some sort of a chemical bond. The analogous case here would be the release of H_2 and the retention of O by the surface. Such a reaction is endothermic in the gas phase, but may be possible under the impact of energetic H_2O formed by collisions with ambient species as observed by Narcisi et al. (1983). If this step were to occur, NO_2 can then be formed by the reaction of N with the adsorbed O and a subsequent ambient O atom. In this case the intensity should be linear with both [N] and [O].

Some of the new, advanced structural materials considered for space-borne observatories consist of ultra-low expansion structures made of SiO_2 doped with TiO_2. These structures are made of honeycombed or bonded frits of this material (2 mm thick) coated with suitable reflectors. They are at special risk of being attacked by the type of reactions outlined above. For example, Reaction (9) is endothermic by about 41 kcal/mol at thermal energies. However, in the low earth orbit environment it becomes exothermic by about 3.4 eV, since O has 5.2 eV in kinetic energy. The excess energy may well appear as glow above the surface, due to excitation of O_2. Surface emissivity changes as TiO_2 is transformed to TiO by Reaction (9) may affect space systems thermal performance.

SPECTRAL RAMIFICATIONS

Each of the processes discussed above may have different internal energy distributions in the product molecules and consequently a unique spectral signature. Thus, we suggest that the glow may be used as an indicator of the

types of interactions occurring at surfaces. Energy losses to the solid products and to the desorption process must be considered, but sufficient exothermicity exists to allow vibrational and electronic excitation in the evolved gas phase species which could result in fluorescence. In this section we will briefly consider potential spectral emissions resulting from the various processes. The actual emission spectrum resulting from these reactions can be obtained only from laboratory or on-orbit observations.

From inspection of Table 2, it is seen that four species could be released into the gas phase with some amount of internal excitation: NO, CO, SiO, and CN. The first three are produced in interactions which are sufficiently exothermic (if reactant kinetic energy is included) that internal excitation up to the dissociation limit is possible. Equipartitioning of available energy into all available degrees of freedom is not expected and a fraction of the gas-phase products may leave with considerable translational, rotational, vibrational, or electronic excitation. The formation of electronic states above the dissociation energy is not considered here but should not necessarily be ruled out.

Silicon monoxide could be excited into any of 11 electronic states (including the ground state) lying below its dissociated energy. [Huber and Herzberg, 1979]. Vibrational emission (from the ground state) would occur at 8.14 μm in the infrared with overtone bands at 4 and 2.7 μm. Furthermore many tens of quanta of vibrational excitation are possible in the SiO product molecule giving rise to a strong infrared glow. Emission from the relatively short-lived (10^{-8} s) A and E states falls in the UV between 210 to 270 nm and 170 to 200 nm respectively [Pearse and Gaydon, 1963]. Emission from the longer lived b-x, f-b, and c-b transition bands would extend from 290 nm to the 420 nm region.

Cyanogen could be created with considerable internal excitation from Reaction (12). It has three accessible states X(ground state), $A(^2\Pi_i)$, and $B(^2\Sigma^+)$. Vibrational emission would occur at 4.9 μm with hot bands extending to 6 μm and beyond. The first overtone bands would start at 2.46 μm. Higher overtone transitions could reach into the visible. The CN Red (A-X, τ = 680 ns) and Violet (B-X, τ = 65 ns) systems emit visible photons. The Red system has structured electronic progressions stretching from 500 nm to beyond 1 μm. The Violet system is dominated in the laboratory by three strong features at 422, 388, and 359 nm.

Carbon monoxide also has 11 accessible electronic states which could give rise to a very rich UV and visible spectrum with bands occurring between 100 nm and 1.6 μm. Some of the possible emission bands from CO are listed in Table 3. The vibrational fundamental and first overtone bands are at 4.67 and 2.35 μm. Again, higher overtones can extend into the visible. The a state is sufficiently long lived to give rise to an extended glow layer above surfaces where this state is created.

TABLE 3

Some CO Electronic Emissions

Name	States	Lifetime[a]	Spectral Region[b] (nm)
Asundi Bands	a'→a	3-4μs	575>1600
Angstrom	B→A	15-22 ns	410-660
Triplet	d→a	-	450-650
Third Positive	b→a	53-69 ns	283-370
Cameron	a→X	7.5-9.5 ms	200-257
Fourth Positive	A→X	9-11 ns	200-275

(a) - (Huber and Herzberg, 1979)

(b) - Pearse and Gaydon, 1963.

Nitric oxide emissions have been described previously. Although six states are accessible, emission should be dominated by vibrational bands in the infrared with high overtone transitions extending into the visible, and by γ, β, and δ band emission in the UV.

The UV electronic transitions are relatively short lived and would give rise to a thin glow layer just above the reactive surface. The longer lived states such as molecules vibrationally excited in the ground state and CO(a) take 5 to 80 ms to decay giving rise to a much more extended glow. For example, for a 10 ms lifetime a molecule leaving the surface translationally equilibrated would give rise to a glow layer of 3m extent. If the molecule left the surface with 1 eV of directed kinetic energy, the glow layer would extend tens of meters.

SUMMARY

We have presented a summary of the relevant observations of the glow occurring above spacecraft surfaces in low-earth orbit and a discussion of the possible reactions of the atmospheric constituents with spacecraft surfaces. The importance of these reactions is not just as a source of the glow which has deleterious effects on our ability to make remote observations from spacecraft, or as the cause of material erosion which have been considered previously. These reactions can change surface composition and properties altering spacecraft thermal, structural, or electrical characteristics. Nitridation, changes from insulator to semiconductor, and emissivity alterations were given as examples. In addition to thermal reaction energetics, these processes have available the large kinetic energy of the atmospheric precursor impacting Shuttle surfaces. We have considered the spectral emissions which could arise from evolved surface reaction products will give rise to a variety of surface specific glows. These glows can be used as a remote diagnostic to provide insight into the changes occurring in on-orbit materials.

REFERENCES

Abreu, V. J., Skinner, W. R., Hays, P. B., and Yee, J. H. (1985), Optical Effects of Spacecraft-Environment Interactions: Spectrometric Observations of the DE-2 Satellite, J. Spacecraft Rockets, 22, 177-180.

Banks, P. M., Williamson, P. R., and Raitt, W. J. (1983), Space Shuttle Glow Observations, Geophys. Res., Lett., 10, 118-121.

Chakrabarti, S. and Sasseen, T. (1985), Investigation of the Vehicle Glow in the Far Ultraviolet, J. Geophys. Res.

Engebretson, J. J. (In Press), AE and DE Mass Spectrometer Observations Relevant to the Shuttle Glow, in Proceedings of the Second Workshop on Spacecraft and Glow, NASA/MSFC.

Green, B. D. (1984), Atomic Recombination into Excited Molecular States - A Possible Mechanism for Shuttle Glow, Geophys. Res. Lett., 11, 576-579.

Green, B. D., Caledonia, G. E., and Wilkerson, T. D. (In Press), The Shuttle Environment: Gases, Particles, and Glow, J. Spacecraft Rockets.

Hanson, W. B., Sanatani, S., and Hoffman, J. H. (1981), Ion Sputtering from Satellite Surfaces, J. Geophys. Res., 86, 11350-11356.

Huber, K. P. and Herzberg, G., Molecular Spectra and Molecular Structure IV, (Van Nostrand, New York, 1979).

Kofsky, I. (1984), Spectroscopic Consequences of Papadopoulos' Discharge Models in Spacecraft Ram Glows, Radio Sci., 19, 578-586.

Korb, L. J. Morant, C. A., Calland, R. M., and Thatcher, C. S. (1981), The Shuttle Orbiter Thermal Protection System, Bull. Am. Ceram. Soc., 60, 1188-1193.

Langhoff, S. R., Jaffe, R. L., Yee, J. H., and Delgarno, A. (1983), The Surface Glow of the Atmospheric C and E Satellites, Geophys. Res. Lett., 10, 896-899.

Mende, S. B., Garriott, O. K., and Banks, P. M. (1983), Observations of Optical Emissions on STS-4, Geophys. Res. Lett., 10, 122-125.

Mende, S. B., Banks, P. M., and Klingelsmith, III, D. A. (1984a), Observation of Orbiting Vehicle Induced Luminosities on the STS-8 Mission, Geophys. Res. Lett., 11, 527-530.

Mende, S. B., Nobles, R., Banks, P. M., Garriott, O. K., and Hoffman, J. (1984b), Measurement of Vehicle Glow on Space Shuttle, J. Spacecraft Rockets, 21, 374-381.

Mende, S. B. and Swenson, G. R. (1985), Vehicle Glow Measurements on the Space Shuttle, AIAA-85-0909, presented at 20th Thermophysics Conference, VA, submitted to J. Spacecraft and Rockets.

Narcisi, R., Trzcinski, E., Federico, G., Wlodyka, L., and Delorey, D. (1983), The Gaseous Environment Around Space Shuttle, AIAA-83-2659, Proceedings of the AIAA Shuttle Environment and Operations Meeting, Washington, D.C.

Papadopoulos, K. (1984), On the Shuttle Glow - The Plasma Alternative, Radio Sci., 19, 571-577.

Pearse, R. W. B. and Gaydon, A. G., The Identification of Molecular Spectra, (Chapman and Hall, London, 1963).

Porter, R. F. and Smith, D. H. (1962), Heats of Reaction of Fluorine with Graphite, J. Phys. Chem., 66, 1563-1563.

Shamir, N., Baldwin, D. A., Darko, T., Rabalais, J.W., and Hochman, P., (1982), Reactions of Homonuclear Diatomic Ions with Metal Surfaces. II. Nitridation of Aℓ, Cu, Mo, and Ni by N_2^+ Beams in the Low Kinetic Energy - Near Threshold Region, J. Chem. Phys., 76, 6417-6424.

Slanger, T. (1983), Conjectures on the Origin of the Surface Glow of Space Shuttle, Geophys. Res. Lett., 10 130-132.

Swenson, G. R., Mende, S. B., and Clifton, K. S. (1985), Ram Vehicle Glow Spectrum; Implication of NO_2 Recombination Continuum, Geophys. Res. Lett. 12, 97-100.

Taylor, J. A., Lancaster, G. M., Ignatiev, A., and Rabalais, J. W. (1978), Interactions of Ion Beams with Surfaces. Reactions of Nitrogen with Silicon and Its Oxides, J. Chem. Phys., 68, 1776-1784.

Torr, M. R. and Torr, D. G. (1985), A Preliminary Spectroscopic Assessment of the Spacelab 1/Shuttle Optical Environment, J. Geophys. Res., 90, 1683-1690.

Von Zahn, U. (1985) private communication.

Wagman, D. D., Evans, W. H., Parker, V. B., Schumm, R. H., Halow, I., Bailey, S. M., Churney, K. L., and Nuttall, R. L. (1982), The NBS Tables of Chemical Thermodynamic Properties, J. Phys. Chem. Ref. Data, 11, Suppl. 2.

Witteborn, F. C., O'Brien, K., and Caroff, L. (1985), Measurement of the Nighttime Infrared Luminosity of Spacelab 1 in the H- and K-Bands, NASA Tech. Memo. 85972.

Yee, J. H. and Abreu, V. J. (1982), Optical Contamination on the Atmospheric Explorer-E Satellite, Proc. SPIE-Opt. Eng., 338, 120-128.

Yee, J. H. and Abreu, V. J. (1983), Visible Glow Induced by Spacecraft-Environment Interaction, Geophys. Res. Lett., 10, 126-129.

Yee, J. H. and Dalgarno, A. (1983), Radiative Lifetime Analysis of the Spacecraft Optical Glow, AIAA-83-2660-CP.

Yee, J. H., Abreu, V. J., and Dalgarno, A. (In Press), The Atmospheric Explorer Optical Glow Near Perigee Altitudes, Geophys. Res. Lett.

APEPNDIX G

Review of the Vehicle Glow

Paper 85-6095-CP

AIAA Shuttle Environment and Operations II Conference

SR-235 is reproduced in its entirety.

AIAA'85

AIAA - 85 - 6095 - CP
REVIEW OF THE VEHICLE GLOW (INVITED)

B. D. GREEN

Physical Sciences Inc., Andover, MA

AIAA Shuttle Environment and Operations II Conference
November 13 - 15, 1985 Houston, Texas

The U.S. Government is authorized to reproduce and sell this report. Permission for further reproduction by others must be obtained from the copyright owner.

For permission to copy or republish, contact the American Institute of Aeronautics and Astronautics
1633 Broadway, New York, NY 10019

REVIEW OF THE SPACECRAFT GLOW

B.D. Green*
Physical Sciences Inc.
Dascomb Research Park
Andover, MA 10810

Abstract

This paper will review the current data base on the glow observed above surfaces of spacecraft, particularly the Shuttle, which are exposed to the energetically impacting atmospheric flux. The various mechanisms which have been proposed will be considered. Several experiments which are planned or have been proposed will also be briefly discussed to indicate the additional knowledge they may provide about the intriguing glow phenomenon.

Introduction

The benefits which could be achieved by space based observation platforms for astronomy or atmospheric remote sensing may be seriously compromised by the presence of a diffuse near field glow phenomenon which has been observed above surfaces subjected to the impact of atmospheric species as the spacecraft sweeps through the low earth orbital atmosphere at 8 km/s. The residual atmosphere appears to be capable of generating molecular excitation in this interaction. However, the exact mechanisms and reactants which give rise to the glow will dictate the approaches used in future efforts to reduce its effects. Whether the glow results from interactions of the ambient flux with contamination, thruster effluents, surface adsorbates, catalytic surfaces, or in the surface materials themselves will determine whether or not reduction is possible and what remedial actions to be taken. A single mechanism has not emerged as the source of the glow. The existing observations often do not agree. It is possible that several different processes could be occurring at different times in the variable environment on-orbit. The existing data base is insufficient to allow the dominant mechanisms to be determined. Future measurement programs must be aimed toward better characterizing and extending the current data base -- spectrally, temporally, and spatially, as well as over a variety of surfaces and orbital conditions both natural (such as altitude, solar flux) and induced (such as contamination levels, thruster firings, water dumps). The role of supporting ground based simulation facilities will also be discussed.

Observations of the Glow Above Surfaces in Low Earth Orbit

A glow has been detected above surfaces of both satellites and the Shuttle. Comparison of the two data bases is complicated by the lack of similarity between the detection systems and geometries. The glow above Shuttle surfaces was first observed (fortuitously) above the tail pod section by Banks and coworkers[1] on the STS-3 mission. Starting with the next mission Steven Mende and coworkers undertook a series of systematic measurements which have accumulated the most extensive data base of Shuttle glow.[2-7] Since these measurements will be described in the next paper in this session,[8] we will only state their results in relation to other observations. The other extensive glow data base on the Shuttle was acquired by the Imaging Spectrometric Observatory (ISO) which was part of the Spacelab 1 mission. This instrument looked directly out of the bay not at Shuttle surfaces but still observed significant spectral emissions not of atmospheric origin. This data has excellent temporal and spectral resolution. M. Torr and D. Torr have just begun to unravel this complex but very intriguing data base,[9] and will present their current progress in Session 14 of this meeting.[10]

The on-orbit environment surrounding satellites should be much cleaner than that of the Shuttle: the satellites are on-orbit for years so payload outgassing has substantially decreased; there are few thruster firings; and there is no lifesupport-induced cloud of H_2O or CO_2. Nevertheless a residual emission not of natural atmospheric origin has been found upon careful inspection of the data. Yee and coworkers[12-15] and M. Torr[16] have analyzed the visible and UV data base from the Atmospheric Explorer (AE) C and E and Dynamics Explorer-2 satellites. Recently, an additional interaction-induced emission in the far ultraviolet has been described by Chakrabarti, et al.[18]

Variation of the Glow Intensity with Altitude and Angle of Attack

The altitude variation provides insight into the reactive source of the glow. The angular dependence will demonstrate the role of kinetic energy and flux. The most extensive data on altitude scaling of glow above spacecraft is from the AE - C and E satellites[12] which were in highly elliptical orbit. This permitted the altitude variation of the glow to be measured during each orbit so that long term fluctuations in atmospheric composition do not compromise these observations. The detection system consists of filtered photometers looking radially outward from the surface of the rotating satellite through a telescope. The telescope baffling protrudes 8 cm out into the boundary layer above the satellite surface so that a portion of the glow may be missed. Alternately, glow may be occurring inside the telescope. Six filtered photometer channels (with ~2.0 nm bandpass) were used for atmospheric observation. An enhanced emission was clearly observed up to altitudes of 450 km[19] in the two red channels centered at 656.3 and 732.0 nm. The altitude scaling of this enhanced emission between 140 and 280 km is found to scale with the atomic oxygen density above 180 km;[12] and to scale as neutral molecular density (N_2 or O_2) squared in the 140-180 km altitude region. [In this latter altitude range the density of N_2 is an order of magnitude greater than O_2.][20] The angular variation of this intensity was found to agree with a modeled $\cos^3\phi$ distribution with respect to the angle of attack.[12] Yee and Abreu have suggested that a flux x impact energy dependence would match this behavior.

Because the Shuttle usually remains at a single altitude during a mission, altitude variation of the glow is limited to comparison of observations from different flights which are months apart.

*AIAA Member

This results in large uncertainties due to detection system response changes or atmospheric variability. The glow was observed from the rear cabin window looking through a 10 m long column just above the tail and engine pods. After carefully correcting for film exposure reciprocity, the intensity was found to be a factor of 3.5 brighter at 240 km than at 305 km.[4] This scaling is not inconsistent with the AE satellite observations. The total intensity between 400 and 800 nm bandpass was found to be several hundred kilorayleighs (1 Rayleigh = 10^6 photons/cm^2s) for STS 5 at 305 km, making the radiance on the order of 1 megarayleigh at 240 km. these intensities are comparable in intensity to emission features from the entire earth limb. On the Shuttle, the variation of the glow with angle relative to the velocity vector was obtained by rolling the Shuttle slowly through 360 degrees. This striking photographic data indicated a much weaker angular dependence of glow scaling as less than linear with cosϕ. The Shuttle tile-surfaces are very structured - there is always a surface facet normal to the velocity vector at even large angles of attack. Thus it is difficult to infer a kinetic energy dependence from this observation. Surfaces not exposed to the ram flux did not glow, the shadowed regions had sharp edges. No glow intensity has been observed in the wake. If present it is at least two orders of magnitude lower than intensities in ram.[21]

Spatial Extent Above Surfaces

Even in the first observation by Banks and coworkers[1] the glow appeared to stand off above the surfaces. Later pictures showed stars shining through the glow layer. A detailed analysis of the glow extent which included tail and viewing geometries was performed by Yee and Dalgarno.[22] They concluded that the glow exponentially decreased above the tail surfaces with a characteristic perpendicular scale length of 20 cm. On Spacelab 1 with a better viewing geometry, Mende and coworkers[6] arrived at the same characteristic distance. Mende and Swenson[6] have also reported on their measurements of glow above different materials mounted on the Remote Manipulator System (RMS). Although the total intensities observed varied with material (see below), the spatial extent of the glow layers were the same for the materials observed. However, the data when corrected for background levels had a half-intensity spatial extent of only 6.0 to 6.5 cm. This may be a geometrical effect due to observing above the curved arm, or perhaps may provide some insight into the physical mechanism causing the glow. The AE satellite observations can only be inferred from modeling but are best explained by a glow of about 1m extent. The variation of the extent of that data with altitude would be very useful in understanding of the glow.

The spatial extent of the glow can be interpreted in several ways. If excitation of the emitting species occurs at the surfaces then the extent is proportional to the distance the excited molecule travels before it emits (distance = velocity x excited state lifetime). The extent could also be representative of the pressure gradient above surfaces, representing the layer in which collisional excitation of neutrals[23] or collisional ionization to create a plasma[24] can occur. Thus the three different distances observed (6 cm above the RMS arm, 20 cm above the Shuttle tail, and 1 m above the ~75 cm radius AE satellite) seem to represent different radiating species or even different mechanisms.

Material Specificity

The Lockheed group studied the glow intensities over different materials on two missions STS 5 (Kapton, Aluminum, and Black Chemglaze Paint) and STS 41D (nine samples including MgF_2, paints with and without overcoats), polyethylene, carbon cloth, and Al_2O_3). The data indicated that there was an order of magnitude variation in intensity above different surfaces. All surfaces glowed to some extent. There appeared to be no correlation with material erosion. MgF_2 optics and black chemglaze paint glowed the brightest, yet these materials suffer no detectable mass loss on-orbit.[25,26] By contrast, polyethylene and aluminum have the weakest glow intensities. Aluminum is very stable on-orbit, while polyethylene is one of the most reactive species on-orbit.[25] Thus, it appears that the glow is the result of a non-reactive interaction of the surface material with the low earth orbital (LEO) environment. The intensity is a function of the ability of the surface to facilitate the emission process -- to allow catalytic recombination, or to transform the kinetic energy of impact into internal excitation, or to effectively reflect the incoming species. (See below.)

Luminosity from Thruster Firings

The luminosity associated with thruster firings has two distinct components. An extremely bright gas phase extended component has been observed only when the rear downward thrusters fire.[6] Their exhaust strikes the wing, is thermalized into a cloud which has a low velocity relative to the Shuttle. These exhaust species can then undergo chemiluminescent reactions with atmospheric species to produce the glow. Unburned fuel or even normal exhaust constituents (H_2O, N_2) are capable of giving rise to line of sight column intensities of 10^{12} photons/cm^2s.[27] After the extended gas phase luminosity associated with thruster firings dissipates, a residual enhanced luminescence persists on Shuttle engine pod surfaces. This decays with a time constant of a few seconds,[6] which is comparable to the time required for an O-atom in the orbital flux [~10^{13} O/cm^2s] to strike each surface site,[23] suggesting thruster effluents adsorbed on Shuttle surfaces after being backscattered, are removed in a chemiluminescent process by O-atom scouring of the Shuttle tile surfaces.

Spectral Distribution

Perhaps the most important observable for glow mechanism identification is spectral distribution. Swenson, Mende and Clifton,[7] Torr and Torr,[9] and Witteborn, et al.,[28] have all published spectral observations of the glow surrounding Shuttle. In a beautiful set of experiments, a handheld camera/spectrometer system, looking through the rear cabin window, was used to monitor the spectral distribution of the glow above the rear engine pods. Film response and window transmission limit the observations to the 400 to 800 nm region. The published spectrum[7] acquired on STS 41D is uncorrected for the structured window transmission, but shows emission having a broad spectral distribution peaking in the red at 680 nm. This data was acquired at an

altitude of 300 km, higher than the 240 km originally planned so that the signal levels were lower than expected. Consequently the signal-to-noise ratio of the spectrum is only about four so that although it is clearly a broad spectral feature, feature, any structure present is obscured in the noise. Swenson, et al.,[7] have faired a smooth curve through the data as their best estimate of the glow spectrum above Shuttle tile surfaces.

By contrast the ISO instrument, which was part of the Spacelab 1 mission, did not observe Shuttle surfaces directly but nevertheless observed emission not attributable to the far field earth limb. The Imaging Spectrometric Observatory[9] is comprised of a bank of five spectrometers with charge-coupled array detectors which permit rapid acquisition of emissions between the vacuum ultraviolet and the near infrared (30 to 1270 nm) with good (0.3 to 0.6 nm) spectral resolution. This mission was somewhat compromised by a delayed launch so that it operated in daylight for much of its duration. The ISO instrument observed contamination levels decaying with mission elapsed time. The enhanced near field emissions were brighter on the first day of the mission observing the wake than they were on the tenth day of the mission looking into the ram. Significant latitudinal variations in both the emission intensity and distributions were observed. Peak intensities of 100 R/Å were observed even late in the mission. The near-field spectral distribution in the red was highly structured and has not been completely assigned. The analysis is complicated because the surface giving rise to the glow is uncertain - it may be the telescope baffles or an external Shuttle surface. Marsha Torr will present her latest conclusions in Session 14 of this meeting tomorrow.

Not just the visible may be affected by glow. Witteborn has observed the Shuttle in the near infrared from the ground using the 1.6 m telescope at the Maui Optical Observatory. The entire Shuttle was observed to have an intensity enhanced above reflected and thermal emissions in two relatively wide bandpasses at 1.6 and 2.2 μm.[28] These infrared intensities are even a factor of two or three brighter than the observed visible levels.

The AE satellite data intensities in six bandpasses between 280 and 732 nm provides spectral coverage of only 2.5 percent of that region. Nevertheless, the enhanced emission rises to the red having a value of 3 R/Å in the 732 nm bandpass at an altitude of 220 km.

A Fabry-Perot interferometer on-board the DE-2 satellite also observed a contaminating glow.[14] This high resolution instrument (0.0018 nm/channel) filtered at 732 nm indicated that the near field satellite glow was attributable to one or more species. [They propose OH(v) as a possibility.]

Chakrabarti has reported[18] an enhanced intensity of Hydrogen Lyman α (121.6 nm) on an Air Force Satellite STP 78-1. He will present his most recent findings later in this session. This observation represents the sole observation of a UV enhancement above spacecraft surfaces. Huffman[29] has previously reported observing no enhancements due to Shuttle operations or due to glow luminosity in his UV spectrometer on STS 4. This instrument covered the wavelength region 110 to 180 nm.

Thus at present the observations do not support each other. This may be attributable to the extremely variable environment on-orbit - both the atmosphere and the near field environment may vary between missions. Additionally, the observation geometries also complicate intercomparisons. In order to test our understanding of the mechanisms responsible for the glow (as discussed in the next section), an extended data base is required. Extended spectral coverage and the spatial dependence of this spectrum are necessary. Because different spatial extents have been observed, different mechanisms (with different spectral distributions) may be occurring. Thus the glow over a variety of surfaces and geometries should also be obtained.

Summary of Proposed Mechanisms

The sparcity of glow observations is more than compensated for by the wealth of proposed mechanisms which could give rise to the glow. This review will treat them in the order an incoming ambient molecule would encounter them: 1) gas phase collisions (both during quiescent and thruster firings or water dumps) giving rise to kinetic energy transfer, chemical, and plasma excitation processes; 2) surface aided chemiluminescence reactions with adsorbates; and 3) surface bulk reactions leading to material loss or composition changes.

In LEO the Shuttle is surrounded by a radially decreasing cloud of its own effluents, pressures in the Shuttle bay are between 10^{-7} and 10^{-4} Torr during various Shuttle activities with the higher pressures correlating with ram observations and thruster firings.[30] At the highest pressures the mean free path between collisions is much less than the Shuttle bay dimensions, and contamination from other parts of the vehicle can be scattered and detected by point sampling mass spectrometers. During periods of little Shuttle activity, and late in the mission, the concentration of species will be very spatially non-homogeneous being dominated by local sources. Thus, general statements of the Shuttle environment are dangerous. Nevertheless, the most prevalent species have been measured to be H_2O and CO_2 (Miller, et al.;[31,32] Narcisi, et al.[33]), although He, O_2, Ar, freons, cleaning agents and other species have also been detected in trace amounts. The gaseous environment surrounding the Shuttle has been recently reviewed.[34]

The natural atmosphere at Shuttle altitudes is composed dominantly of atomic oxygen, with some N_2. Molecular oxygen, helium, nitric oxide, atomic nitrogen, argon, and atomic hydrogen are all present in trace amounts below the one percent level. This atmosphere is not constant, but undergoes diurnal, seasonal and latitudinal variations.

As the Shuttle and its cloud of contaminants approaches atmospheric species at 8 km/s, the cloud and ambient constituents can interact at molecular velocities much in excess of thermal. This kinetic energy of the reactants can overcome barriers to reaction that exist at room temperature and can allow processes which are endothermic at room temperature to proceed on-orbit.[23,27] As a result reactions producing chemiluminescence and collisions producing excitation of internal molecular (vibrational, rotational) modes are possible. Based on measured contaminant column densities and estimated rate constants, these processes should be

efficient at creating infrared fluorescence at the levels[27] of 10^{11} photons/cm^{2}s. However, they do not occur at a sufficient rate to generate significant visible glow intensities for measured contamination levels. However, if the column densities were considerably higher due to ram pressure build-up, then these gas phase reactions would generate a glow layer, the extent of which would reflect the concentration and density gradients above the surfaces.

If the incoming ambient species are nearly elastically reflected by Shuttle surfaces then the interaction between incoming and reflected ambient species may be energetic enough to cause ionization as suggested by Papadopoulos.[35] The gyroradii of these electrons are such that they remain in the vicinity of the Shuttle, suffer additional collisions with energetic neutrals until they are energetic enough to ionize the ambient N_2 causing an avalanche breakdown. This mechanism effectively transforms orbital kinetic energy into a discharge which can release a great deal of energy, some of which goes into molecular excitation and fluorescence. This mechanism would also depend on the gas composition above surfaces as they affect ionization levels. The resulting fluorescence would contain both ambient and contaminant molecular emissions.[35] For this process the spatial extent of this glow layer is the region capable of sustaining a discharge. However, an exponential decrease with distance above the surface is not necessarily expected. A variation with surface material could result from reflection efficiencies. Ion enhancements and energetic electrons have been observed in ram,[31,36] but these enhancements are probably not sufficient to explain the observed radiance levels during passive Shuttle operational periods.

During a typical RCS thruster firing, 10^{25} molecules (dominantly H_2O, N_2 and H_2) are released in 80 ms. The plume molecules traveling at ~3.5 km/s expand out and displace the ambient atmosphere. Collisions within the thruster plume and with the atmospheric flux will result in reactions, collisional excitation or backscatter. Radiances in the megarayleigh range (10^{12} photons/cm^{2}s) can easily result from these interactions. Similarly collision induced plasma processes could be significant in the interaction of the energetic plume effluent and ambient atmosphere.

Self-contamination of payloads while on-orbit has been of concern for years.[37] The mean free paths between collisions are sufficient to result in backscattering of contamination to Shuttle surfaces. In fact the IECM/mass spectrometer could only detect contaminant species which had been backscattered into its aperture. Its field-of-view is 0.1 sr looking directly out of the payload bay.[31,32] In addition, thruster events will result in backscattered effluents reaching Shuttle surfaces. Narcisi, et al.[33] with good temporal resolution observed H_2O, N_2 and H_2 enhancements during thruster events. During periods when the Shuttle is being actively stabilized, the flux of backscattered thruster effluents to Shuttle surfaces could equal the ambient flux.[23] The backscattered outgassing flux should be at least an order of magnitude smaller. Consequently, the Shuttle surfaces (instruments, and test materials) are being constantly coated with a stream of molecular contaminants, some fraction of which are adsorbed onto the porous surfaces. Simultaneously, the reactive O-atom atmospheric flux is scouring the surfaces potentially resulting in chemiluminescent product formation or collisional desorption and excitation by either atmospheric O or N_2. The temporal behavior of the enhanced glow above surfaces after thruster events[6] described above may reflect the time required for removal of the adsorbate layer by the ambient flux. The interaction of the ambient atmosphere with the common adsorbates likely to be present on Shuttle tile surfaces, should result in NO, CO and OH formation.[23] Moreover, it appeared, based on reasonable reaction efficiencies, that these species could easily generate the megarayleigh glow radiance levels observed.

A surface glow emission has been suggested by Prince.[38] In this mechanism the energetic ambient oxygen atom chemisorbs onto the Shuttle surface emitting a photon (or electron) in the process. This emission would occur at the surface. Because of the density of states below the Fermi-level of the surface, a near continuous emission could result. These interactions are extremely short ranged (2Å). Consequently, the nature of the interaction is dominated by the outermost layer "seen" by the incoming species. Even a fraction of a monolayer of absorbate on the surface will change the nature of the interaction;[39] i.e., the adsorbate very effectively shields the substrate. Atomic O-adsorbate reactions may then occur rather than chemisorption. Additionally, emission from this process has been observed only above metals. There is no experimental evidence to suggest that the process would occur on insulator materials such as the tile borosilicate glasses, Kapton, or MgF_2. Future experiments with spatial resolution of the glow will define the orbital conditions under which this chemisorptive surface emission occurs.

Green first suggested the possibility that atmospheric N_2 could dissociate upon impact with spacecraft surfaces based on purely energetic grounds.[40] There is at present no experimental evidence to support this hypothesis. It was put forward as a means of providing N-atoms adsorbed on surfaces. Ambient N and NO (which should dissociate on impact) will also provide N on the surface. The O and N atoms in the ambient flux may not be readily adsorbed since the collisional energy cannot be as easily transformed into internal potential energy. If reflected atoms undergo collisions in the gas layer above the surface, they may remain in the vicinity of the surface and be adsorbed. Thus, the relative concentration of O and N on the surfaces (may be surface specific) is unknown.

A key point is that the surface can then act as a catalytic substrate which allows these atoms to recombine into ground and excited molecular states of N_2, NO, O_2[34,40] and NO_2[7] as they leave the surface. These species have been observed in heterogeneous recombination on metal surfaces in the laboratory by varying mole fractions of N and O.[40,41] There appears to be no strong preference for recombination partner. The molecular states populated will depend on the nature of the interaction between excited species and the particular surface material. The same molecular species could give rise to different glow intensities and even different spectral distributions over various surfaces. Spectrally resolved emissions can thus provide insight into the dynamics of the creation

process. For these surface-catalyzed recombinations (and for the surface reactions considered next) the extent of the glow has been interpreted to represent the region over which excited species are emitting -- the product of the emitter velocity and radiative lifetime of the excited state.

There is no reason to expect the desorbed molecule to be in thermal equilibrium with the surface either translationally, vibrationally, rotationally, or electronically. Such an equilibrium is the exception rather than the rule.[42] Swenson, et al.,[7] have invoked a translationally hot NO_2^* desorbed from the surface to reconcile the known NO_2^* lifetime with the observed glow layer thickness. In fact those authors strongly believe NO_2 is the sole source of the glow above tile surfaces.

Extremely vibrationally excited diatomics can also be created in recombination (see references in Refs. 34, 40, 41). In fact within the uncertainties of the synthetic spectral model and the noise in the orbital data, emission from highly vibrationally excited NO matches the observed glow spectral distribution at least as well as NO_2 electronic chemiluminescence. Only one incoming ambient species in 10^6 must participate in the generation of a visible photon to match the observed glow intensities. There is still sufficient residual atmosphere present in LEO to give rise to observable fluorescence from this transformation of kinetic energy into electronic excitation. Future measurements must provide extended spatial and temporal observations to discriminate the magnitudes of these various processes, i.e., the spectral distribution as a function of time after a thruster firing or the distribution as a function of time immediately after surface exposure to ram. The impact in other spectral regions (such as the infrared) will depend greatly on the emitting species. Kofsky and Barrett[43] have concluded that the infrared fluorescence intensities will be comparable to the visible for NO_2 glow constituents. By contrast, Green, et al.,[27] have shown that if highly vibrationally excited NO is the dominant glow species, the resulting infrared fluorescence will be four orders of magnitude more intense and more spatially extended.

Again it is our belief that several of these processes occur over the range of conditions encountered on-orbit. Only future measurements can define the domain of dominance for each.

The last set of mechanisms considered is the reaction of the atmospheric species with the bulk spacecraft material. This class of mechanisms was first suggested by Slanger[44] who proposed OH as the source of the glow. Subsequent spectral modeling of OH vibrational overtone emission[14] did not match the Shuttle observations of the Lockheed group[7] or the ISO data[9] but was in rough accord with the AE and DE observations.[16] As for CO and NO, our lack of knowledge about the molecular dipole moment function and rotational dependence of the Einstein coefficients at these high vibrational levels seriously affect the accuracy of the spectral modeling. Recent work on CO has improved our understanding of its dipole moment function.[45] However, because glow is clearly observed above materials which do not undergo orbital degradation, chemiluminescent reactions involving the surface materials cannot be the only glow mechanism.

Some Future Measurements Programs

Following are brief descriptions of just a few of the programs directed toward the measurement of various aspects of the glow. It is certainly incomplete. G. Fazio of Harvard had a gimballed infrared astronomical payload on the Spacelab mission this past summer. His liquid He cooled system was capable of observing infrared emission between 2 and 120 μm in a series of bandpasses. He observed no additional radiance at any wavelength above the surface of the PDP package when it was suspended near his field-of-view. Unfortunately his background levels were higher than expected and this data only bounds the IR (2 to 3 μm) photon flux as being less than 10 times the observed visible levels.

M. Torr at NASA Marshall Space Flight Center is hoping to coordinate a series of experiments to monitor the glow above several surfaces using existing hardware. These measurements would occur in calendar 1986 or 1987. This program was planned to grow out of the workshop held there last May.

At that workshop, M. Mumma, of NASA Goddard, described his planned glow package. He hopes to measure the glow in the infrared using a circular variable filter radiometer to provide spectral resolution ($\Delta\lambda/\lambda \sim 0.04$). This CVF would be flown as a hitchhiker payload and would be configured to look out of the bay. It is planned to observe emissions between 0.9 and 5.5 μm using six bandpass limited detectors. This instrument could be on a mission in calendar 1986.

Ball Aerospace has provided a getaway special cannister to the students at the University of Colorado (Boulder). They are assembling an 1/8 m Ebert-Fastie configuration UV spectrometer which will look over the Shuttle rear stabilizer surfaces using a scanning mirror. The spectral region covered is 190 to 300 nm.

Mende has proposed an infrared CVF system which would allow the glow to be observed over a number of surfaces. There are several other observational missions planned.

In addition to on-orbit observations, there are several groups planning to look at glow above surfaces in the laboratory using translationally energetic species impinging on targets. Physical Sciences Inc. as part of a program for NASA has developed a source for generating high fluxes (in excess of orbital) of 5 eV oxygen atoms. We have also observed emission above target surfaces. G. Caledonia will present these results in Session 13 tomorrow.[46] Groups at the Aerospace Corporation and Martin Marietta are also planning to look for glows in the laboratory.

Summary

Since its discovery the diffuse glow above spacecraft surfaces has been the object of great interest and concern. The observational data base is still sparce and often contradictory. The Lockheed data presented in the next paper forms the most extensive set of observations. It appears that no single mechanism can explain all of the glow observations and indeed it would be unreasonable that a single mechanism could dominate over the extremely variable conditions encountered in low earth orbit. Certainly the extended gas phase

luminescence during thruster firings and the longer lived component just above surfaces after these firings are different in character than the glow during passive observational periods. Satellites which have much smaller thruster and outgassing contamination levels still observe glow luminosities which are constant if not increasing after years.[19] Consequently chemiluminescent recombination processes where the surface provides the inert (catalytic) substrate are likely to be a source of glow above spacecraft surfaces. Kinetic analyses and spectral modeling support this conclusion. The key to our understanding of the glow is an extended data base to provide spectral (ultraviolet through infrared); temporal (to determine the interplay of processes after events such as thruster firings or exposure to ram), spatial (to discriminate the role of emission at the surface and different regimes above the surface where plasmas or species with different radiative lifetimes may dominate) and surface specific information (to isolate reactive from catalytic process). The glow may have a tremendous impact on our ability to use low earth platforms for observing our atmosphere or deep space. Certainly space telescope systems may be compromised. Hopefully in the next few years our understanding of the glow above surfaces exposed to the energetically impacting ambient flux will improve so that preventative or remedial actions can be undertaken.

Acknowledgments. This effort was supported by the Spacecraft Environment Branch at the Air Force Geophysics Laboratory and by PSI internal research funds.

References

[1]Banks, P.M., Williamson, P.R., and Raitt, W.J., "Space Shuttle Glow Observations," Geophys. Res. Lett., 10, 118, 1983.

[2]Mende, S.B., Garriott, O.K., and Banks, P.M., "Observations of Optical Emissions on STS-4," Geophys. Res. Lett., 10, 122, 1983.

[3]Mende, S.B., "Vehicle Glow," AIAA-83-2607-CP, presented at Shuttle Environment and Operations Meeting, Washington, DC, 1983.

[4]Mende, S.B., Nobles, R., Banks, P.M., Garriott, D.K., and Hoffman J., "Measurement of Vehicle Glow and Space Shuttle," J. Spacecraft Rockets, 21, 374, 1984.

[5]Mende, S.B., Banks, P.M., and Klingelsmith, III, D.A., "Observation of Orbiting Vehicle Induced Luminosities on the STS-8 Mission," Geophys. Res. Lett., 11, 527, 1984.

[6]Mende, S.B. and Swenson, G.R., "Vehicle Glow Measurements on the Space Shuttle," AIAA-85-0909, presented at AIAA 20th Thermophysics Conference, Virginia, 1985, submitted to J. Spacecraft.

[7]Swenson, G.R., Mende, S.B. and Clifton, K.S. "Ram Vehicle Glow Spectrum: Implication of NO_2 Recombination Continuum," Geophys. Res. Lett., 12, 97, 1985.

[8]Mende, S.B., "Shuttle Glow Observations and Interpretation" (Invited) AIAA-85-6096-CP, Shuttle Environment and Operations Meeting II, Houston, November, 1985.

[9]Torr, M.R. and Torr, D.G, "A Preliminary Spectroscopic Assessment of the Spacelab 1/Shuttle Optical Environment, J. Geophys. Res., 90, 1683, 1985.

[10]Torr, M. and Torr, D.G., "The Optical Environment of the Spacelab 1 Mission" (Invited), AIAA-85-7024-CP, Shuttle Environment and Operations Meeting II, Houston, November 1985.

[11]Torr, M.R., Hays, P.H., Kennedy, B.C. and Walker, J.C.G., "Intercalibration of Airglow Observations with the Atmospheric Explorer Satellite," Planet. Space. Sci., 25, 173 (1977).

[12]Yee, J.H. and Abreu, V.J., "Optical Contamination on the Atmospheric Explorer-E Satellite," Proc. SPIE-Soc. Opt. Eng., 338, 120, 1982.

[13]Yee, J.H and Abreu, V.J., Visible Glow Induced by Spacecraft - Environment Interaction, Geophys. Res. Lett., 10, 126, 1983.

[14]Abreu, V.J., Skinner, W.R., Hays, P.B., and Yee, J.H., "Optical Effects of Spacecraft-Environment Interaction: Spectrometric Observations by the DE-2 Satellite," J. Spacecraft Rockets 22, 177, 1985.

[15]Yee, J.H., Abreu, V.J., and Dalgarno, A., "The Atmospheric Explorer Optical Glow Near Perigee Altitudes," Geophys. Res. Lett. 12, 651, 1985.

[16]Langhoff, S.R., Jaffe, R.L., Yee, J.H., and Dalgarno, A., "The Surface Glow of the Atmospheric Explorer C and E Satellites," Geophys. Res. Lett., 10, 896, 1983.

[17]Torr, M.R., "Optical Emissions Induced by Spacecraft-Atmosphere Interactions," Geophys. Res. Lett., 10, 114, 1983.

[18]Chakrabarti, S. and Sasseen, T., "Investigation of the Vehicle Glow in the Far Ultraviolet," Submitted to J. Geophys. Res., also Chakrabarti, S. and Bowyer, S., "The Space Shuttle for Ultraviolet Environment," AIAA-85-6099-CP Shuttle Environment and Operations, Meeting, Houston, November 1985.

[19]Yee, J.H., Private Communication, 1985.

[20]U.S. Standard Atmosphere 1976, 227 pp., U.S. Government Printing Office, Washington, DC, October 1976.

[21]Mende, S.B., Private Communication, 1985

[22]Yee, J.H. and Dalgarno, A., "Radiative Lifetime Analysis of the Spacecraft Optical Glow," AIAA-83-2660-CP presented at Shuttle Environment and Operations Meeting, 1983.

[23]Green, B.D., Marinelli, W.J. and Rawlins, W.T., "Spectral Identification/Elimination of Molecular Species in Spacecraft Glow," Proceedings of the Second Workshop on Spacecraft Glow, NASA/MSFC, May 1985.

[24]Papadopoulos, K., "On the Shuttle Glow (The Plasma Alternative)," Radio Science, 19, 571, 1984.

[25]Visentine, J.T., Leger, L.J., Kuminecz, J.F., Spiker, I.J., "STS-8 Atomic Oxygen Effects Experiment," AIAA-85-0415, AIAA 23rd Aerospace Sciences, Meeting, Reno, January 1985.

[26]Whitaker, A.F., Little, S.A. Harwell, R.J., Griner, D.B., and DeHaye R.F., "Orbital Atomic Oxygen Effects on Thermal Control and Optical Materials - STS-8 Results," AIAA-85-0416, AIAA 23rd Aerospace Sciences Meeting, Reno, January. 1985

[27]Green, B.D., Murad, E. and Rawlins, W.T., "The Nature of the Glow and its Ramifications on Space Based Observations," AIAA-85-0910 presented at 20th Thermophysics Conference (VA, June 1985).

[28]Witteborn, F.C., O'Brient, K., and Caroff, L., "Measurements of the Nighttime Infrared Luminosity of Spacelab 1 in the H- and K-bands," NASA Tech. Memo. 85972, 1985.

[29]Huffman, R.E., LeBlanc, F.J., Larrabee, J.C. Paulsen, D.E. and Baisley, V.C., "Ultraviolet Horizon Radiance Measurements from Shuttle," AIAA-83-2628-CP, Shuttle Environment and Operations Meeting, Washington, D.C., November 1983.

[30]Shawhan, S.D., Murphy, G.B., and Pickett, J.S., "Plasma Diagnostics Package Initial Assessment of the Shuttle Orbiter Plasma Environment," J. Spacecraft, 21, 389, 1984.

[31]Miller, E., ed., "STS-2, -3, -4 Induced Environment Contamination Monitor (IECM)," NASA TM-82524, February 1983.

[32]Miller, E., ed., "Induced Environment Contamination Monitor - Preliminary Results from the Spacelab 1 Flight," NASA TM-86461, August 1984.

[33]Narcisi, R.S., Trzcinski, E, Frederico, G., and Wlodyka, L., "The Gaseous Environment Around Space Shuttle," AIAA-83-2659-CP, Presented at Shuttle Environment and Operations Meeting, Washington, D.C., 1983.

[34]Green, B.D., Caledonia, G.E., and Wilkerson, T.D., "The Shuttle Environment: Gases, Particles, and Glow," J. Spacecraft and Rockets, 22, 500, 1985.

[35]Kofsky, I.L., "Spectroscopic Consequences of Papadopoulos' Discharge Model in Spacecraft Ram Glows," Radio Sci., 19, 578,1984.

[36]McMahon, W.J., Salter, R.H., Hills, R.S., and Delory, D., "Measured Electron Contribution to Shuttle Plasma Environment," AIAA-83-2598-CP Shuttle Environment and Operations Meeting, Washington, D.C., November 1983.

[37]Scialdone, J.J., "Self-contamination and Environment of an Orbiting Spacecraft," NASA-TN D-6645, May 1972; and Scialdone, J.J., "An Estimate of the Outgassing of Space Payloads, Their Internal Pressures, Contaminations, and Gaseous Influences on the Environment," AIAA-85-0957 presented at AIAA 20th Thermophysics Conference, VA, June 1985.

[38]Prince, R.H., "On Spacecraft-Induced Optical Emission: A Proposed Second Surface Luminescent Continuum Component," Geophys. Res. Lett., 12, 453, 1985.

[39]Bozco, F., Yales, J.T., Jr., Arias, J., Metiu, H., and Martin, R.M., "A Surface Penning Ionization Study of the CO/Ni(111) System," J. Chem. Phys., 78, 4256 (1983).

[40]Green, B.D., "Atomic Recombination into Excite Molecular States - A Possible Mechanism for Shuttle Glow, Geophys. Res. Lett., 11, 576, 1984.

[41]Chu, A-L, Reeves, R.R., and Halstead, J.A., "Surface Catalyzed Formation of Electronically Excited Nitrogen Dioxide and Oxygen," submitted to J. Phys. Chem., 1985.

[42]Tolk, N., Albridge, R., Haglund, R., Memdenhall, M. and Tully, J., "Neutral-Particle Erosion and Optical Radiation Processes Produced by Particle and Photon Beams on Surfaces," Proceedings of Second Workshop on Spacecraft Glow NASA/MSFC, May 1985.

[43]Kofsky, I.L. and Barrett J.L. "Infrared Emission from NO_2^* and NO^* Desorbed from LEO Spacecraft and Surfaces," Proceedings of Second Workshop on Spacecraft Glow, NASA/MSFC, May 1985, submitted to J. Spacecraft and Rockets, June 1985.

[44]Slanger, T.G., "Conjectures on the Origin of the Surface Glow of Space Vehicles," Geophys. Res. Lett., 10, 130, 1983.

[45]Chackerian, C., Jr., Farrenq, R., Guelachvili, G., Rossetti, C., and Urban, W., "Experimental Determination of the $^1\Sigma^+$ State Electric Dipole Moment Function of Carbon Monoxide up to a Large Internuclear Separation," Can. J. Phys., 62, October 1984.

[46]Caledonia, G.E. and Krech, R.M., "Development of a High Flux Source of Energetic Oxygen Atoms for Material Degradation Studies," AIAA-85-7015-CP, Shuttle Environment and Operations Meeting II, Houston, November 1985.

APPENDIX H

Chemical Interactions in Low-Earth Orbit

Gordon Research Conference on High Temperature Chemistry (1986)

VG87-7 is reproduced in its entirety.

VG87-7

CHEMICAL INTERACTIONS IN LOW EARTH ORBIT

B.D. GREEN

PHYSICAL SCIENCES INC.

GORDON RESEARCH CONFERENCE ON
HIGH TEMPERATURE CHEMISTRY

23 JULY 1986

VG87-7

CHEMICAL INTERACTIONS IN LOW EARTH ORBIT

B.D. GREEN

PHYSICAL SCIENCES INC.

GORDON RESEARCH CONFERENCE ON
HIGH TEMPERATURE CHEMISTRY

23 JULY 1986

VG87-7

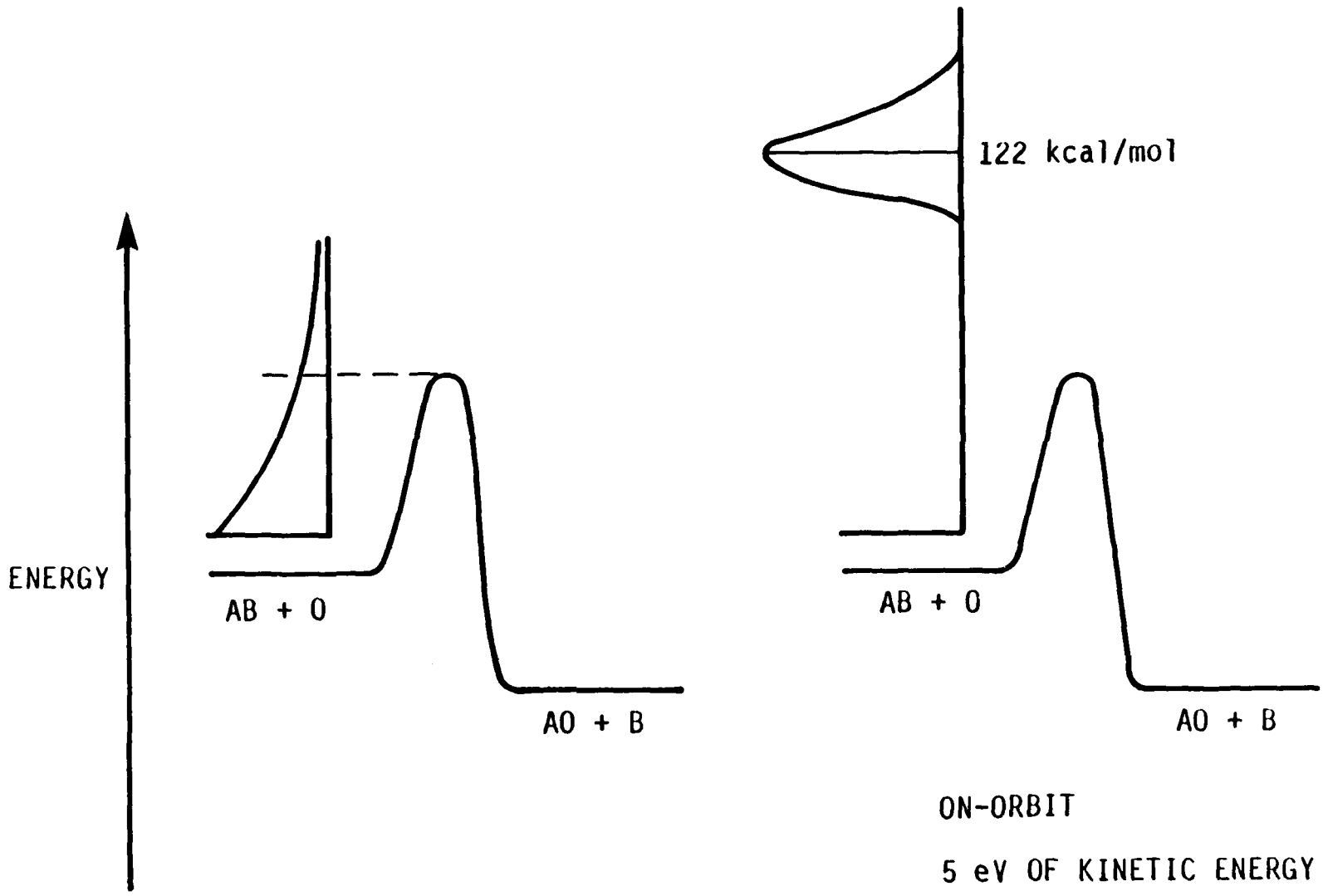

ON-ORBIT

5 eV OF KINETIC ENERGY

TEMPERATURE OF 1000K

THE AMBIENT ATMOSPHERE

- SHUTTLE MISSIONS 240-300 km
- ATMOSPHERIC DENSITY $10^9/cm^3$ ($\sim 10^{-8}$T)
- TEMPERATURE ≈ EXOSPHERIC 800-2000 K
- MEAN FREE PATH 1 km
- COMPOSITION AT 300 km

O	N_2	HE	O_2	H	AR
5.4(8)	9.6(7)	7.6(6)	3.9(6)	1.0(5)	1.6(5)
83%	15%	1.2%	0.6%	--	--

- VARIABILITIES
- IONOSPHERE
  - F2 LAYER
  - HIGHEST PLASMA DENSITY 10^5 - 10^6 cm^3 [0.1% IONIZED]
  - EXTREMELY VARIABLE WITH SEASON/SOLAR ACTIVITY
  - F2 PEAK LOWER DAY / HIGHER NIGHT

OBSERVATIONS

- SHUTTLE RETURN SAMPLES FROM ORBIT (1 WEEK EXPOSURE)
- SURFACES EXPOSED TO RESIDUAL ATMOSPHERE
  - ERODED - MASS LOSS VERY MATERIAL SPECIFIC
  - MODIFIED
    - STRUCTURAL CRACKS/FLAKES FOUND
    - ELECTRICAL CONDUCTIVITY $Ag \rightarrow AgO$
  - GLOWS OBSERVED

OXIDE FORMATION AND FATE

- Ag: RAPIDLY FORMS TRANSPARENT OXIDE, MECHANICALLY UNSTABLE - CRACKS AND FLAKES
- Ni, Cu: MORE SLOWLY FORMS OXIDE LAYER
- Al: FORMED EXPANDED OXIDE LAYER, GAINS MASS
- C: DISAPPEARS - CO
- Os: DISAPPEARS - OsO_4
- W: SLOWLY DISAPPEARS

PETERS, GREGORY AND SWANN APPL. OPT. 1986

SILVER OXIDE FORMATION

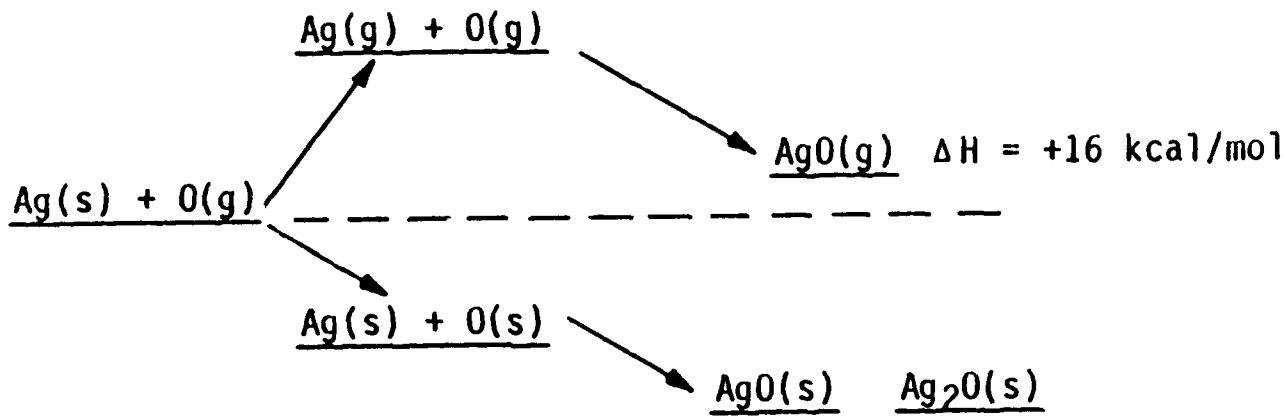

- RAPID REACTION; EXPOSED SURFACE EXPANSION
- POOR MECHANICAL PROPERTIES $Ag_2O(s)$ RESULT CONSTANT EXPOSURE FRESH SURFACES
- CLEARLY SURFACE REACTION
- ONLY CONDENSED PHASE OXIDE IS ALLOWED THERMODYNAMICALLY

COPPER (AND NICKEL) OXIDE FORMATION

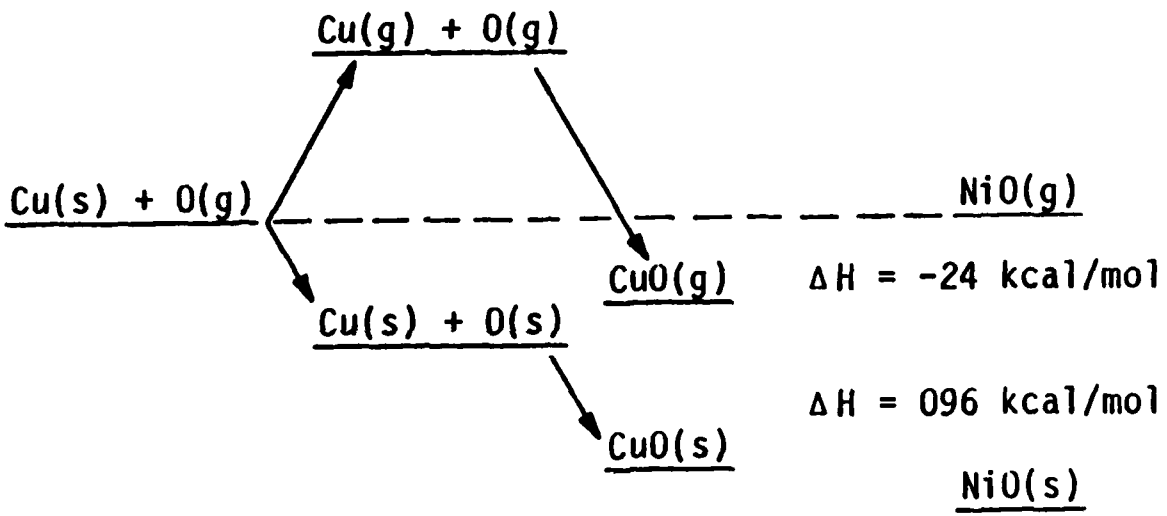

- GAS PHASE PRODUCTS NET EXOTHERMIC; NO MASS LOSS SEEN
- SURFACE REACTION PATHWAY, PRODUCT REMAIN ON SURFACE

CO FORMATION

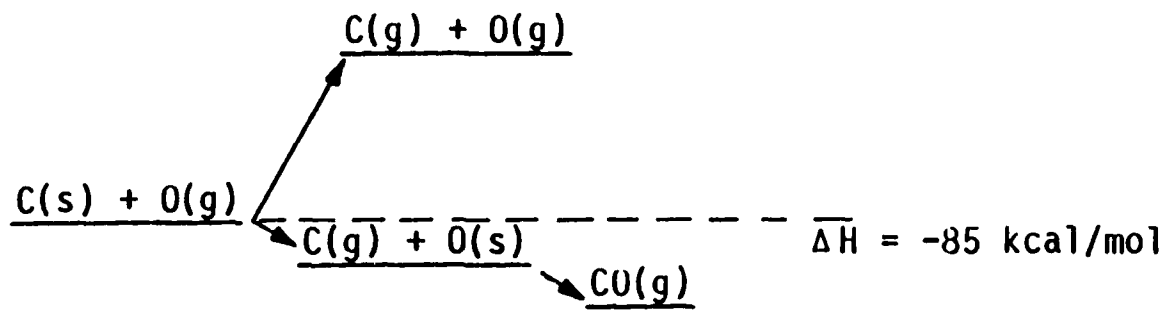

- CARBON BLACK REMOVED FROM SURFACES COMPLETELY
- THERMAL EXPERIMENTS LANGMUIR-HENSHELWOOD DOMINATE RIDEAL[1] THEORY RIDEAL GIVE MORE CO* [2]
- IMPACT ON GLOW
- LABORATORY BEAM STUDIES[3] DO NOT INDICATE STRONG DEPENDENCE ON ENERGY OF IMPACT UP TO 1.0 eV

[1] KORI + HALPERN CPL 1983
[2] TULLY JCP 1980
[3] ARNOLD AIAA MEETING

ALUMINUM OXIDE FORMATION

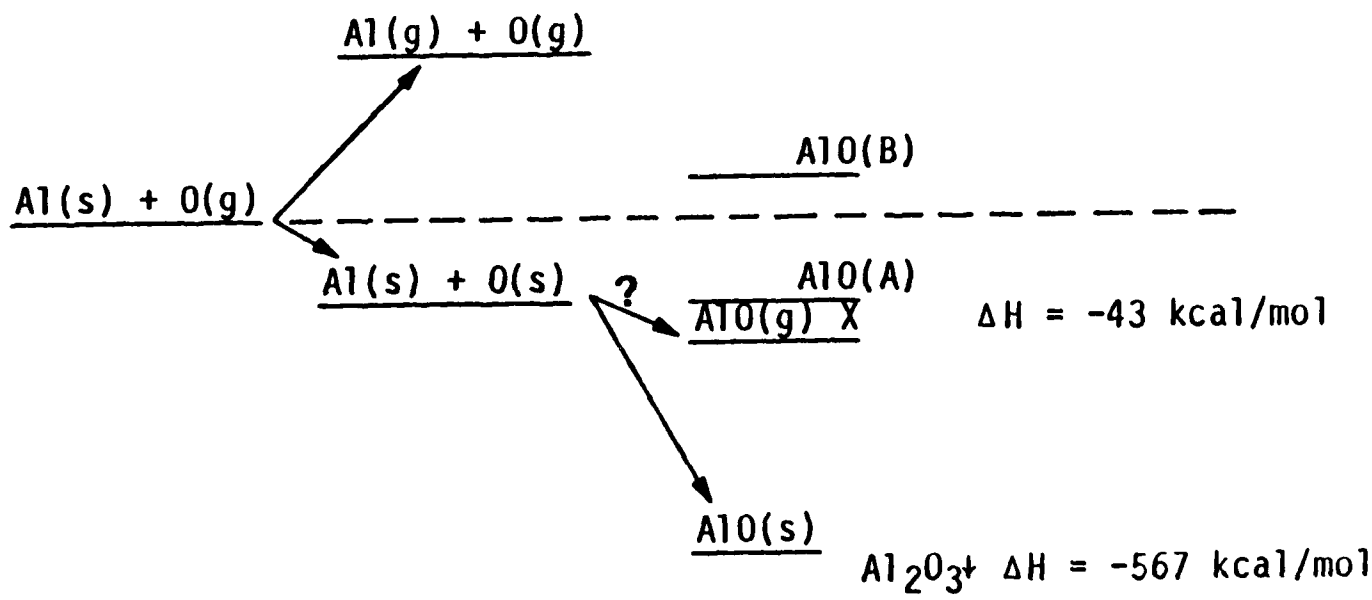

- EXPOSED SURFACE EXPANSION
- AlO(g) FORMATION FROM SURFACE ATOMS IS EXOTHERMIC
- ORBITAL OBSERVATIONS FAVOR AlO(s)
- LABORATORY OBSERVATION OF AlO(g) B STATE
  - ENDOTHERMIC UNLESS KINETIC ENERGY PLAYS A ROLE

TUNGSTEN OXIDE FORMATION

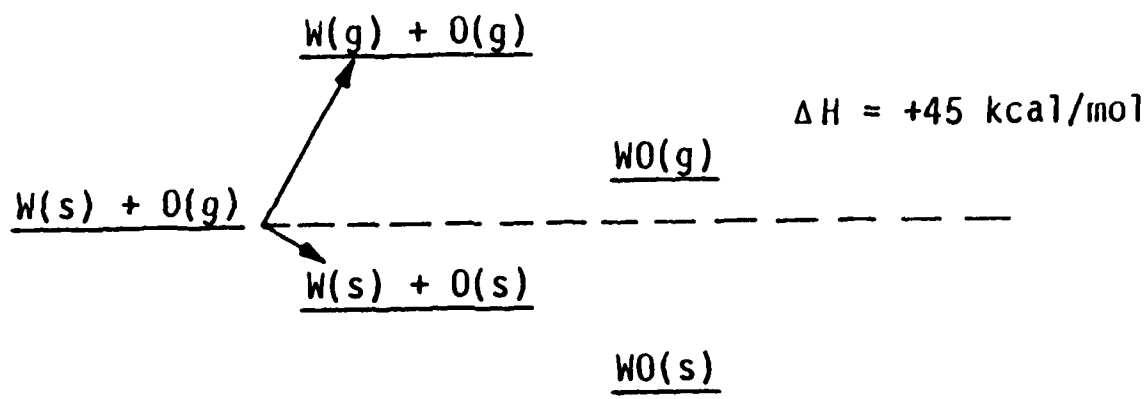

- W IS SLOWLY REMOVED, NO OXIDE IS FORMED
- GOLD IS NOT SPUTTERED, SO KINETIC ENERGY SPUTTER REMOVAL W NOT LIKELY
- WO(g) FORMED? $O_{fast} + W(s) \rightarrow WO(g)$ RIDEAL MECHANISM?

SURFACE MODIFICATION

- ESCA ANALYSIS OF POLYETHYLENE FILM (50Å)

	$-CH_2-CH_2-$	C-O	C=O OH	O
CONTROL	99.2			0.8
ORBITAL	81.5	4.5	3.1	9.9

- ESCA ANALYSIS OF Z306 (BLACK) PAINT
  - CARBON FILLED POLYURETHANE PAINT FILLED WITH SILICA
  - EROSION PROCEEDS UNTIL SiO_2 LAYER FORMS PROTECTIVE BARRIER

STRUCTURAL IMPACTS

- REACTION EFFICIENCIES UP TO 18% (ATOM REMOVED/ATOM INCIDENT)
- SPACE STATION STRUCTURAL SUPPORTS (GRAPHITE-EPOXY) LOSE 70% OF MASS DURING 30 YEAR LIFETIME
- SOLAR CELL Ag INTERCONNECTS BECOME AgO(INSULATE)
- PROTECTIVE COATINGS
  - METALLIZED FAILS - FRAGILE
  - FLUOROPOLYMERS - BRITTLE

SPECTRAL DISTRIBUTION OF GLOW OBSERVATIONS

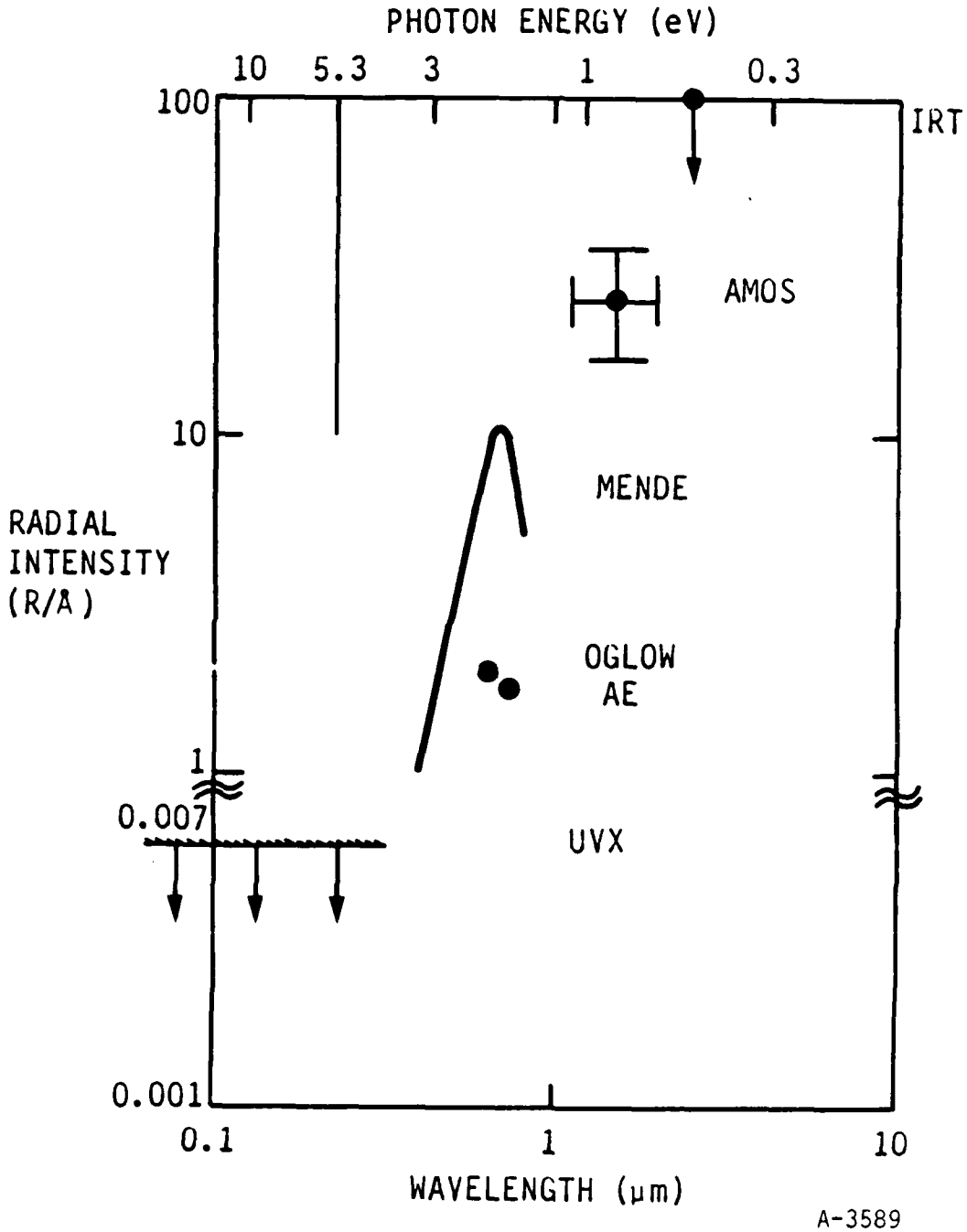

A-3589

LABORATORY FAST ATOM/MOLECULE SOURCES

- ARC-HEATED SUPERSONIC BEAMS
- RF DISCHARGES
- SHOCK TUBES
- CHARGE EXCHANGE
- PHOTODETACHMENT OF NEGATIVE ION BEAMS
- TOROIDAL PLASMA IONS REFLECTED AND NEUTRALIZED ON SURFACES
- PHOTODISSOCIATION OF O_3
- LASER SUSTAINED/SEEDED DISCHARGE EXPANSION
- LASER INDUCED BREAKDOWN

ARNOLD AND PEPLINSKI (1984) AEROSPACE REPORT

$$p = 1.8 \exp(-0.18/E_t)$$

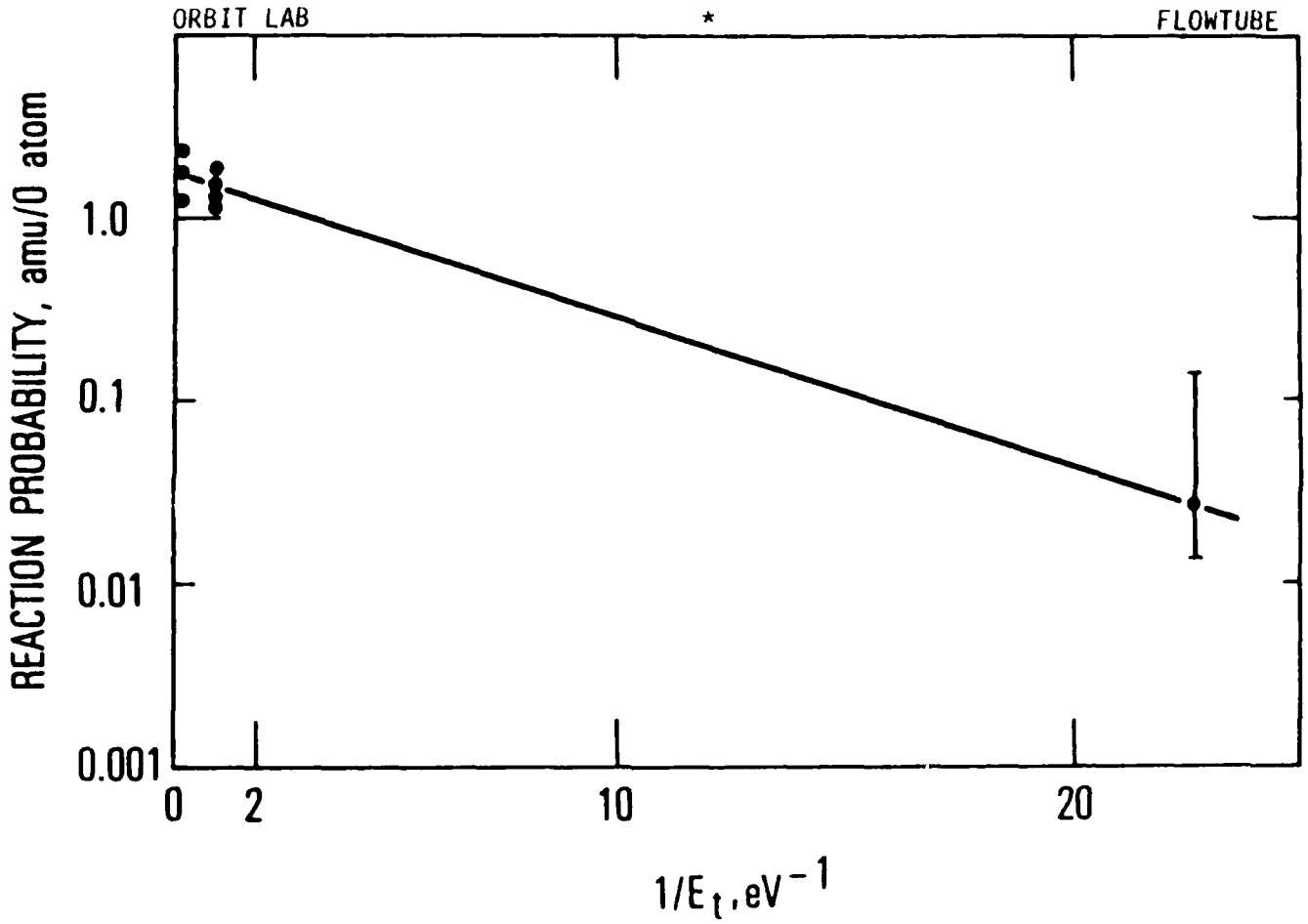

EMISSION FROM N_2 IN ACT-1 DEVICE

LANGER et al. (1986) GRL

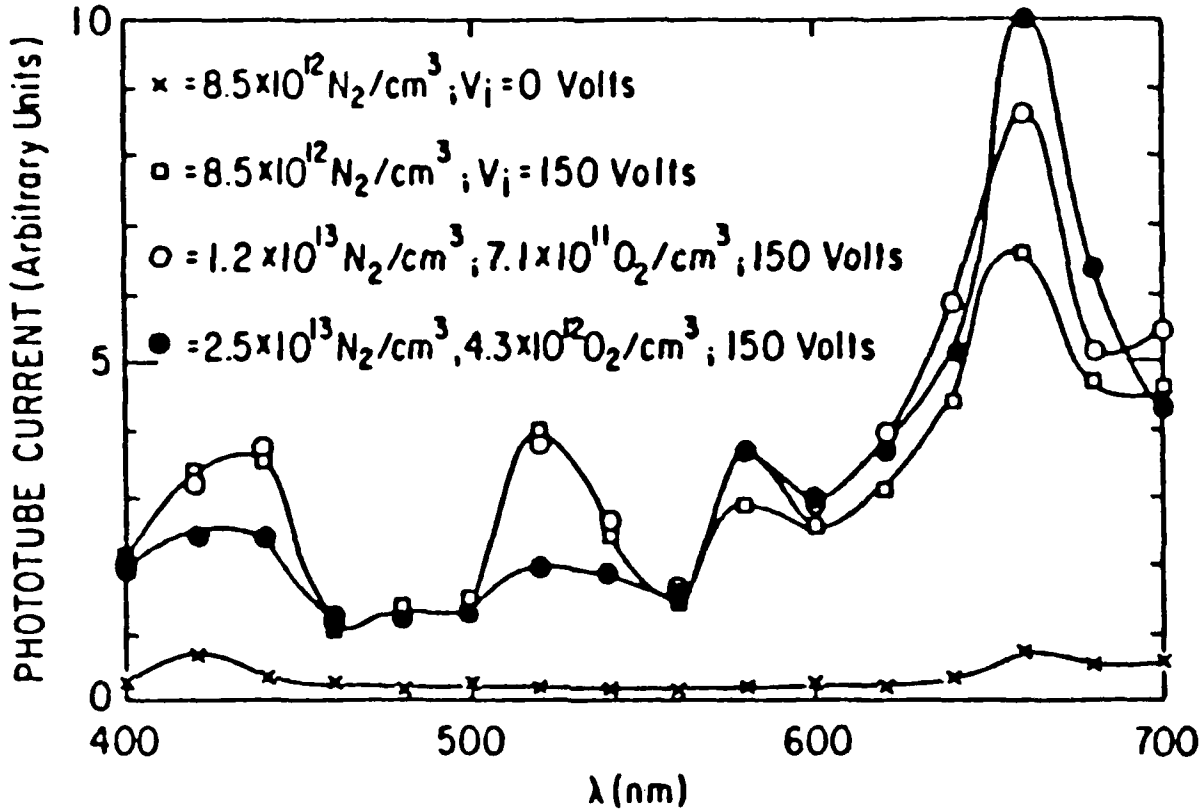

AlO* FORMATION IN LASER INDUCED BREAKDOWN EXPERIMENT

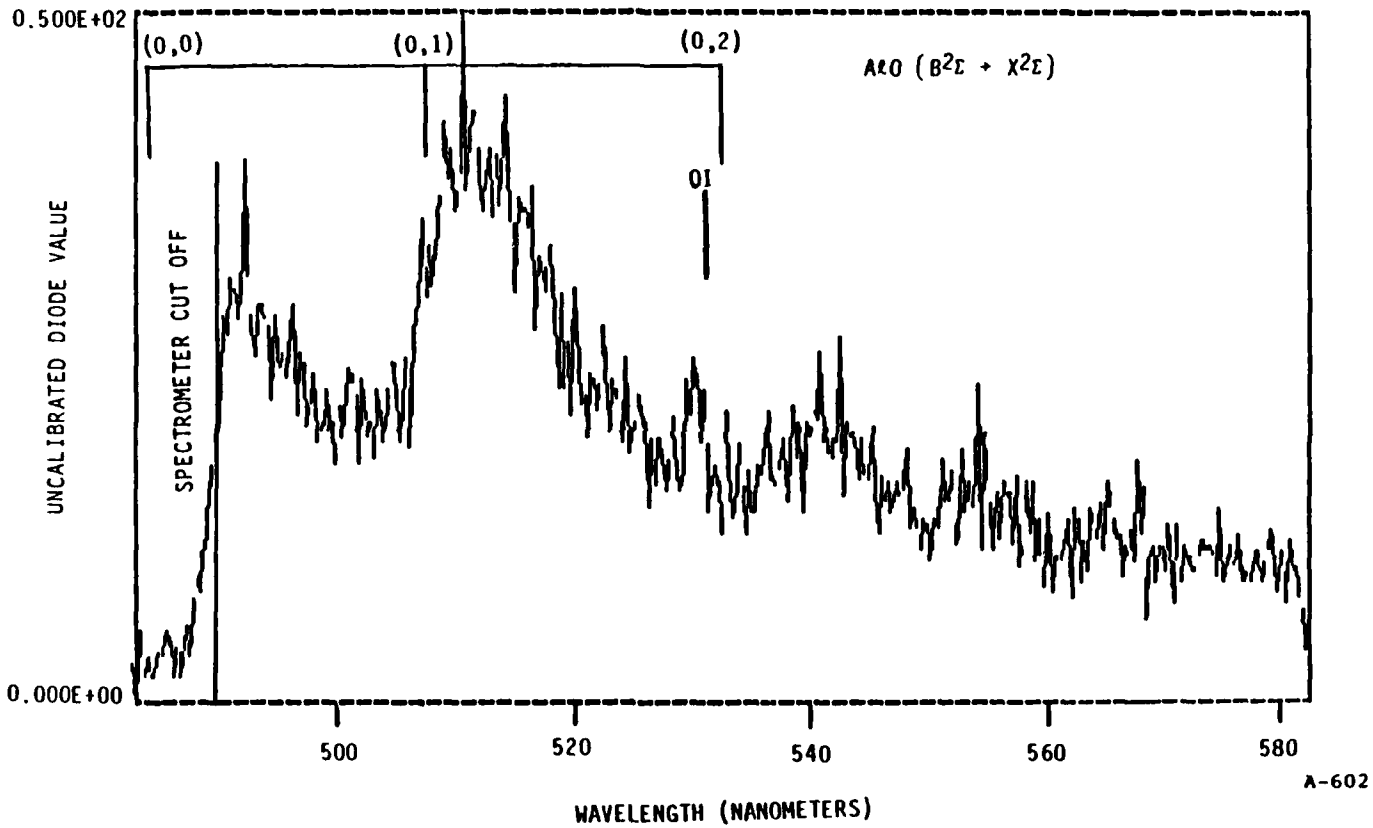

KINETIC vs INTERNAL ENERGY

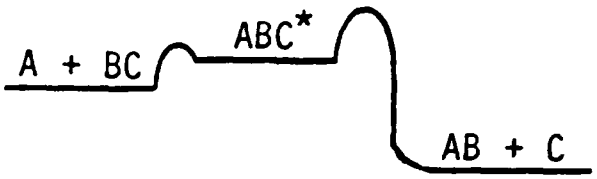

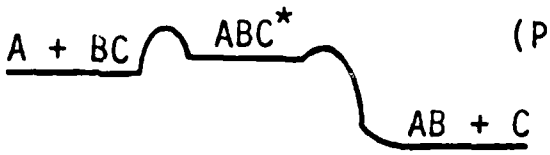

(POLANYI 1969)

INTERNAL MORE EFFICIENT

KINETIC ENERGY MORE EFFICIENT

- INTERNAL BETTER:
  - $He + H_2 \rightarrow HeH^+ + H$ (TURNER (LEE) 1984)
  - $C_2H_2^+ + H_2 \rightarrow C_2H_3^+ + H$
  - $NH_3^+ + CH_3OH \rightarrow CH_3OH_2^+ + NH_2$; $NH_3^+ + CH_3OH \rightarrow NH_4^+ + CH_3O$ (MARX 1986)
- NO DEPENDENCE (7.4-12.4 kcal/mol)
  - $O + C_2H_3Br \rightarrow C_2H_2BrO + H$; $O + C_2H_3Br \rightarrow CH_2Br + CHO$; $O + C_2H_3Br \rightarrow Br + C_2H_3O$ (He (LEE) 1982)

CONCLUSIONS

- MANY ORBITAL OBVSERVATIONS / THERMODYNAMICALLY REASONABLE IN RETROSPECT
- LABORATORY EXPERIMENTS AND THEORETICAL CALCULATIONS ARE NEEDED TO ELUCIDATE REACTION PATHWAYS
  - ADSORBATE/SURFACE REACTIONS
  - BEAM/SURFACE REACTIONS (THERMAL - eV)
- KINETIC ENERGY LEADS TO NON-EQUILIBRIUM PARTITIONING IN PRODUCTS
  - EROSION
  - GLOW
  - LABORATORY

ORBITAL INTERACTIONS

- MANY OBSERVATIONS NOT UNDERSTOOD
  - WIDELY DISSEMINATED
  - NEW SETS OF NON-INTUITIVE PROCESSES INVOLVED
  - INTERESTING SCIENCE FORTUITOUSLY
- NEED UNDERSTANDING
  - PERFORM BETTER EXPERIMENTS ON-ORBIT
  - EXPLORE NEW PROCESSES NOT ARTIFACTS
- SHUTTLE MOVES 8 km/s IN ITS ORBIT
  - RESIDUAL ATMOSPHERIC SPECIES IMPACT SURFACES
  - KINETIC ENERGIES ~5 to 10 eV (100 to 250 kcal/mol)
  - EROSION AND CHEMILUMINESCENCE
  - ROLE KINETIC ENERGY, NOT TEMPERATURE, ON REACTION RATES AND PATHWAYS

CONCLUSIONS

- MANY ORBITAL OBSERVATIONS THERMODYNAMICALLY REASONABLE IN RETROSPECT
- LABORATORY EXPERIMENTS AND THEORETICAL CALCULATIONS ARE NEEDED TO ELUCIDATE REACTION PATHWAYS
  - ADSORBATE/SURFACE REACTIONS
  - BEAM/SURFACE REACTIONS (THERMAL - eV)
  - CHEMILUMINESCENCE STUDIES
- KINETIC ENERGY LEADS TO NON-EQUILIBRIUM PARTITIONING IN PRODUCTS
  - EROSION
  - GLOW
  - LABORATORY
- KINETIC ENERGY IS ANOTHER TOOL TO PROBE POTENTIAL ENERGY SURFACES

APPENDIX I

Spectral Signatures of Micron-Sized Particles in the Shuttle Optical Environment

Applied Optics 26, 3052 (1987)

PSI-139/SR-241 is reproduced in its entirety.

PSI-139/
SR-241

SPECTRAL SIGNATURES OF MICRON-SIZED PARTICLES IN THE SHUTTLE OPTICAL ENVIRONMENT

W.T. Rawlins and B.D. Green
Physical Sciences Inc.
P.O. Box 3100, Research Park
Andover, MA 01810

Abstract

Solar-illuminated particulates surrounding the space Shuttle have been observed repeatedly in Shuttle missions. Particulate loadings are especially severe after ventings, temporarily obscuring stellar radiances and precluding remote observations. However, even very low particulate loadings can interfere optically with measurements of earth limb emissions. Depending on wavelength and particle size, the important optical contributions can be scattering of solar radiation, scattering of earth radiation, and particle self-emission. In the latter case, the particles radiate at a temperature which is achieved through radiative equilibrium with the earth and the sun. In general, for grey or black particles, solar scattering will dominate in the visible and self-emission will dominate in the infrared beyond 4 μm, and the effects can be predicted in a straightforward manner. However, for likely contaminant particles such as ice, the real and imaginary components of the complex index of refraction follow complex and highly structured behavior with wavelength. As a result, the spectral behavior of the scattering and emission contributions will exhibit pronounced wavelength dependencies, e.g., strong emission/absorption bands near 3 and 12 μm, which will in turn be sensitive to particle size in the micron range. We compare predicted particle brightnesses for ice as functions of wavelength through the visible and infrared, and as functions of particle size between the volume absorption and geometric scattering

regimes. Predicted brightnesses are compared to expected atmospheric limb radiances in various spectral bandpasses to illustrate conditions under which earth limb sensors would be affected and the means for identifying particulate contributions.

I. Introduction

Dispersed particulates in the vicinity of Shuttle have long been of concern due to their potential to interfere with Shuttle-borne optical measurements. The scattering/emission signatures of particulate clouds or even individual particles can impact passive and active optical probes (e.g., of earth limb airglow emission) in the ultraviolet, visible, and infrared regions of the optical spectrum. Thus, it is important to assess not only the degree and characteristics of particulate loadings at various points throughout the Shuttle flights, but also the resulting spectral signatures for a variety of illumination conditions and detection geometries. We describe here the use of Mie scattering theory to predict particulate spectral signatures for a variety of observation conditions.

The primary factors which influence particulate optical effects are: 1) the wavelength-dependent complex refractive index of the particles, which is of course strongly dependent upon particle composition and perhaps also somewhat dependent upon particle temperature; 2) the wavelength range of the measurements, since the radiation from particles of a given size depends markedly on the spectral behavior of not only the Mie cross sections for scattering and extinction but also the light sources with which the particles are illuminated; 3) sensor configuration, i.e., field of view of the near field, fixed wavelength or spectrally scanning, scan rate, monochromatic or interferometric scanning, etc.; and 4) the time-dependent characteristics of

the particle field, i.e., number of particles in a given field of view at a given time, their sizes, shapes, spatial distribution, and velocity vectors, and the correlation of these with source activities aboard the Shuttle. The first three factors can be addressed theoretically and are the subject of this paper. The results of this treatment may then be coupled with the Shuttle-borne observations of particle fields to predict optical effects for specific sensors. Initial observations of the particle fields for early Shuttle missions were carried out by Miller and co-workers[1] using photographic stereo-imaging of solar-illuminated particles. A similar experiment, designated Particle Analysis Camera for Shuttle (PACS)[2] and employing additional illumination of the near field by an ultraviolet strobe, was successfully flown in early 1986 on Space Transportation System Mission STS 61-C by M. Ahmadjian and R. Murphy of the Air Force Geophysics Laboratory; the results of these observations will be analyzed using these calculational methods and will be reported elsewhere.

Observations and characterizations of the particulate environment of Shuttle are reviewed by Green, et al.[3] In general, particulate loadings are found to be small, except during brief periods following venting episodes. Since spacecraft water dumps are prolific sources of particulates, it is likely that ice is the principal particulate species observed near Shuttle. However, thruster firings also appear to eject particles; these may be metallic or carbonaceous materials having significantly different optical properties. In addition, activities around Shuttle, e.g., a satellite launch, other activity in the bay, thermal stresses, or astronaut extravehicular activity (EVA), could cause particles to be dislodged from surrounding surfaces; these

particles may well be large, irregularly shaped, and of unknown composition. Since it is likely that sensitive optical measurements will be conducted during periods of minimal activity, the principal contamination as indicated by the data base will arise from sparse (1 to 10 particles in the field of view) fields of small (<< 1 mm diameter) ice particles formed either directly from earlier liquid vents or by flaking from accumulated frost deposits on the vent nozzles. The particle shapes and relative size distributions formed by these two mechanisms are difficult to anticipate without a detailed treatment of the fluid dynamics of the phenomena occurring in the liquid vent. As discussed further below, we have assumed spherical shapes to simplify the present parameter study.

The optical properties of ice vary dramatically across the optical spectrum. Ice particles are nearly perfect scatterers in the visible, having almost no imaginary component to the complex index of refraction, but exhibit significant absorption in the infrared through bands near 3, 12, and 50 μm. Thus, the relative contributions of light scattering and self-emission will vary significantly with particle size and wavelength in the infrared. In addition, the computation of scattering and absorption efficiencies for these particles in the visible and infrared covers a large range of particle size/wavelength ratio, from the Rayleigh (small particle) limit to the anomalous and ordinary diffraction ranges of Mie theory, resulting in scattering and absorption effects which are difficult to anticipate without rigorous computation of the cross sections.

In this paper, we use the Mie theory to compute absorption and scattering efficiencies of single spherical ice particles of radius 0.1 to 30 μm for

wavelengths of 0.1 to 100 μm. We then couple these values with the spectral radiance of the sun and earth in order to determine the effective particle brightness to an observer on-board Shuttle. Finally, we will use the predicted particle spectra to assess the potential for interference with Shuttle-borne optical measurements.

II. Absorption and Scattering Efficiencies

The expressions for Mie scattering involve series whose terms contain spherical Bessel functions with complex argument and first and second derivatives of the Legendre polynomials;[4,5] the number of terms required for evaluating the series with reasonable accuracy is of the order of the size parameter $x = 2\pi r/\lambda$. The operative equations are:

$$Q_E = \frac{2}{x^2} \sum_{n=1}^{\infty} (2n + 1) \left[\mathrm{Re}(a_n) + \mathrm{Re}(b_n)\right]$$

$$Q_S = \frac{2}{x^2} \sum_{n=1}^{\infty} (2n + 1)\left[|a_n|^2 + |b_n|^2\right]$$

$$Q_A = Q_E - Q_S$$

$$i(\theta) = \frac{1}{2}\{|S_1(\theta)|^2 + |S_2(\theta)|^2\}$$

where

$$S_1(\theta) = \sum_{n=1}^{\infty} \frac{2n+1}{n(n+1)}\{a_n\pi_n(\cos\theta) + b_n\tau_n(\cos\theta)\}$$

$$S_2(\theta) = \sum_{n=1}^{\infty} \frac{2n+1}{n(n+1)}\{b_n\pi_n(\cos\theta) + a_n\tau_n(\cos\theta)\} .$$

The Mie coefficients a_n and b_n and the phase functions π_n and τ_n are given on pp. 123 ff. of Ref. 4. We have computed values of the absorption and scattering efficiencies, Q_A and Q_S, and the angular differential scattered intensities $i(\theta)$, for unpolarized light and spherical particles, using the refractive index data from the compilation of Warren[6] and a downward recurrence numerical method[7] validated for size parameters up to $x = 1500$.

It should be noted that the refractive index data of Warren[6] are appropriate for bulk ice (Ih) at temperatures of 266 K and are therefore somewhat uncertain for small particles at the lower temperatures encountered here. In addition, non-spherical particles are likely to appear under some (or perhaps all) conditions, most notably at the large sizes. Particle shape effects have been treated theoretically (see, for example, Refs. 8-9 for specific effects in ice crystals for large size parameter), and tend to manifest themselves primarily in the degree of polarization of the scattered light.[4] Additional minor effects on the scattering phase function may cause changes in the fine details of the predicted differential scattering patterns. In view of the extreme difficulty of treating shape effects adequately, we have chosen to examine the general scattering characteristics for spherical particles, and to defer more detailed treatments until they are warranted by the <u>in situ</u> data base.

Computed values of Q_A and Q_S for three different particle radii are plotted in Figures 1 through 3. As might be anticipated, the small particles exhibit predominantly scattering at visible wavelengths (0.3 to 0.8 μm) and absorption at long wavelengths, with the absorption occurring in broad but discrete bands. However, as the particle size increases, the scattering

efficiency extends well into the infrared, and the infrared absorption both increases substantially and loses spectral structure, approaching the characteristics of a blackbody at wavelengths beyond 3 μm.

Example angular scattering patterns for different size parameters are shown in Figure 4. The complex behavior with increasing particle size is readily apparent but difficult to generalize. However, it is clear that forward scattering ($\theta \sim 0°$) is an extremely important effect for mid-sized to large particles, and backward scattering ($\theta \sim 180°$) also becomes important for large particles. It should be noted that $i(\theta)$ and Q_S are related by:[4]

$$Q_S = \left(\frac{\lambda}{2\pi r}\right)^2 2 \int_0^{\pi} i(\theta) \sin\theta \, d\theta \tag{1}$$

Hence the intense forward scattering lobe makes little contribution to the spatially integrated scattered intensity. In practical terms, observation angles for natural solar scattering will probably be restricted to 30 to 150 deg to avoid viewing the source directly or shadowing the particles with the orbiter. However, more acute forward scattering can be an important consideration in multiple scattering conditions (e.g., "whiteout").

In order to model the sparse particle field, we must compute the naturally occurring single-particle radiances. Thus, we must superimpose on these cross-sections the spectral radiance of the principal visible and infrared light sources, the sun and the earth. These are displayed in Figure 5; we have taken the solar spectral radiance from Ref. 10 and the earth radiance curves from Ref. 11. The curves for earthshine represent computations of blackbody radiation from the earth's surface as propagated vertically to space, with atmospheric absorption taken into account. The magnitude and spectral distribution of the earth radiance depend upon the local conditions;

we have used the extreme cases of tropical and subarctic winter conditions. Note from these curves that, in low earth orbit, the earth is brighter than the sun in the long-wavelength infrared ($\lambda > 5\ \mu m$). Thus, we expect earthshine to control the particulate radiation and infrared scattering signatures with negligible diurnal effects, while the sun contributes mainly to ultraviolet and visible scattering on the day side. For the present study, we do not consider contributions from earth-reflected solar radiation on the day side, zodiacal light and lunar-reflected solar radiation on the night side, or spacecraft light sources.

III. Particle Absorption/Emission

The power radiated at a wavelength λ by a single spherical particle of radius r and temperature T is given by:

$$I_R(\lambda) = 4(\pi r)^2 Q_A^r(\lambda) N(\lambda,T) \tag{2}$$

where Q_A^r is the absorption efficiency (analogous to a single-particle emissivity) computed from the refractive index and $N(\lambda,T)$ is the Planck blackbody function. To evaluate the particle temperatures, we consider that, following nucleation, the particles cool radiatively to a steady state temperature which represents radiative equilibrium, i.e., the radiative output of the particle balances the power absorbed from the radiation field of the earth and sun. (It is straightforward to show that gas-particle collisional effects are negligible at orbital altitudes, even for the high collision energies encountered at orbital velocities; similarly, intraparticle heat transport is sufficiently rapid to ensure equal surface and bulk temperatures.) For low earth orbit (altitude << earth radius), the radiative equilibrium condition is given by:

$$\pi r^2 \int_0^\infty (J_\lambda + \pi I_\lambda)\, Q_A^r(\lambda) d\lambda = \int_0^\infty I_R(\lambda) d\lambda \tag{3}$$

where J_λ and πI_λ are the spectral irradiances of the sun and earth, respectively. Equation (3) is transcendental in T and must be solved iteratively to determine the particle temperatures. Solutions for different particle sizes and illumination conditions are shown in Figures 6 and 7. Inspection of the running integrals for the left and right hand sides of Eq. (3) reveals that most of the absorption arises from earthshine absorption in the strong 10 to 12 μm band, while solar absorption near 3 μm makes an additional small contribution in the daytime; most of the particle emission occurs at wavelengths of 12 to 50 μm. It is important to note that, for the larger particle sizes, one must carry the emission integral out to a wavelength of 100 μm to achieve adequate accuracy.

It is interesting to consider Eq. (3) in terms of analytical approximations. Let us represent the integrated earth radiance by a blackbody at surface temperature T_E with an effective emissivity ε. Let us further represent the particle emissivities as constant average values $\overline{Q_A}$ and $\overline{Q_A}'$, where $\overline{Q_A}$ is the average of $Q_A(\lambda)$ over the range of significant particle radiation (10 to 100 μm) and $\overline{Q_A}'$ is the average value responsible for most of the absorption (10 to 15 μm). Equation (3) then becomes:

$$\int_0^\infty \overline{Q_A}' \, \varepsilon \, N(\lambda, T_E) d\lambda = 4 \int_0^\infty \overline{Q_A} \, N(\lambda, T) d\lambda \tag{4}$$

We can now evaluate the blackbody integrals to obtain:

$$T = \frac{1}{\sqrt{2}} T_E \left(\frac{\varepsilon \overline{Q_A}'}{\overline{Q_A}} \right)^{1/4} \tag{5}$$

The value $\varepsilon^{1/4}$ is near unity, so the particle temperature is primarily governed by the spectral distribution of $Q_A(\lambda)$ at long wavelengths. For

smaller particles, $r < 10$ μm, we have $\overline{Q_A}' > \overline{Q_A}$, so the particle temperatures are somewhat larger than $T_E/\sqrt{2}$. However, for the large particles, $r \sim 30$ μm and greater, we see that $\overline{Q_A}' \approx \overline{Q_A}$, i.e., the particles are effectively "black" in the infrared, and thus the temperature will decrease with increasing particle size to approach a constant value at large r of $\sim T_E/\sqrt{2}$. Indeed, for large particles the right-hand side of Eq. (3) can be cast into an analytically soluble form:

$$P = \int_0^\infty (J_\lambda + \pi I_\lambda) Q_A^r(\lambda) d\lambda = 4\pi \overline{Q_A} \int_0^\infty N(\lambda, T) d\lambda \tag{6}$$

This gives the relationship:

$$T = 458 \left(\frac{P}{\overline{Q_A}} \right)^{1/4} \tag{7}$$

We can evaluate the absorption integral P exactly, and determine from the Mie calculations for $r = 30$ μm the average value $\overline{Q_A} = (1.2 \pm 0.2)$ for $10 < \lambda < 100$ μm, giving values for T in good agreement with those obtained from numerical solution of Eq. (3). Thus from the "black" approximation to the particle radiation for large r, we can obtain accurate determinations of the particle temperature in radiative steady-state.

Finally, we must consider the time required for the particles to cool to steady-state conditions following condensation. The cooling rate at a temperature T is given by:

$$\frac{dT}{dt} = \frac{\int_0^\infty I_R(\lambda) d\lambda}{\rho V C} \tag{8}$$

where ρ, V, and C are the density, volume, and specific heat of the particle, respectively. From the calculated radiated powers, we estimate lower bound

cooling rates on the order of 10 K/s for small particles ($r < 3$ μm), approaching ~1 K/s for $r = 30$ μm. Thus, we expect the small particles to cool within tens of seconds, while the 30 μm particles may require as much as one minute to reach steady-state. Furthermore, since Q_A becomes independent of λ and r for large particles, we have $dT/dt \propto I_R/V \propto 1/r$, so very large particles of a few hundred μm radius would require several minutes to reach steady-state conditions. Thus, the steady-state assumption is appropriate for particles in the range of a few μm radius or smaller, providing the observations are not made within a few seconds of venting, but may not be generally applicable to very large particles in the hundred μm size range.

It should be noted that the steady-state ice particle temperatures are as much as 100 K below the freezing point, i.e., well below the range for which the refractive index data are valid. This constitutes a major uncertainty in these calculations, and points to the need for fundamental refractive index measurements at cryogenic temperatures.

IV. Light Scattering

The scattered light spectrum arises from two contributions: scattering of sunlight, which is strongly dependent upon observation angle, and scattering of infrared radiation from the earth, which acts as a distributed source over all angles. For the case of solar scattering, the scattered intensity in W cm^{-2} μm^{-1} at a distance z from the particle is I_S/z^2, where the normalized intensity is given by:

$$I_S(\theta,\lambda) = \left(\frac{\lambda}{2\pi}\right)^2 J_\lambda i(\theta,\lambda) \tag{9}$$

where $i(\theta,\lambda)$ is evaluated in the Mie calculations as described above. We have evaluated $I_S(\theta,\lambda)$ for nominal observation angles of 90 deg (sideways), 30 deg

(forward), and 150 deg (backward). The 30 and 150 deg scattered intensities generally exceed those for 90 deg for the particle size parameters considered here, with the differences being as much as two orders of magnitude for the 30 μm particles. However, in real scenarios, it seems likely that the detector will be held at approximately right angles to the sun in most cases where the near field is sunlit. When the near field is not sunlit, the visible scattered light from the particles should be near zero, the possible residual contributions being from indirect solar reflections or Shuttle-borne light sources.

The representation of earthshine scattering must incorporate the spatially distributed nature of the source. From simple geometry, a particle at altitude h can "view" radiation from the earth's surface at a range of $(2R_E h)^{1/2}$ where R_E is the radius of the earth. For h = 200 km, the extent of the source is ~1600 km in each direction. Thus, for all practical purposes, the earth can be represented as a flat, infinite Lambertian surface as shown in Figure 8. In this approximation, the observation angle θ is given by:

$$\theta = \theta_D - \theta_E \tag{10}$$

where θ_E is the angle of an earthshine ray with respect to the normal to the surface, and θ_D is the angle of the detector line of sight with respect to the earth normal. The angular distribution of earth radiation follows Lambert's law:

$$\pi \mathscr{I}_\lambda(\theta_E) d\theta_E = \frac{1}{2}\pi I_\lambda \cos\theta_E \, d\theta_E \tag{11}$$

The normalized scattered intensity (analogous to I_S given in Eq. (9) above) is then:

$$I_E = \left(\frac{\lambda}{2\pi}\right)^2 \frac{\pi I_\lambda}{2} \int_{-\pi/2}^{\pi/2} \cos\theta_E \; i(\theta) \; d\theta_E \tag{12}$$

Substituting from Eq. (10), we obtain:

$$I_E = \left(\frac{\lambda}{2\pi}\right)^2 \frac{\pi I_\lambda}{2} \int_{\pi/2-\theta_D}^{\pi/2+\theta_D} \cos(\theta_D - \theta) \; i(\theta) \; d\theta \tag{13}$$

A general solution of Eq. (13) for all θ_D is rather laborious. However, for an earth-limb viewing aspect typical of most orbital atmospheric sensors, θ_D is between 80 and 90 deg, and the solution is straightforward. In this case, we have $\cos(\theta_D - \theta) \cong \sin\theta$ to within 10 percent, and Eq. (13) becomes:

$$I_E = \left(\frac{\lambda}{2\pi}\right)^2 \frac{\pi I_\lambda}{2} \int_0^{\pi} \sin\theta \; i(\theta) \; d\theta \tag{14}$$

Substituting Q_S from Eq. (1), we obtain:

$$I_E = \frac{1}{4} \pi r^2 \; I_\lambda Q_S \tag{15}$$

It should be noted that Eq. (15) provides a significantly different description of earthshine scattering than the assumption of $\theta = 90$ deg, since it provides for significant contributions due to forward and backward scattering of earth radiation from the horizon.

V. Predicted Particle Brightness Spectra

The spectral radiant intensity, in W sr^{-1} μm^{-1}, due to scattering and self-emission is given by:

$$R_\lambda = \frac{I_R}{\pi} + I_S + I_E \tag{16}$$

Some sample predictions for R_λ are shown in Figures 9 through 12 for several different illumination conditions. The variation in the single-particle spectrum with particle size is illustrated in Figure 9 for solar-illuminated particles with $\theta = 90$ deg and a tropical earth; the contributions due to solar scattering and self-emission are shown by the dashed curves. In general the spectra may be divided into three spectral regimes: 0.1 to 3 μm, dominated by solar scattering; 3 to 20 μm, dominated by earthshine scattering; and 20 to 100 μm, dominated by self-emission. For small particles, the earthshine scattering is a negligible contribution in the infrared, and the infrared signature is both weak and controlled by self-emission beyond 10 μm. However, as the particle size increases, earthshine scattering becomes much more important, contributing significantly to the spectral structure between 4 and 10 μm. This is illustrated in Figure 10. The effect of a colder earth, as might be encountered in a polar orbit, is to reduce the infrared intensity by as much as a factor of two, with an additional shift in spectral intensity to the red as a result of the somewhat lower steady-state particle temperature.

The solar scattering spectrum exhibits the basic envelope of the solar spectrum but contains a superimposed detailed structure, as in Figure 11. This structure, which is a consequence of interfering wave-particle interactions, is a sensitive function of particle size and observation angle. Furthermore, the overall intensity of the scattered light is greatly increased if the scattering angle is off the perpendicular. The effect of forward scattering, as much as two orders of magnitude, is illustrated in Figure 12; the effect of backward scattering is similar to this but not as large in magnitude. This type of spectral signature, if observed by a scanning airglow

spectrometer, could be mistaken for a complex molecular near-continuum. We will return to this point in the next section.

The spectra shown here exhibit pronounced oscillations which are characteristic of spherical particles for a given exact size. The actual contaminant particles will exhibit similar but probably not identical oscillations. Furthermore, for collections of particles of different sizes, the single-particle spectra must be summed over the size distribution within the field of view, further altering the characteristics of the scattering fine structure. Thus, the observed spectra of contaminant particles will exhibit the general characteristics of the predicted spectra shown here, but not the identical high-resolution structure.

For simplicity, we have not considered the effects of illumination by lunar- or earth-reflected sunlight. The latter case would be treated as a distributed source in a manner analogous to that for infrared earthshine, with a local albedo depending upon wavelength and terrain. The earth's albedo in the visible can be quite large, especially over ice fields or cloud cover, so in some conditions the visible light scattering may be more intense and less dependent upon solar angle than we indicate here. In addition, the intensity distribution of the scattered light could be shifted towards longer wavelengths if the source's surface reflectance is relatively poor in the blue, or if the blue portion of the source radiation is removed by atmospheric Rayleigh scattering. Solar reflection effects are difficult to model a priori, and we await experimental demonstration of the conditions for which they are important.

VI. Applications and Discussion

The fundamental spectral intensities predicted from Eq. (16) can be applied to a variety of detector designs and configurations. To convert the values of R_λ into radiance units, one must divide by an effective cross-section of the detector's field-of-view. For a typical baffled detector system, this quantity is $z^2\Omega_D$, where z is the distance of the particle from the detector and Ω_D is the effective solid angle of the detector. For a telescoped system, we anticipate that most of the significant particle radiation will occur in the near field, i.e., the particles will be out of focus and the detector will be overfilled. In this case the limiting area is just the area of the limiting aperture stop. The resulting predicted radiances can then be integrated over specific spectral bandpasses and/or coupled with detector responsivity curves to assess the visibility of particles for the actual experimental conditions. We discuss briefly three example detector systems: photographic imaging of particles, scanning ultraviolet/visible spectrometry, and infrared interferometry.

Photographic imaging of particles provides a means of characterizing particle sizes and distributions in the near field.[1,2] In this case, the detector (film) integrates over the visible spectrum, and either the sun or a Shuttle-borne light source such as a strobe is required to illuminate the particles. Use of two cameras with overlapping fields of view provides a stereoscopic image which permits determination of particle range, size, and velocity vector, and thereby absolute intensity. Shuttle-borne light sources offer increased flexibility, as one can explore a range of backscattering angles, polarizations, and spectral bandpasses in order to test the predictions of the spectral model. This type of validation in the visible can

permit more confident prediction of effects in the infrared for similar particle distributions.

Spectrally scanning ultraviolet/visible spectrometers are widely used in aeronomy and have been used repeatedly in satellite and Shuttle-borne airglow measurements.[12,13] Since these instruments usually employ gated diode array detectors, the spectral signature of the particle field will be superimposed upon that of the atmosphere. If the particle field is illuminated by direct or reflected sunlight, the resulting composite scattered-light spectrum would appear at high resolution as a broad, complex quasi-continuum containing partially resolved and apparently random spectral structure (cf. Figure 11). The envelope of this spectrum would reflect the spectral signature of the illumination source, e.g., peaked near 0.5 μm for direct solar radiation and further to the red for lunar or earth reflections. Spectral behavior qualitatively similar to this has been observed in past Shuttle missions,[13] but there is insufficient supporting data to determine conclusively whether those observations were due to particulates. Nevertheless, the observed signal levels reported in Ref. 13 for 700 to 800 nm are in general accord with our predictions for forward scattering by single particles in the 3 to 30 μm size range. It should be noted that, in order to more accurately assess light scattering effects in the vacuum ultraviolet, the detailed high-resolution spectrum of the sun must be considered, since discrete atomic lines dominate the blackbody continuum at wavelengths less than 0.2 μm.

In the case of a scanning interferometer, particle effects can be manifested in two different ways. If the particle is moving rapidly across the field-of-view, it appears as a transient in the interferogram, and one is

primarily interested in the particle radiance integrated over the bandpass of the instrument as compared to the integrated radiance of the steady source being scanned by the device. For single particles in the infrared (2 to 20 μm), a particle diameter of several hundred μm (in the geometric scattering regime) is required before the integrated particle brightness can interfere with earth limb measurements. However, if a particle or collection of particles remains in the field-of-view as an apparently steady radiation source, the actual spectrally resolved signature is the quantity of interest. In this case, even relatively small integrated particle radiance can have a substantial spectral effect in the infrared, since ice particles exhibit most of their intensity in atmospheric spectral "windows" between adjacent molecular bands.

Comparison of our predictions with infrared atmospheric limb radiance models[14,15] indicates that, for a typical aperture of ~100 cm^2, particles in the 0.3 μm size range should not interfere with infrared spectral measurements unless present in large quantities (10^{4-5} particles in the field-of-view), but single particles in the 30 μm size range can dominate 9 to 14 μm earth limb emission from ~120 km tangent heights or higher. The threshold for single-particle interference with high altitude IR limb radiance measurements appears to be in the 1 to 3 μm size range, and arises primarily in the 8 to 12 μm wavelength range as a result of earthshine scattering. Self-emission by larger particles can also be a factor at wavelengths beyond 20 μm. These comparisons are illustrated in Figures 13 and 14 for daytime and nightime conditions.

VII. Conclusions

We have assembled a model for predicting the detailed spectral signatures of particulates in the near field of Shuttle, using ice as a benchmark particulate species. These computations identify the separate contributions of angle-dependent solar scattering, earthshine scattering, and self-emission to the naturally occurring brightness spectra of single spherical ice particles throughout the ultraviolet, visible, and infrared. Major elements which need to be validated by experiment include particle identity, the wavelength-dependent refractive index as a function of temperature, and near-field distributions of number, size, shape, and velocity. Calculations of this type can be used in support of diagnostic design and data interpretation for Shuttle-borne experiments to characterize particulate scattering in the visible and to optically probe atmospheric emissions through a tenuous particle field.

The predicted spectral distributions have interesting implications for the interpretation of spectrally resolved remote observations of aeronomic data obtained from Shuttle. Stereocamera experiments[1,2] indicate that, while the near-field particulate distribution is often sparse, it is rarely zero for long periods of time. These imaging experiments can detect only particles larger than a few tens of microns in diameter; we have shown here that even single particles in the 1 μm size range can affect spectral measurements. Thus, it seems that the appearance of particulate spectral signatures in Shuttle aeronomic data will be more likely the rule than the exception, even when great care is exercised in performing the measurements during low-contamination periods. It then falls upon the experimenter to somehow identify particulate contributions and remove them from the data. This could be

done most comprehensively by obtaining spectrally resolved images of the near-field particulate distributions during the aeronomic measurements, perhaps with a companion sensor. Alternatively, investigators should obtain spectra during periods when particulate signatures are likely to predominate in order to unambiguously identify their appearance.

Acknowledgments

The authors are grateful to G. E. Caledonia and A. Modak for many helpful discussions, and to B. Claflin for capable assistance with the computations. We also acknowledge many helpful discussions with M. Ahmadjian, E. Murad, C. Pike, and R. Murphy of the Air Force Geophysics Laboratory. This research was supported by the Spacecraft Interactions Branch of the Air Force Geophysics Laboratory.

References

1. E.R. Miller, ed., "STS-2, -3, -4 Induced Environment Contamination Monitor (IECM) Summary Report," and E. Miller, ed., "Induced Environment Contamination Monitor-Preliminary Results from the Spacelab 1 Flight," private communication.
2. F.J. Redd, D.R. Bunnell, and M. Ahmadjian, "Particle Analysis Camera for Shuttle (PACS): the First Hitchhiker (HHG-1)," Proceedings of AIAA Shuttle Environment and Operations II Conference, p. 104, Houston, November 1985.
3. B.D. Green, G.E. Caledonia, and T.D. Wilkerson, "The Shuttle Environment: Gases, Particulates, and Glow," J. Spacecraft Rockets 22, 500 (1985).
4. H.C. van de Hulst, Light Scattering by Small Particles, John Wiley and Sons, New York, 1957.
5. M. Born and E. Wolf, Principles of Optics, Pergamon Press, New York, 1959.
6. S.G. Warren, "Optical Constants of Ice from the Ultraviolet to the Microwave," Appl. Opt. 23, 1206 (1984).
7. J.V. Dave, "Subroutines for Computing the Parameters of the Electromagnetic Radiation Scattered by a Sphere," IBM Report No. 320-3237, IBM Scientific Center, Palo Alto, CA, May 1968.
8. Q. Cai and K.N. Liou, "Polarized Light Scattering by Hexagonal Ice Crystals: Theory," Appl. Opt. 21, 3569 (1982).
9. K.N. Liou, Q. Cai, J.B. Pollack, and J.N. Cuzzi, "Light Scattering by Randomly Oriented Cubes and Parallelpipeds," Appl. Opt. 22, 3001 (1983).
10. S.L. Valley, ed., Handbook of Geophysics and Space Environments, McGraw-Hill, New York, 1965.

11. F.X. Kneizys, E.P. Shettle, W.O. Gallery, J.H. Chetwynd, Jr., L.W. Abreu, J.E.A. Selby, R.W. Fenn, and R.A. McClatchey, "Atmospheric Transmittance/Radiance: Computer Code LOWTRAN 5," AFGL-TR-80-0067, ADA 088215, Air Force Geophysics Laboratory, Bedford, MA February 1980.

12. R.E. Huffman, F.J. LeBlanc, J.C. Larrabee, and D.E. Paulsen, "Satellite Vacuum Ultraviolet Airglow and Auroral Observations," J. Geophys. Res. 85, 2201 (1980).

13. M.R. Torr and D.G. Torr, "A Preliminary Spectroscopic Assessment of the Spacelab 1/Shuttle Optical Environment," J. Geophys. Res. 90, 1683 (1985).

14. T.C. Degges and H.J.P. Smith, "A High Altitude Infrared Radiance Model," AFGL-TR-77-0271, ADA 059242, Air Force Geophysics Laboratory, Bedford, MA, 1977.

15. R.D. Sharma, "Infrared Airglow," in Handbook of Geophysics, Chap. 13, Air Force Geophysics Laboratory, Hanscom AFB, MA, in press, 1986.

Fig. 1 Single-particle efficiencies for absorption and scattering of light by spherical ice particles, 0.3 μm radius.

Fig. 2 Single-particle efficiencies for absorption and scattering of light by spherical ice particles, 3 μm radius.

Fig. 3 Single-particle efficiencies for absorption and scattering of light by spherical ice particles, 30 μm radius.

Fig. 4 Angular scattering patterns for ice particles in the visible.

Fig. 5 Spectral radiant flux of sun and earth.

Fig. 6 Particle temperatures in radiative steady-state, tropic earth.

Fig. 7 Particle temperatures in radiative steady-state, arctic earth.

Fig. 8 Geometry for scattering of earth radiation by particle at altitude h, detector angle θ_D with respect to earth normal.

Fig. 9 Single-particle radiant intensities, tropic earth, 90° solar scattering. The dashed curves on the left and right illustrate the contributions of solar scattering and self-emission, respectively.

Fig. 10 Single-particle radiant intensities in the infrared, tropical earth, no sun.

Fig. 11 Single-particle solar scattering spectrum, $r = 30$ μm, $\theta = 90°$.

Fig. 12 Single-particle radiant intensities, tropic earth, forward solar scattering ($\theta = 30°$).

Fig. 13 Comparison of predicted single particle brightness to daytime IR limb radiance (Ref. 15). The modeled limb radiance spectra are given for 10 km (tangent height) intervals.

Fig. 14 Comparison of predicted single particle brightness to nighttime IR limb radiance (Ref. 15). The modeled limb radiance spectra are given for 10 km (tangent height) intervals.

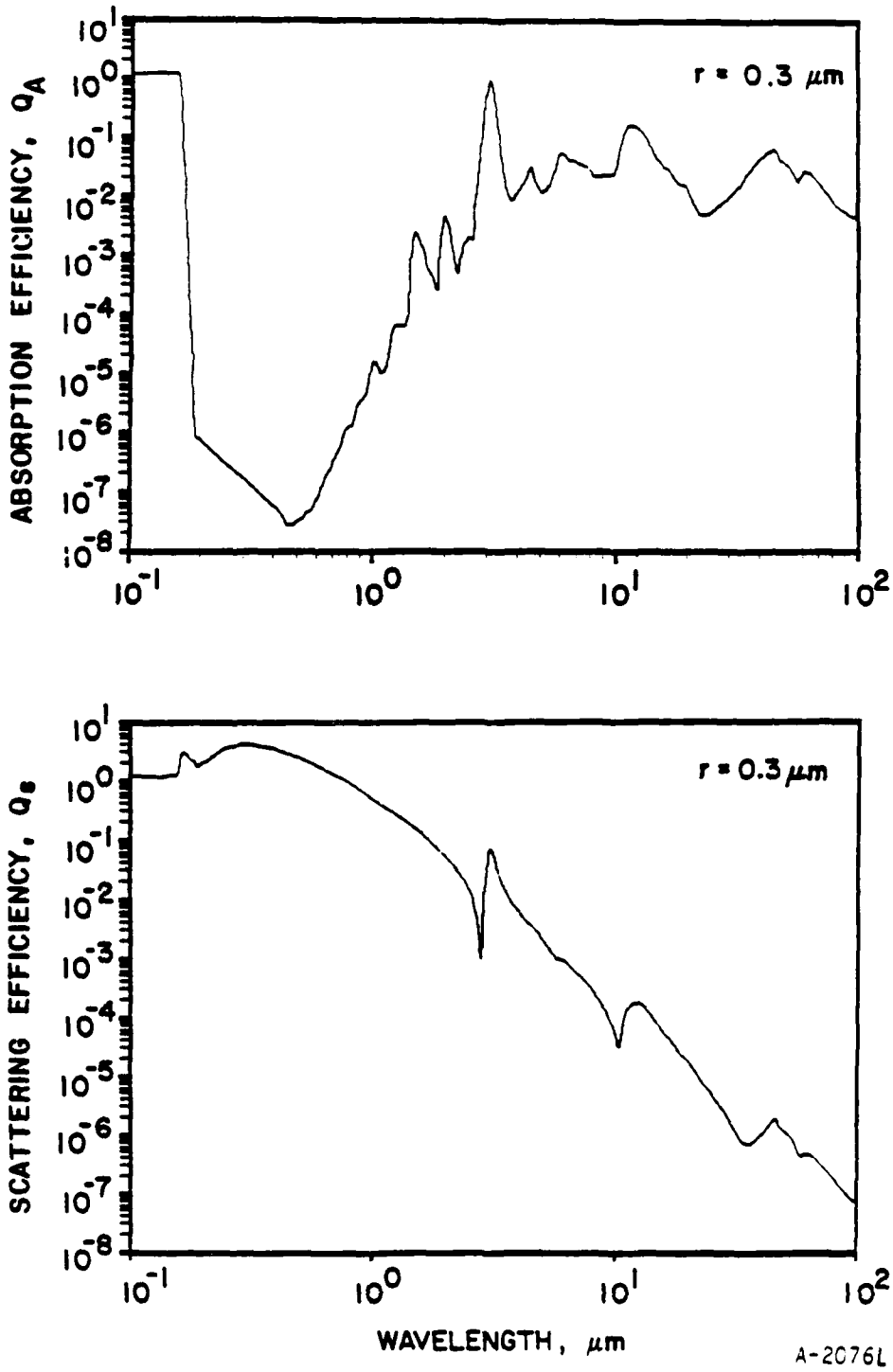

Fig. 1 Single-particle efficiencies for absorption and scattering of light by spherical ice particles, 0.3 μm radius.

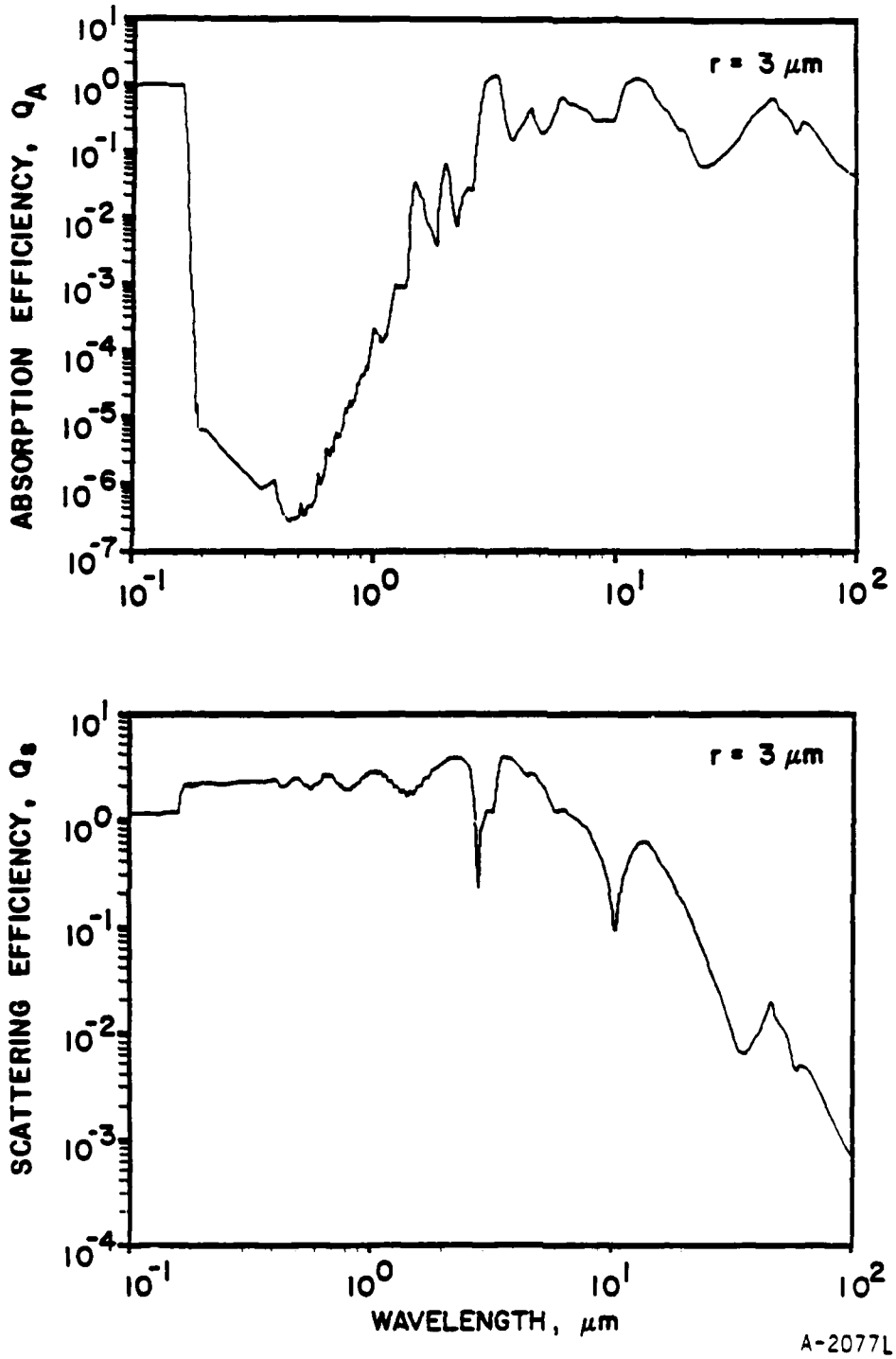

Fig. 2 Single-particle efficiencies for absorption and scattering of light by spherical ice particles, 3 μm radius.

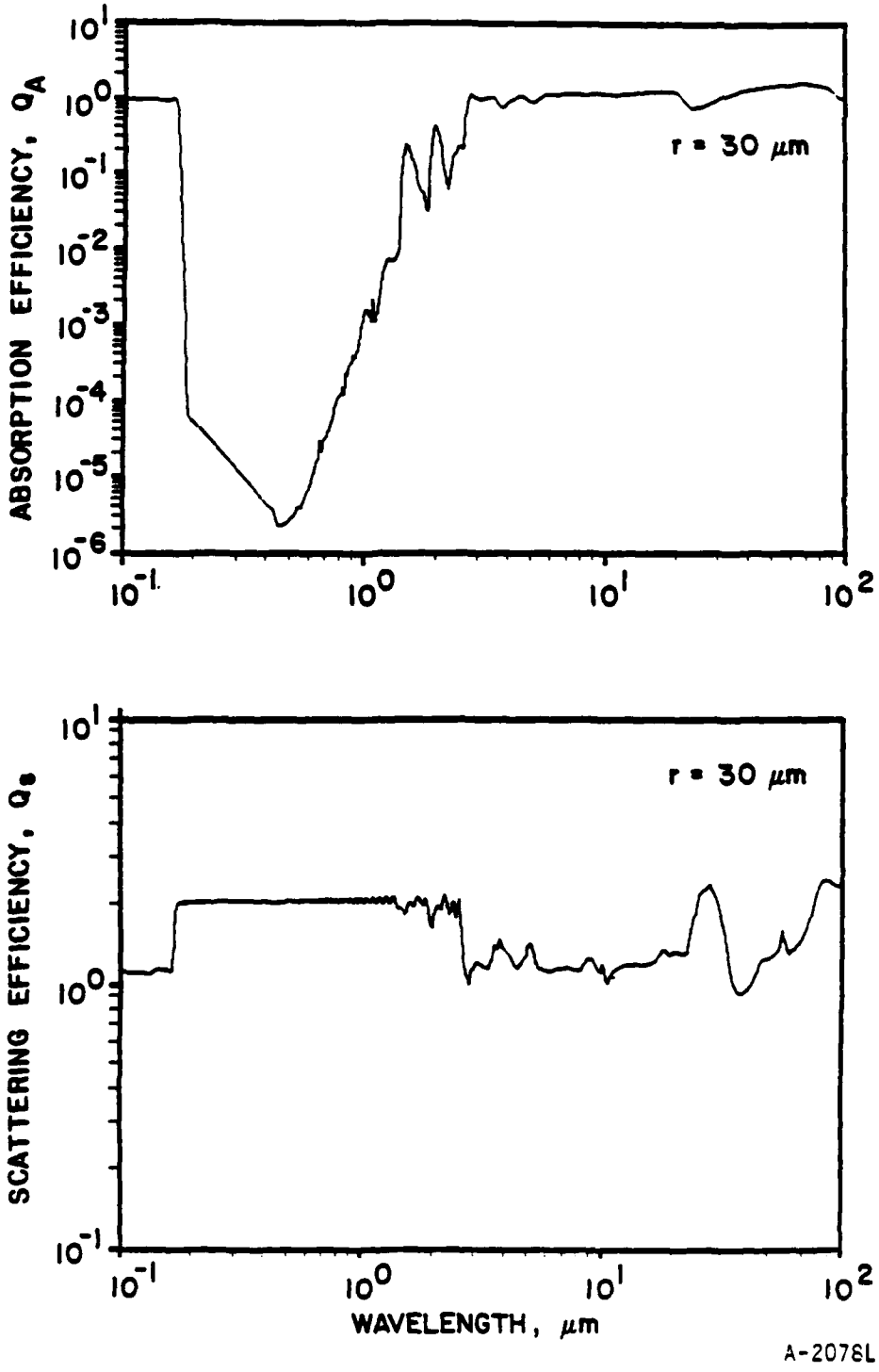

Fig. 3 Single-particle efficiencies for absorption and scattering of light by spherical ice particles, 30 radius.

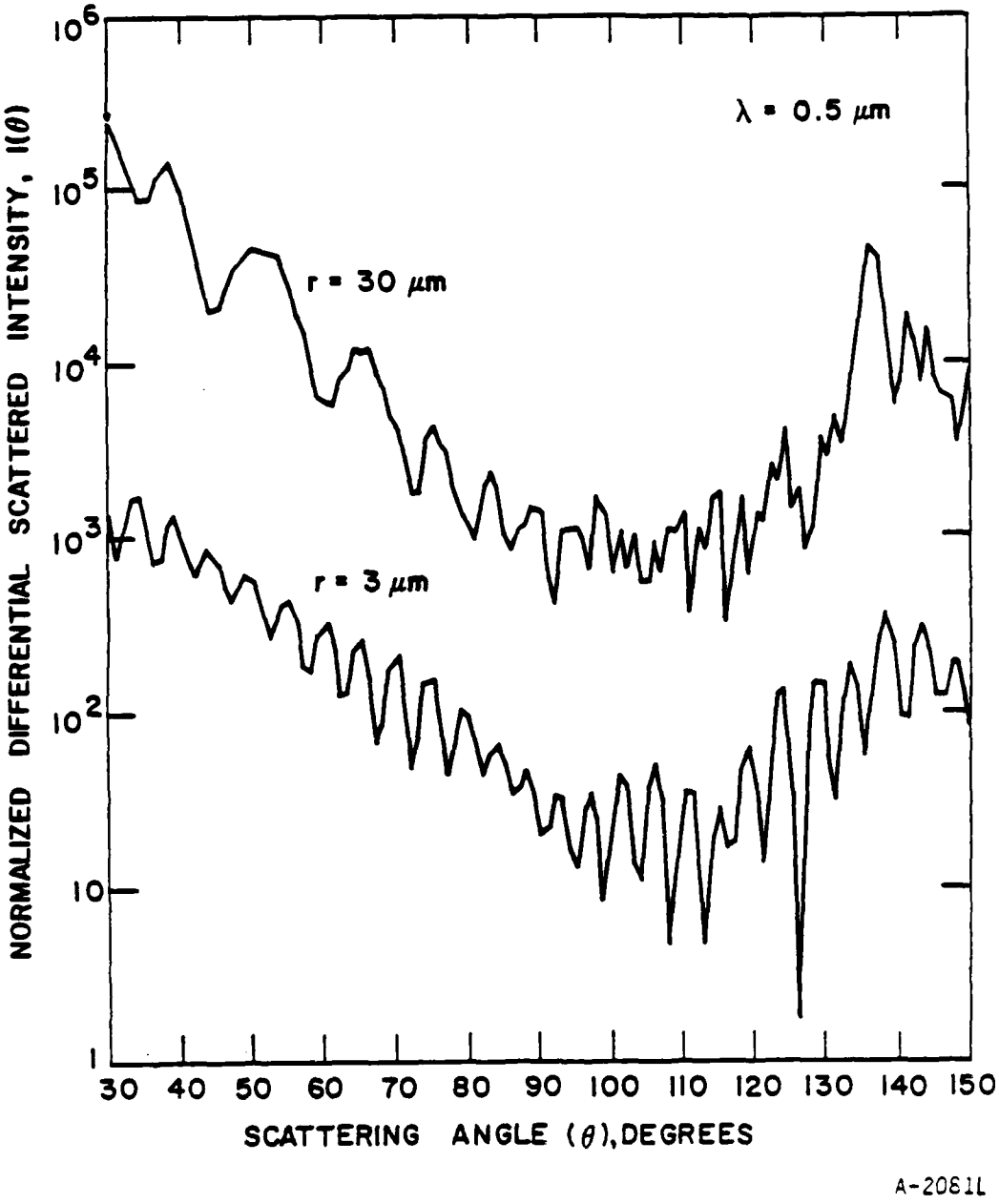

Fig. 4 Angular scattering for ice particles in the visible.

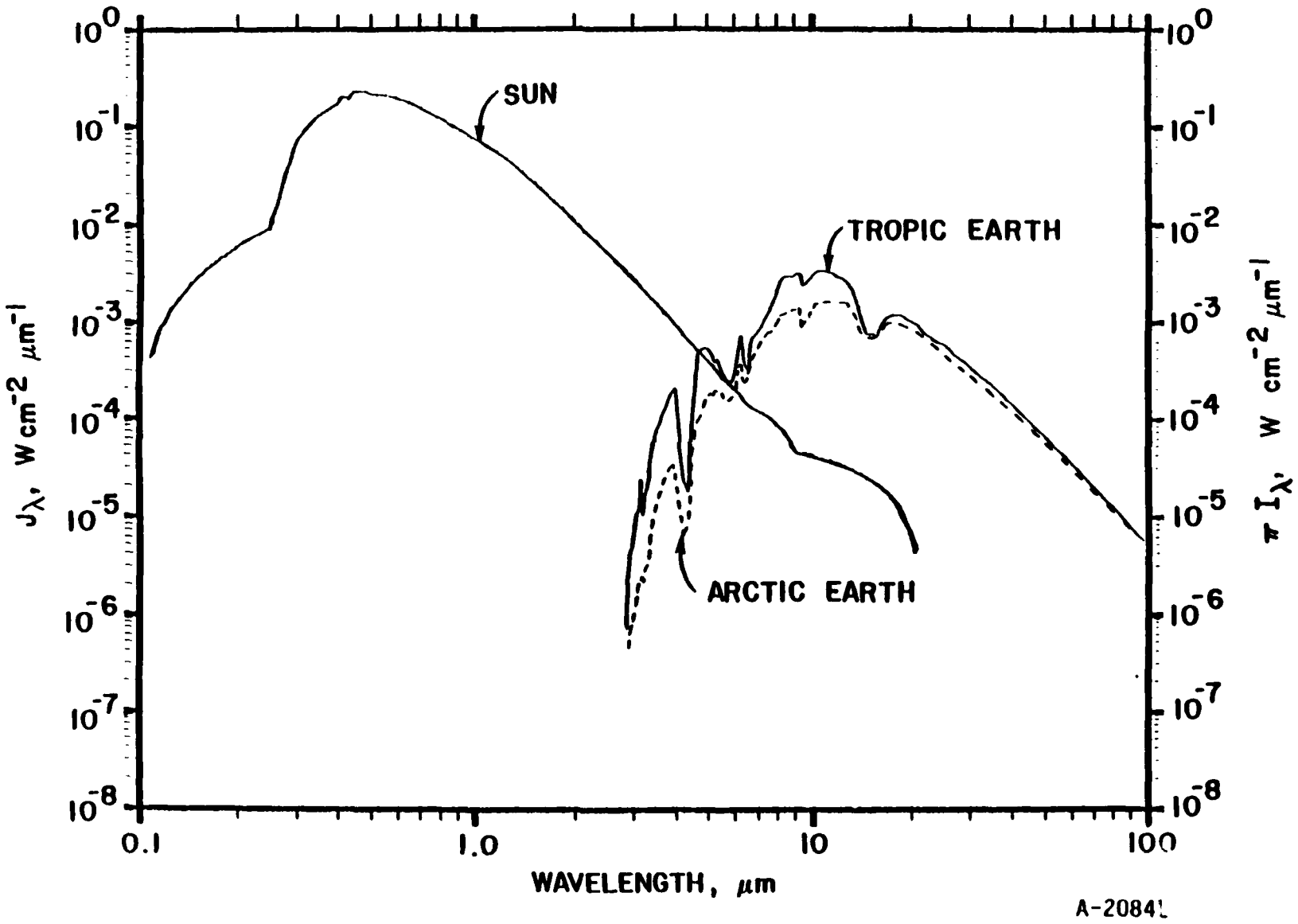

Fig. 5 Spectral radiant flux of sun and earth.

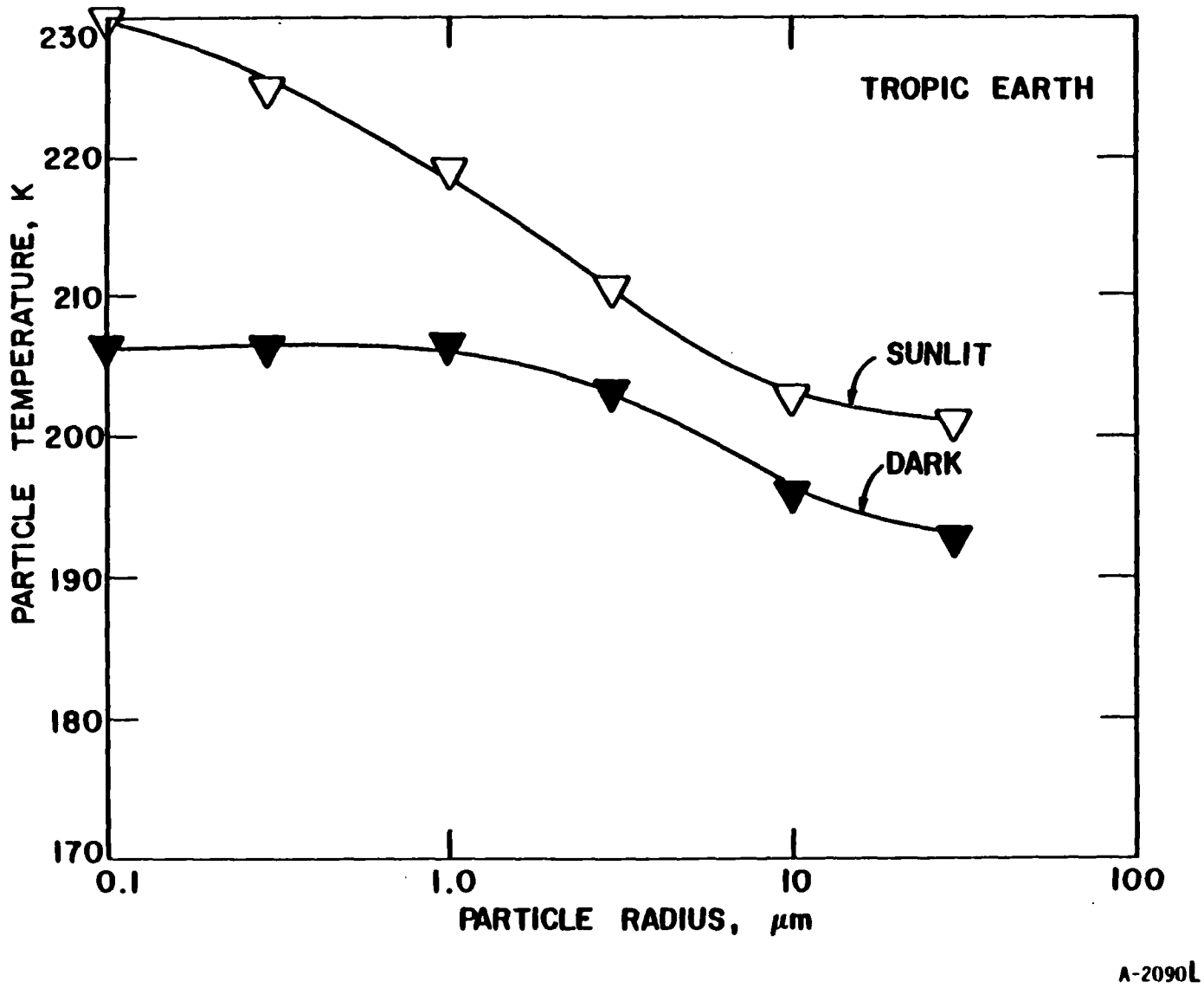

Fig. 6 Particle temperatures in radiative steady-state, tropic earth.

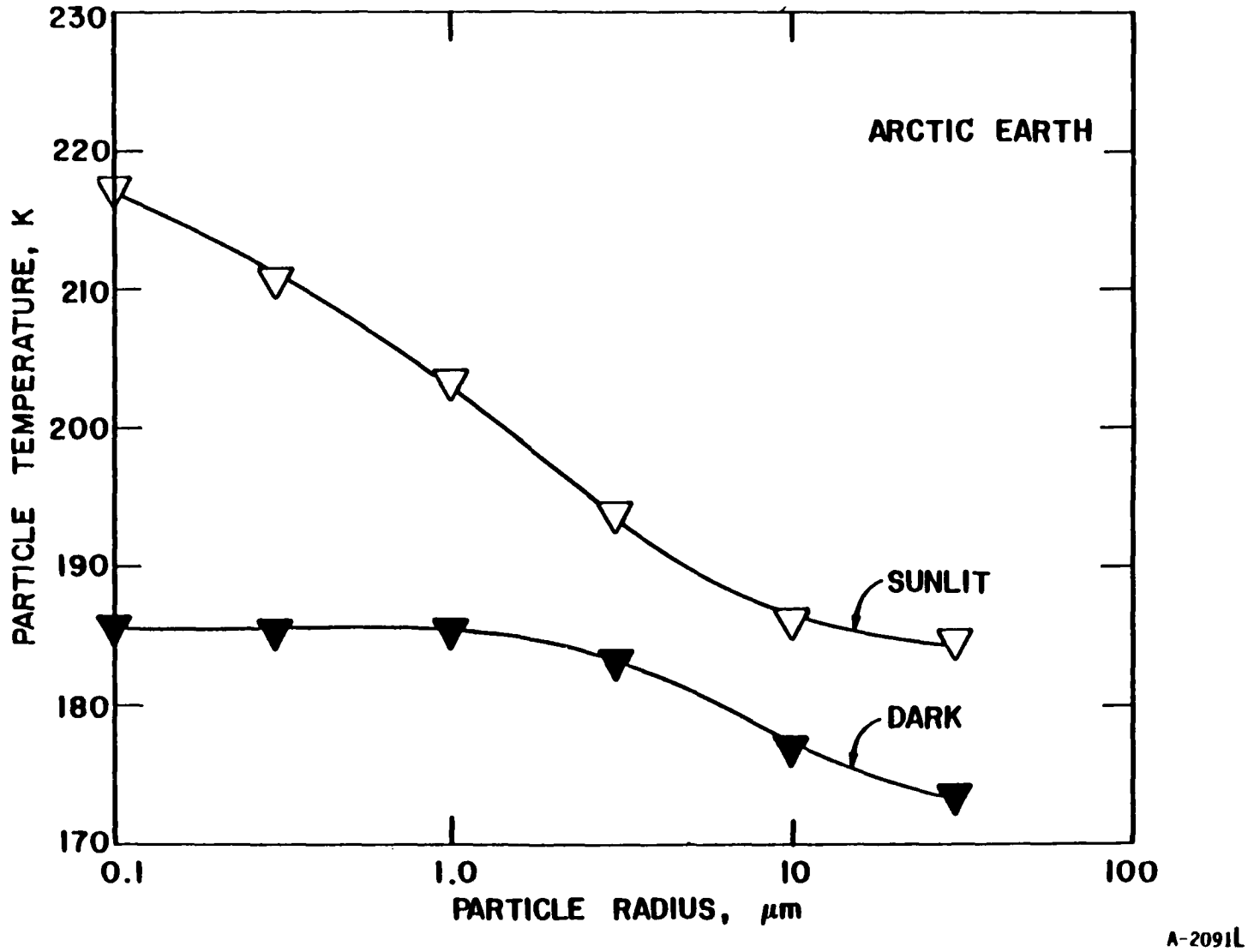

Fig. 7 Particle temperatures in radiative steady-state, arctic earth.

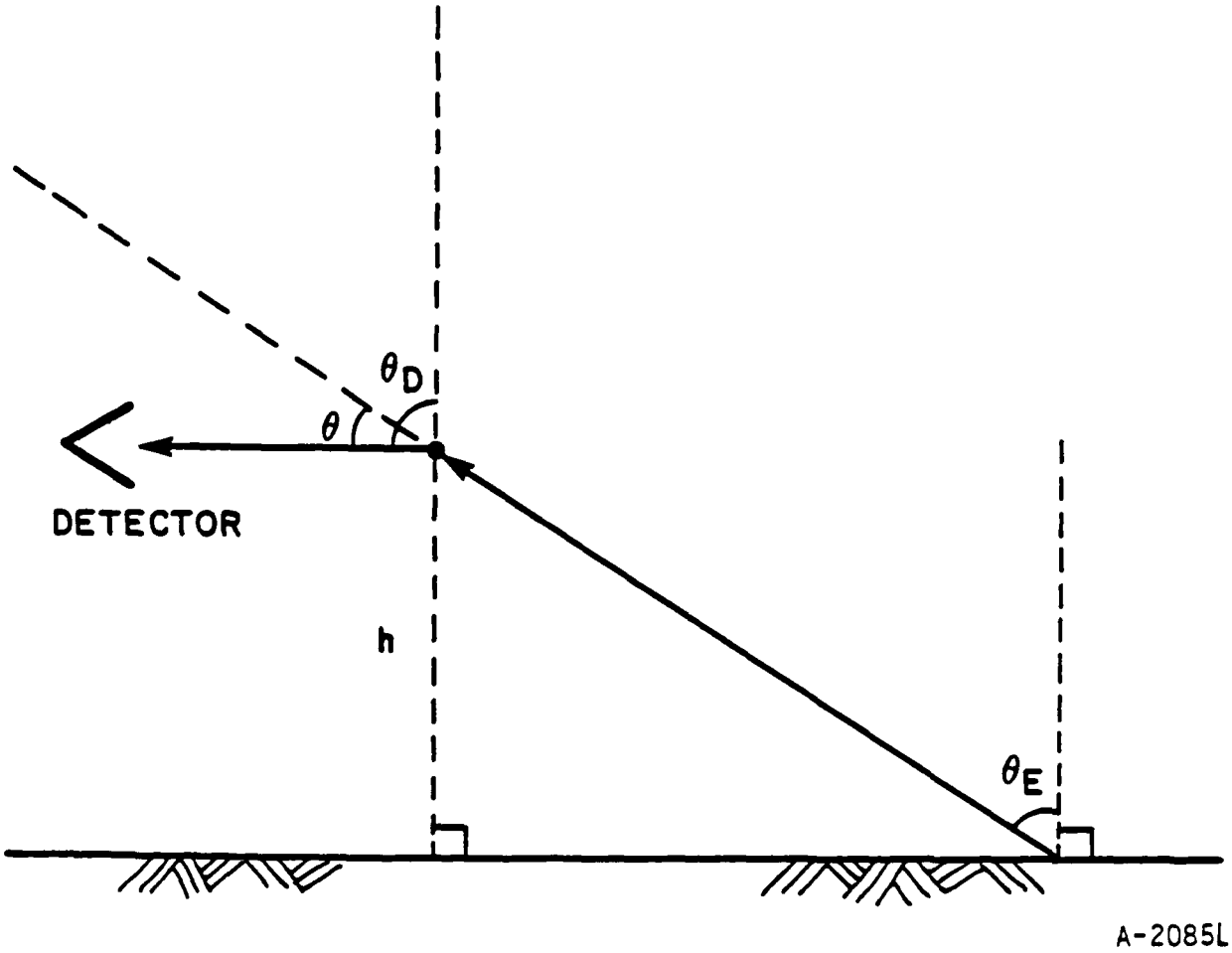

Fig. 8 Geometry for scattering of earth radiation by particle at altitude h, detector angle θ_D with respect to earth normal.

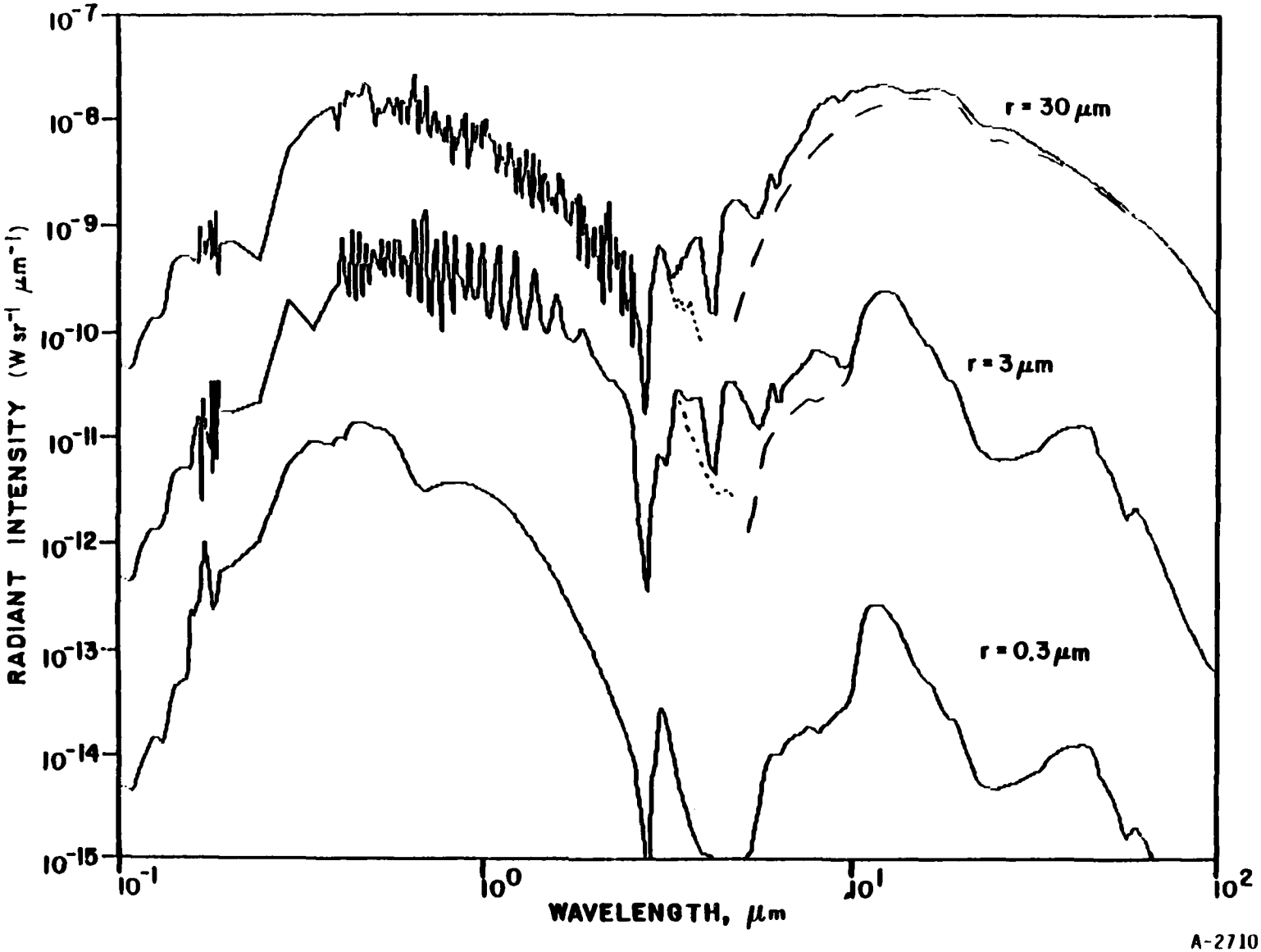

Fig. 9 Single-particle radiant intensities, tropic earth, 90° solar scattering. The dashed curves on the left and right illustrate the contributions of solar scattering and self-emission, respectively.

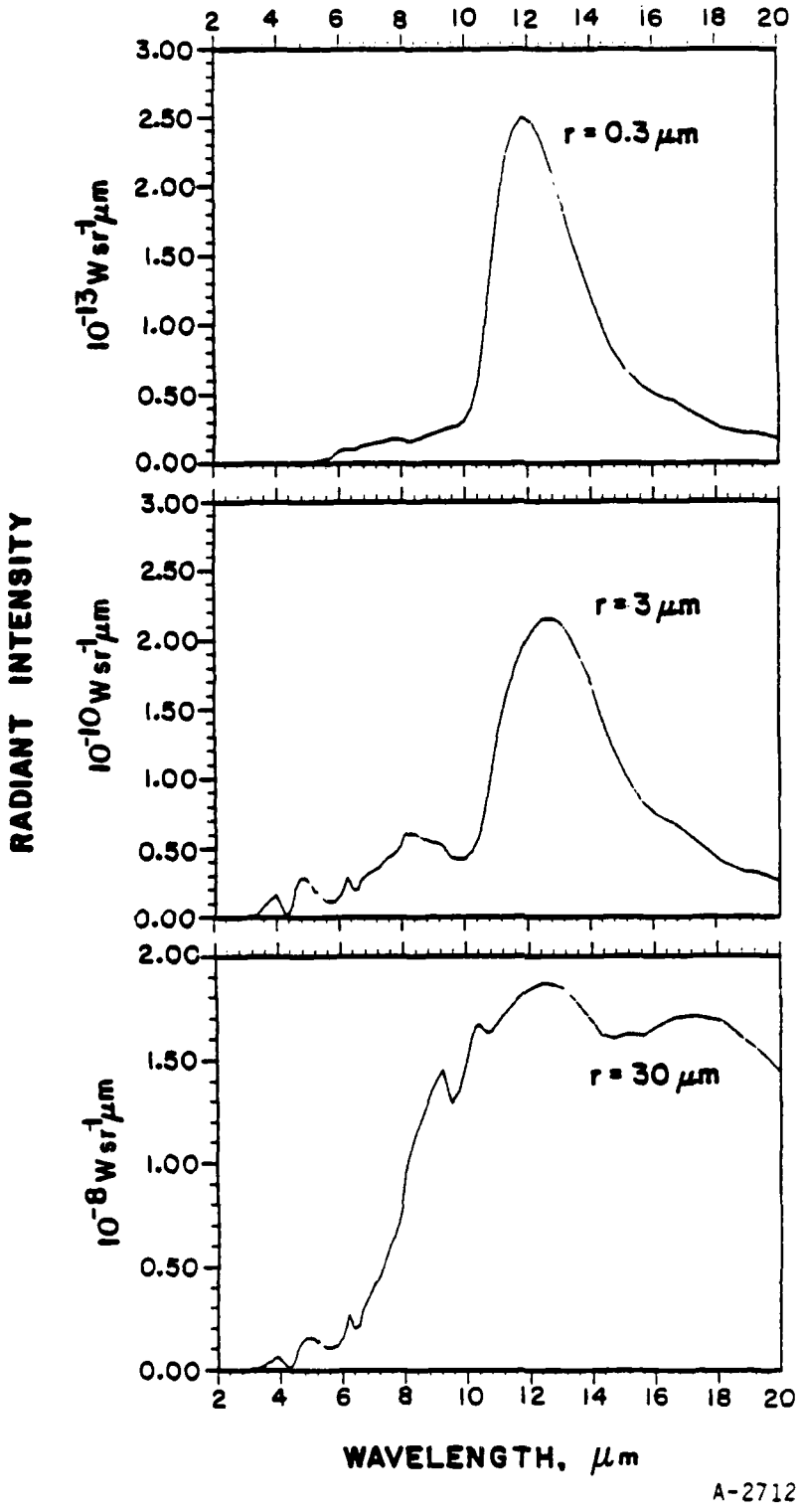

Fig. 10 Single-particle radiant intensities in the infrared, topical earth, no sun

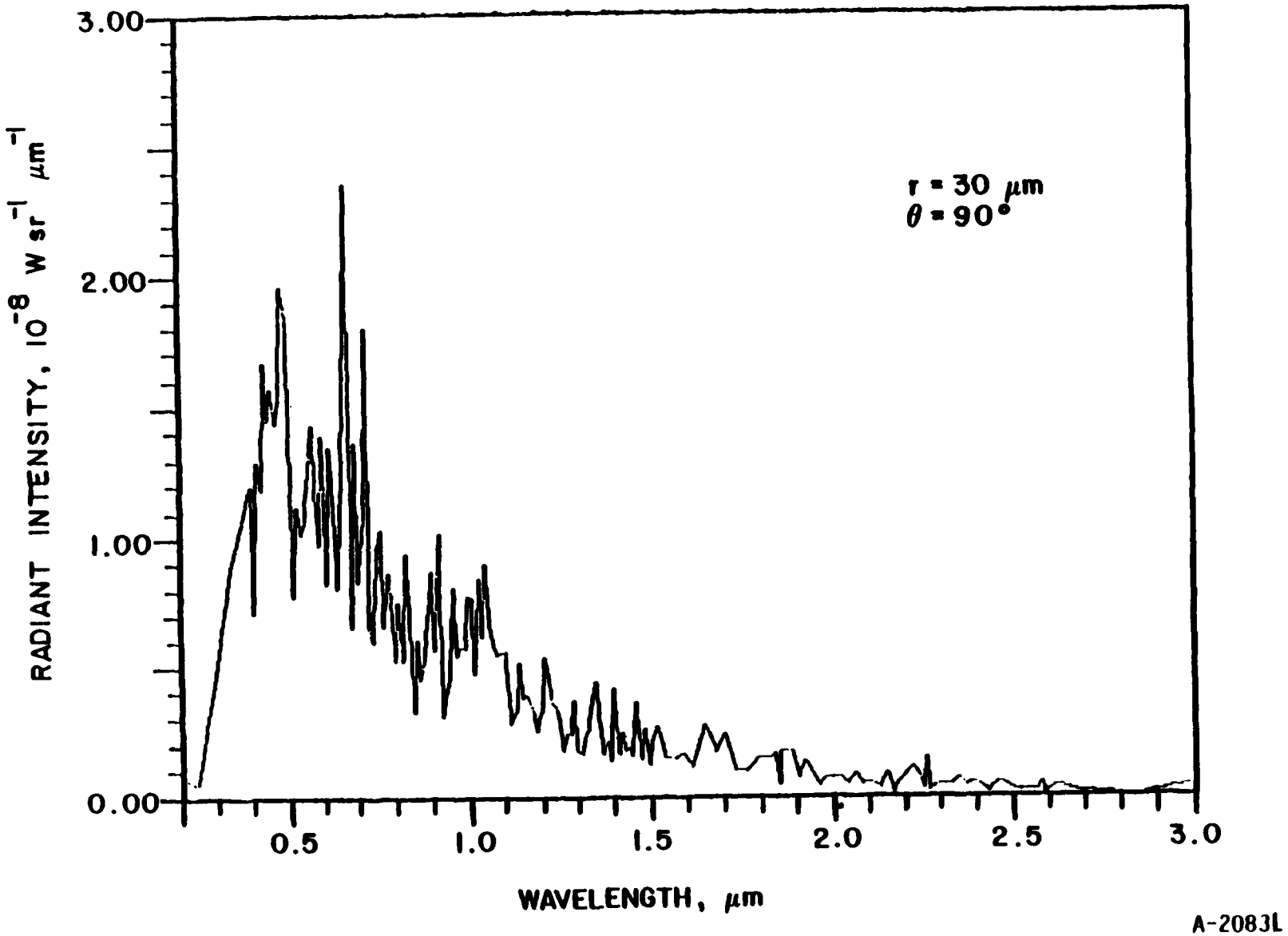

Fig. 11 Single-particle solar scattering spectrum, r = 30 μm, Θ = 90°.

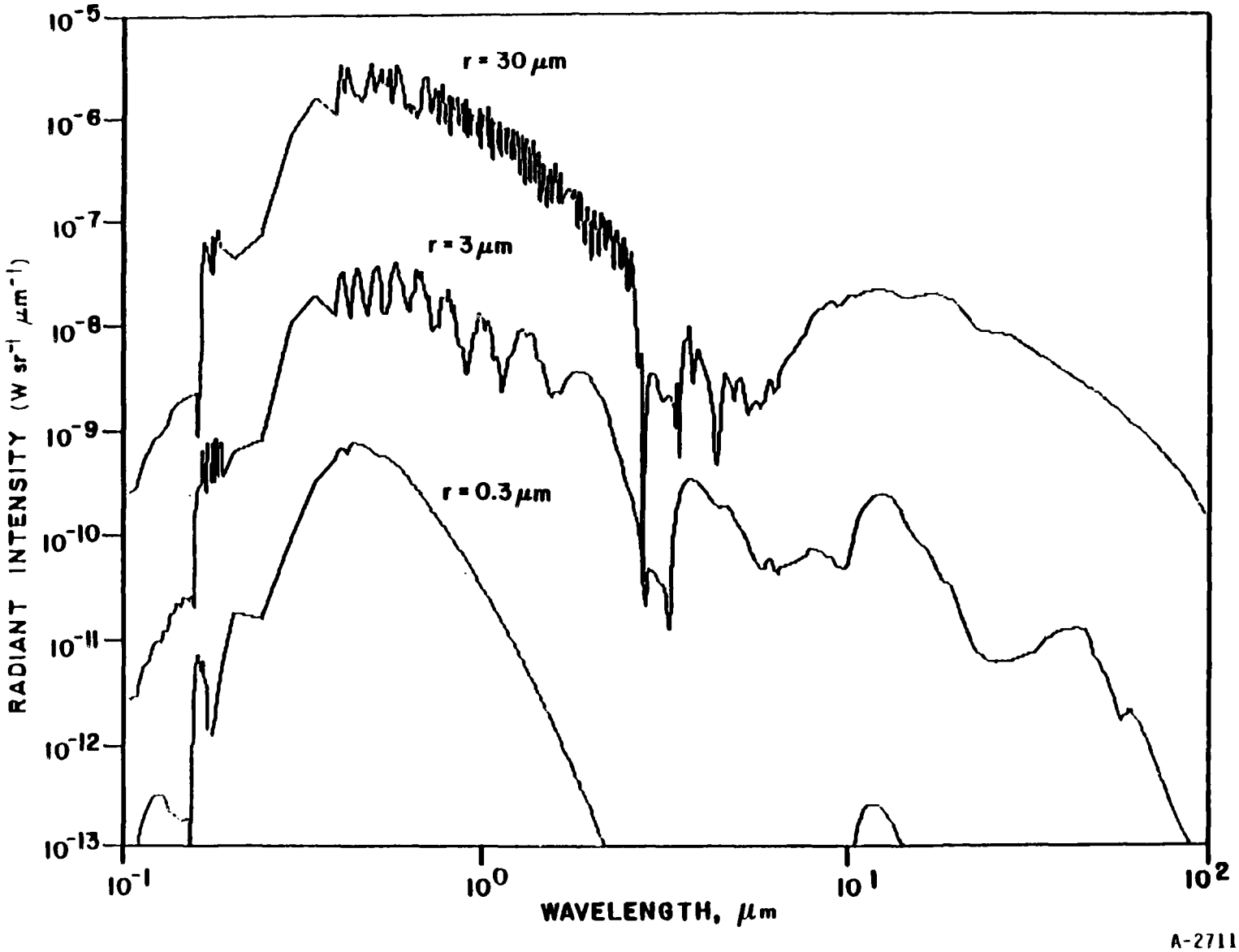

Fig. 12 Single-particle radiant intensities, topical earth, forward solar scattering ($\Theta = 30°$).

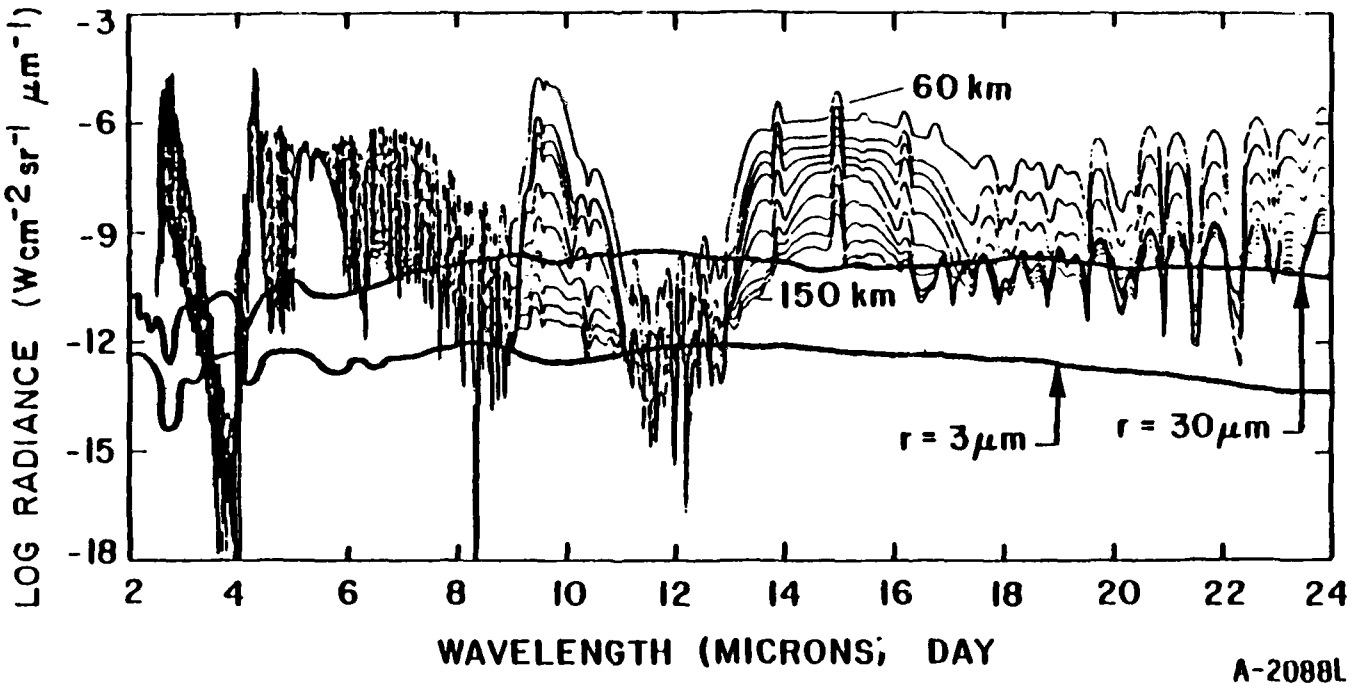

Fig. 13 Comparison of predicted single particle brightness to daytime IR limb radiance (Ref. 15). The modeled limb radiance spectra are given for 10 km (tangent height) intervals.

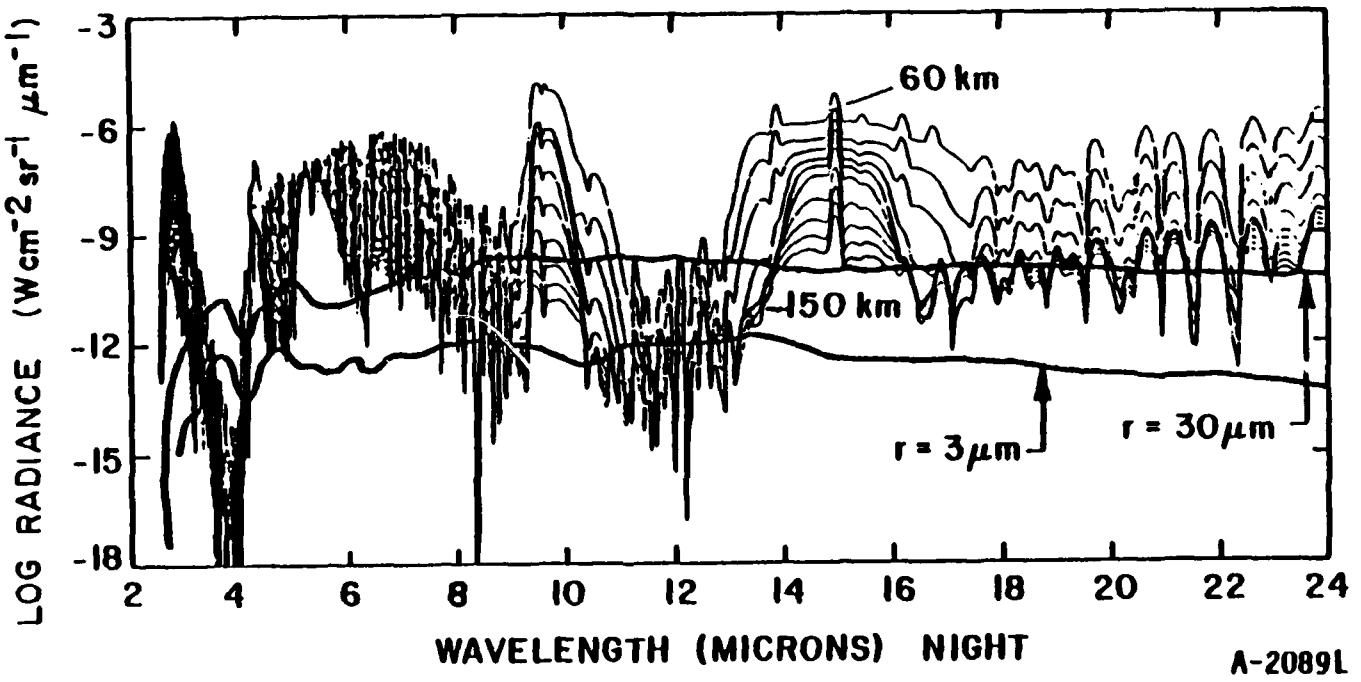

Fig. 14 Comparison of predicted single particle brightness to nighttime IR limb radiance (Ref. 15). The modeled limb radiance spectra are given for 10 km (tangent height) intervals.

APPENDIX J

Error Budget Calculations for Stereo Camera Pairs

Briefing by EKTRON Applied Imaging

Reproduced in its entirety.

EKTRON
23 Crosby Drive
Bedford, MA 01730

AGENDA

SHUTTLE CONTAMINATION STUDY

12/17/85

9:30 am	WELCOME TO EKTRON/EIKONIX	WJ
9:45 am	INTRODUCTION - TECHNICAL	DG
10:00 am	OVERVIEW OF MEASUREMENTS EFFORT	WJ
10:10 am	ERROR BUDGET	WJ
10:30 am	MODEL AND IMPLEMENTATION	BG
11:15 am	BREAK	
11:30 pm	TOUR AND VISION LAB DEMO	ALL
12:30 pm	ADJOURN	

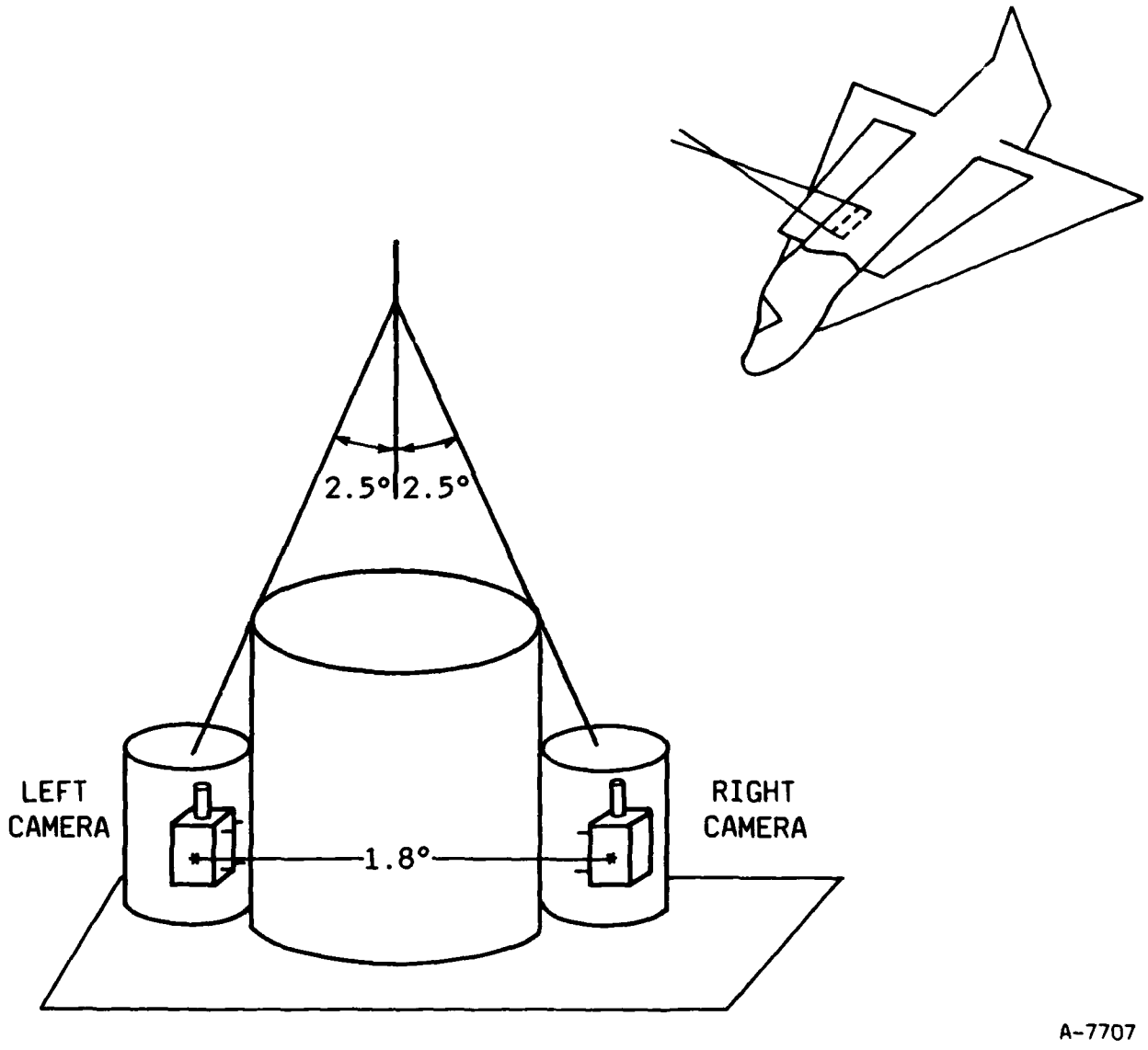

System Overview

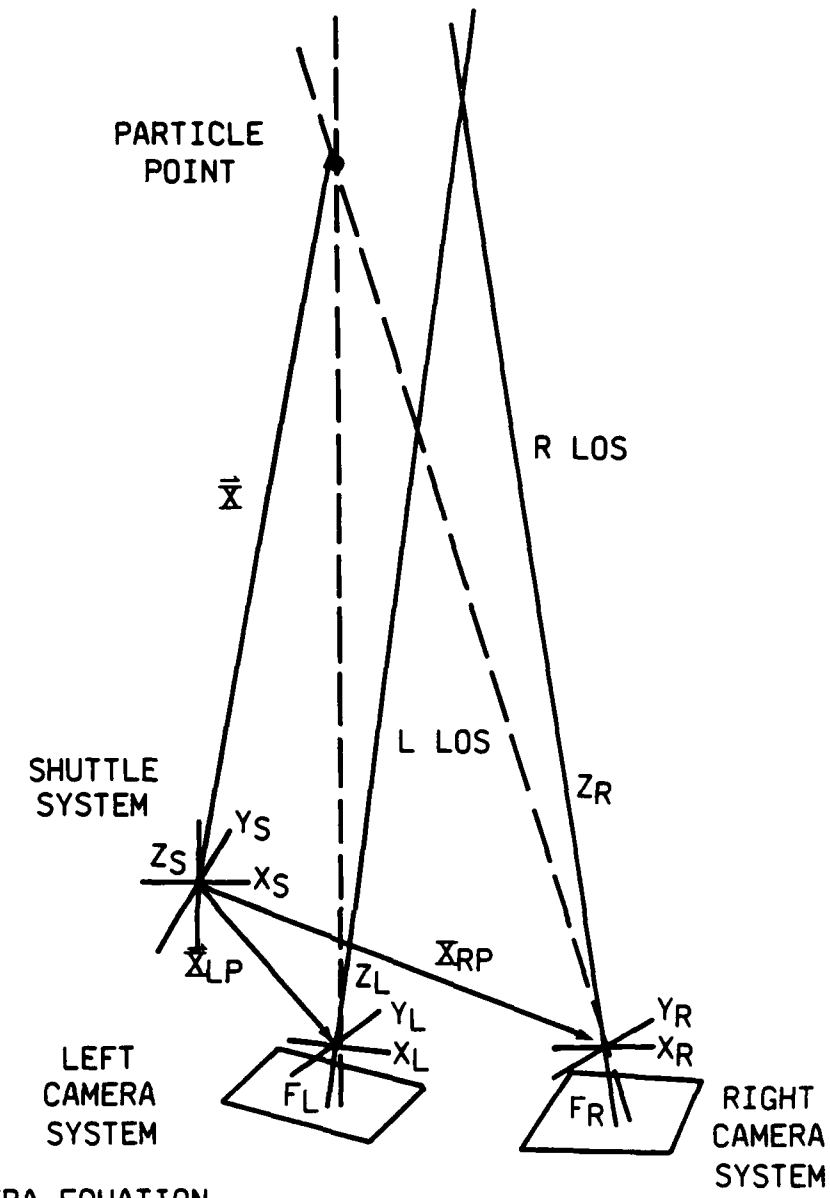

CAMERA EQUATION

$$-\frac{1}{r_i}\begin{pmatrix} x_i \\ y_i \\ F_i \end{pmatrix} = \frac{[T_i]}{R_i}\left(\vec{X} - \vec{X}_{ip}\right)$$

A-7706

Shuttle Contamination Measurements

Essential System Model

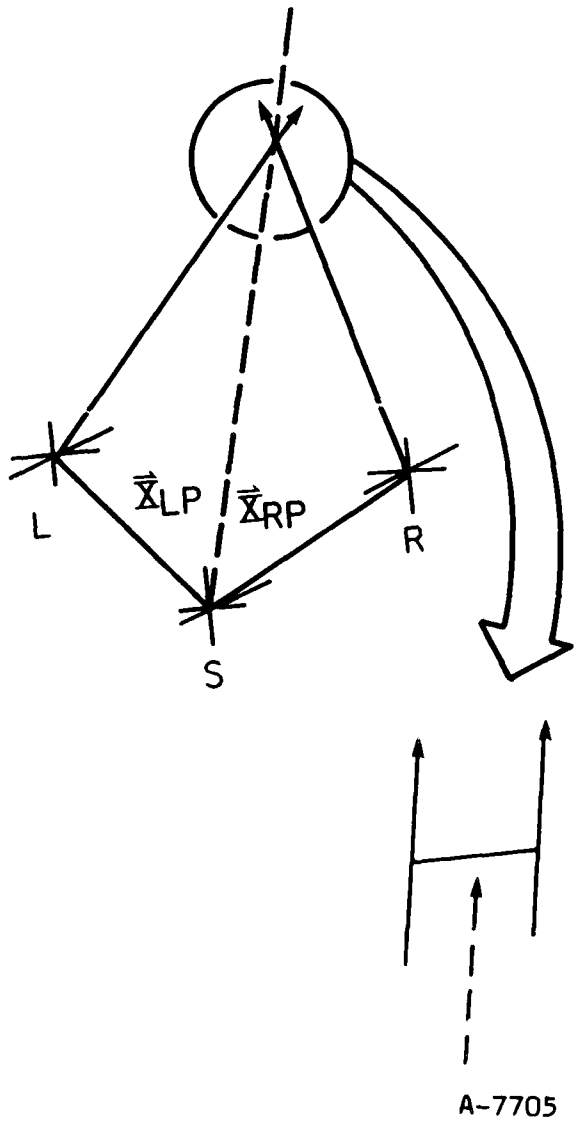

Triangulation Pointing Errors

PARTICLE POSITION ERROR BUDGET

Source	Unpropagated Error	Propagated Error (1 σ each axis)	
		at 10 ft	at 100 ft
Interior Orientation Each Camera			
Focal Length	0.075 in.	2 in.	20 in.
Film Plane Disp.	0.004 in.	0.7 in.	7 in.
Film Plane Rot.	$\leq$ 0.5 deg	1 in.	10 in.
Radial Lens Dist.	$\leq$ 0.001 in.	0.15 in.	1.5 in.
Measurement Error	0.001 in.	0.15 in.	1.5 in.
Exterior Orientation Each Camera			
Angular Orientation	0.1 deg	0.3 in.	3 in.
Perspective Center Disp.	0.1 in.	0.3 in.	0.3 in.
Base to Shuttle			
Angular Orientation	0.25 deg	0.7 in.	7 in.
Displacement	0.5 in.	0.5 in.	0.5 in.
RSS		2.5 in.	25 in.

FOR $|\vec{D}| = 90\text{ft}$

AND $\Delta t = 5\text{ s}$

$$\vec{V}_t = \frac{\vec{D}}{\Delta t}$$

$$\vec{V} = \frac{\vec{D}_e}{\Delta t} = \frac{\vec{D} + \delta\vec{r}_2 - \delta\vec{r}_1}{\Delta t}$$

$$\text{or } \delta\vec{V} = \frac{\delta\vec{r}_2 - \delta\vec{r}}{\Delta t}$$

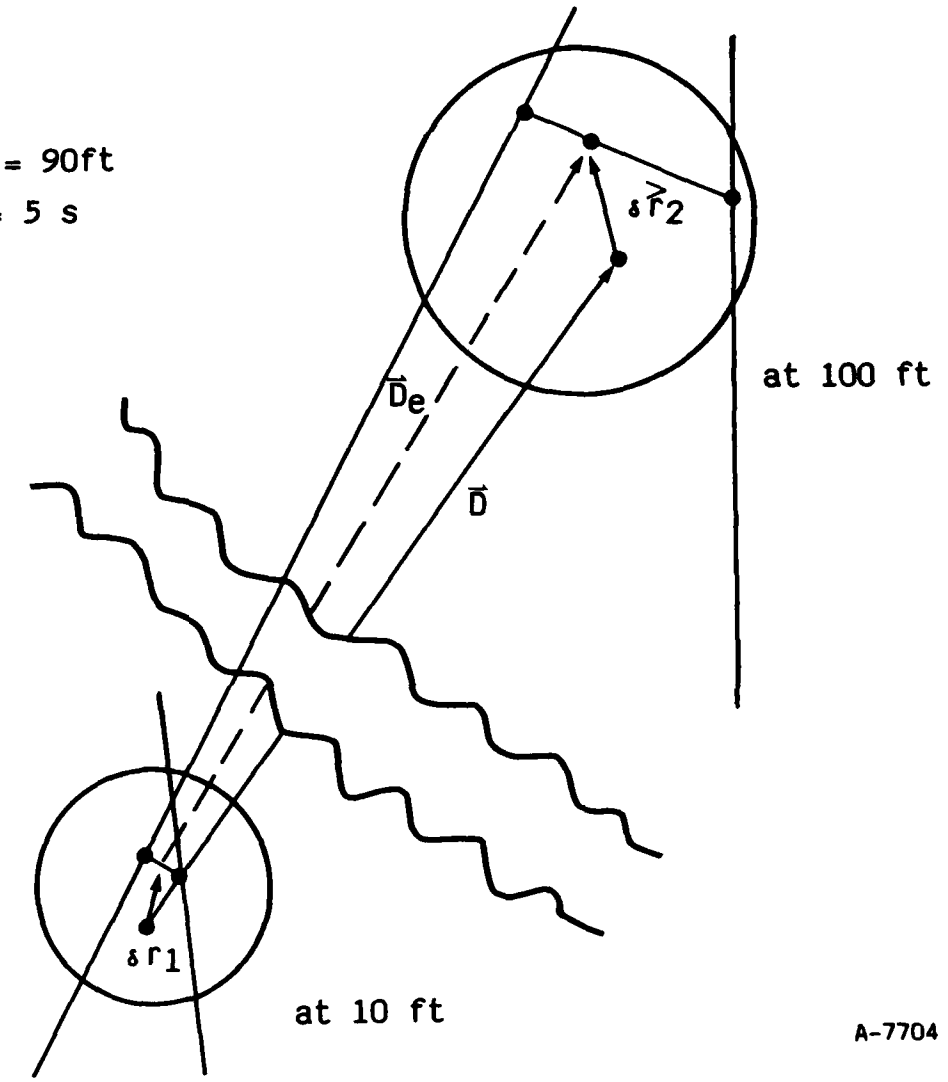

Velocity Error

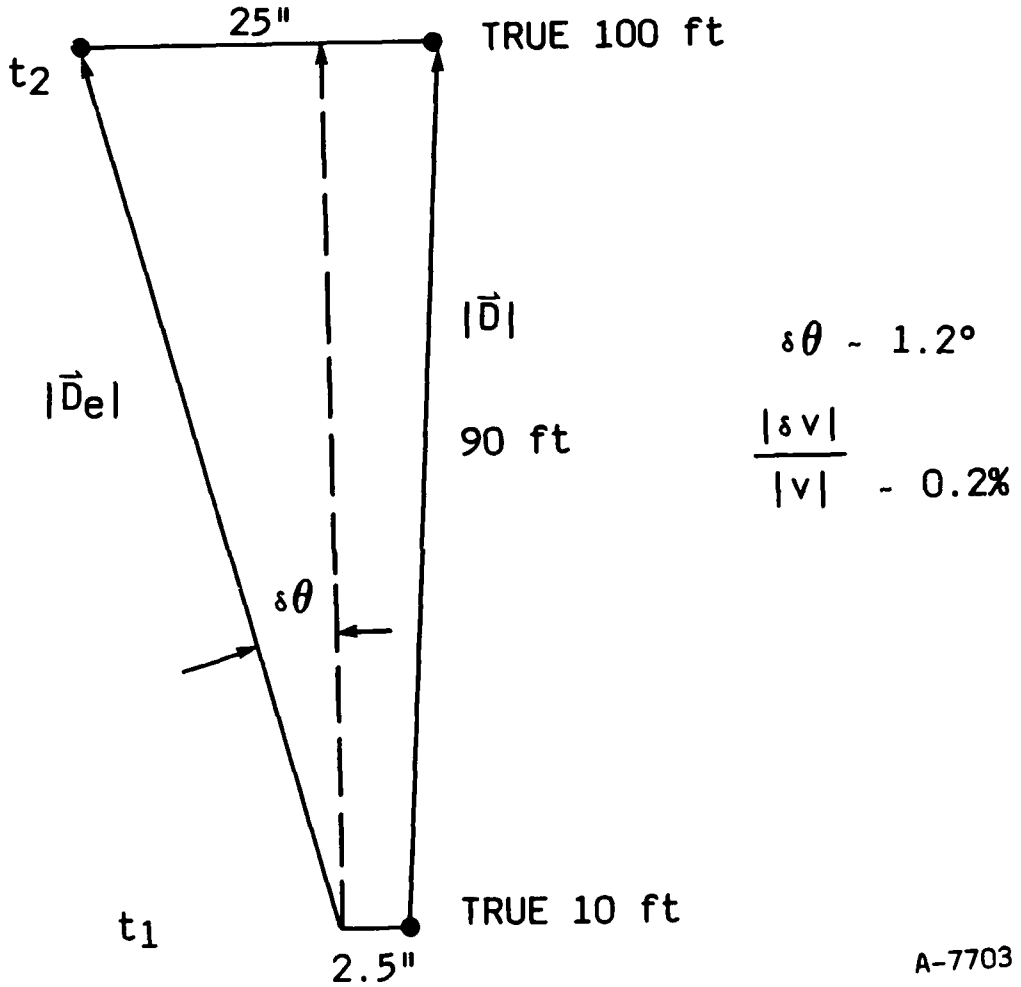

$\delta\theta \sim 1.2°$

$\frac{|\delta v|}{|v|} \sim 0.2\%$

Worst Case Velocity Errors (1σ)

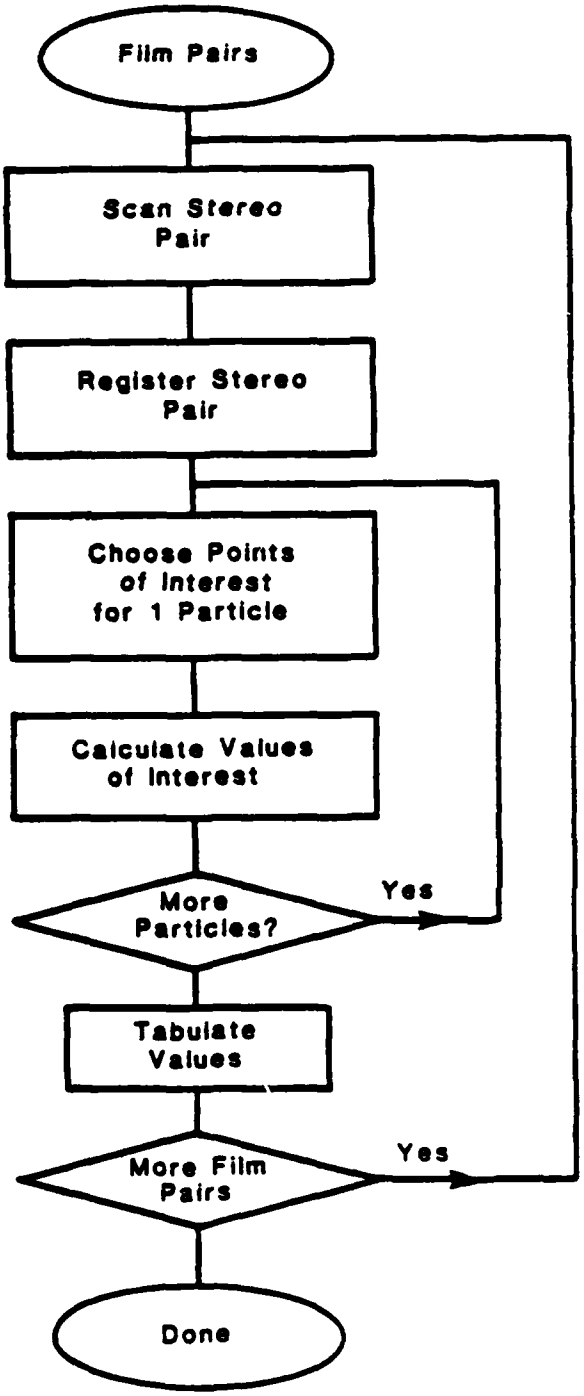

General Flow of Data Reduction

CHOOSING POINTS OF INTEREST

- TO FIND POINTS OF INTEREST, THE LEFT AND RIGHT HAND IMAGES ARE SUPERIMPOSED IN RED AND GREEN
- TO DO THIS, EACH IMAGE IS OPTICALLY RECORDED TO OCCUPY ONLY 16 GRAY LEVELS, AND THEN RECOMBINED
- THE OPERATOR WILL POINT TO CORRESPONDING SEGMENTS; SOFTWARE WILL DETERMINE ENDPOINTS AND WIDTHS
- VALUES FOUND WILL BE STORED IN INTERNAL DATA FILE N. INT. DAT

DETAIL OF SCANNING STEREO PAIR

- FILMS FED SIDE-BY-SIDE INTO DIGITIZER
- PAIR OF FRAMES SCANNED SIMULTANEOUSLY INTO 1536 x 512 FILE - N. RAW (25 μm/SAMPLE)
- FRAMES SEPARATED INTO LEFT AND RIGHT HAND IMAGES (N.L., N.R.)
- HEADERS CONTAIN UPPER-LEFT-HAND CORNER COORDINATES IN N. RAW

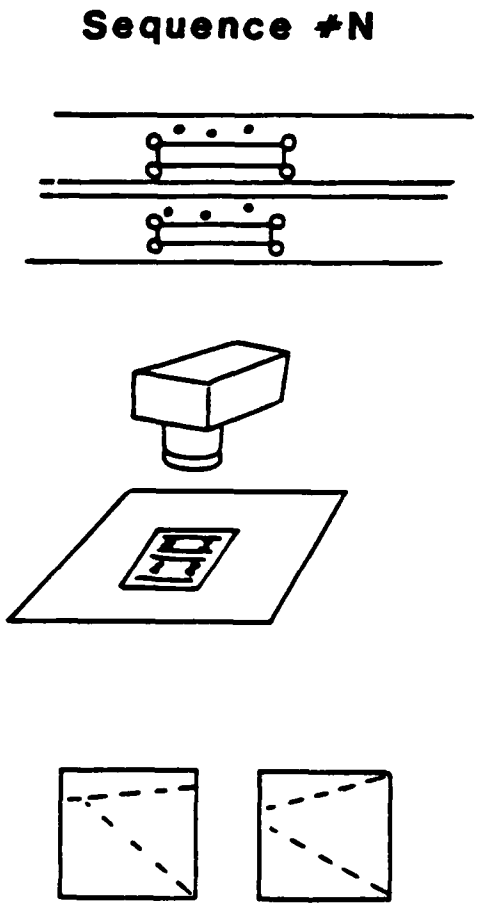

DETAIL OF STEREO PAIR REGISTRATION

- REGISTRATION MEANS DETERMINING RELATION OF FILM PLANE COORDINATES TO CAMERA IMAGE PLANE COORDINATES
- BASIC ELEMENTS TO USE ARE FIDUCIALS ON EDGES OF FRAMES

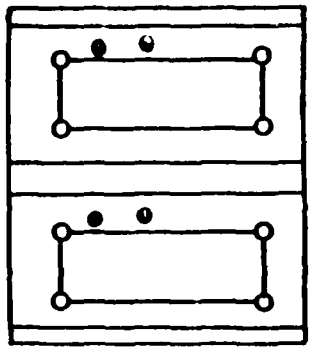

- N. RAW CONTAINS FIDUCIALS
- REGIONS WILL BE EXTRACTED AND DISPLAYED

- OPERATOR COARSELY LOCATES POSITIONS OF FIDUCIALS WITH TABLET
- SOFTWARE WILL AUTOMATICALLY CENTROID OBJECTS LOCATED

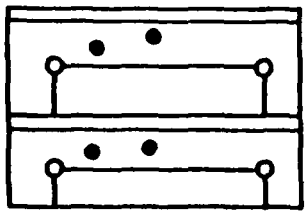

- COORDINATES OF ASSOCIATED FIDUCIALS WILL BE STORED IN HEADERS OF N.L., N.R.
- TRANSFORMERS TO CAMERA IMAGE PLANES CALCULATED AND STORED IN HEADERS OF N.L., N.R.

OUTPUT FILE ORGANIZATION

- HAVE TWO FILES - N. INT. DAT, N. OUT. DAT
- N. INT. DAT HAS FILM PLANE DATA
  N. OUT. DAT HAS SPATIAL DATA

IMAGE SEQUENCE #N

PARTICLE #1

EXPOSURE #1 $\left(X_1^L, Y_1^L\right), \left(X_2^L, Y_2^L\right), \left(X_1^R, Y_1^R\right), \left(X_2^R, Y_2^R\right), W_L, W_R$

EXPOSURE #2 $\left(X_3^L, Y_3^L\right), \left(X_4^L, Y_4^L\right), \left(X_3^R, Y_3^R\right), \left(X_4^R, Y_4^R\right), W_L, W_R$

EXPOSURE #3 $\left(X_5^L, Y_5^L\right), \left(X_6^L, Y_6^L\right), \left(X_5^R, Y_5^R\right), \left(X_6^R, Y_6^R\right), W_L, W_R$

EXPOSURE #4 $\left(X_7^L, Y_7^L\right), \left(X_8^L, Y_8^L\right), \left(X_7^R, Y_7^R\right), \left(X_8^R, Y_8^R\right), W_L, W_R$

PARTICLE #2

.
.
.

OUTPUT FILE ORGANIZATION

N. INT. DAT

IMAGE SEQUENCE #N

PARTICLE #1

EXPOSURE #1 $(X_1, Y_1, Z_1); (V_{x1}, V_{y1}, V_{z1}), e_1$

EXPOSURE #2 $(X_2, Y_2, Z_2); (V_{x2}, V_{y2}, V_{z2}), e_2$

EXPOSURE #3 $(X_3, Y_3, Z_3); (V_{x3}, V_{y3}, V_{z3}), e_3$

EXPOSURE #4 $(X_4, Y_4, Z_4); (V_{x4}, V_{y4}, V_{z4}), e_4$

PARTICLE #2

.
.
.

APEPNDIX K

Catalogue of PACS Film Data

Reproduced in its entirety.

APPENDIX

Catalogue of PACS Film Data

Orbit - counted from ascending node

MET in hours:minutes

Number of sets (four frames in set) in sequence

Black: sets of film overexposed - too much scattered sunlight from baffles or earth

Part: sets containing easily visible particles

Sky: sets containing only stars

Earth: sets having earth in field of view

Orientation: (incomplete) Shuttle attitude

Notes: comments on exposures or mission events

Orbit	MET start	MET end	Black	Part	Sky	Earth	Orientation	Notes
3	0:03:31	0:03:53	29				-ZLV+XVV	Sunlit earth
3	0:03:55	0:03:57		2				Grey frames progressively murkier; orbit 3 sunset 0:03:57:27
3	0:03:59	0:04:01				2	maneuver	Second set Earth limb
3	0:04:03	0:04:07			3		IH	Slewing to stable star pattern
3/4		0:04:29			11			same star field
4	0:04:31					1	maneuver	Earth limb appears; Orbit 4 sunrise 4:32
4				2				particles against white-many different directions
4	0:04:37	0:05:27	26				-ZLV+XVV	sunlit earth
4	0:05:29					1		Earth dark
4	0:05:31			1				Third frame possible strobed particle against earth
4/5						16		Clear fields; Orbit 5 sunrise 06:03
5	0:06:05			1				Many particles-same basic direction
5			25					
5	0:06:57	0:06:59		2				Grey Murky sets; Orbit 5 sunset 6:59
5/6	0:07:01	0:07:33				17		clear; Orbit 6 sunrise 7:34
6	0:07:35			1				large particle coming from the left-other smaller particles
6						1		Grey mottled set-no obvious particles
6	0:07:39	0:08:29	26					Orbit 6 sunset 8:30
6/7	0:08:31	0:08:57				13		Earth limb appearing on thirteenth set's last frame
7	0:08:59	0:09:05			4		maneuver	slewing; Orbit 7 sunrise 9:05
7	0:09:07	0:09:29		12			-YSI	Storm of particles! sun??? backscatter; satellite launched
7		0:09:57	14				mnvr to ...	14 black; sunlit earth in foreground
7	0:09:59	0:10:01		2			-ZLV+XVV	few slow movers-same "size"; Orbit 7 sunset 10:01; 1 grey
7/8	0:10:03	0:10:29			14		+ZLV+XVV	slewing to +ZLV+XVV
8	0:10:21	0:10:35				3	maneuver	1st has earth limb-2 sets clear; Orbit 8 sunrise 10:36
8	0:10:37	0:10:39		2				1st has fast moving particle from left-2nd has smaller storm
8	0:10:41	0:11:31	26				-ZLV+XVV	sun on Earth; Orbit 8 sunset 11:32; Fuel cell purge 11:19
8	0:11:33	0:11:37				3		
8/9	0:11:39	0:12:01			12		deep space	maneuver to deep space
9	0:12:03	0:12:07				3	maneuver	1st has earth limb and cities 2 clear;Orbit 9 sunrise 12:07
9	0:12:09			1				large rock lower left hand corner 1st frame most go left to right
9	0:12:11					1		filiagree pattern-over Pakistan
9	0:12:13		15				+YSI...	3 sets of grey coming out of black
9		0:13:08		11			Nose South	Varied motion & sizes-roughly ten per set (i.e. not storm)Orbit 9 SS 13:03
9/10	0:13:05	0:13:23			10			stable star field
10	0:13:25	0:13:39				8		1,2 Earth limb 3,4,5 clear 6,7,8 cities; Orbit 10 SR 13:38
10	0:13:41			1				left to right about 5 particles

5/6/86

PACS film catalogue

Orbit	MET start	MET end	Black	Part	Sky	Earth	Orientation	Notes
10	0:13:43		17					17th grey w/no particles
10		0:14:33		9				Orbit 10 SS 14:34;1st-few faint ; 2nd-large low L; 3rd faint few; 4th med one; 5th-one on left; 6th-faint middle; 7th-3 diff clarities; 8th-diff dir; 9th-afew
10	0:14:35	0:14:53			10			
11	0:14:55	0:15:09				8		1,2 Earth limb 3-few cities 4-8 not much; Orbit 11 SR 15:10
11	0:15:11	0:15:13		2				1-diff directions,med size,sparse; 2nd-very few,one or two
11	0:15:15		15					15th is grey w/no particles
11		0:16:05		11				1 to 4-grey with 0 or 1 particle; 5-one from bottom; 6-grey; 7-long one 8-diff dir; 9-big one; 10-crossing pair; 11-few diff dir; Orbit 11 SS 16:05
12	0:16:07	0:16:25			10			
12	0:16:27	0:16:41				8		2 Earth limb sets 6 empty; Orbit 12 SR 16:41
12	0:16:43			1				Particles from top left- 5 or 6
12	0:16:45		14					
12		0:17:37		11				7 very sparse sets; 8-THE WORM!; 9-sparse with long one on last frame; 10-sparse; 11-intersection; Orbit 12 SS 17:36
12/13	0:17:39				10			
13	0:17:59	0:18:13				8		2 earth limb with cities 8th-dark on last frame; Orbit 13 SR 18:12
13	0:18:15			1				few sparse faint ones
13	0:18:17		17					2 or 3 grey w/no particles
13		0:19:07		9				1-bunch at bottom middle; 2-bot to top; 3-top to bot; 4-grey; 5-long tails; 6-long dark L to R; 7, 8, 9 sparse; Orbit 13 SS 19:08
13/14	0:19:09	0:19:27			10			
14	0:19:29	0:19:43				8		2 earth limb, 3-few cities, from 4 on clear; Orbit 14 SR 19:43
14	0:19:45			1				few particles
14	0:19:47					1		mottled grey-striated-clouds over Canary Islands
14	0:19:49		20					last 4 or 5 grey,last frames 2stars
14		0:20:39		6				1-out of focus smudge 2-upper right; 3-large ones, smudge; 4-one maybe; 5-a few; 6-grey; Orbit 14 SS 20:39
14/15	0:20:41				10			stable pattern; Fuel cell purge 20:53
15	0:21:01	0:21:15				8		2 earth limb,4th Carrib. cities; Orbit 15 SR 21:14; Supply water dump start 21:16
15	0:21:17			1				about ten particle tracks
15	0:21:19		14					
15		0:22:09		12				STORMY,then clear to few large ones per set; Orbit 15 SS 22:10; Dump Stop 21:50
15/16	0:22:11	0:22:43			17		maneuver	slew to new stable pattern +X+ZSI
16	0:22:45					1	+X+ZSI	Earth limb w/many cities; Gulf coast of Florida; Orbit 16 SR 22:45
16				2		2		Particles against Earth limb as cities retreat
16	0:22:51'	0:23:37	24				maneuver	2 sets slightly brighter during black section, entry to light part is crisp

Orbit	MET start	MET end	Black	Part	Sky	Earth	Orientation	Notes
16	0:23:39					1	UVX1IH	grey flower shaped splotches 6 dark spots; Australian Outback
16	0:23:41			1		1		clear; Orbit 16 SS 23:41; two large stationary particles
16						1		earth limb appearing at bottom left hand corner-opposite previous pattern
16		0:23:49				3		clearly earth limb; Sun +X+Z
16/17	0:23:51				14			steady star field; Orbit 17 SR 1:00;16:56
17				5	5			particles against star field-light leak?-growing murky-several large hunks
17	1:00:37?			4			maneuver	can no longer see stars and only a few particles show up against grey
17		1:01:09	17				UVX2IH	
17	1:01:11					1		R-light leak appears w/ ground in upper LH corner-cross track?; Orb 17 SS 1:12
17	1:01:13					1		clear field
17	1:01:15	1:01:21				4		Earth limb low right corner to up L
17/18	1:01:23	1:01:49			13			Orbit 18 SR 1:48
18	1:01:51	1:02:09		10				1-particles w/right fuzz and stars; 2-darker; 3-grey fuzzy stripe; 4-a few;
							maneuver	5-long dark tracks growing murky; 6-10 growing too grey to see
18	1:02:11	1:02:41	16				UVX3IH	maneuver to UVX3 2:35
18	1:02:43					1		ground view dark grey with a few black dots; Orb 18 SS 2:43
18	1:02:45			1		1		particles? with light leak?
18	1:02:47	1:02:53				4		clear fields
18	1:02:55	1:02:57				2		Earth limb appearing from low left corner
19	1:02:59	1:03:19			12		maneuver	Orbit 19 SR 3:19; begin maneuver 3:01
19	1:03:21	1:03:23		2				1-right light leak? long track to Left; 2-Murk w/cluster low left & large fuzz
								track from top
19	1:03:25	1:04:16	24					PACS OFF/ON 3:26 to 3:29; Orb 19 SS 4:14
19	1:04:18					1	Bias -ZSI	Grey w/spot mid right edge; Sun into bay
19	1:04:20	1:04:28				5		clear fields
19	1:04:30	1:04:32				2		small cities
20	1:04:34	1:04:37				3		clear fields
20	1:04:38					1		city low left-Guam
20	1:04:40	1:04:42				2		clear fields
20	1:04:44	1:04:48				3		Earth limb appearing low left hand corner VERY BRIGHT sun behind it
20	1:04:50	1:05:28	20					Orbit 20 SR 4:50
20	1:05:30		1				maneuver	white spot against black--sun directly in field of view
20	1:05:32	1:05:46	8					Orbit 20 SS 5:45
20	1:05:48				1		CHAMP	light leak low left corner
20						1		Earth limb w/T-storm shaped bright spot low left
20						1		Earth limb mid right hand side
20	1:05:54					1		Earth limb-big spot

PACS film catalogue

Orbit	MET start	MET end	Black	Part	Sky	Earth	Orientation	Notes
20/21						6		Earth limb stable position last 8; Orbit 21 SR 6:21
21	1 06:22					8		7 clear fields 8-large trifoliate light leak right
21	1 06:24	1:07:16	27					Orbit 21 SS 1:07:00
21	1 07:18					1	maneuver	Dark grey bulge appearing right
21	1 07:22	1:07:24				3		Earth limb very bright 1 bright earth spot
21	1:07:26					1		clear field
21	1:07:28			1				3rd frame possible strobed particle
21/22						3	-ZLV ...	clear fields
22	1:07:36					1	NOSE NORTH	with city moving up
22						2		clear fields
22	1:07:42					1		another small set of blotches
22						1		clear field
22	1:07:46			1				possible strobe
22						3		clear fields; Orbit 22 SR 7:52
22	1:07:54	1:08:48	28					Fuel cell purge 08:19; Orbit 22 SS 8:48
22/23	1:08:50	1:09:24				18		clear fields, maybe particles in 12, 14, and 16; Orbit 23 SR 9:23
23	1:09:26	1:10:18	27					Supply water dump start 09:37, stop 10:14; Orbit 23 SS 10:19
23	1:10:20			1		1		light leak low right corner improves with time-triangle of particles
23/24	1:10:22	1:10:36				8		clear fields
24	1:10:38					1		two fuzzy streaks
24	1:10:40					1		clear set
24	1:10:42					1		city Saudi Arabia
24	1:10:44					3		clear sets
24	1:10:50					2		faint tracks vertical-earth lights
24	1:10:54					2		clear to greying on the edge; Orb 24 SR 10:54
24	1:10:58	1:11:50	27					Orb 24 SS 11:50
24/25	1:11:52	1:12:26				18		many earth lights w/clear structure-Mecca-Saudi Arabia; Orb 25 SR 12:26
25	1:12 28	1:13:22	28					Orbit 25 SS 13:21
25/26	1:13:24	1:13:58				18		some cities in set 10-West Africa, otherwise clear; Orbit 26 SR 13:57
26	1:14:00	1:14:51	27					Orbit 26 SS 14:52
26/27	1:14:53	1:15:19				19		1st set-smallish light leak low right; last set-greying from the corners, a few city streaks; #13 Coast of Brazil
27	1:15:21	1:16:23	27					Orbit 27 SR 15:28; SS 16:23
27/28	1:16:25	1:16:59				18		clear fields-one or two streaks of western Sahara; Orb 28 SR 16:59
28	1:17:01	1:17:55	28					Orbit 28 SS 17:54
28/29	1:17:57'	1:18:31				18		last set-city lights of Canary Islands w/ clear structure; Orbit 29 SR 18:30
29	1:18:33	1:19:25	27					Fuel cell purge 19:03; Orbit 29 SS 19:03

5/6/86

Orbit	MET start	MET end	Black	Part	Sky	Earth	Orientation	Notes
29/30	1:19:27	1:20:01				18	-ZLVNN	1 set w/cities; Orbit 30 SR 20:01
30	1:20:03	1:20:57	28					Orbit 30 SS 20:57
30/31	1:20:59	1:21:33				18		1 set large cloud, 2 w/cities; #13 Mexico coast; #16 Florida; Orb 31 SR 21:32
31	1:21:35		24				+X+ZSI	Maneuver to UVX10
31	1:22:23			1			UVX10	grey with black plume low R and squarish black spot on right mid edge- particle in first 2 frames
31	1:22:25			1	1			Pleiades & Particles; L to R segments
31	1:22:27			1	1			long thin segmented track &odd grey smudge-47 SEGMENTS!; Orb 31 SS 22:28
31	1:22:29			1	1			segments in about 4 tracks
31/32					15			Pleiades
32	1:23:03	1:23:07				3		Earth limb, pleiades, land-Gulf coast; Orb 322 SR 23:03; Particles in set #3
32	1:23:09			1				grey ground view w/diagonal stripes
32	1:23:11	1:23:55	23				maneuver	maneuver to UVX5
32	1:23:57					1	Bias +YSI	Dark grey curtain over left side with same squarish black mark mid right edge
32	1:23:59			1		1		long particle track with Earth limb; Orb 32 SS 23:59
32	2:00:01	2:00:03				2		Earth limb
32/33					16		maneuver	Orbit 33 SR 2:00:35:03
33		2:00:42	4	1			+XYZSI	first set has one particle track displayed against stars, the rest are grey and don't really look like there are any particles
33	2:00:44	2:01:26	21				UVX7	
33	2:01:28					1		grey Earth view with dark striped diagonals-squarish black on right
33	2:01:30					1		Bright at first/slight grey diagonals w/ light leak right; Orb 33 SS 1:30
33	2:01:32	2:01:36				3		Earth limb low right to up left
33/34					15		maneuver	slowly changing field; Orb 34 SR 2:06; maneuver between 1:54 and 2:15
34	2:02:08			1				light leak beginning at right-perhaps a few tracks in fourth frame
34	2:02:10			1				large rock from top/few thin tracks on fourth frame
34	2:02:12			1				More particles/diff directions and sizes light leak on right/large particle
34	2:02:14	2:02:58	22				deep space	never gets black/particles in the dark; Done maneuvering 2:15
34/35	2:03:00	2:03:38			21			slowly changing fields; Orb 34 SS 3:01; Orb 35 SR 3:37
35	2:03:40			1				pie shaped particle top on frame 3
35	2:03:42	2:04:04		12			maneuver	particles discernible through grey for a while; Begin maneuver 3:59:26
35	2:04:06	2:04:32	14				GG	Orbit 35 SS 4:32; end maneuver 4:18:30
35	2:04:34					1		dark vertical curtain of grey over left side, square light leak to right
35/36	2:04:36	2:05:10			18			slowly changing fields; Orb 36 SR 5:08
36	2:05:12	2:05:14		2	2			4th frame shows clear particles
36	2:05:16					1		Dark vertical curtain over left side
36	2:05:18	2:06:00	22				maneuver	Can still see vertical curtain; Out of GG 5:47:38; Sun though field of view 5:58

PACS film catalogue

Orbit	MET start	MET end	Black	Part	Sky	Earth	Orientation	Notes
36	2:06:02	2:06:04		2				predominant motion left to right many particles; Orb 36 SS 2:06:03:45; Thruster?
36/37	2:06:06				13		UVX4	short slew to stable field
37	2:06:32	2:06:36				3		Earth limb nearly vertical right to left
37						2		clear fields; Orbit 37 SR 6:39
37	2:06:42			1*				definitely particles here that do not move; approximately 75 particles
37	2:06:44					1		ground view with dark features to right; particles persist; Over Atlantic
37	2:06:46	2:07:36	26				maneuver	much of this is not black; Orbit 37 SS 7:34
37	2:07:38	2:07:48			6		-XYZSI	steady field
38	2:07:50	2:07:54				3		Earth limb bottom left to top right
38		2:08:12		0*		9	maneuver	clear fields; Fuel cell purge 08:04; Supply water dump start 07:59; Orb38 SR 8:10 North Pacific South of Japan, looking toward wake.
38	2:08:14	2:09:06	27				-ZLV NNorth	last set dark grey; Supply water dump stop 08:38; Orbit 38 SS 9:05
38/39	2:09:08	2:09:42				18		vertical city streaks; Orbit 39 SR 9:41; Bangladesh set 16
39	2:09:44	2:10:30	28					last 2 sets very dark grey
39/40	2:10:31	2:11:14				18		cities w/structure 9th set on; Orb 39 SS 10:37; Orb 40 SR 11:12 set #14 Arab Emirates Muscat
40	2:11:16	2:12:07	27					last set dark grey; Orbit 40 SS 12:08
40/41	2:12:09	2:12:45				19		1st-light leak low R some cities w/structure; 14th-strobed pie shaped particle Orbit 41 SR 12:44
41	2:12:47	2:13:39	27					Orbit 41 SS 13:39
41/42	2:13:41	2:14:15				18		vertical streaks from time to time; Orb 42 SR 14:15
42	2:14:17	2:15:11	28					Orbit 42 SS 15:10
42/43	2:15:13	2:15:47				18		one or two streaks; Orbit 43 SR 15:46
43	2:15:49	2:16:41	27					Orbit 43 SS 16:41
43/44	2:16:43	2:17:17				18		one or two sets of vertical streaks; Orb 44 SR 17:17
44	2:17:19	2:18:13	28					grey either side of black; Fuel cell purge 17:46; Orbit 44 SS 18:12
44/45	2:18:15	2:18:49				18		some sets with vertical streaks; Orb 45 SR 18:48; Waste Water Dump start 18:42
45	2:18:51	2:19:43	27					Orb 45 SS 19:43
45	2:19:45			1				particles bottom left to top right
45/46	2:19:47	2:20:21				18		few vertical streaks; Orbit 46 SR 20:19; Waste Water Dump stop 19:54
46	2:20:23	2:20:41	10				maneuver	maneuver to UVX11 +XZ-YSI
46	2:20:43	2:20:45		2				2 sets predominant motion left to right in grey
46	2:20:47	2:20:57	6					grey
46	2:20:59	2:21:03		3				Particles in grey
46	2:21:05	2:21:13	5				+XZ-YSI	grey seem to be one frame out of sinc; Orbit 46 SS 21:14
46	2:21:15	2:21:17				2		1 ground view/1 dark spot upper right
46	2:21:19	2:21:23				3		

5/6/86

PACS film catalogue

Orbit	MET start	MET end	Black	Part	Sky	Earth	Orientation	Notes
46/47	2:21:25	2:21:27				2		Earth limb left upper corner to low right corner
47		2:21:51			12			Orb 47 SR 21:50; steady field with slow drift
47	2:21:53	2:21:57		3			maneuver	light leak on right
47	2:21:59	2:22:43	23				Bias Nose..	
47	2:22:45	2:22:47		2			to Earth	nice segmented particle; Orbit 47 SS 22:46
47/48	2:22:49	2:23:21				17		15-17 city lights of Gulf coast moving L to R; Orbit 48 SR 23:21
48	2:23:23	3:00:15	27					
48	3:00:17			1				Large number of stationary particles. About 70 particles, one with halo.
48								Orb 48 SS 3:00:17:08
48/49	3:00:19	3:00:37				10		clear fields
49	3:00:39			1		1		one particle or city
49	3:00:41					1		city to the left
49	3:00:43	3:00:53				6		last set turning grey w/one or two dark spots; Orbit 49 SR 00:53
49	3:00:55	3:01:45	26					
49	3:01:47	3:01:51		3		3		mottled with stationary particles; Last set with band of particles; Orb 49 SS 01:48
49/50	3:01:53	3:02:25				17		last two sets get grey; Orb 50 SR 02:24
50		3:03:17	26					
50	3:03:19	3:03:25		2		4		3 stationary particles against mottled grey for two sets; Orb 50 SS 3:19
50/51	3:03:27	3:03:35				5		
51	3:03:37					1	maneuver	Earth limb
51	3:03:39	3:03:57			10		+ZSI	slewing; Orbit 51 SR 03:55
51	3:03:59	3:04:03		3				
51		3:04:47	22					last set grey
51/52	3:04:49	3:05:27			20			Orbit 51 SS 04:50; Orbit 52 SR 05:26
52	3:05:29	3:05:33		3				light leak beginning right; random velocites; tail to nose; approximately 6 per set
52	3:05:35	3:06:17	22					
52	3:06:19				1			grey with stars
52	3:06:21	3:06:23		2				1 slow moving particle that persists through 2 sets; approaching; Orb 52 SS 06:21
52/53	3:06:25	3:07:00			19			Fuel cell purge 06:36; Orbit 53 SR 06:57
53	3:07:02	3:07:04		2				a few
53		3:07:48	22					last set grey
53	3:07:50	3:07:54		3				a few fine particles; Orbit 53 SS 07:52
53	3:07:56				1		maneuver	slewing
53/54	3:07:58	3:08:18			11		+X+ZSI	Orion's head triangle; Supply water dump start 08:05
54	3:08:20				1		maneuver	slewing
54	3:08:22					1		Earth limb almost vertically in the middle
54	3:08:24	3:08:28				3		few cities in the 2nd set; Orbit 54 SR 08:28

5/6/86

PACS film catalogue

Orbit	MET start	MET end	Black	Part	Sky	Earth	Orientation	Notes
54	3:08:30	3:08:38	5				ROTR	PTC
54	3:08:40	3:08:42		2				Small Storm! Dump; more than 450 particles; varying size and direction
54	3:08:44	3:08:52	5					Supply water dump stop 08:50
54	3:08:54			1				lots of particles! Smaller storm! approx. 300 particles
54	3:08:56	3:09:24	15					sometimes small dark square to right w/ lighter grey background; Orb 54 SS 09:23
54/55	3:09:26	3:09:58			17			slewing; Orb 55 SR 09:59
55	3:10:00					1		Earth limb
55	3:10:02	3:10:08	4					first is grey
55	3:10:10	3:10:12		2				first set has particles, second might
55	3:10:14	3:10:22	5					
55	3:10:24			1				
55	3:10:26	3:10:54	15					a few lighter sections; Orb 55 SS 10:54
55/56	3:10:56	3:11:08			7			Cricket shaped dark spot, then slewing
56	3:11:10					1		Earth limb
56	3:11:12	3:11:20				5		
56	3:11:22					1		city structure; Riyadh, Saudi Arabia
56	3:11:24	3:11:30				4		last limb; Orb 56 SR 11:30
56	3:11:32			1				one fuzzy particle
56	3:11:34	3:11:38	3					never fully black
56	3:11:40			1				light leak to right
56	3:11:42	3:12:24	22					periods of lighter grey: 11:42, 11:50-11:54, 12:00-12:08, 12:16-12:20
56	3:12:26			1				Orb 57 SR 13:02
56/57	3:12:28	3:12:38			6			slewing
57	3:12:40					1		Earth limb across upper left
57	3:12:42	3:12:46			3			
57	3:12:48					1		Earth limb across lower left
57	3:12:50	3:13:02			7			slewing; Orb 57 SR 13:02
57	3:13:04			1				light leak developing low left
57	3:13:06	3:13:08	2					never fully black
57	3:13:10			1				
57	3:13:12	3:13:56	23					1st grey, lighter; 13:20-13:26, 13:32-13:38, 13:46-13:50; Orb 57 SS 13:57
57								19th has particle-13:48; 23rd has mottled zebra striped ground view-13:56
57/58	3:13:58	3:14:16			10			slewing
58	3:14:18					1		Earth limb
58	3:14:20	3:14:34		1	7			7th has particle; Orb 58 SR 14:33
58	3:14:36	3:14:38	2					
58	3:14:40	3:14:42		2				2nd circular light leak; 6 particles, 1 w/ halo

5/6/86

PACS film catalogue

Orbit	MET start	MET end	Black	Part	Sky	Earth	Orientation	Notes
58	3:14:44	3:15:26	22					Lighter; 14:50-14:56, 15:04-15:08, 15:16-15:22
58	3:15:28					1		Earth limb low horizontal; Orb 58 SS 15:28
58/59	3:15:30	3:15:46			9			
59	3:15:48					1		Earth limb
59	3:15:50	3:16:04		1	8			8th has particle; Orb 59 SR 16:04
59	3:16:06	3:16:08	2					
59	3:16:10	3:16:12		2				
59	3:16:14	3:16:56	22					Lighter; 16:20-16:26, 16:34-16:38, 16:46-16:52
59	3:16:58					1		Beautiful horizontal earth limb; Orb 59 SS 16:59
59/60	3:17:00	3:17:34				18		Orb 60 SR 17:35; Fuel cell purge 17:31
60	3:17:36			1				particles against Earth limb
60	3:17:38		1					not fully black-sun near FOV
60	3:17:40	3:17:42		2				
60	3:17:44	3:18:28	23					Lighter; 17:44, 17:52-17:56, 18:04-18:08, 18:16-18:20
60	3:18:30				1			slewing; Orb 60 SS 18:30
60	3:18:32			1				long segmented streak across upper left corner
60/61	3:18:34	3:19:04			16		maneuver	Barrel roll! Really Neat! limb 18:36; limb 18:58-19:02; circular light leak 19:04
—	3:19:06	4:02:03	11				-ZLV+XVV	PACS off in middle of black; Orb 61 SR 19:08
65	4:02:05					1		Orb 65 SS 4:02:06:06; clouds
65	4:02:07			1				KU Antenna; many particles; PLBD ops
65/66	4:02:09	4:02:45				18		mostly clear; Orb 66 SR 2:42
66	4:02:47		28				maneuver	Orb 66 SS 03:37
66	4:03:41	4:03:42			1		CHAMP	time changes between 2 and 3
66	4:03:43	4:03:44			1	1		sky,Earth limb, comet, Beautiful Earth view
66	4:03:45					1		gorgeous Earth view
67	4:03:47	4:03:49				2		mottled
67	4:03:51					1		mottled with dark spot
67	4:03:53					1		grey upper left corner
67	4:03:55					1		clear fields
67	4:03:57	4:03:58				1		cities 2/3
67	4:03:59	4:04:17				10		clear fields; Orb 67 SR 04:13
67	4:04:19					1		grey mottled Earth view
67	4:04:21	4:04:31	5					
67	4:04:33	4:04:40		5			ROTR	PTC; #5 with antenna-4:40 Time 1/2
67	4:04:42	4:04:58	9				CHAMP	not fully black ??? 4:48
67	4:05:00 ,	4:05:12		7				first of these has particles; Orb 67 SS 05:08
67	4:05:14	4:05:16			2	2		Earth limb sunset, comet

5/6/86

PACS film catalogue

Orbit	MET start	MET end	Black	Part	Sky	Earth	Orientation	Notes
68	4:05:18					1		Earth view
68	4:05:20	4:05:26				4		clear
68	4:05:28					1		cities
68	4:05:30	4:05:46				9	maneuver	clear mostly; Fuel cell purge 05:40; Orb 68 SR 05:44; Maneuver 5:30-5:37
68	4:05:48			1			-ZLV+XVV	approx. 10 stationary particles
68	4:05:50					1		mottled dark view
68	4:05:52	4:06:42	26					Orb 68 SS 6:39
68	4:06:44	4:06:48				3		mottled
69	4:06:50					7		clear
69		4:07:18				8		few streaks right to left; Orb 69 SR 7:15
69	4:07:20			1				7 stationary particles; 1 w/halo
69	4:07:22	4:08:12	26					Orb 69 SS 8:10
69/70	4:08:14	4:08:48				18		Orb 70 SR 8:46
70	4:08:50		1					light leak developing right
70	4:08:51	4:08:52				1		clouds at sunrise; time change 2/3
70	4:08:53	4:09:44	26					more clouds on 25th set 9:41; Orb 70 SS 9:41
70/71	4:09:45	4:10:19				18		start time change 3/4; clouds 9:52; Ethiopia 10:01, Muscat 10:07, Napal 10:13 Orb 71 SR 10:17
71	4:10:21		1					light leak right
71	4:10:23	4:11:13	26					26th has antenna; Orb 71 SS 11:12
71/72	4:11:15	4:11:53				20		20th is mottled grey Earth view-clouds 11:15,11:23; some cities throughout-
72								11:17, 11:29, 11:41, 11:47, 11:49, 11:51; Orb 72 SR 11:48
72	4:11:55	4:12:45	26					Orb 72 SS 12:43
72/73	4:12:47	4:13:23				19		17th chain of city lights (Iran) 13:19; clouds 12:47-12:55; Orb 73 SR 13:20
73	4:13:25	4:14:17	27					26, 27 grey with blotches; Orb 73 SS 14:15
73/74	4:14:19	4:14:55				19		Clouds 14:19, 14:25; city 14:49, 14:53, 14:55; Orb 74 SR 14:51
74	4:14:57	4:15:47	26					26 has antenna; Orb 74 SS 15:46
74/75	4:15:49	4:16:25				19		cities: 16:01, Caracas 16:03, Morocco 16:17, 16:23; clouds 15:49, 15:55 Orb 75 SR 16:22
75	4:16:27	4:17:19	27					27 has antenna, first grey; Fuel cell purge 16:33; Orb 75 SS 17:17
75	4:17:21	4:17:23				2		
75/76	4:17:25	4:17:49			13		maneuver	slewing with a few stable sets
81	5:01:48	5:02:26	20				-ZLV+XVV	PACS off; Orb 81 SS 02:23
81/82	5:02:28	5:03:02				18		Clouds 02:28-02:40; Orb 82 SR 03:00
82	5:03:04			1				
82	5:03:06					1		mottled
82	5:03:08	5:03:18	6				maneuver	sides black, dramatic drop

5/6/86

PACS film catalogue

Orbit	MET start	MET end	Black	Part	Sky	Earth	Orientation	Notes
82	5:03:20	5:03:28		5				5th antenna
82	5:03:30	5:03:50	11				IH +X+ZSI	never very dark; IH +X+ZSI 3:41
82	5:03:52				1			Orion
82	5:03:54				1			Orion's head triangle confirmed-belt stars in view; Orb 82 SS 03:55
82	5:03:56			1	1			Orion with many particles Great Nebula in Orion; EVENT
82/83	5:03:58	5:04:38			21		GG	Orb 83 SR 04:31; Maneuver 4:00-4:15; GG 4:15-4:30
83	5:04:40			1			maneuver	
83	5:04:42	5:05:28	24				-XYZSI	varying darkness; Orb 83 SS 5:26
83	5:05:30					1	maneuver	Beautiful Earth limb
83/84	5:05:32	5:06:04				17	-ZLV+XVV	clouds-05:38; city 05:48, 05:54; Fuel cell purge 5:44; Orb 84 SR 6:02
								Waste water dump #2 starts 5:52
84	5:06:06	5:06:08		2				lots of particles many directions; dump
84	5:06:09	5:06:59	26					25th has mottled view-06:57; Orb 84 SS 6:57; Waste water dump #2 stop 6:41
84/85	5:07:01	5:07:39				20		last two sets dark; cloud 07:01-07:03; city 07:21, 07:25; Orb 85 SR 7:33
85	5:07:41	5:08:31	26					last is grey; Orb 85 SS 8:28
85/86	5:08:33	5:09:09				19		08:33-clouds-08:39, 09:09/08:41 city 08:47, 08:51, 08:55, 08:57
								Orb 86 SR 9:04
86	5:09:11	5:10:01	26					Orb 86 SS 9:59
86/87	5:10:03	5:10:39				19		clouds 10:03-10:09; cities with structure; Orb 87 SR 10:35
87								(spider (Persian Gulf) -10:25) [10:13, 10:15, 10:23, 10:27]
87	5:10:41					1		grey mottled view
87	5:10:43	5:11:33	26					Orb 87 SS 11:30
87/88	5:11:35	5:12:11				19		clouds 11:35-11:43; city 11:47, 11:59, 12:07; Orb 88 SR 12:06
88	5:12:13	5:13:03	26					Orb 88 SS 13:01
88/89	5:13:05	5:13:43				20		cities w/structure 13:35, 13:39; clouds 13:05-13:17; Orb 89 SR 13:38
89	5:13:45	5:14:35	26					Orb 89 SS 14:32
89/90	5:14:37	5:15:15				20		mottled grey 20th set; city 15:13; clouds 14:37-14:43; Orb 90 SR 15:09
90	5:15:17	5:16:07	26					Orb 90 SS 16:04
90/91	5:16:09	5:16:45				19		clouds thru 16:19; sunset; Algeria 16:37; Fuel cell purge 16:31; Orb 91 SR 16:40
91	5:16:47	5:17:35	25					Orb 91 SS 17:35
91	5:17:36	5:17:39				2	maneuver	time 3/4
91/92	5:17:40	5:18:04			13			slewing
			19					This is the end of the data; sprocket holes black
								sunrise/sunset from planned timeline, not as flown

5/6/86

APPENDIX L

EKTRON Final Report

Reproduced in its entirety.

EKTRON
APPLIED IMAGING
A Kodak Company
23 Crosby Drive, Bedford, Massachusetts 01730 • (617) 275-0475

PACS IMAGE PROCESSING
FINAL REPORT

Contract No. Subcontract PC060

EAI/2533901

November 18, 1986

TABLE OF CONTENTS

Section	Title	Page
1.0	**INTRODUCTION**	1-1
2.0	**TECHNICAL BACKGROUND**	2-1
3.0	**WORK PERFORMED**	3-1
	3.1 Histogram Manipulations	3-1
	3.2 Edge Methods	3-2
	3.3 Local Contrast Segmentation Operators	3-3
	3.4 Zonal Filtering	3-4
4.0	**RESULTS**	4-1
	4.1 Evaluation Criteria	4-1
	4.2 Evaluation Results	4-2
5.0	**CONCLUSIONS AND RECOMMENDATIONS**	5-1
	APPENDIX A	A-1

LIST OF FIGURES

Figure	Title	Page
4-1	Original Images	4-4
4-2	Histogram Equalized Images	4-4
4-3	Zonal Filtered Images	4-5
4-4	Roberts Edge Operator	4-5
4-5	Sobel Edge Operator	4-6
4-6	Local Contrast	4-6
4-7(a)	MET 0:14:21 Original	4-7
4-7(b)	MET 0:14:21 Histogram Equalized	4-7
4-8(a)	MET 0:17:31 Original	4-8
4-8(b)	MET 0:17:31 Histogram Equalized	4-8
4-9(a)	MET 0:21:51 Original	4-9
4-9(b)	MET 0:21:51 Histogram Equalized	4-9
4-10(a)	MET 0:22:47 Original	4-10
4-10(b)	MET 0:22:47 Histogram Equalized	4-10
4-11(a)	MET 1:05:50 Original	4-11
4-11(b)	MET 1:05:50 Histogram Equalized	4-11
4-12(a)	MET 1:10:18 Original	4-12
4-12(b)	MET 1:10:18 Histogram Equalized	4-12
4-13(a)	MET 1:22:27 Original	4-13
4-13(b)	MET 1:22:27 Histogram Equalized	4-13
4-14(a)	MET 1:23:07 Original	4-14
4-14(b)	MET 1:23:07 Histogram Equalized	4-14

LIST OF FIGURES (Cont.)

Figure	Title		Page
4-15(a)	MET 2:02:18	Original	4-15
4-15(b)	MET 2:02:18	Histogram Equalized	4-15
4-16(a)	MET 2:06:04	Original	4-16
4-16(b)	MET 2:06:04	Histogram Equalized	4-16
4-17(a)	MET 2:06:42	Original	4-17
4-17(b)	MET 2:06:42	Histogram Equalized	4-17
4-18(a)	MET 2:06:44	Original	4-18
4-18(b)	MET 2:06:44	Histogram Equalized	4-18
4-19(a)	MET 2:23:21	Original	4-19
4-19(b)	MET 2:23:21	Histogram Equalized	4-19
4-20(a)	MET 1:22:27	Compare to Figures 4-13 (a)&(b) Some Improvement in Detail . . .	4-20
4-20(b)	MET 1:22:27	Compare to Figures 4-13 (a)&(b) Note Gain in Detail	4-20
4-20(c)	MET 1:22:27	Compare to Figures 4-13 (a)&(b) No Real Improvement	4-21
4-20(d)	MET 1:22:27	Compare to Figures 4-13 (a)&(b) No Real Improvement	4-21

LIST OF TABLES

Table	Title	Page
A-1	Nominal Error Budget	A-2
A-2	Particle Position Error Estimate (1 sigma, each axis) in Shuttle Coordinate System	A-3

1.0 INTRODUCTION

EKTRON was contracted by PSI of Andover to perform image analysis on film data returned by the PACS system. This included development of an analytical model and error budget analysis for stereoscopic data reduction. Following the failure of one of the cameras, EKTRON was tasked with extracting as much information as possible out of the film that was returned; in particular, image enhancement techniques were to be explored which would either bring out faint particle tracks or give a better understanding of the behavior of the camera system.

2.0 TECHNICAL BACKGROUND

The original PACS experiment was to examine the contamination background of the Shuttle bay by gathering stereoscopic imagery with a fixed acquisition schedule. Every two minutes a series of four frames was to have been exposed, with the members of the series to have varying exposure times or illumination conditions.

The camera systems used 16mm film (KODAK Pan Film 2484 (ESTAR-AH Base)). The camera focus was set at 70 feet in order to optimize the viewing of small particles.

Before the flight of Shuttle Columbia, EKTRON developed a plan to reduce the data that was to be returned by the PACS. The plan included development of an imaging model for the stereoscopic system that would allow determination of size, distance, and velocity of particles that appeared on conjugate frames. A software processing plan was created, and many of the necessary modules were implemented prior to the flight. An error budget was also prepared and presented (refer to *Appendix A*).

After the flight of the Shuttle Columbia and the failure of one of the camera systems, a re-evaluation of the program plan was called for. It was decided that EKTRON would process copies of the original film and attempt the following:

- enhance the images to bring out faint tracks or small particles
- examine tracks in greater detail to get a cross-sectional view of their structure
- attempt to use the blur circle to get an approximation to range and/or size.

3.0 WORK PERFORMED

With the above plan in mind, EKTRON digitized several frames at two resolutions and used them as a testbed for algorithmic evaluation. The frames were chosen subjectively: one showed a mixture of types of particle tracks (wide, thin, long, short, etc.), one included a view of Florida, and another included Comet Halley. Resolution was either at 512 x 512 or 1024 x 1024 pixels per frame (i.e., 32 or 16 microns per pixel).

Several families of algorithms were examined for image enhancement. They included:

Histogram Manipulations (including Equalization)

Edge Operators (including Roberts, Sobel, and Laplace types)

Local Contrast Segmenters

"Zonal" Filtering.

All the operations modify the data, and they will all be described more fully below.

3.1 Histogram Manipulations

The histogram of an image is the graph of gray level versus the occurrence frequency of gray level. Whereas an image might have a nominal dynamic range of 8 bits (256 gray levels), in practice very few of those levels are widely populated, so that only 4 or 5 bits of dynamic range are actually used.

More to the point, the gray levels that are used are usually clustered together or in a few clusters; meaningful patterns are masked by the eye's inability to distinguish similar gray scale values.

Linear histogram manipulation methods simply rescale the data so that the small differences within a cluster appear larger. If there is more than one cluster in the histogram, the permissible scale factor might be small. It is, therefore, usually better to use nonlinear transformations. Among the many possibilities, two stand out. One is the use of a logarithmic transform; this has the effect of giving a very good separation to dark values while compressing bright values. The other is histogram equalization. In this method, gray values are reassigned so as to make the histogram as flat as possible. This is especially useful in the case of a histogram with several narrow clusters, because each cluster is stretched out.

3.2 Edge Methods

One of the ways of distinguishing objects within an image is to form an edge image; this should effectively encircle each individual object by its boundary. Once that is done, there are several ways to approach segmenting the image into the distinct objects.

There are perhaps as many edge operators as there are researchers in image processing, all with advantages in certain particular cases. Several of the more generally useful variety were examined: the Roberts Edge Operator, the Sobel Edge Operator, and the Laplace Edge Operator. For various reasons, they were all found wanting.

In order to discuss the different operators, fix a digital image as an array of integer values $P(j,i)$, where $1 < j < \#$ rows and $1 < i < \#$ columns.

The Roberts Edge Operator replaces each pixel P(j,i) by the value:

$$R(j,i) = abs(P(j+1,i+1)-P(j,i))+abs(P(j+1,i)-P(j,i+1))$$

The Sobel Edge Operator looks similar:

$$S(j,i) = sqrt(DV^2 + DH^2),$$

$$DV = P(j-1,i-1)-P(j-1,i+1) + P(j+1,i-1)-P(j+1,i+1) + 2*(P(j,i-1)-P(j,i+1))$$

$$DH = P(j-1,i-1)-P(j+1,i-1) + P(j-1,i+1)-P(j+1,i+1) + 2*(p(j-1,i)-P(j+1,i))$$

The Laplace Edge Operator is actually a family of operators, L_n, where n > 0 is an integer. L_n is a 3n x 3n matrix formed from the fundamental matrix:

$$L_1 = \begin{matrix} 0 & -1 & 0 \\ -1 & 4 & -1 \\ 0 & -1 & 0 \end{matrix}$$

For n > 1, each element is replaced by an n x n constant matrix with the same value.

There are also edge operators designed specifically for horizontal and vertical edges, but those are not of particular interest for the imagery in hand; in fact it can be seen from its definition that the Sobel operator essentially incorporates them into a unified measure.

3.3 Local Contrast Segmentation Operators

In many sorts of images there are no good edges as such, but there are clear regions distinguished by their texture.

Local contrast operators segment the image by assigning local texture measures for each point; regions of similar texture are then transformed into regions of roughly constant value.

There are probably as many local contrast measures as there are edge measures. They all have a free parameter (the window size); proper choice of a window size is somewhat ad hoc, but is normally related to the size of expected features. Once a window size has been chosen, some of the simpler measures are local average (smoothing) and local variance. A whole other class are the rank operators: each point is replaced by that pixel value which has a certain rank in the histogram of the window centered at the point. Examples of rank which are frequently used are the median, the maximum, and the minimum.

Another measure that frequently is useful is the following:

T(i,j) = (max(window)-min(window)) / (max(window)+min(window))

Notice that in regions of constant (or nearly so) grayscale the measure T is very close to 0, while in regions with a wide disparity of grayscales, the measure is close to 1.

3.4 Zonal Filtering

An interesting class of operators are the "zonal" filters; more precisely they are formed from the short space spectral transform. Essentially, a window is dragged across an image; the data within the window is scaled, tapered, and Fourier transformed. The transform is then filtered. The result is inverse Fourier transformed, given a fixed DC value, and added to an output matrix.

The filters that can be applied to the spectral data range from linear bandpass to nonlinear enhancements. A simple example of such enhancement is to multiply each spectral component by its magnitude, and then to scale so as to keep the maximum amplitude unchanged.

There are several parameters in the zonal filter, among them the window size, the amount of overlap in consecutive windows, the amount of scaling prior to tapering, and the degree of spectral filtering.

4.0 RESULTS

As a result of the processing, it was determined that the most useful approaches were, respectively, Histogram Manipulations (especially equalization) and Zonal Filtering. The reasons can be explained as follows:

- the imagery is typically low-contrast, with a nonuniform background, and with most objects of interest being slightly out of focus
- traditional convolution-type edge operators like Sobel, Laplace, and Roberts do not perform well on objects with blurred edges; furthermore the nonuniform background tends to further confuse the edge image that results
- local contrast methods have a great deal of difficulty dealing with images of low contrast (the contrast variations that would be used to segment the image just aren't there)
- by contrast, histogram manipulations (especially equalization) are designed to maximize the spread of the useful data into a full data range; thus, if the data is restricted to several narrow bands, then the result of manipulating the histogram will be to spread each band, improving viewability
- zonal filtering, by its very nature, does not care overly much about local background variations (it removes them, in fact), and it can be tuned to deal with low contrast. Similarly, it can be tuned to sharpen an image as well.

One of the immediate results from the processing is that there are many more particles captured by the film than meet the unaided eye. A second result is that particle tracks are wider than they first appear.

4.1 Evaluation Criteria

The evaluation of different enhancement methods can be approached in two ways: from the point of view of a human

observer, and from the point of view of automatic interpretation. It was decided that all methods tested would be evaluated on the basis of the former; there was no effort made to automatically extract data of interest.

Given that the methods would be judged on how they improve a human operator's understanding of what is in the image, the methods were then judged further on:

- were previously faint objects made brighter or more distinguishable from the background
- was internal structure made more apparent
- was background noise suppressed.

4.2 Evaluation Results

A preliminary set of frames were digitized and processed by several of the above methods (refer to Figures 4-1 thru 4-6). From these, it was determined that the edge and local contrast methods did not do well. A list of test frames was acquired from PSI; of this list 14 frames were digitized and processed (refer to Figures 4-7 thru 4-14).

The logarithmic transformation does a very good job of improving viewability of bright objects in a bright field (on the film, of dark objects in a dark field). In fact, some particles can be detected in seemingly empty regions.

Histogram equalization does a better job of bringing out faint tracks. The blur circles for stars and the width of tracks is similarly improved. However, viewability of internal structure is not improved, and in some cases is reduced.

Zonal filtering also showed promise for detecting faint tracks. In addition, because there tend to be artifacts in the filtered image due to ringing, the potential for automatic processing at a later date is enhanced.

Figure 4-1 Original Images

Figure 4-2 Histogram Equalized Images

Figure 4-3 Zonal Filtered Images

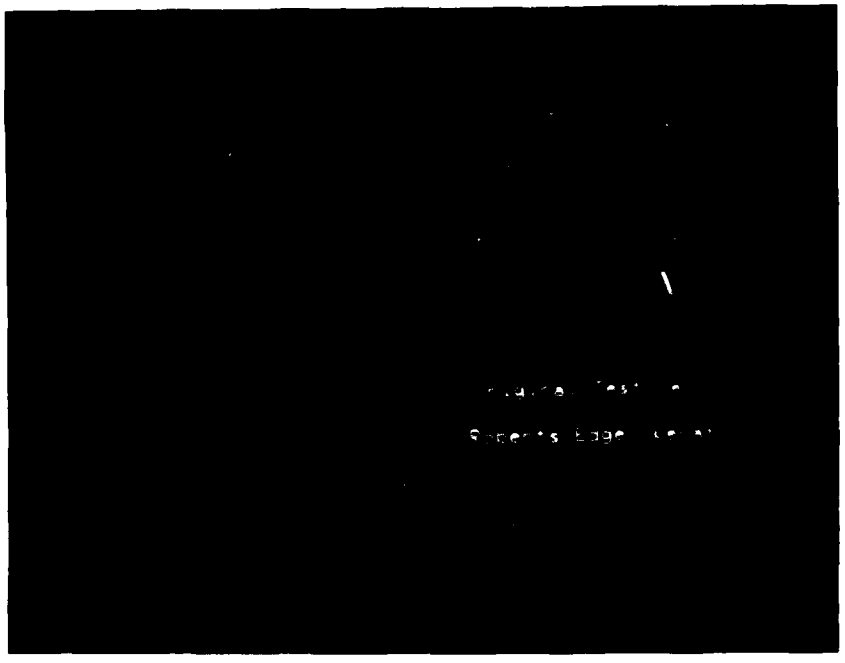

Figure 4-4 Roberts Edge Operator

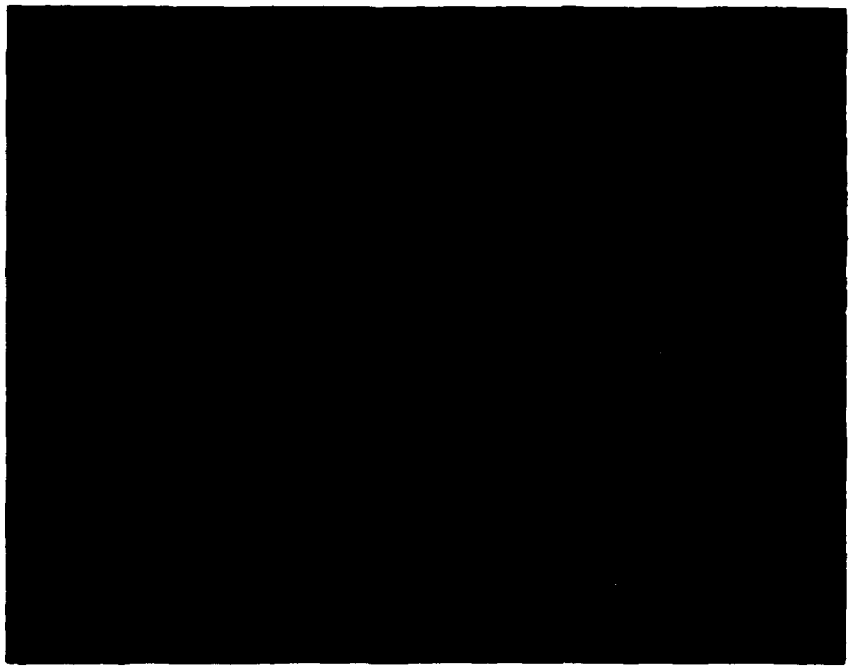

Figure 4-5 Sobel Edge Operator

Figure 4-6 Local Contrast

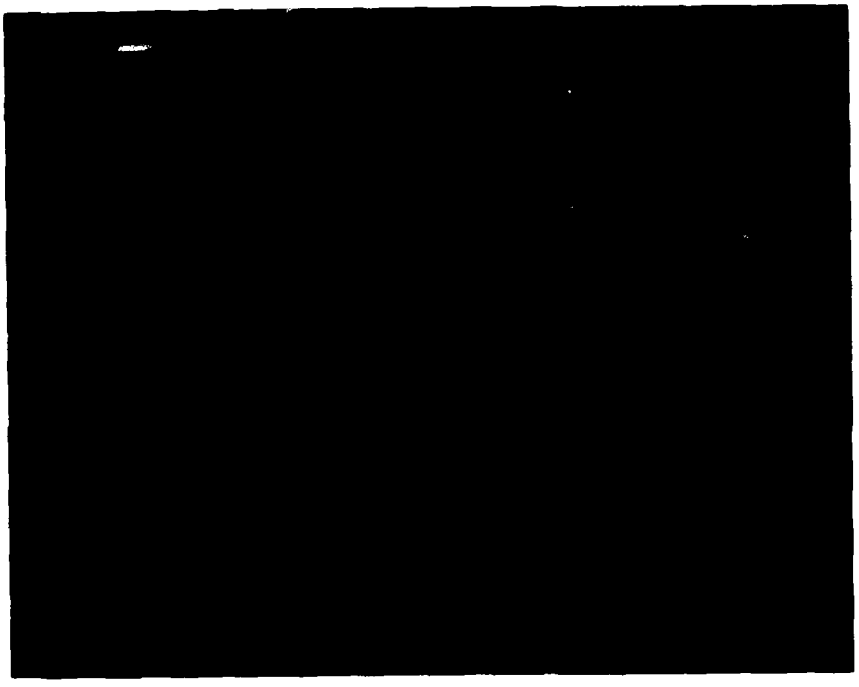

Figure 4-7(a) MET 0:14:21 Original

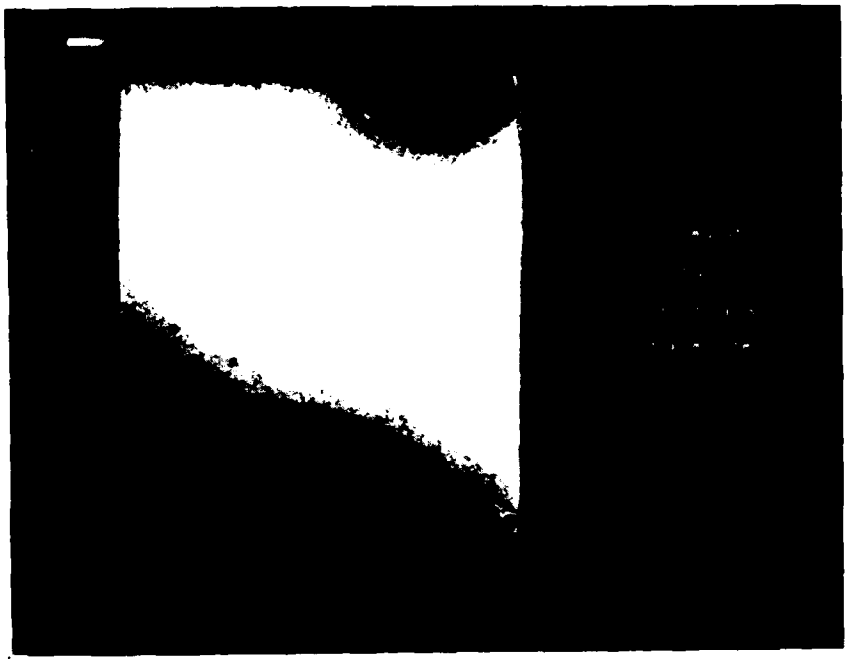

Figure 4-7(b) MET 0:14:21 Histogram Equalized

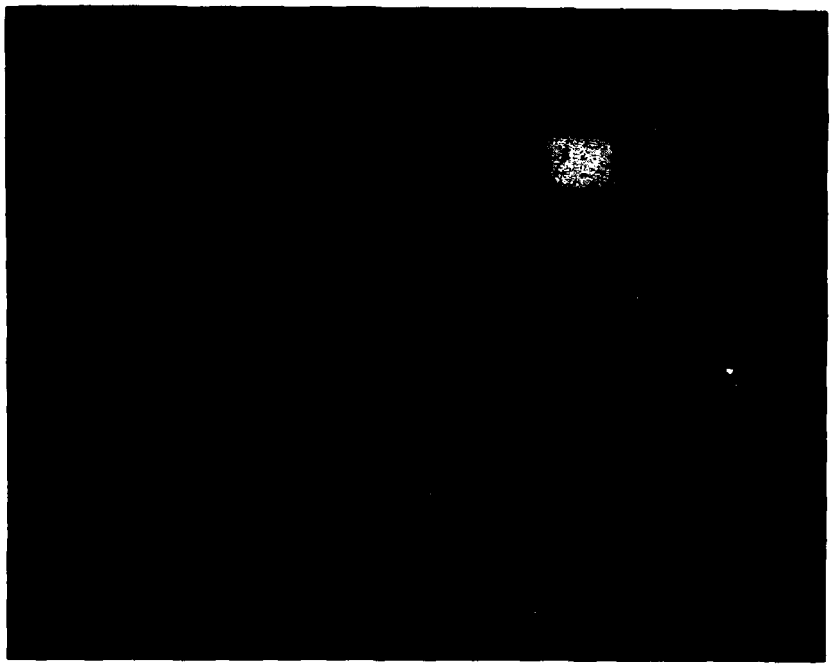

Figure 4-8(a) MET 0:17:31 Original

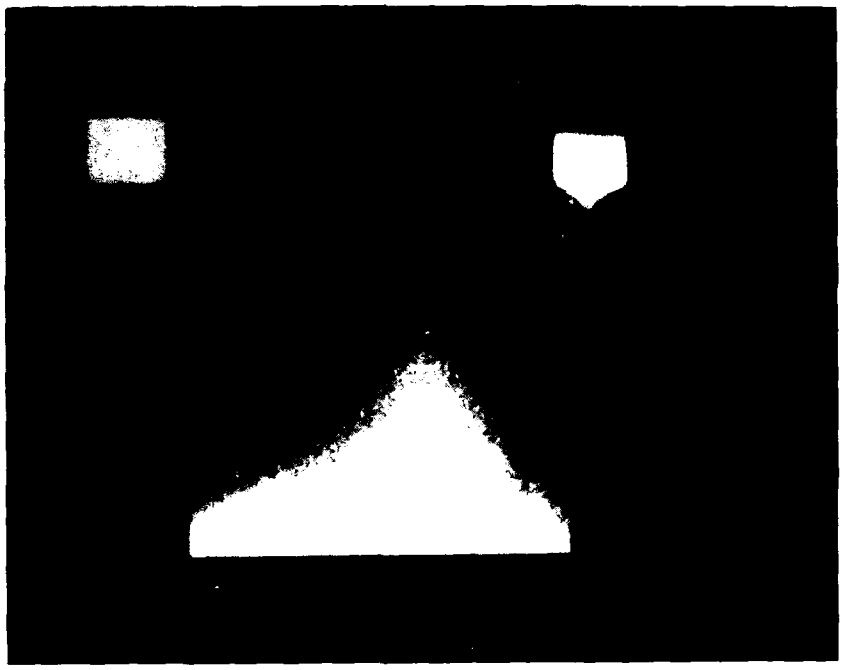

Figure 4-8(b) MET 0:17:31 Histogram Equalized

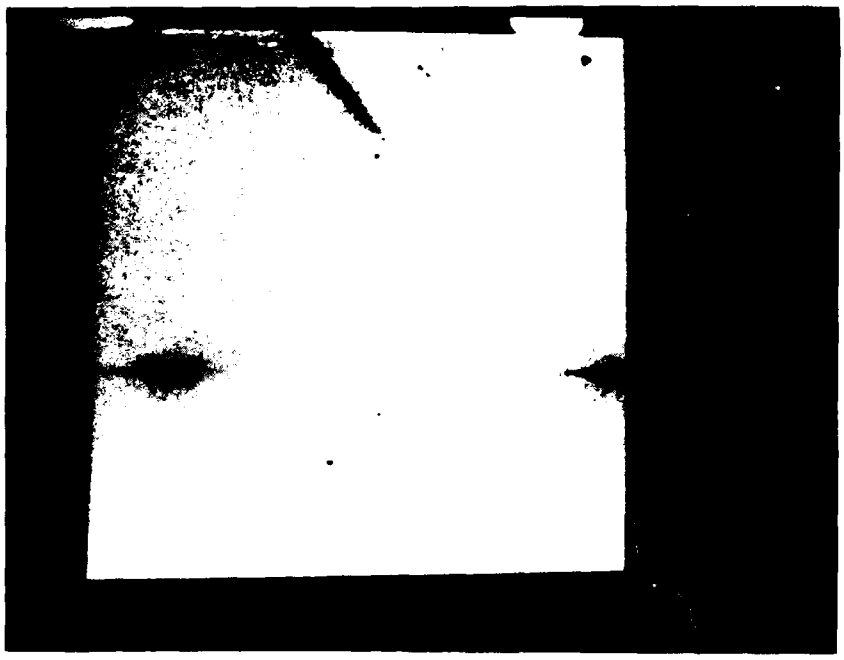

Figure 4-9(a) MET 0:21:51 Original

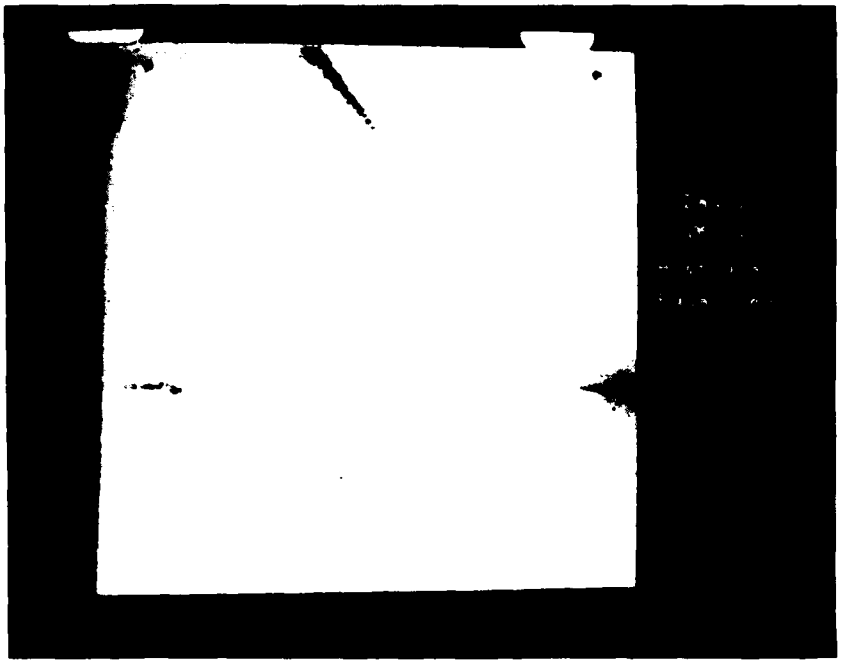

Figure 4-9(b) MET 0:21:51 Histogram Equalized

Figure 4-10(a) MET 0:22:47 Original

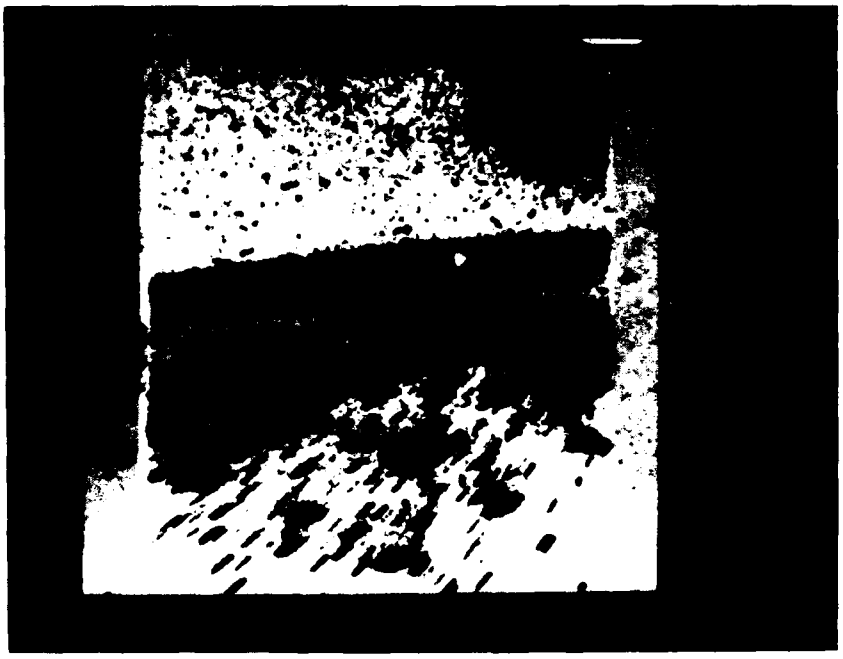

Figure 4-10(b) MET 0:22:47 Histogram Equalized

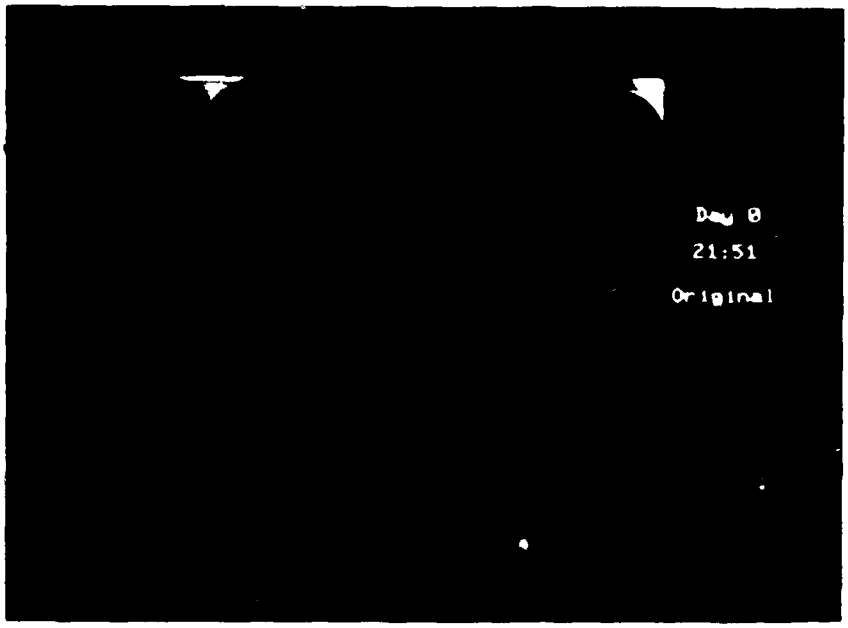

Figure 4-11(a) MET 1:05:50 Original

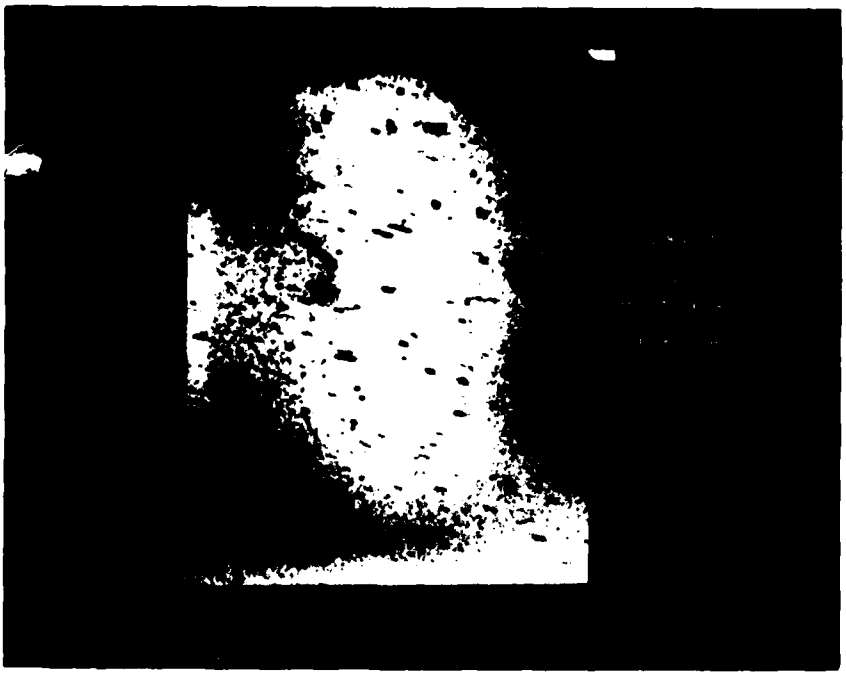

Figure 4-11(b) MET 1:05:50 Histogram Equalized

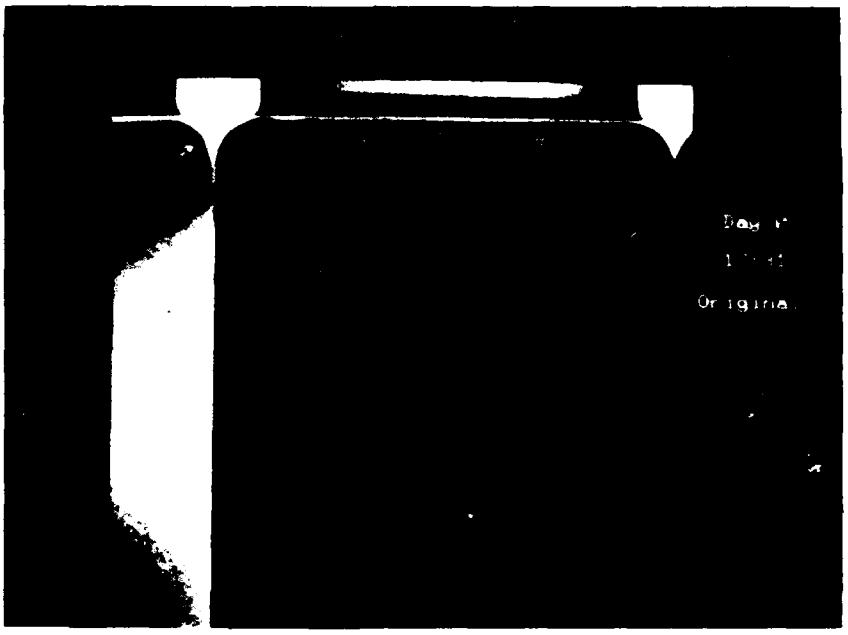

Figure 4-12(a) MET 1:10:18 Original

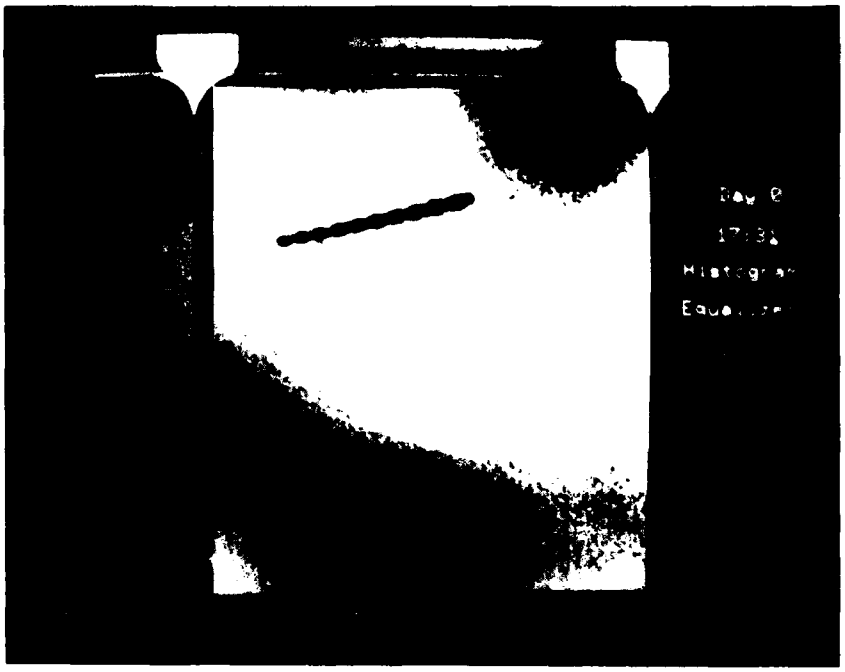

Figure 4-12(b) MET 1:10:18 Histogram Equalized

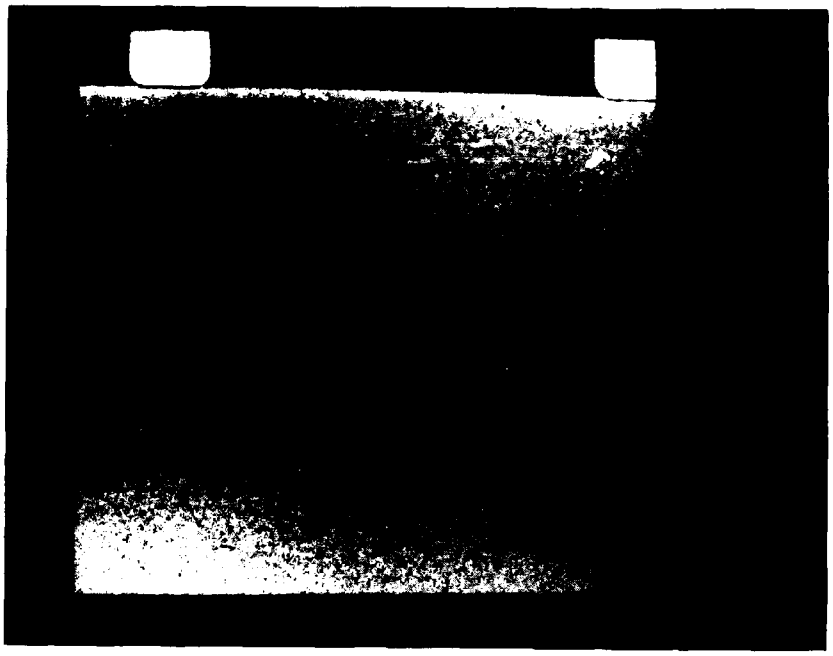

Figure 4-13(a) MET 1:22:27 Original

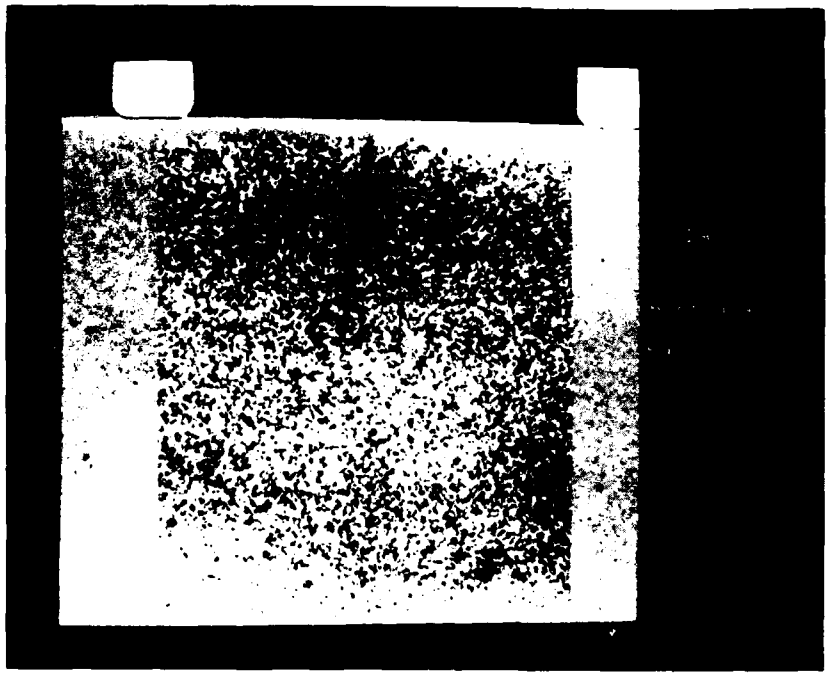

Figure 4-13(b) MET 1:22:27 Histogram Equalized

Figure 4-14(a) MET 1:23:07 Original

Figure 4-14(b) MET 1:23:07 Histogram Equalized

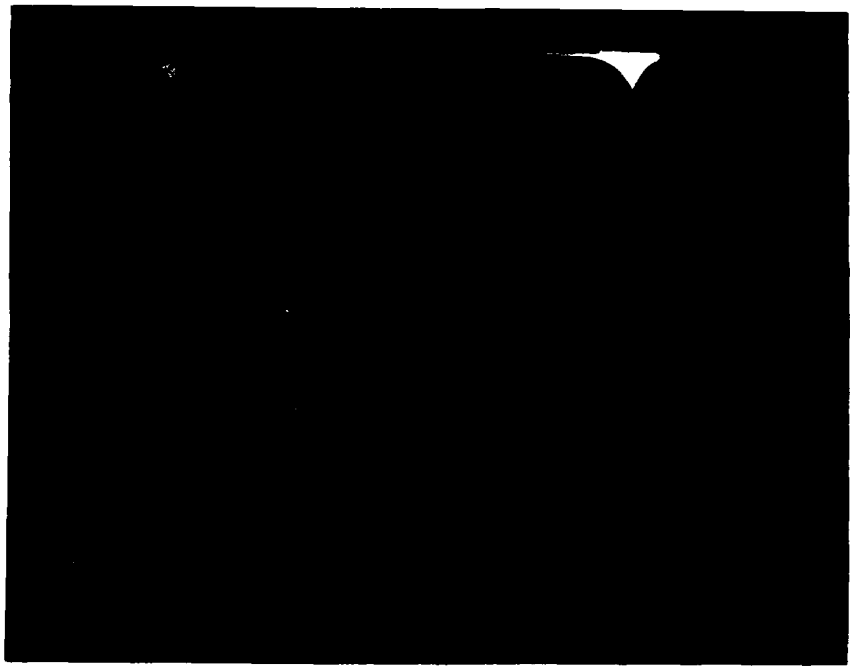

Figure 4-15(a) MET 2:02:18 Original

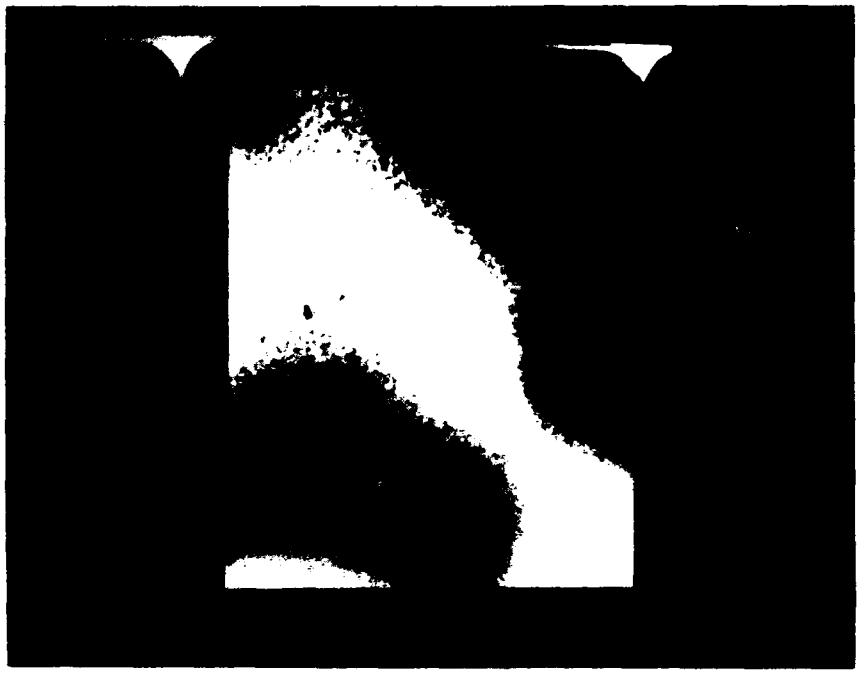

Figure 4-15(b) MET 2:02:18 Histogram Equalized

Figure 4-16(a) MET 2:06:04 Original

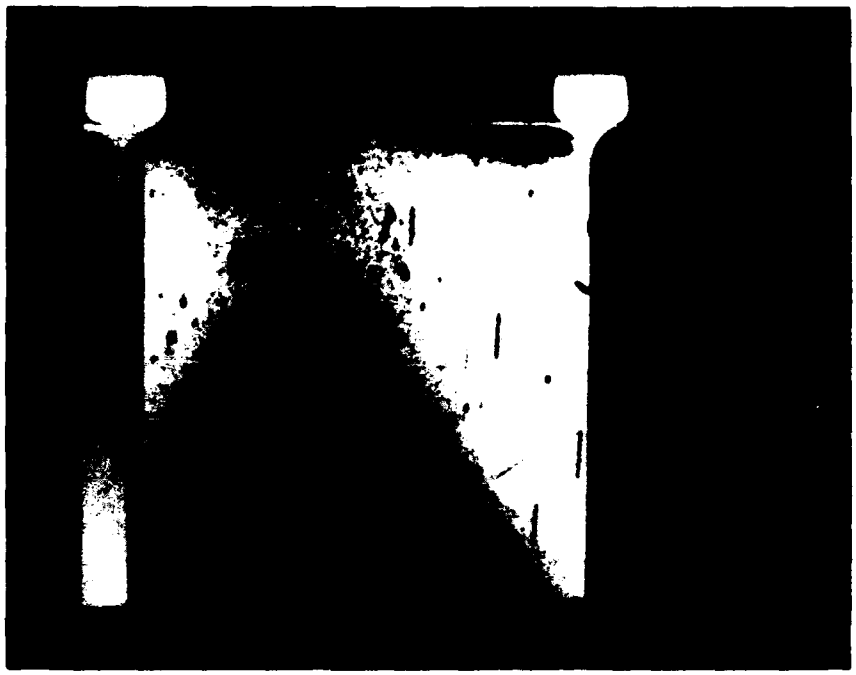

Figure 4-16(b) MET 2:06:04 Histogram Equalized

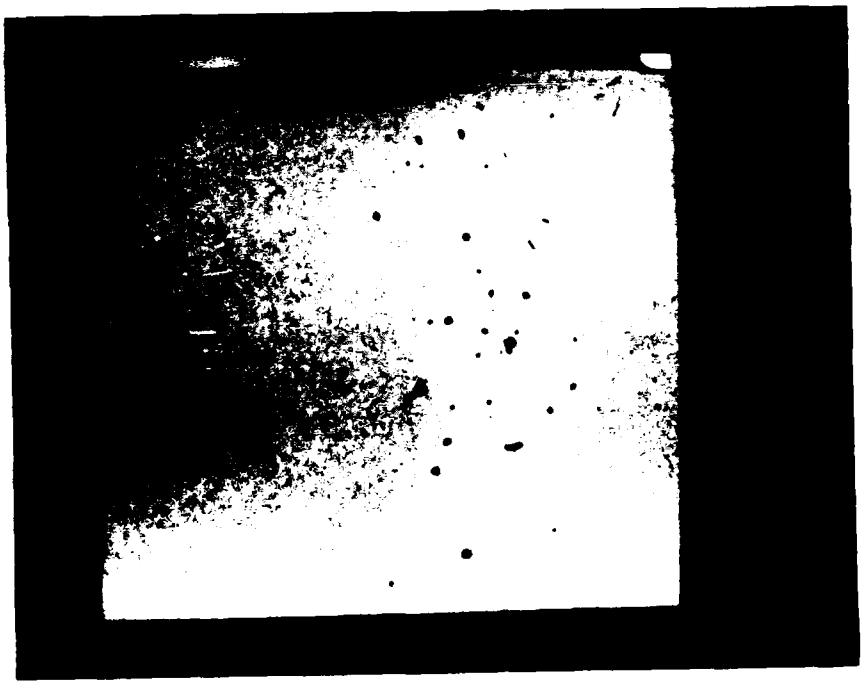

Figure 4-17(a) MET 2:06:42 Original

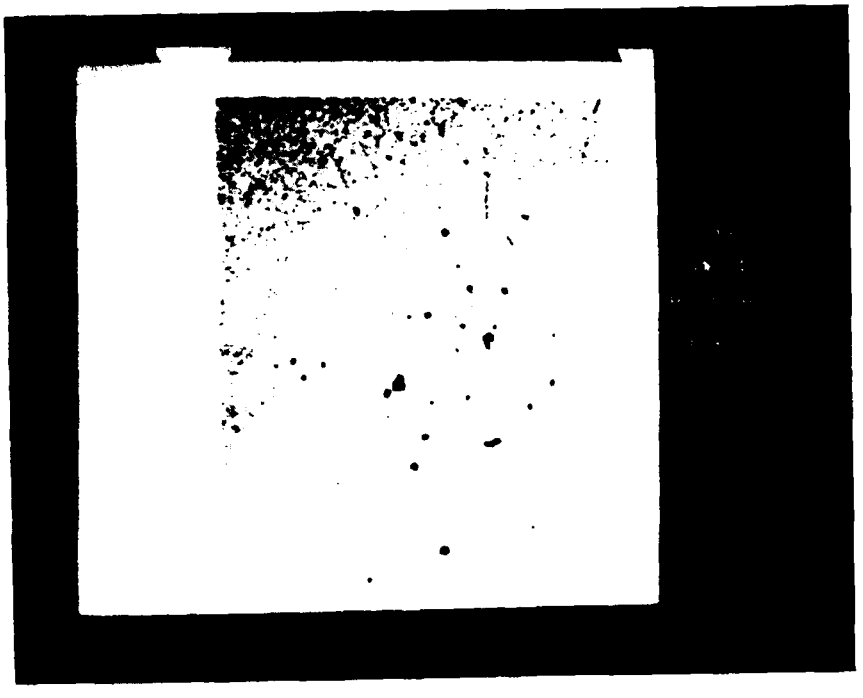

Figure 4-17(b) MET 2:06:42 Histogram Equalized

Figure 4-18(a) MET 2:06:44 Original

Figure 4-18(b) MET 2:06:44 Histogram Equalized

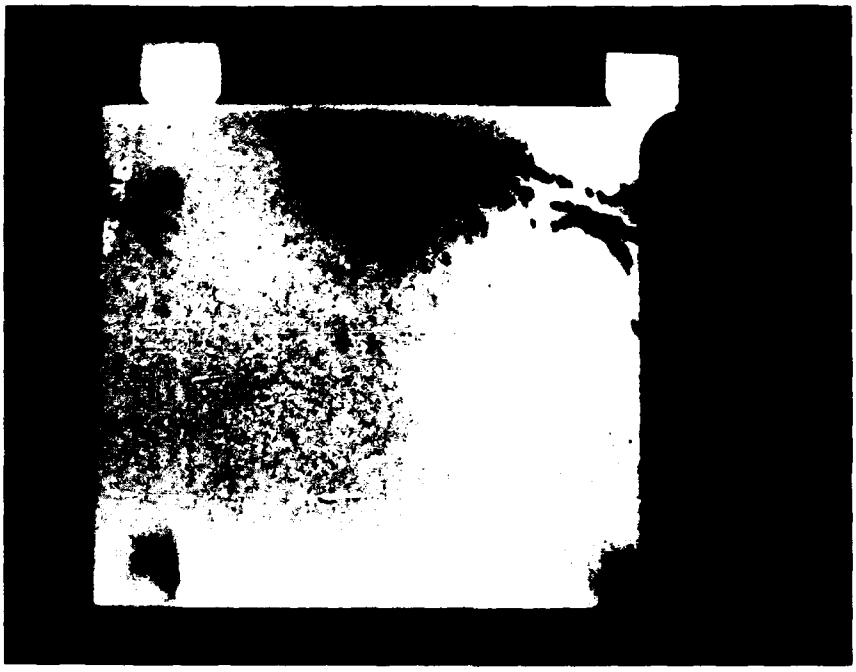

Figure 4-19(a) MET 2:23:21 Original

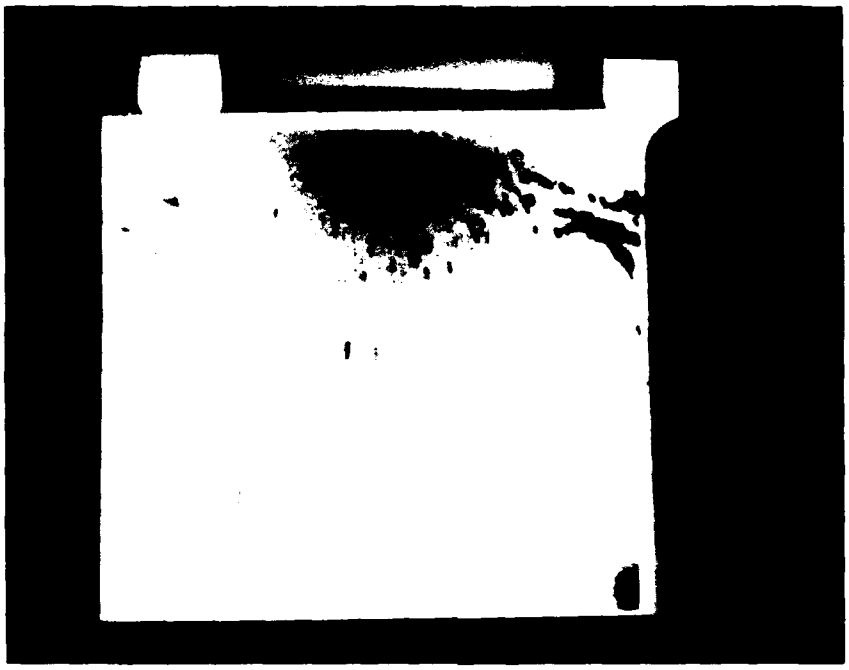

Figure 4-19(b) MET 2:23:21 Histogram Equalized

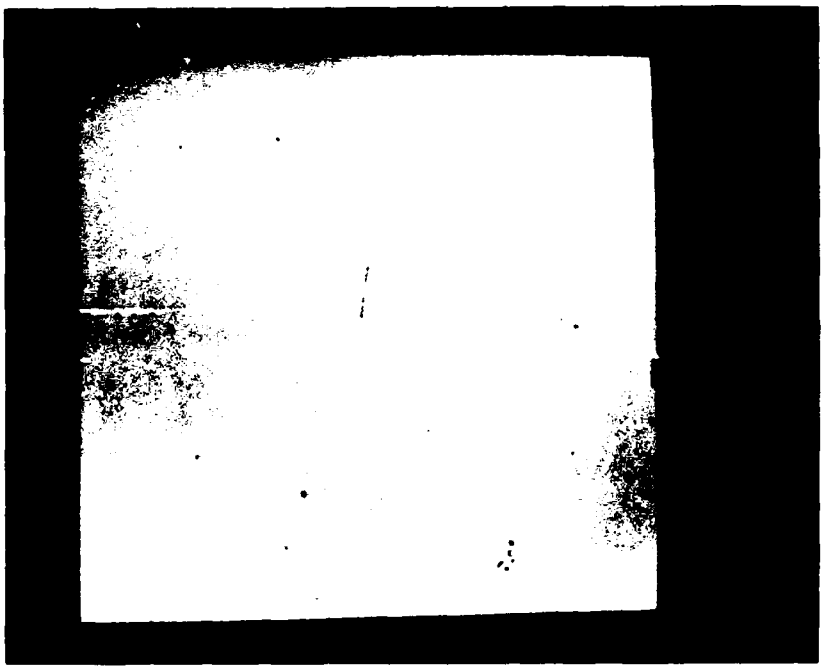

Figure 4-20(a) MET 1:22:27 Compare to Figures 4-13 (a)&(b)
Some Improvement in Detail

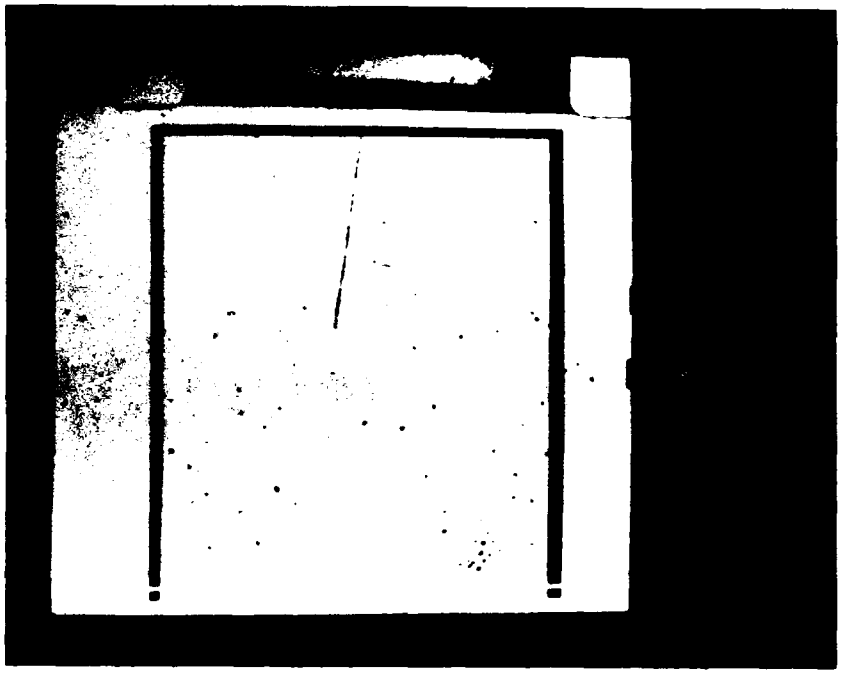

Figure 4-20(b) MET 1:22:27 Compare to Figures 4-13 (a)&(b)
Note Gain in Detail

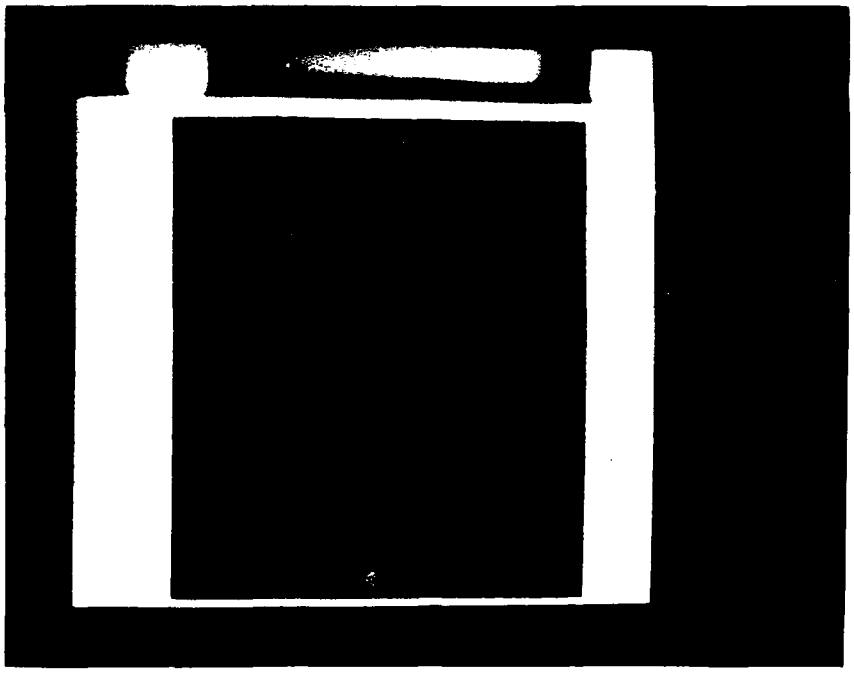

Figure 4-20(c) MET 1:22:27 Compare to Figures 4-13 (a)&(b)
No Real Improvement

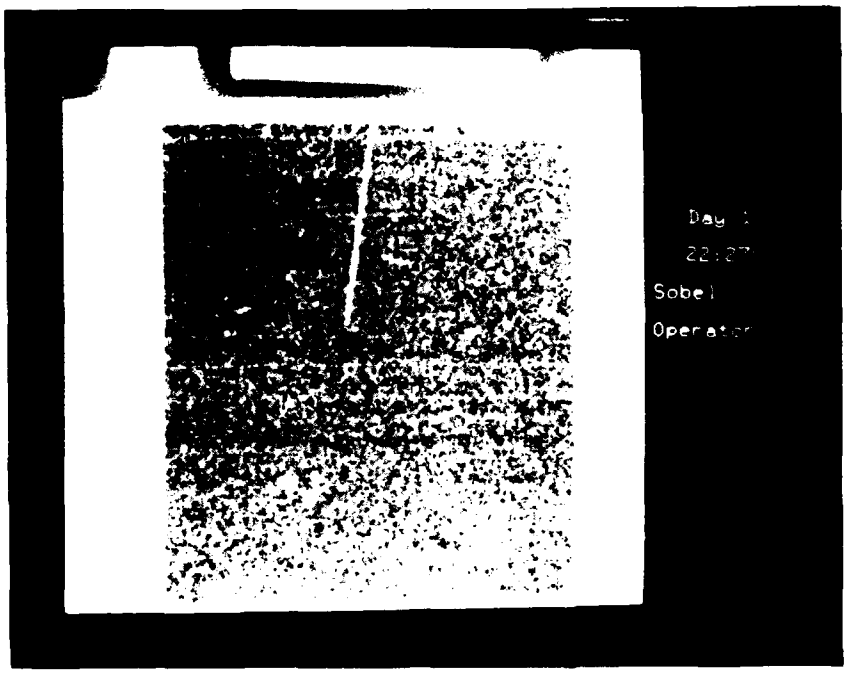

Figure 4-20(d) MET 1:22:27 Compare to Figures 4-13 (a)&(b)
No Real Improvement

5.0 CONCLUSIONS AND RECOMMENDATIONS

The processing performed generally made the imagery easier to interpret. That is good, so long as the purpose of the enhancement is to perform such activities as counting of particles or (with stereoscopic imagery) determining position and velocity. However, the enhancement methods do modify the data, making radiometric evaluation impossible.

On the other hand, film is difficult to use as a radiometer. A film digitizer measures the film transmittance; this transmittance is essentially the exponential of the film density. The relationship between film density and input exposure is given by the D-LogE curve. This is a roughly S-shaped curve, with a broad area which is linear. Putting the equations together, one concludes that there is a power law relationship between input exposure and film transmittance, at least in the region where the D-LogE curve is linear. Moreover, this power law relationship depends critically upon the development protocol.

An alternative is **now** possible that would allow one to use film for what it does best (namely: measurement of numerical density and position/velocity) while gathering radiometric data in a more reliable mode. For radiometric data a solid-state sensor is much more desirable. As an example, there are now solid-state 1024 x 1024 pixel arrays available from both Kodak and Texas Instruments; in fact the Kodak array is available in a digital camera. These arrays have a linear response to exposure and can be calibrated periodically in flight, making them ideal adjuncts to the film system. They can also be used in a staring mode to improve signal detectability. Thus, if one allows such a sensor to gather exposure data over the period that the film system collects geometric data, at the end of the mission one would have two complementary data sets and could make more reliable conclusions about the nature of detected particles.

APPENDIX A

APPENDIX A

The PACS system geometry can be modeled as a standard stereo camera set-up. The errors that can occur can be divided into interior camera orientation errors and exterior camera orientation errors. The interior errors include uncertainty in the focal length, uncertainties in the film plane, and plain measurement errors. The exterior errors include the angular orientation, perspective placement, and location within the shuttle bay. Nominal values for all these error sources are in Table A-1.

The standard camera equations allow one to estimate the induced errors in position due to each of the above errors. These are summarized in Table A-2. Notice that the RMS error in position is about 3.3" for a particle ten feet from the camera.

Velocity errors can be deduced from the positional inaccuracy as follows. For a moving particle, the error circle radius grows linearly with time. By using a worst case approximation, one finds that the magnitude of the velocity variation is about

$$\text{delta } v = (3/\sqrt{2})\ r_0 + (3/4)(r_0{}^2)/|v_0|$$

Using the figure of r_0 = 3.3", and a velocity of about 120"/sec, one gets that delta v = 7"/sec.

Table A-1

Nominal Error Budget

Error Source	**Value, Each Axis**
Interior Orientation	
Focal Length	0.1"
Film Plane Displacement	0.004"
Film Plane Angular Orientation	< 1 Degree
Image Plane to Film Plane	0.002"
Measurement	0.001"
Exterior Orientation, each Camera to Base	
Angular Orientation	0.1 Degree
Perspective Center	0.1"
Base to Shuttle	
Angular Orientation	0.25 Degree
Displacement	0.5"

Table A-2

Particle Position Error Estimate
(1 sigma, each axis)
in Shuttle Coordinate System

Error Source	10 Feet Distant	100 Feet Distant
Interior Orientation		
Focal Length	3"	30"
Film Plane Displacement	0.7"	7"
Film Plane Angle	10^{-4}"	10^{-3}"
Image Plane to Film	0.25"	2.5"
Measurement Error	0.15"	1.5"
Exterior Orientation, Camera to Base		
Angular Orientation	0.3"	3"
Perspective Center	0.3"	3"
Base to Shuttle		
Angular Orientation	0.7"	7"
Displacement	0.7"	7"

APPENDIX M

Briefing to CIRRIS Staff

27 July 1986

Reproduced in its entirety.

PACS

PARTICLE ANALYSIS CAMERAS FOR SHUTTLE

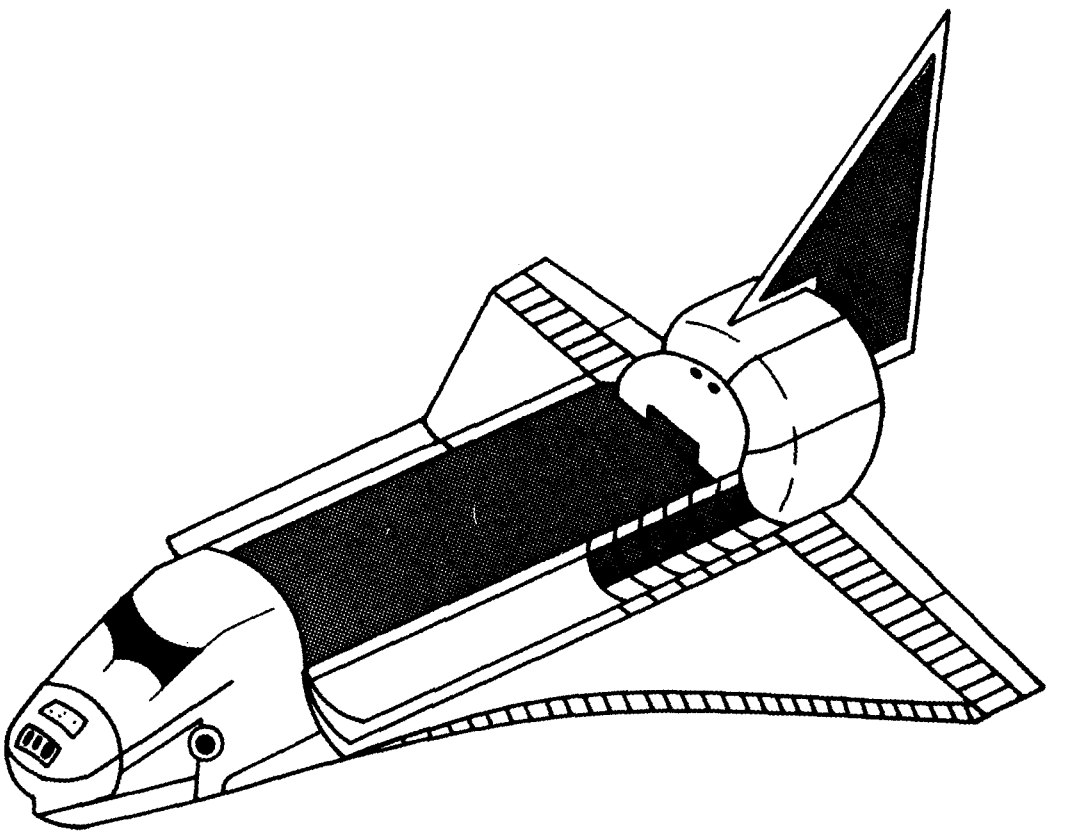

A-7717

OBJECTIVES:

- QUANTIFY PARTICULATE ENVIRONMENT SURROUNDING SHUTTLE THROUGHOUT ORBITAL MISSION
  - STEREO COVERAGE → x, y, z, V_x, V_y, V_z
  - IDENTIFY SOURCES
  - EVENTS - DUMPS/PURGES
    MANEUVERS
    OPERATIONS
- USE STROBE FOR NIGHTTIME OBSERVATIONS
- FAST FILM TO PERMIT SMALL PARTICLE DETECTION

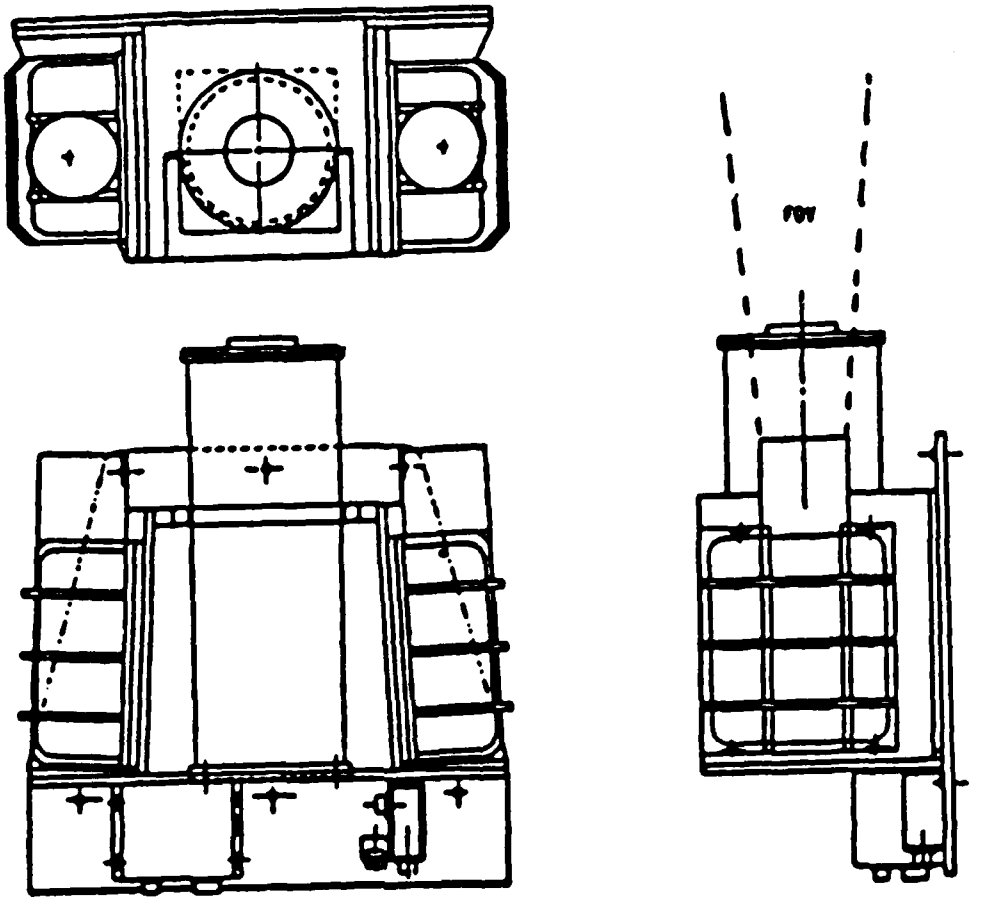

Figure 1. Diagram of PACS Assembly

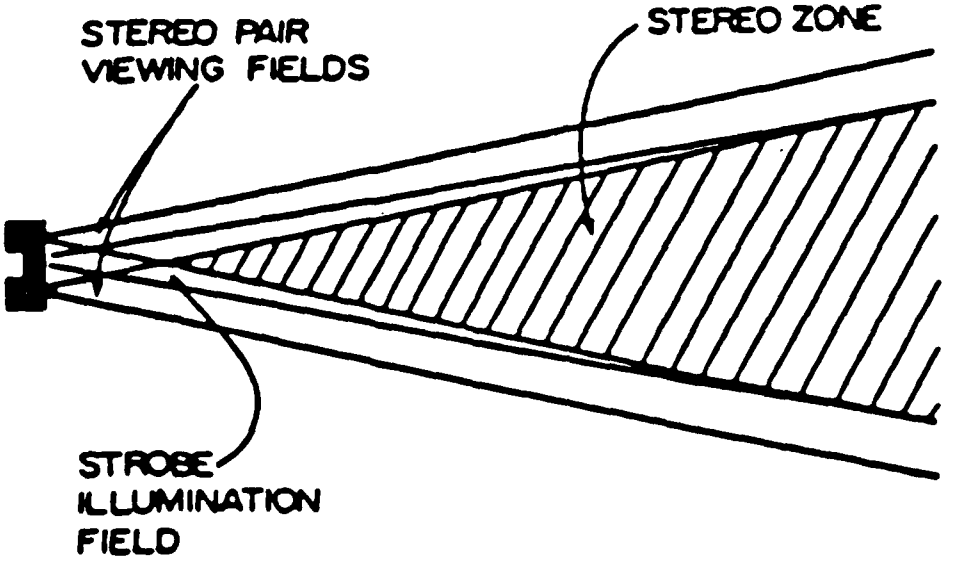

Figure 2. Diagram of PACS Fields of View

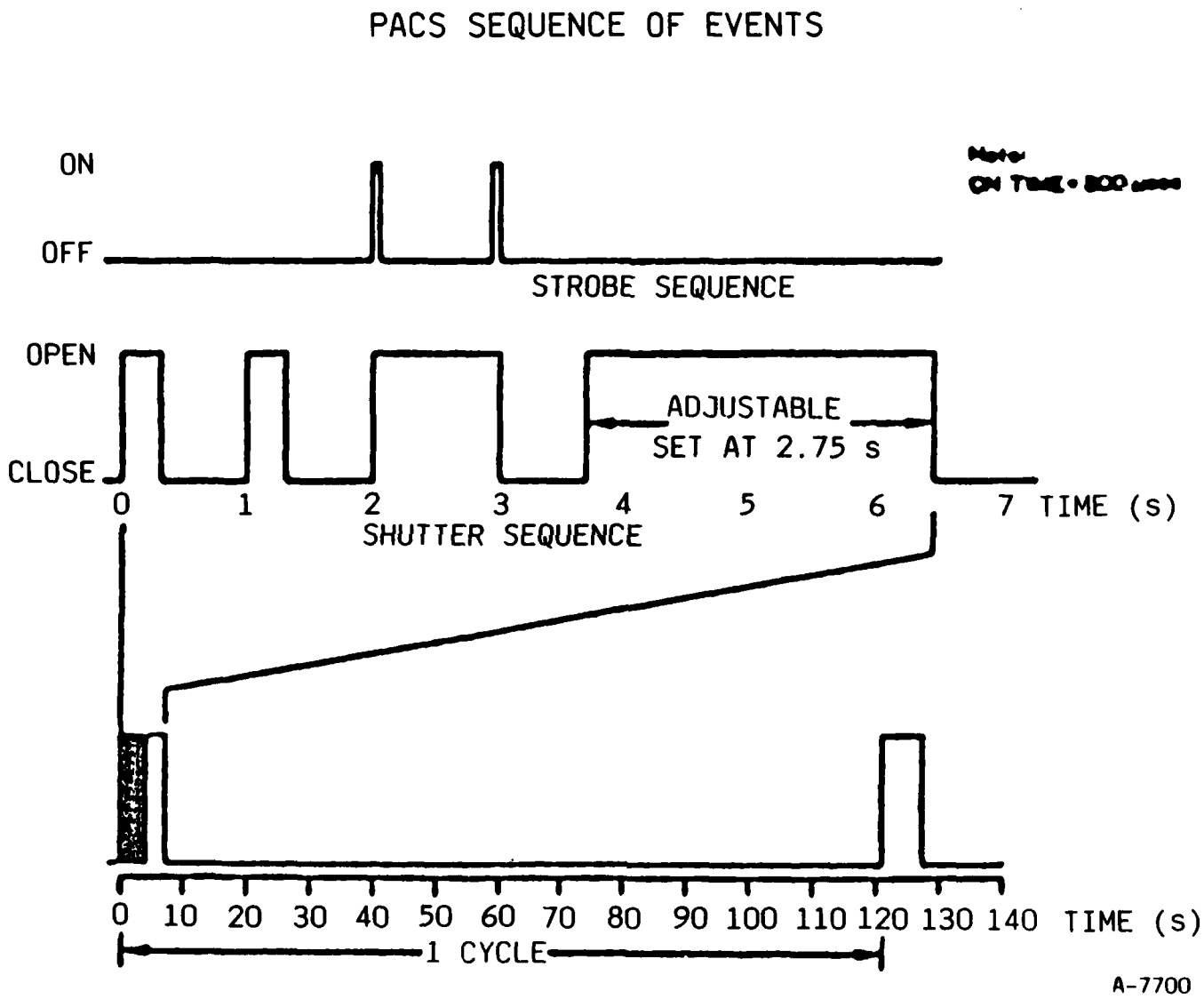

Figure 4. Analog Representation of PACS Sequence

PACS

- PRINCIPAL INVESTIGATOR: M. AHMADJIAN
- PAYLOAD ASSEMBLY: EPSILON (H. MIRANDA)
- PAYLOAD INTEGRATION: USU (D. BUNNELL)
- AT HITCHHIKER POCC: M. AHMADJIAN/D. GREEN
- ANALYSIS: PHK K. YATES, C. PIKE
  LSP M. AHMADJIAN
  PSI D. GREEN, C. WHITE, T. RAWLINS
  EKTRON B. GOLD, B. JUMPER
  H. MIRANDA

FLIGHT HISTORY

- STS-61 (COLUMBIA - FIRST FLIGHT IN 2 YEARS)
- ON PAD FOR 4 WEEKS - HEAVY RAINS
- LAUNCH 6:55 AM EST 12 JAN 1986
- ACHIEVE 290 km CIRCULAR ORBIT, 28° INCLINATION
- PACS ON HITCHHIKER/G PALLET
- PACS TURNED ON AT 0/3:30 MISSION ELAPSED TIME
- FILM JAMMED IN CAMERA 1
- K_u BAND ANTENNA NEAR FOV INCREASE BACKGROUND
- CAMERA 2 OPERATED SUCCESSFULLY THROUGHOUT MISSION
- LAND AT EDWARDS AFB 5:59 AM PST 18 JAN 1986

ORBITAL EVENTS

- LAUNCH RCA TV SATELLITE (12,000 lbs) 0/9:32 MET
- WATER DUMPS (4 SUPPLY, 1 WASTE)
- > 1 ORBIT DEEP SPACE VIEWING ALL DISABLED
- > 1 ORBIT GRAVITY GRADIENT BAY WAKE (CIRRIS 1A CONFIGURATION)
- VARIETY ATTITUDES - PTC, BAKE OUTS, SUN INERTIAL
- PAYLOAD BAY DOOR OPERATIONS LAST NIGHTS

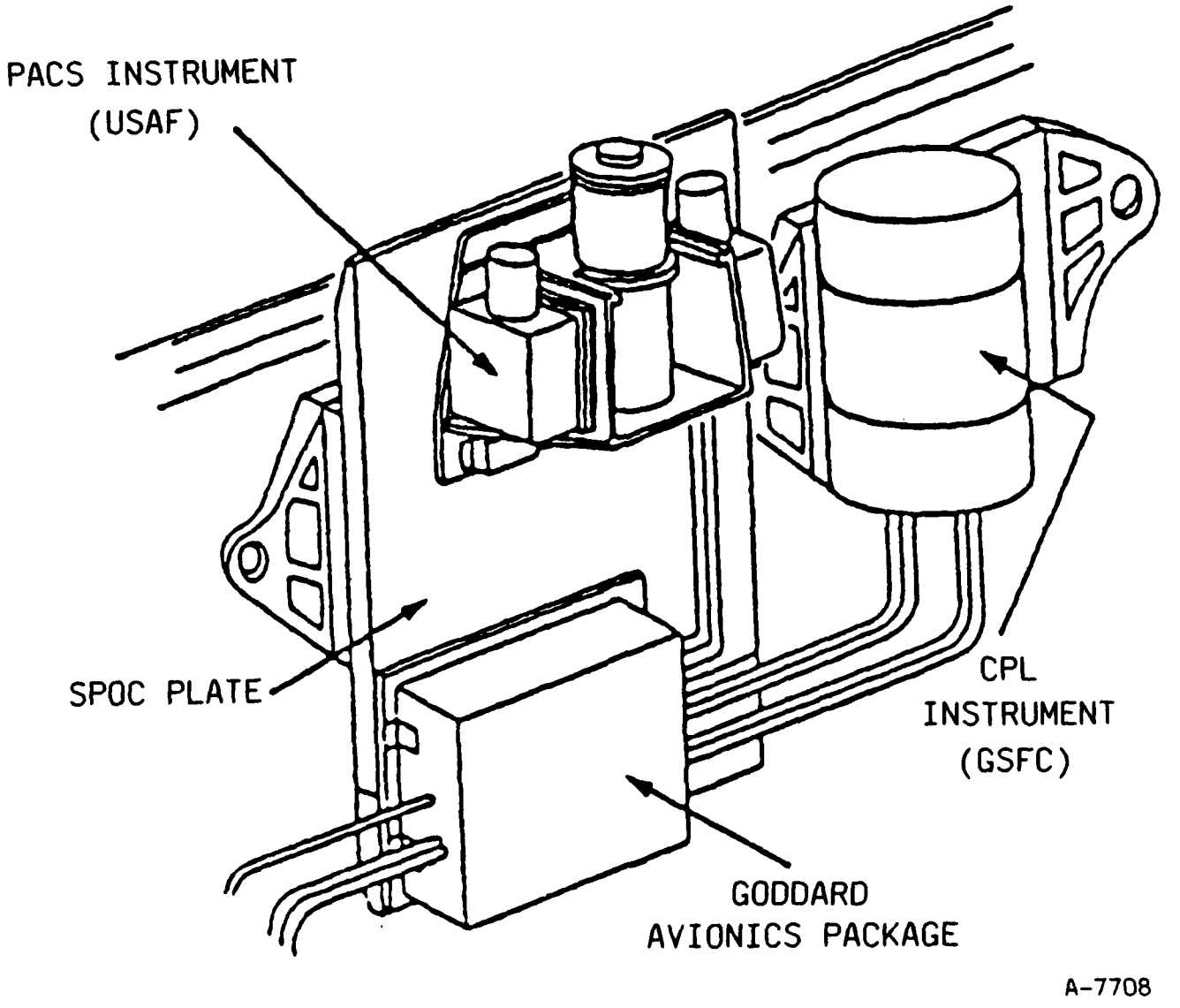

Figure 3. HITCHHIKER G-1 Physical Layout

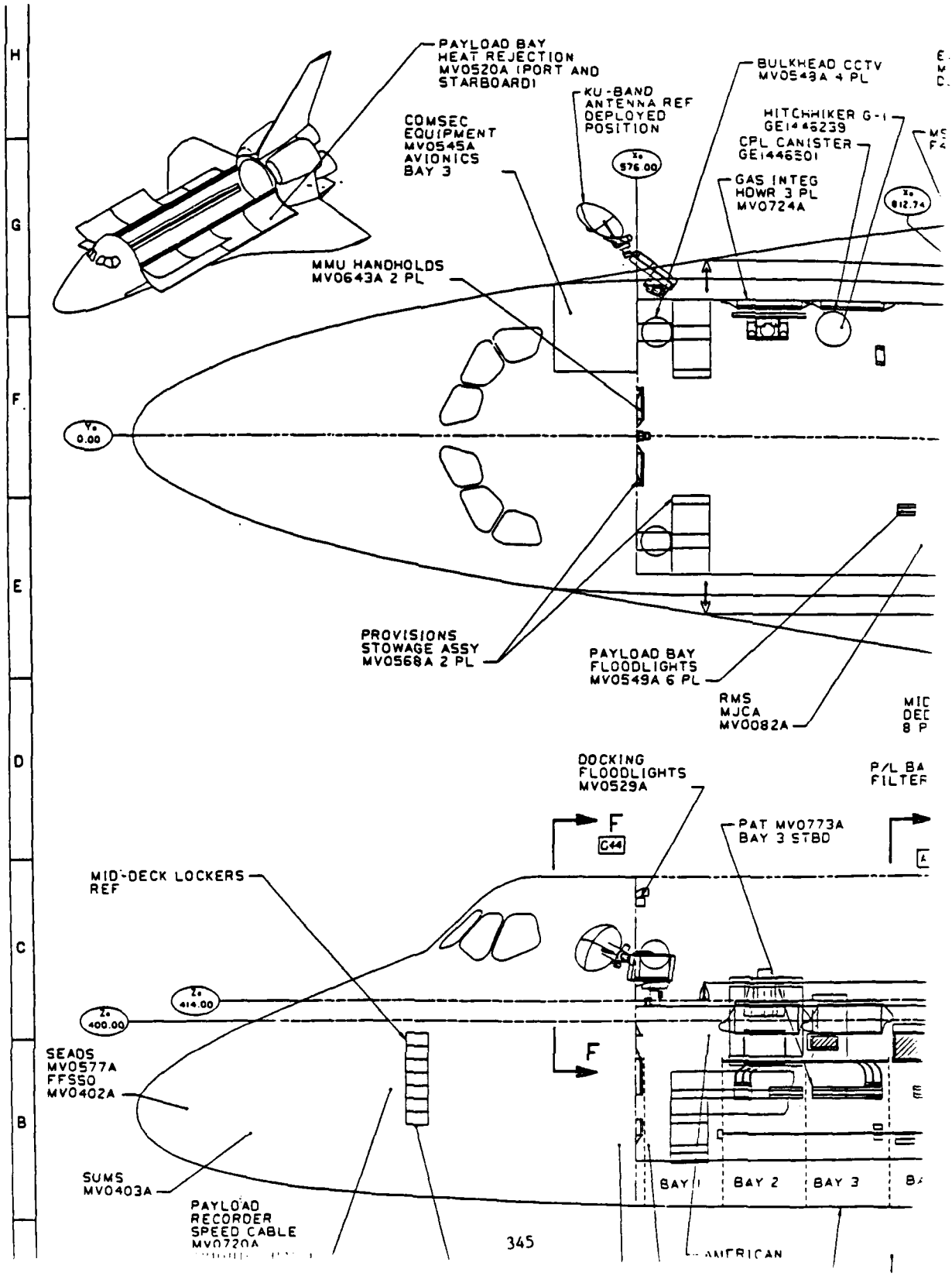
PAYLOAD BAY
HEAT REJECTION
MV0520A (PORT AND
STARBOARD)
KU-BAND
ANTENNA REF
DEPLOYED
POSITION
BULKHEAD CCTV
MV0543A 4 PL
COMSEC
EQUIPMENT
MV0545A
AVIONICS
BAY 3
HITCHHIKER G-1
GE1446239
CPL CANISTER
GE1446501
GAS INTEG
HDWR 3 PL
MV0724A
MMU HANDHOLDS
MV0643A 2 PL
PROVISIONS
STOWAGE ASSY
MV0568A 2 PL
PAYLOAD BAY
FLOODLIGHTS
MV0549A 6 PL
RMS
MJCA
MV0082A
DOCKING
FLOODLIGHTS
MV0529A
PAT MV0773A
BAY 3 STBD
MID-DECK LOCKERS
REF
SEADS
MV0577A
FFSSO
MV0402A
SUMS
MV0403A
PAYLOAD
RECORDER
SPEED CABLE
BAY 1
BAY 2
BAY 3
H
G
F
E
D
C
B

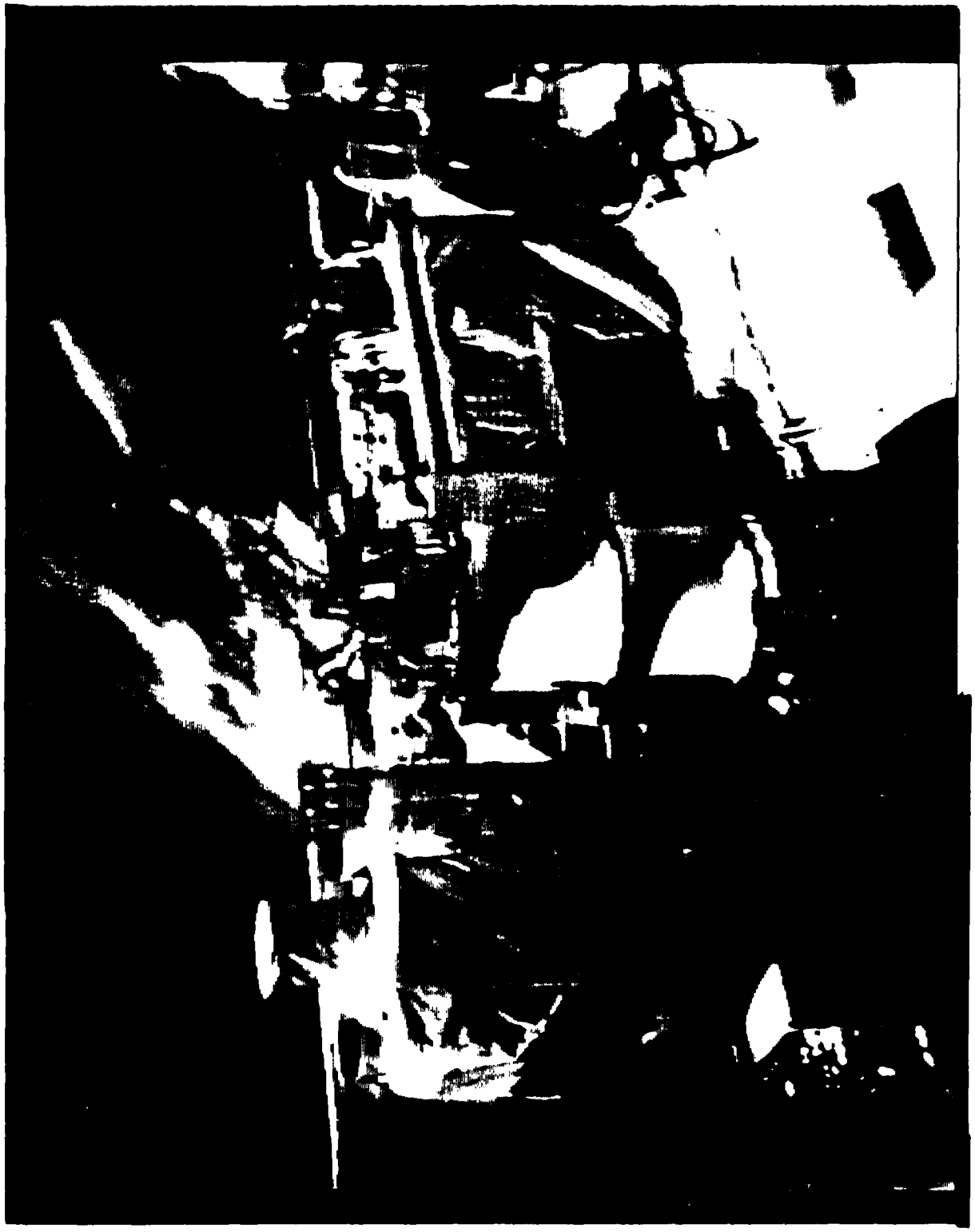

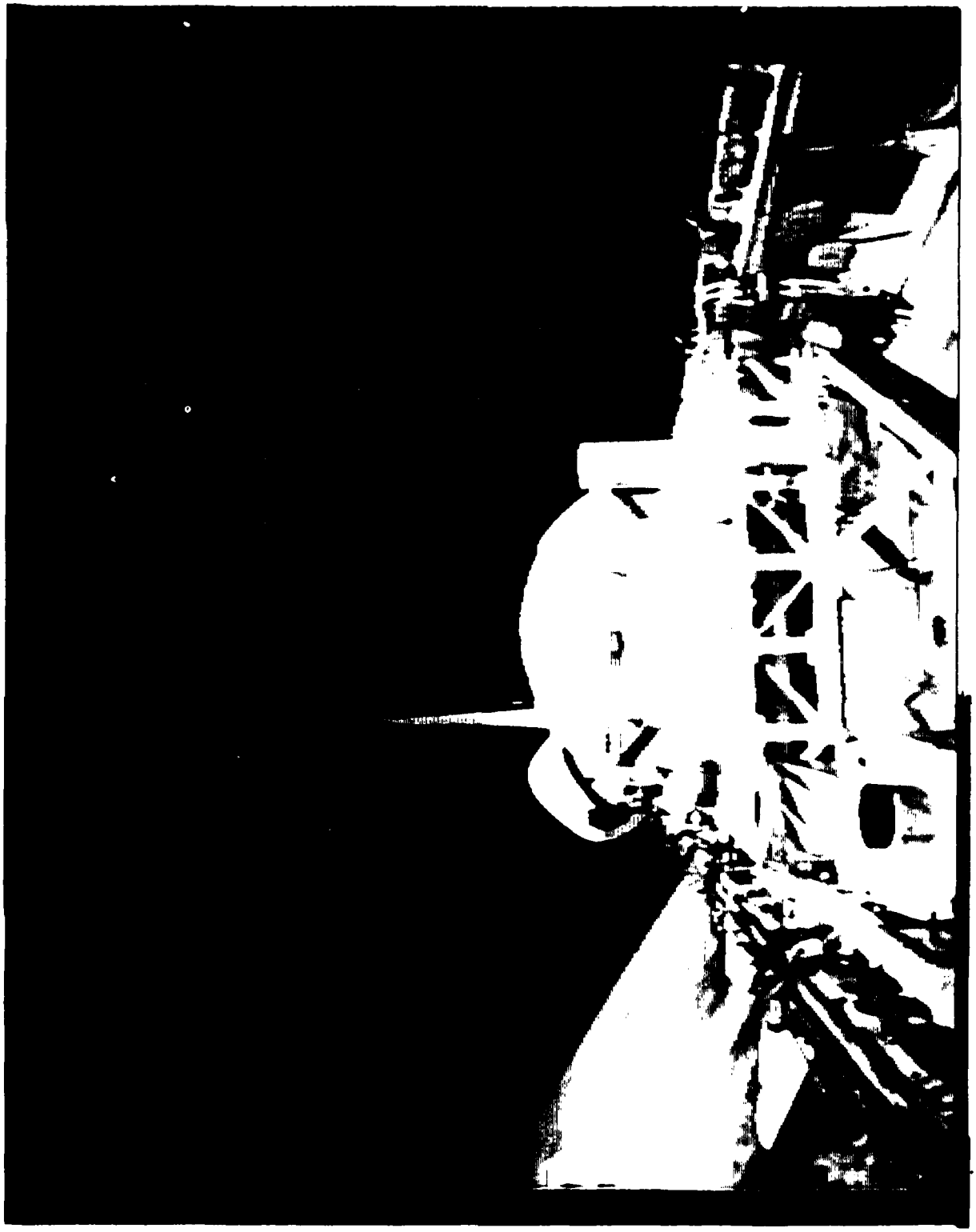

POST FLIGHT

- REMOVE FILM AT KSC ON ~28 JAN 1986
- DEVELOPED BY AEROSPACE CORPORATION
- FILM TRANSFER LSP → PHK → PSI ON 3 FEB 1986
- QUICK LOOK WORKING GROUP AT PSI ON 3 MAR 1986
- ANNOTATED FILM CATALOGUE ON 6 MAY 1986
  - 14788 FRAMES OF FILM DATA
  - 83 ORBITS OF DATA
  - EVENTS/ATTITUDES
  - PARTICLES

PACS film catalogue

Orbit	MET start	MET end	Black	Part	Sky	Earth	Orientation	Notes
3	03:31	03:53	29				-ZLV+XVV	Sunlit earth
3	03:55	03:57		2			maneuver	Grey frames progressively murkier; sunset orbit 3
3	03:59	04:01				2		Second set Earth limb
3	04:03	04:07			3			Slewing to stable star pattern
3/4		04:29			11			same star field
4	04:31					1	maneuver	Earth limb appears (4:23-4:34 timeline maneuver)
4				2				particles against white-many different directions
4	04:37	05:27	26				-ZLV+XVV	by 5:02 -ZLV+XVV;sunlit earth
4	05:29					1		Earth dark
4	05:31			1				Third frame possible strobed particle against earth
4/5						16		Clear fields
5	06:05			1				Many particles-same basic direction
5			25					
5	06:57	06:59		2			-ZLV	Grey murky sets; sunset 6:59
5/6	07:01	07:33				17		clear
6	07:35			1				large particle coming from the right-other smaller particles; sunrise 7:35
6						1		Grey mottled set-no obvious particles
6	07:39	08:29	26					
6/7	08:31					13		Earth limb appearing on thirteenth sets, last frame
7	08:59	09:05			4			slewing
7	09:07	09:29		12			deep space	Storm of particles(sun???) backscatter; satellite launched
7		09:59	15					14 black; 1 grey; sunlit earth in foreground
7	10:01			1				few slow movers-same "size"; sunset 10:01
7/8	10:03	10:29			14			slewing
8	10:21	10:35				3		1st has earth limb-2 sets clear
8	10:37	10:39		2				1st has fast moving particle from right-2nd has smaller storm
8	10:41	11:31	26				-ZLV	sun on Earth; Fuel cell purge 11:19
8	11:33	11:37				3		
8/9	11:39	12:01			12		deep space	
9	12:03	12:07				3		1st has earth limb and cities 2 clear
9	12:09			1				large rock lower right hand corner. 1st frame most on right to left
9	12:11					1		filigree pattern-over Pakistan
9	12:13		15				+Y sun...	3 sets of grey coming out of black
9		13:08		11			inertial...	Varied motion & sizes-roughly ten per set (i.e. not storm)
9/10	13:05	13:23			10		nose...	stable star field
10	13:25	13:39				8	south	1,2 Earth limb 3,4,5 clear 6,7,8 cities
10	13:41			1				right to left about 5 particles

ANALYSIS APPROACH

- PREFLIGHT
  - SCATTERING CALCULATIONS FOR EXPECTED RADIANCE LEVELS (SOLAR ANGLE, WAVELENGTH, SIZE)
  - ALGORITHMS FOR DETERMINING x, y, z, V_x, V_y, V_z, r_p
- FLIGHT
  - GATHER ALL AVAILABLE DATA ON ATTITUDES, SUN ANGLES, MISSION EVENTS (TALES OF WOE)
- POST FLIGHT
  - SORT DATA (OVEREXPOSED, SKY, EARTH, PARTICLES)
  - ADD ATTITUDES, COMMENTS
  - LOOK FOR TRENDS
  - STELLAR MAGNITUDES TO GET INTENSITY CALIBRATION
  - BACKGROUND SUBTRACTION
  - DETAILED TIMELINE AND POINTING INFORMATION

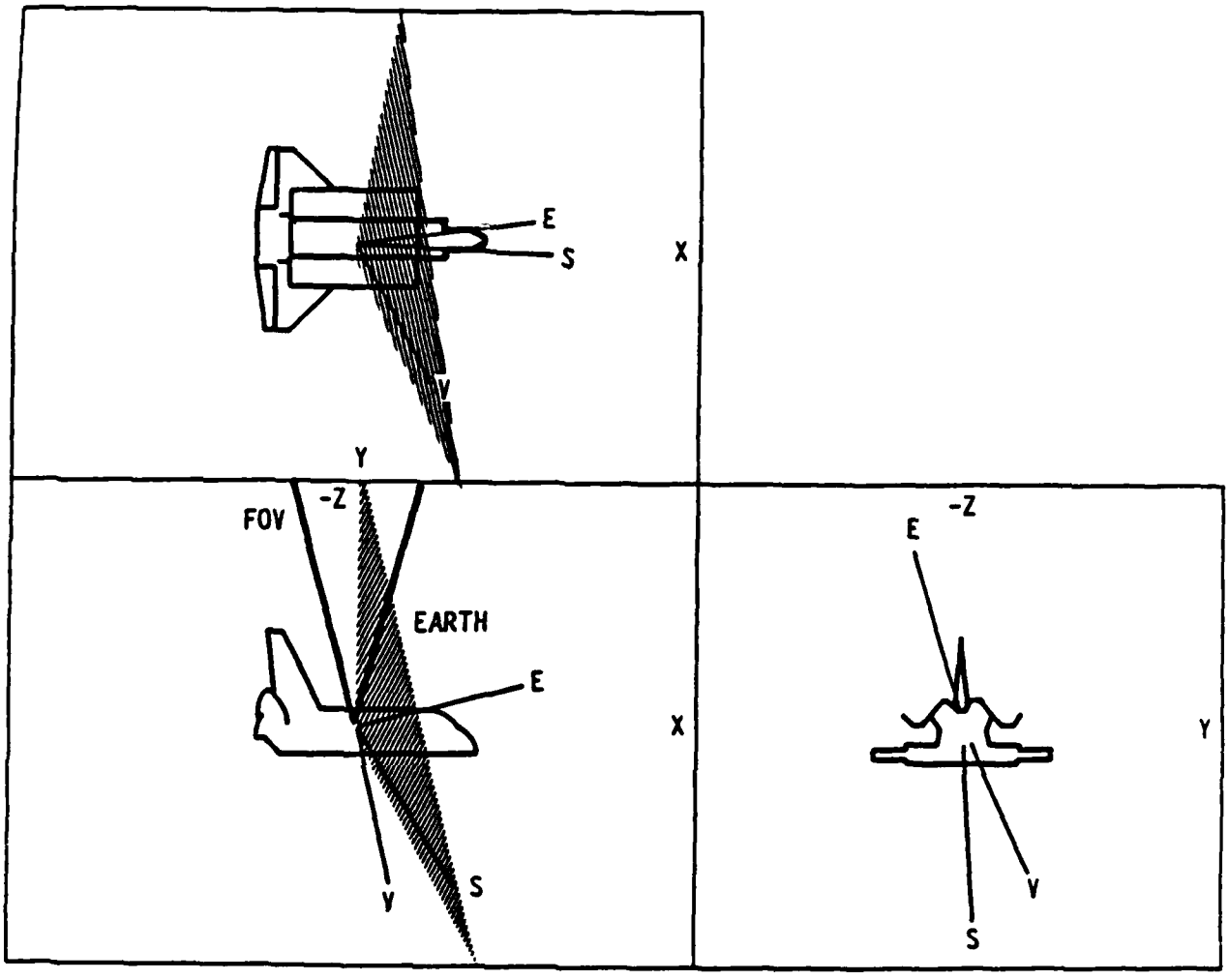

A-2923

Figure 1. Shuttle Ground System Attitude Display. V is Velocity Vector, S is Sun Sector and E is Center of Earth Vector. Solid Angle Subtended by Earth is Indicated, as PACS Field of View

VG86-160

FRACTION OF FILM EXPOSURES HAVING PARTICLES AT SUNRISE/SUNSET

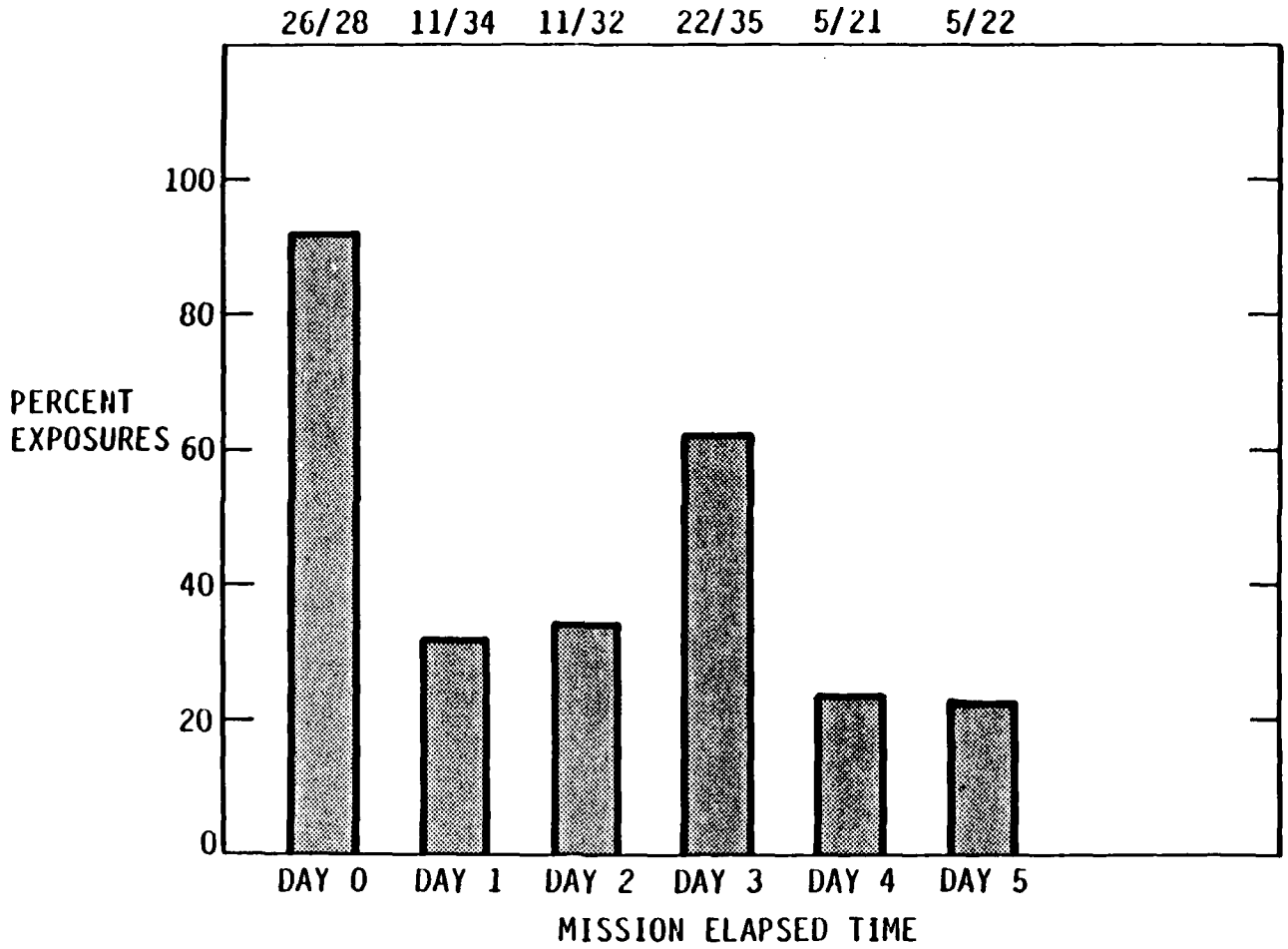

A-3153

VG86-160

PACS: PARTICLE HISTORY - FLIGHT DAY 0 - + YSI

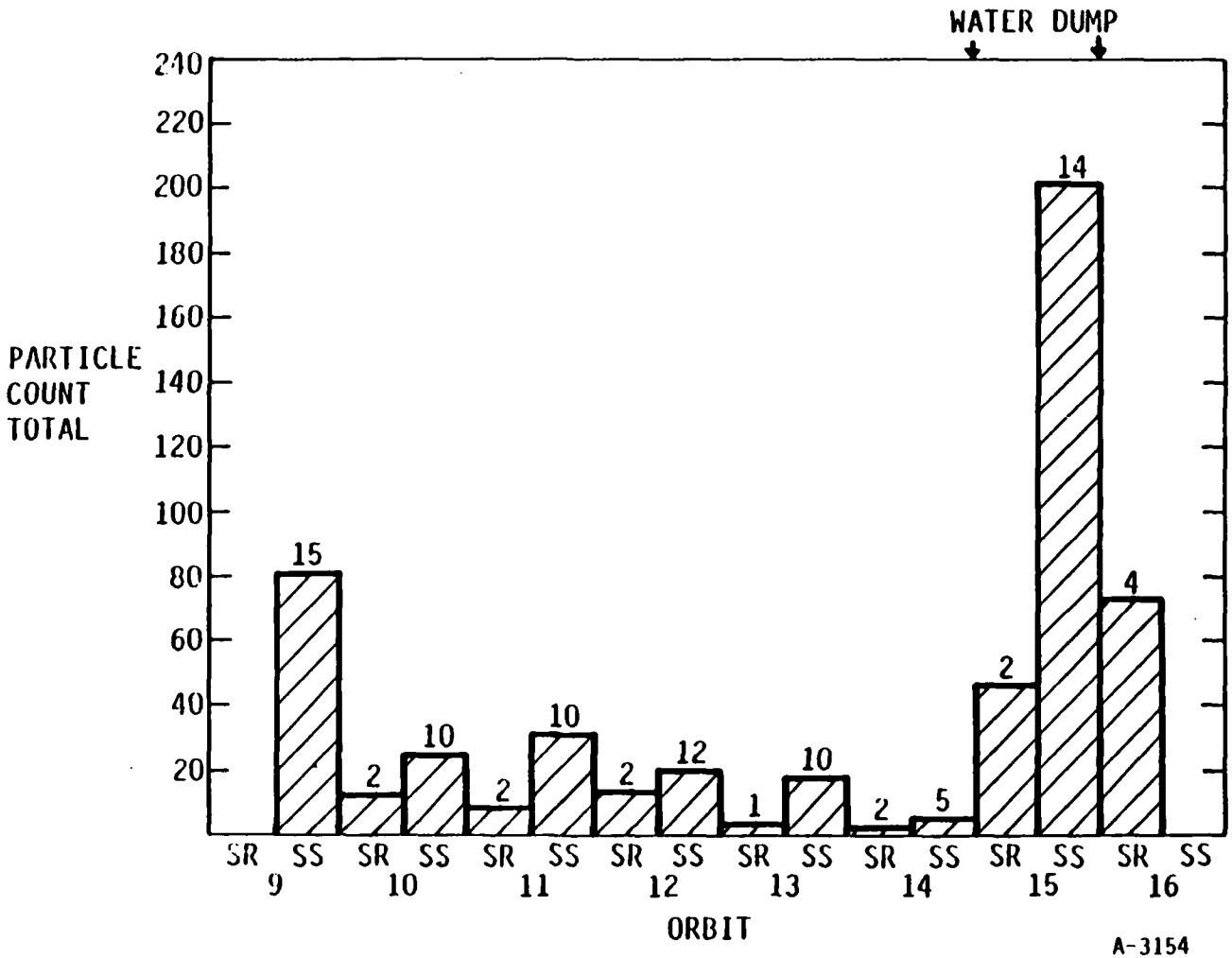

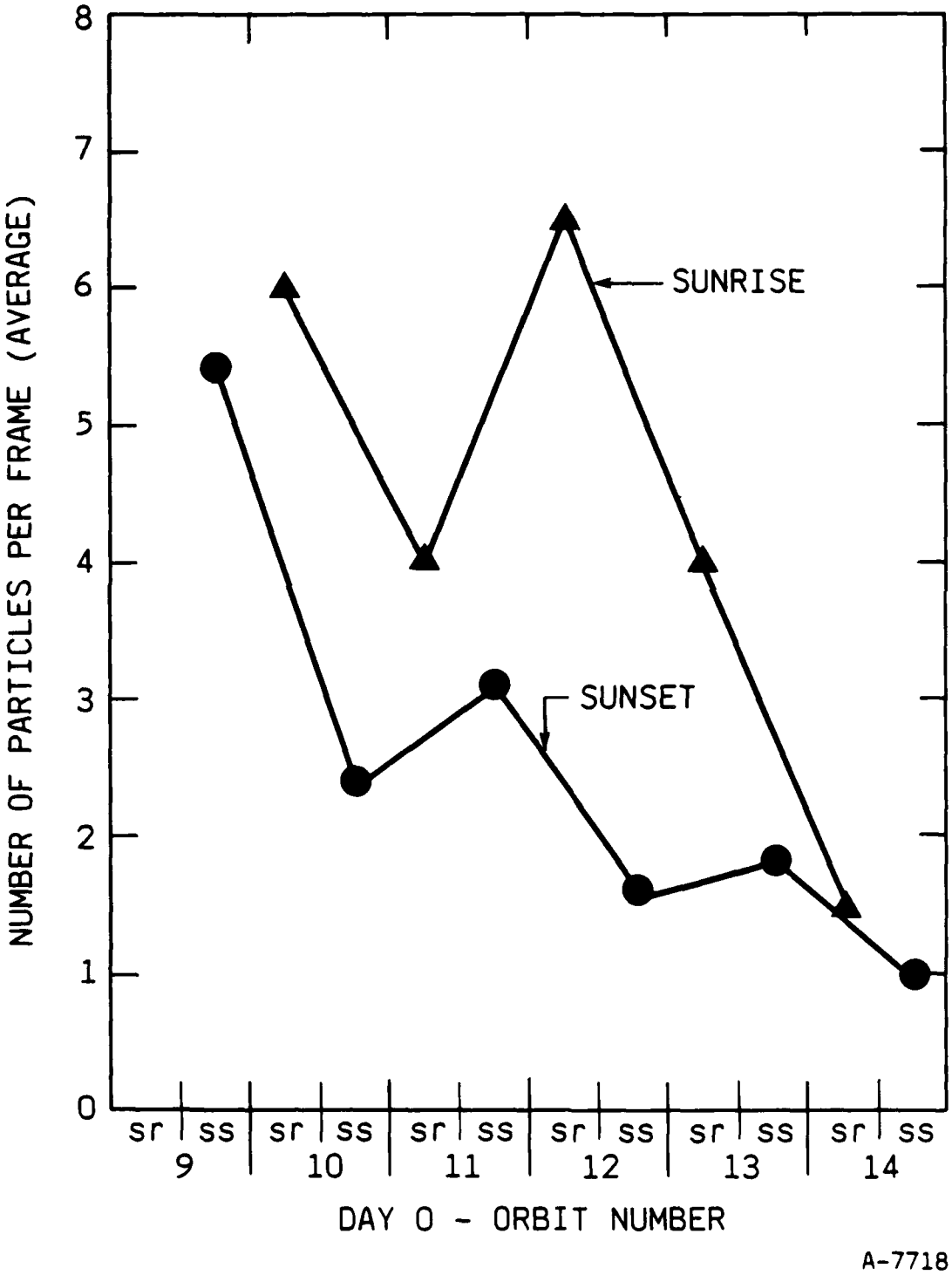
8
7
6
5
4
3
2
1
0
NUMBER OF PARTICLES PER FRAME (AVERAGE)
SUNRISE
SUNSET
sr ss sr ss sr ss sr ss sr ss sr ss
9 10 11 12 13 14
DAY O - ORBIT NUMBER

A-7718

VG86-194

PARTICLE DECAY AFTER SUPPLY WATER DUMP (VISUAL PARTICLE COUNT)

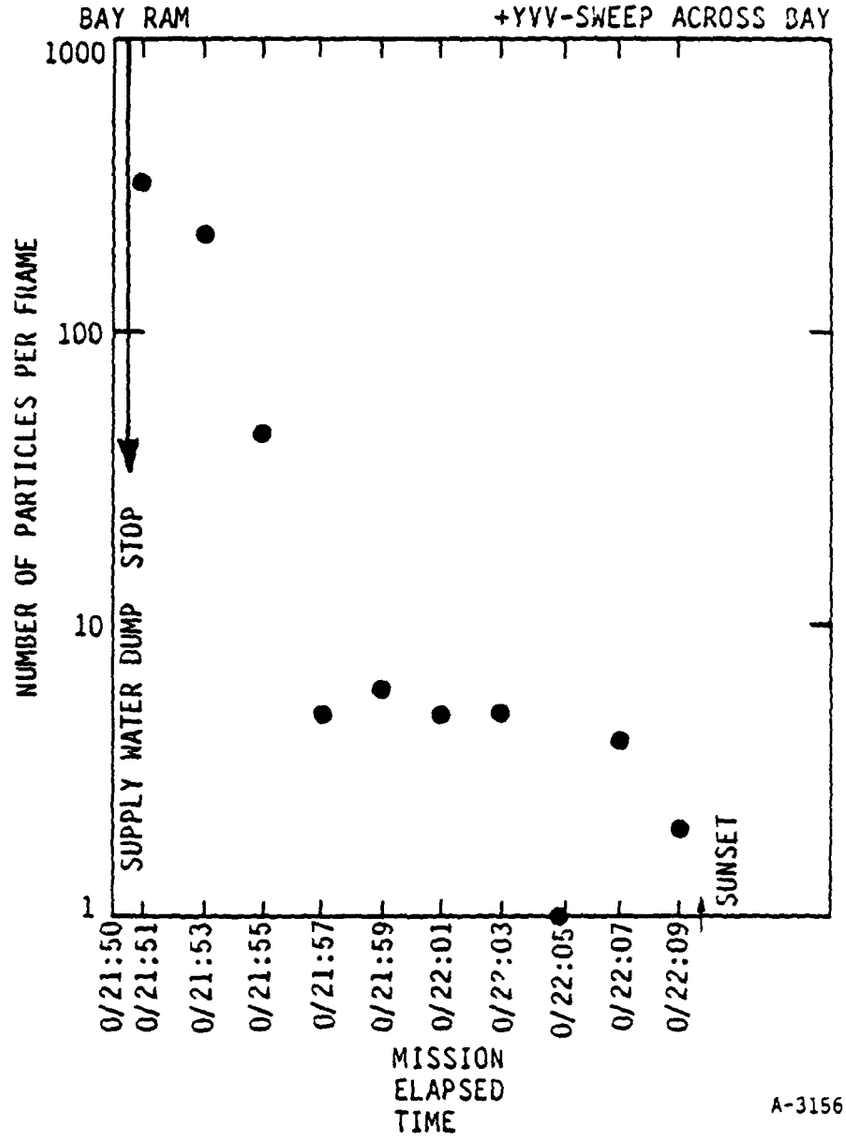

- SEE PARTICLES NEXT SET (+1 min.) AFTER START OF PUMP
- TYPICAL TRACK 1/8° × 1-1/2°/S

NASA-IECM DATA
WATER DUMP DECAY

VG86-194

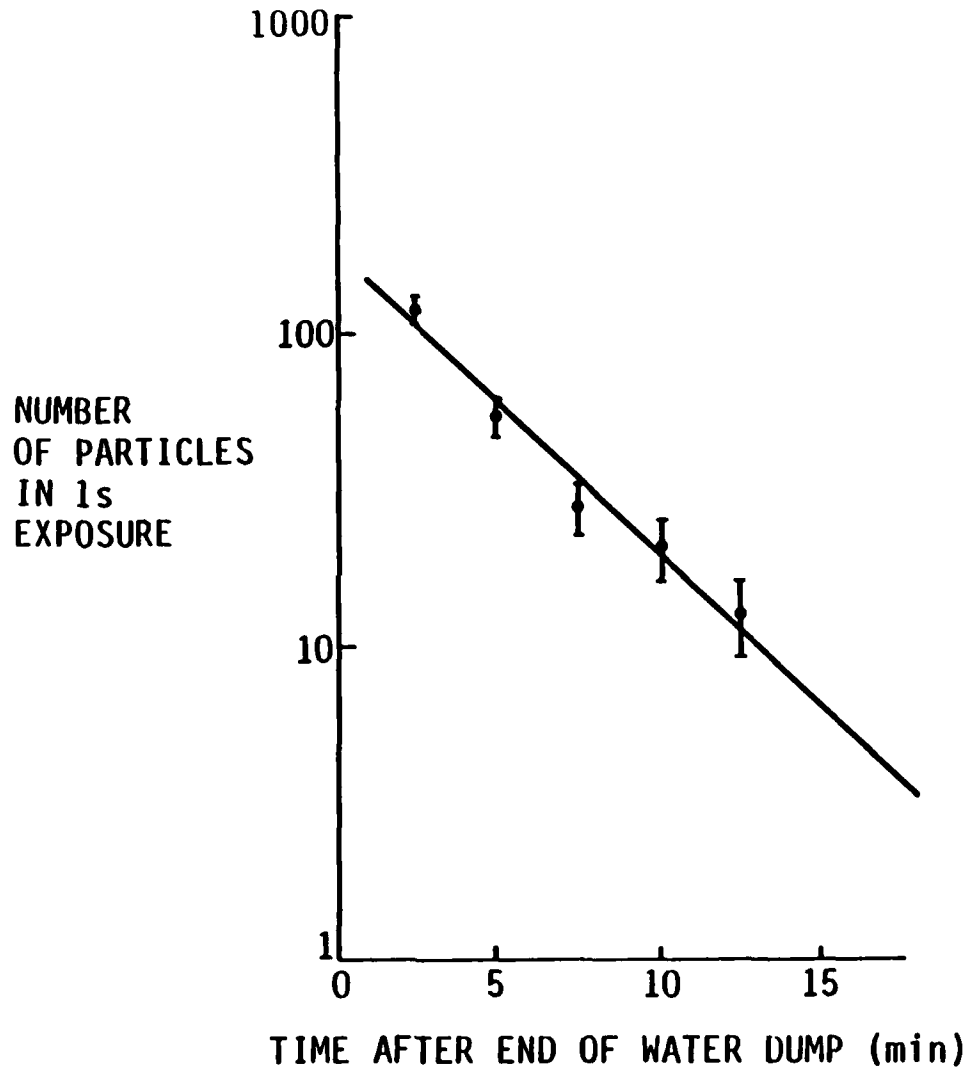

A-3385

VG86-160

PARTICLES IN FIELD OF VIEW DURING PACS PRIME MEASUREMENT SEQUENCE (DEEP SPACE VIEWING - ALL DISABLED)

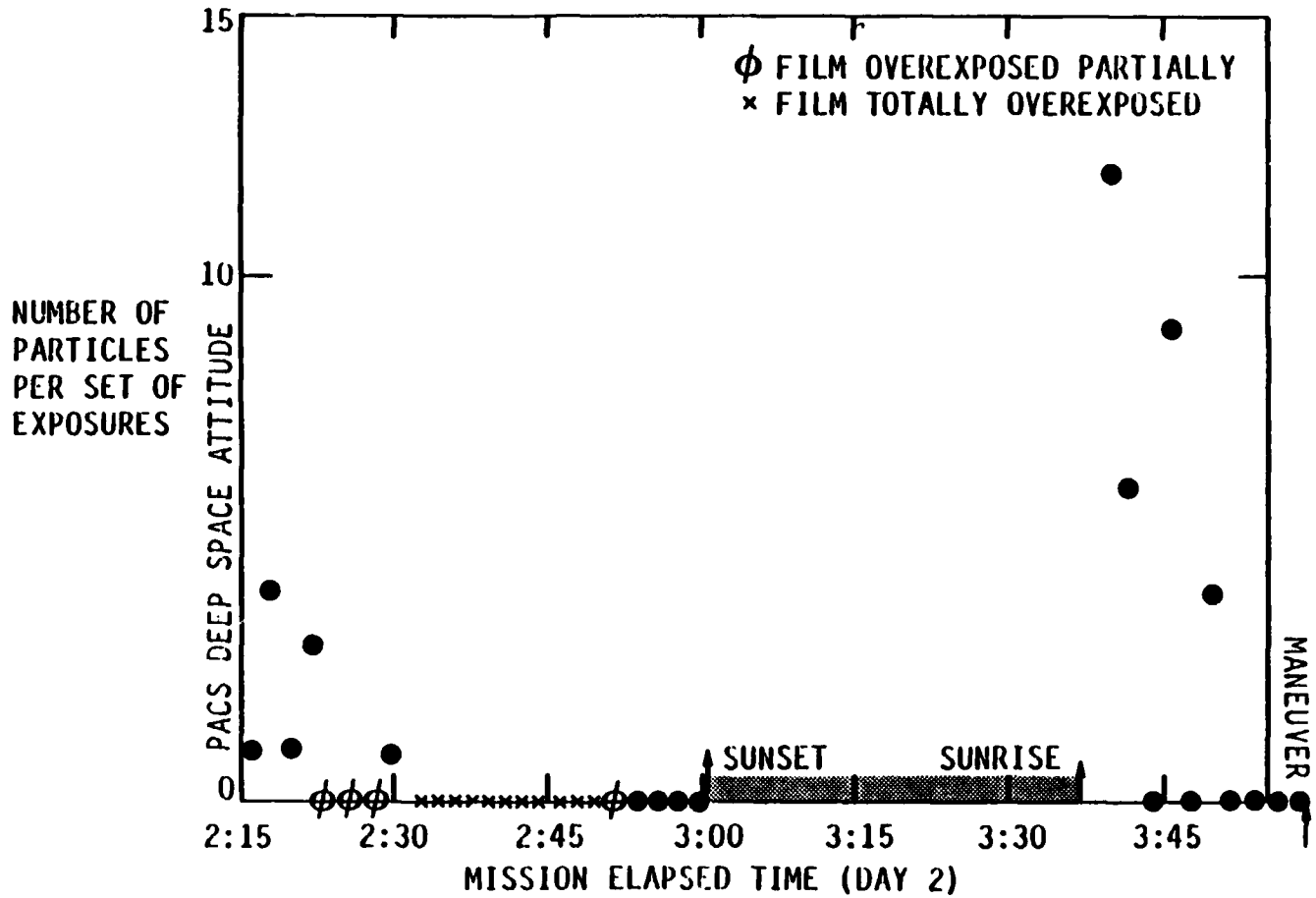

A-3157

VG86-160

PARTICLES IN FIELD OF VIEW WHEN GRAVITY GRADIENT ATTITUDE BAY IN WAKE (ALL DISABLED)

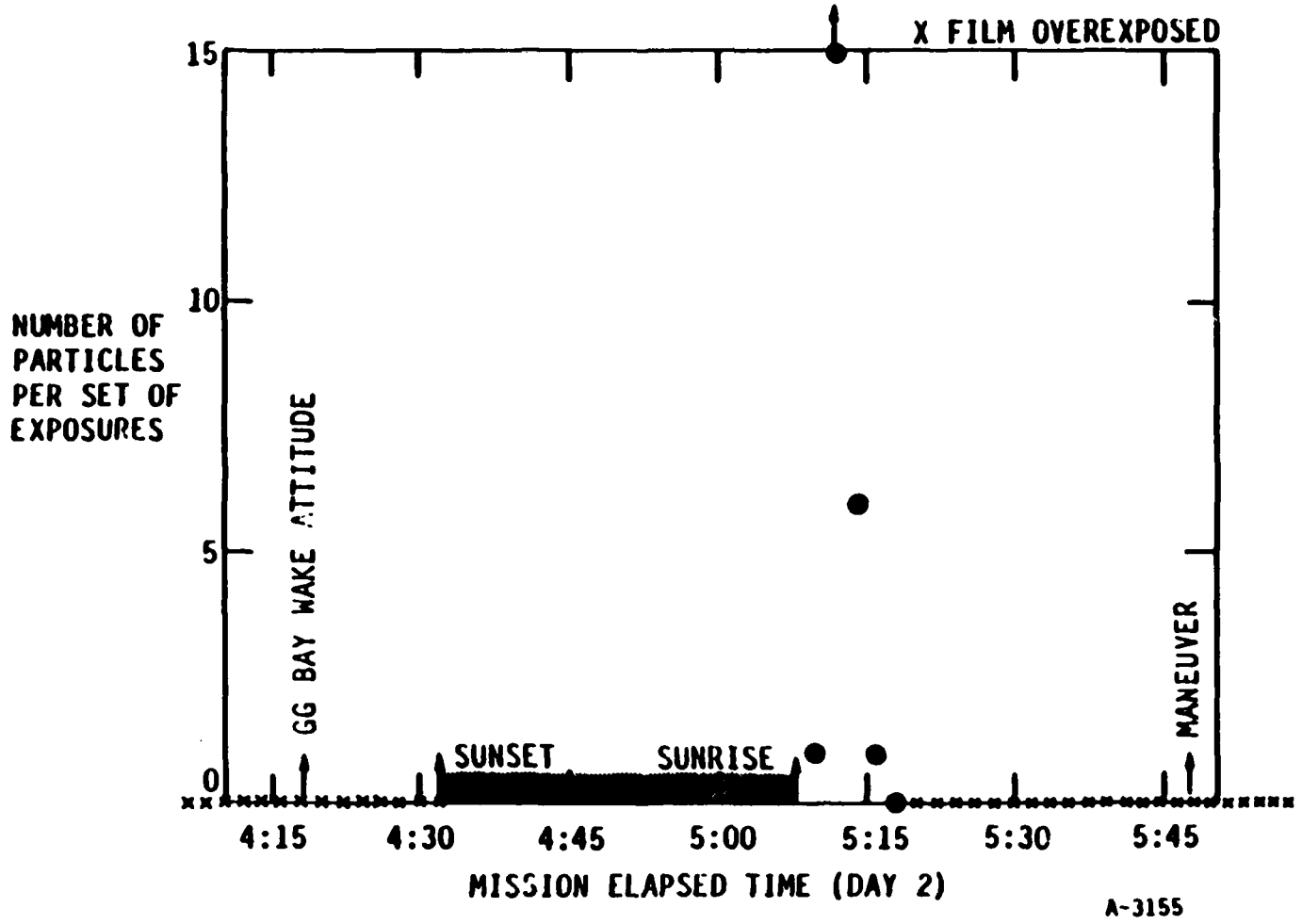

INDUCED ENVIRONMENT CONTAMINATION MONITOR

5911-14

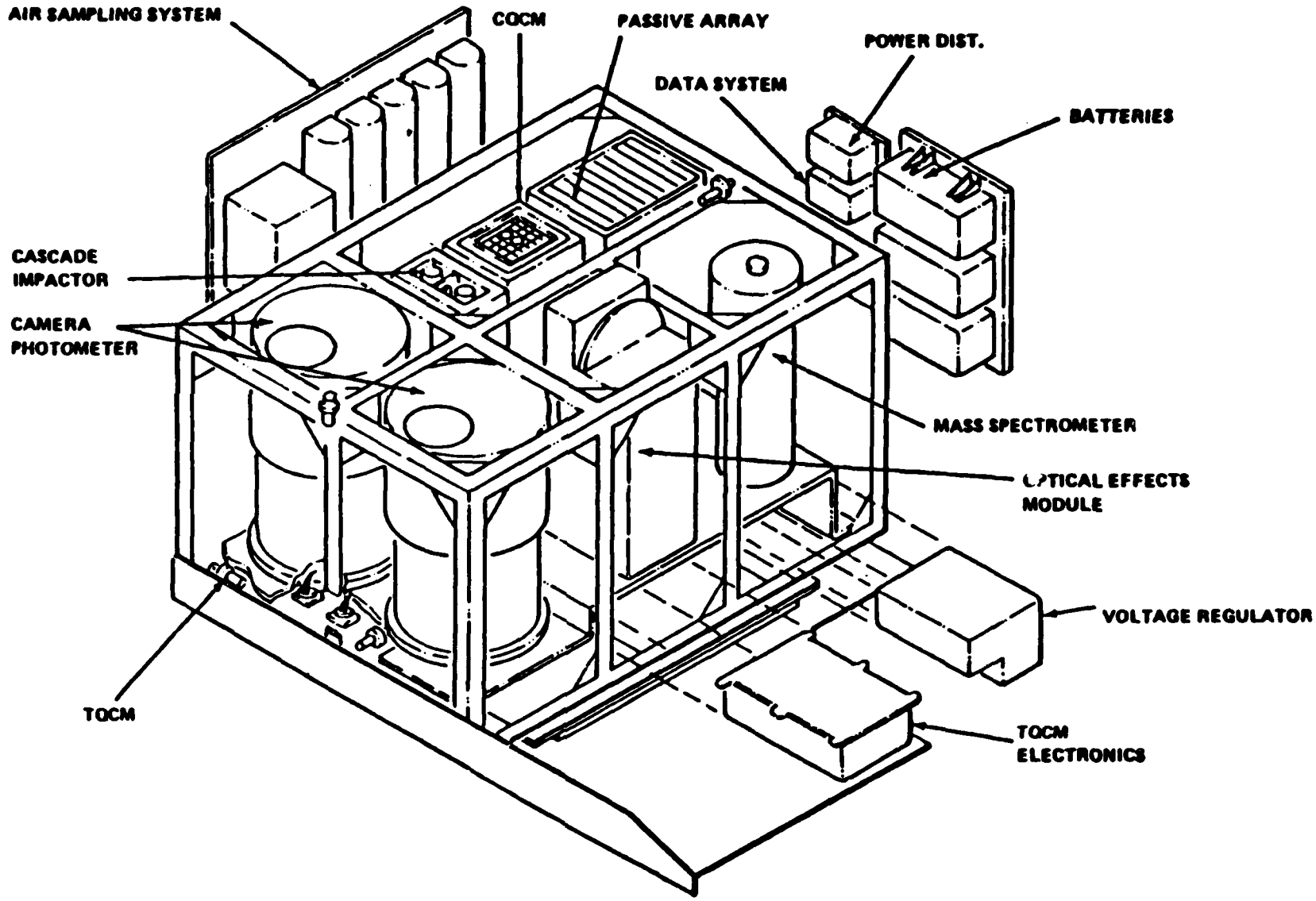

FROM E.R. MILLER STS-2 IECM QUICK LOOK REPORT, NASA TM-82457

SUMMARY OF CONTAMINATION FROM STS-2, -3, -4

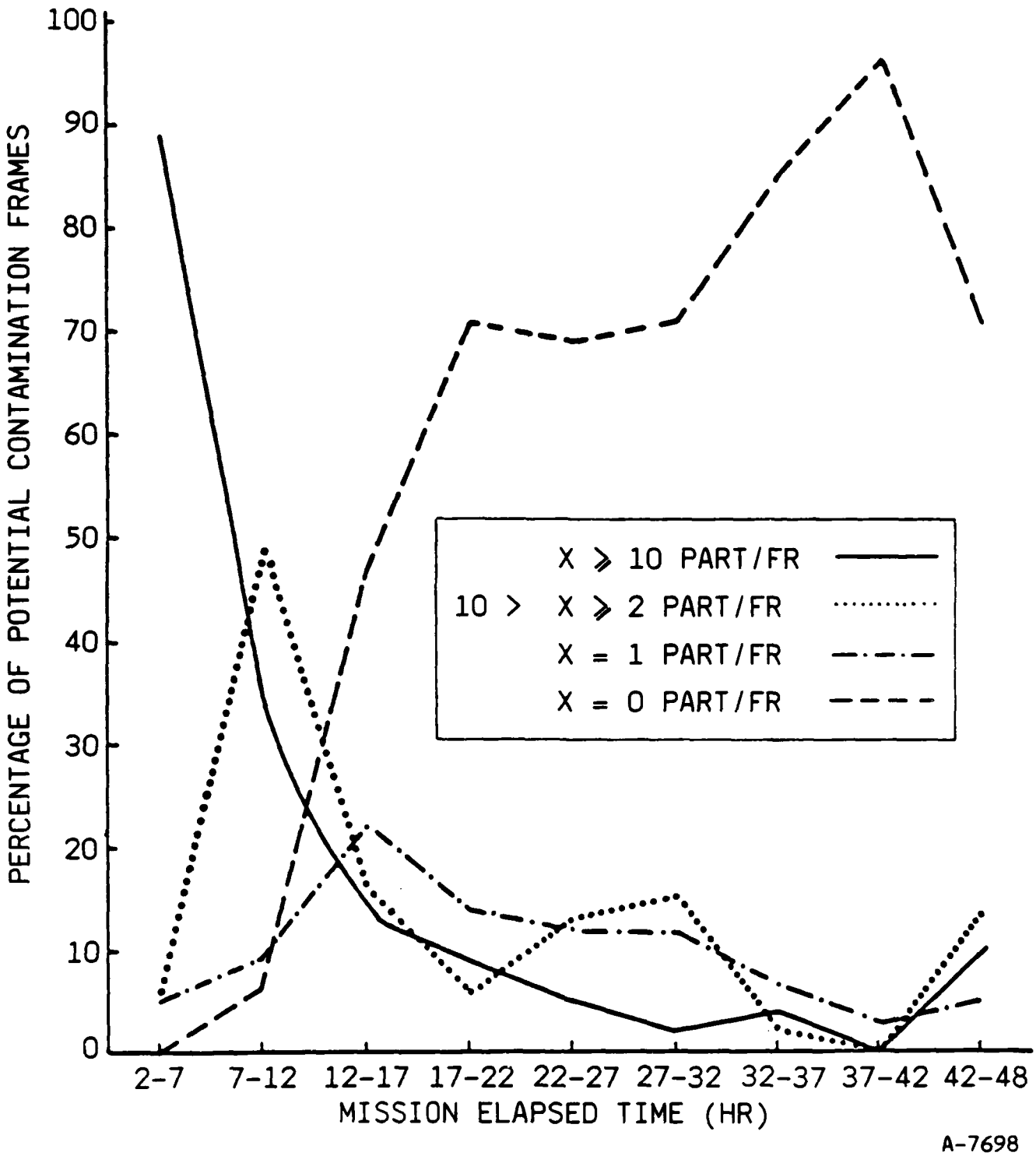

A-7698

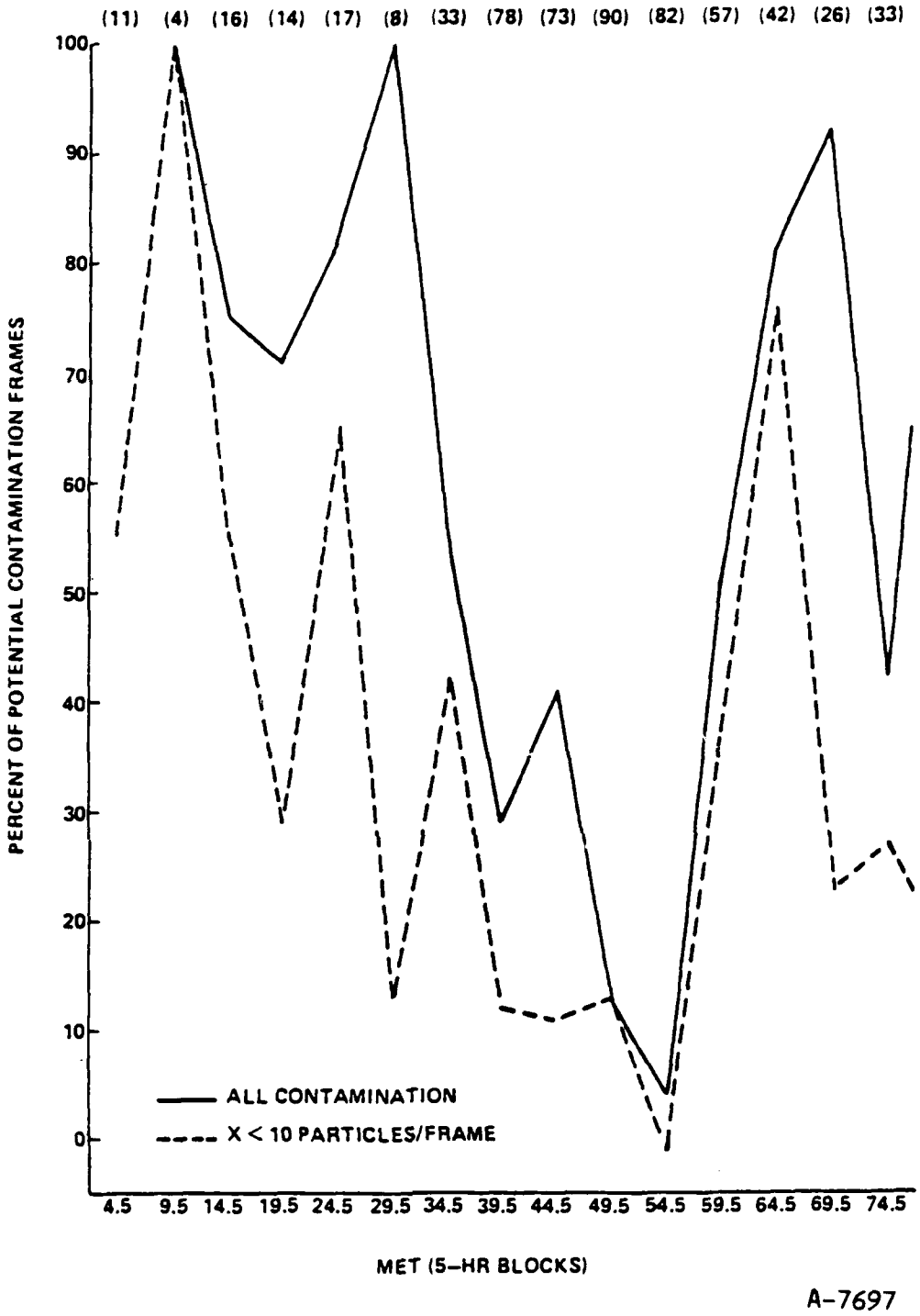

Figure VI-1. Correlation of observed contamination with mission elapsed time (MET) taken in 5-hour blocks. Contamination is portrayed as a percent of those frames capable of showing contaminant particles. Numbers at the top of the figure indicate the size of the data sample (number of potential contamination frames obtained) during each 5-hour period.

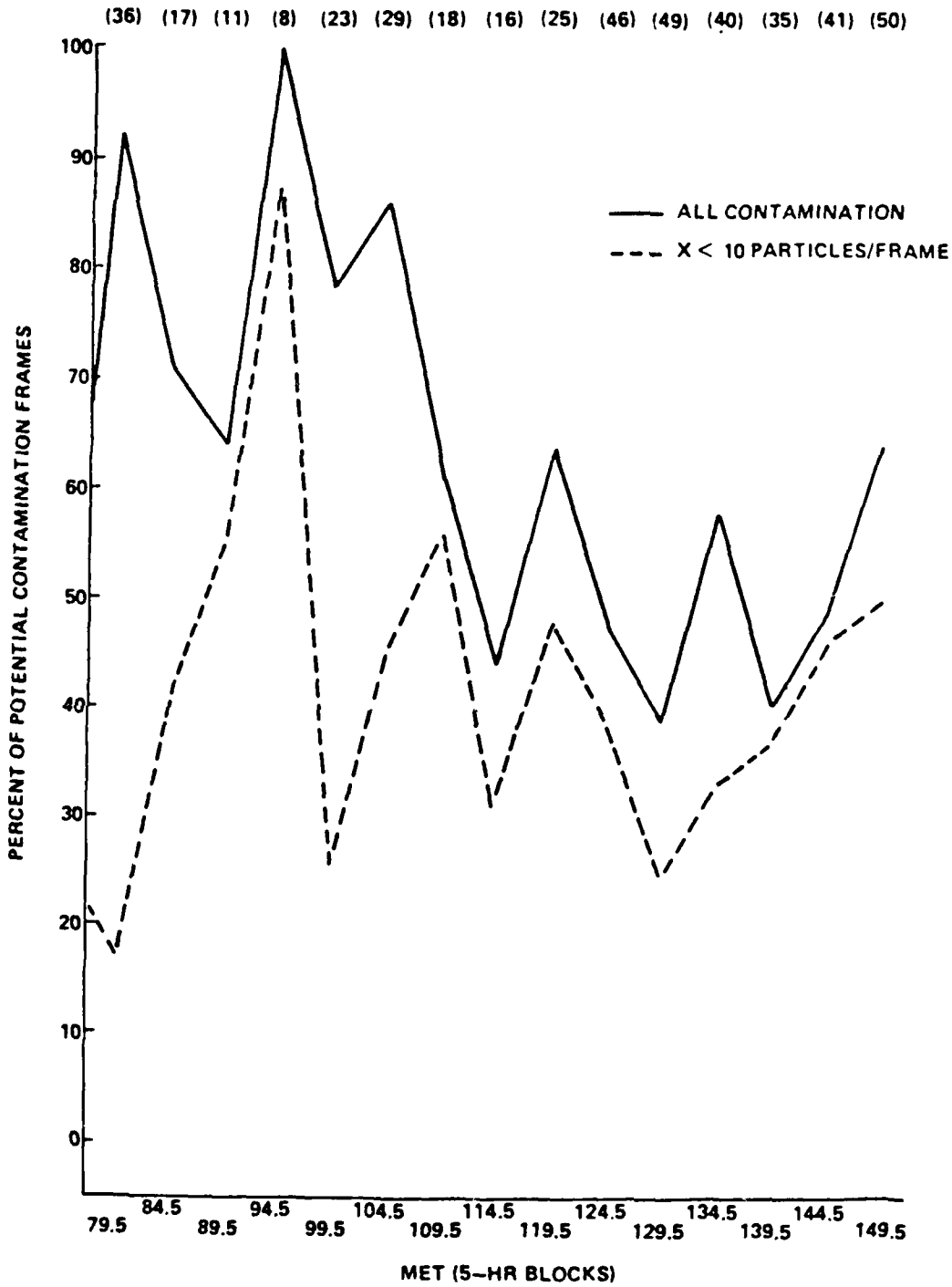

Figure VI-1. (Concluded)

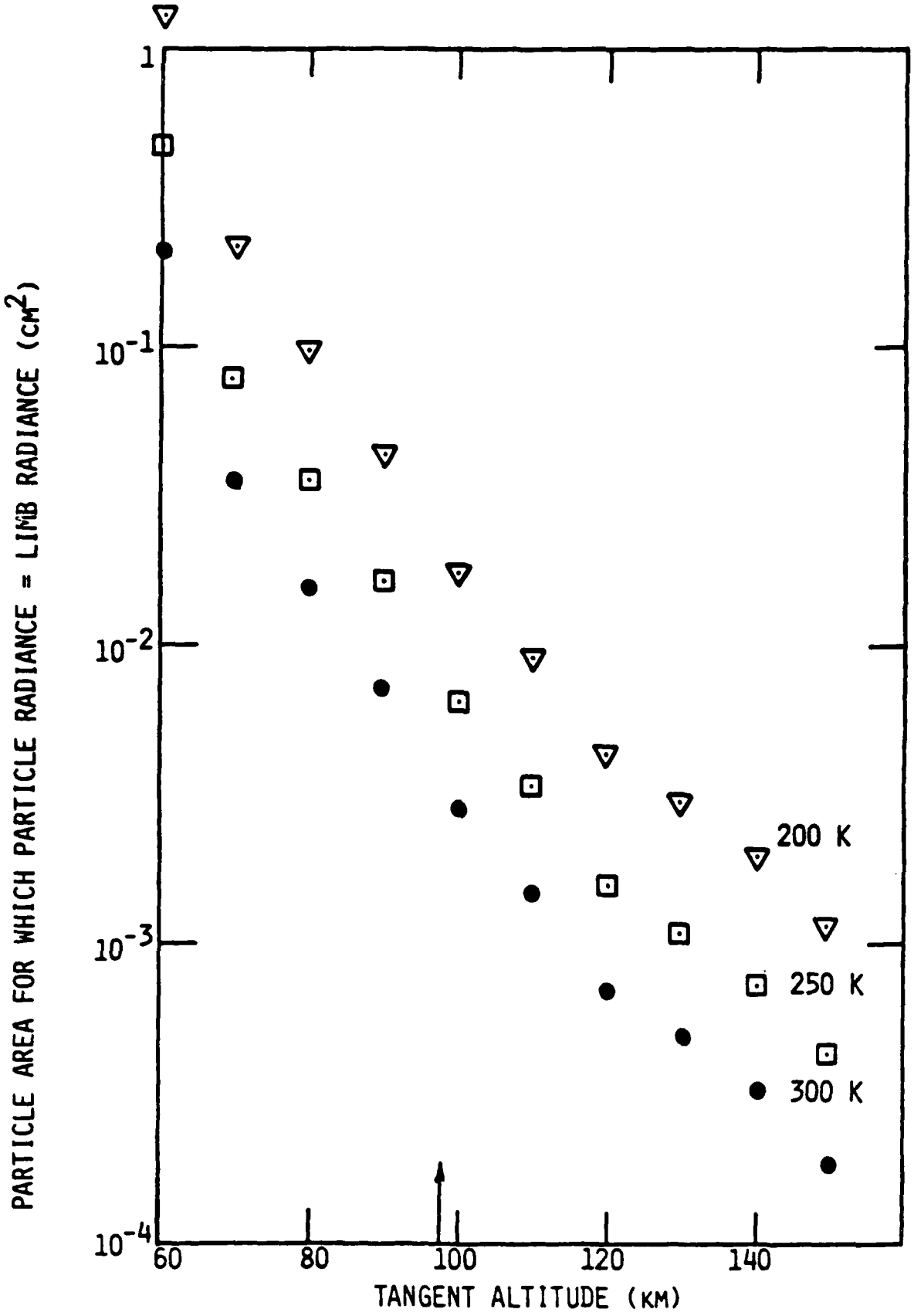

Particle areas which give rise to radiances equal to sunlit earth limb values as a function of tangent height altitude for several temperatures assuming unit emissivity for the particle.

IECM PRELIMINARY RESULTS

- STS 2 (FEW FRAMES)
  - DRAG OBSERVED ON PARTICLES
  - SIZES 45-300 μm
  - VELOCITIES ~0.1-3 m/s
  - AVERAGE 0.7 ± 0.4 m/s
  - MORE PARTICLES AT SUNRISE
- ALGORITHMS IN PLACE
  - SPACELAB 1 DATA NEXT

NEED MIE SCATTERING CALCULATIONS TO USE PHOTOGRAPHIC DATA TO ESTIMATE CIRRIS IMPACT

PARTICLE BRIGHTNESS

- EMISSION, W sr^{-1} μm^{-1}:
  - $I_R(r,\lambda) = 4(\pi r)^2 Q_A(r,\lambda) N(\lambda,T)$
  - DETERMINE T FROM RADIATIVE STEADY-STATE (HEATING BY EARTH, SUN)
- SOLAR SCATTERING, W sr^{-1} μm^{-1}:
  - $I_S(r,\lambda,\theta) = (\lambda/2\pi)^2 J_\lambda f(r,\lambda,\theta)$
  - STRONG ANGULAR DEPENDENCE
- EARTHSHINE SCATTERING, W sr^{-1} μm^{-1}:
  - TREAT EARTH AS DISTRIBUTED, LAMBERTIAN RADIATOR
  - $I_E(r,\lambda) = \pi R^2 I_\lambda Q_S/4$
- TOTAL SPECTRAL RADIANT INTENSITY, W sr^{-1} μm^{-1}:
  - $R_\lambda = I_R + I_S + I_E$

VG86-57

REFRACTIVE INDEX FOR ICE
(S.G. WARREN, APPL. OPT. 23, 1206(1984)

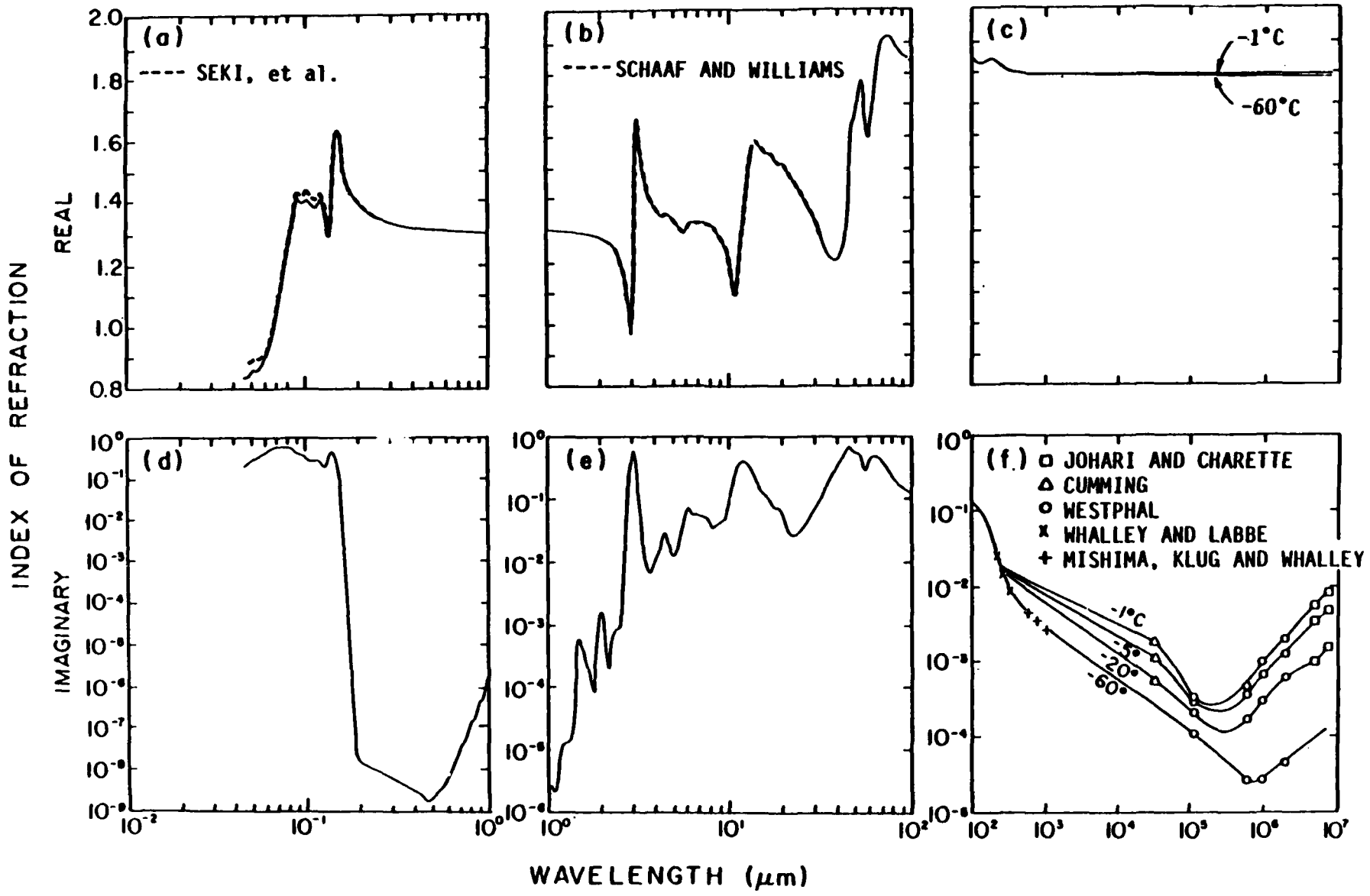

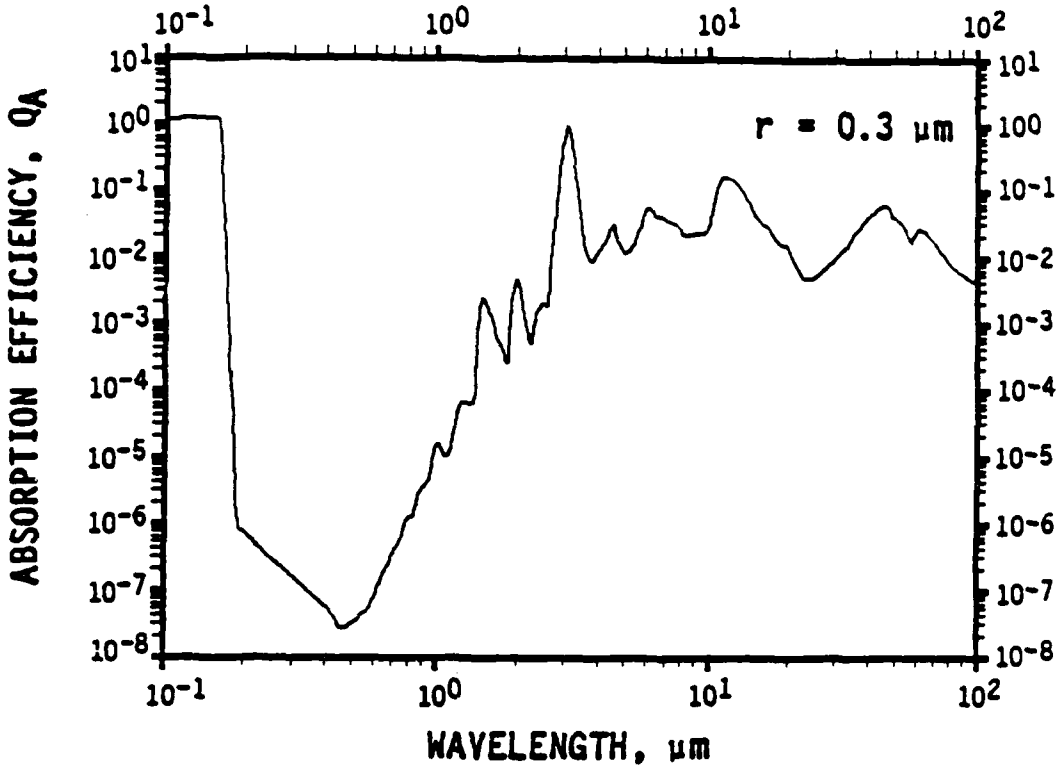
r = 0.3 μm
ABSORPTION EFFICIENCY, Q_A
WAVELENGTH, μm

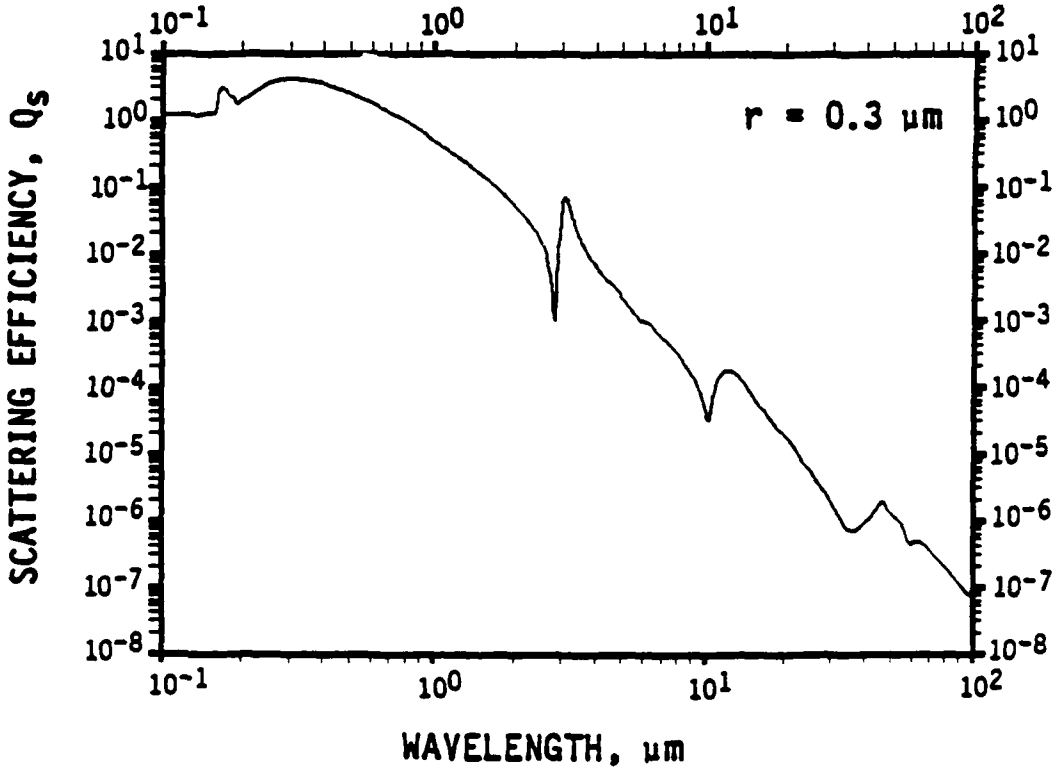
r = 0.3 μm
SCATTERING EFFICIENCY, Q_S
WAVELENGTH, μm

A-2076

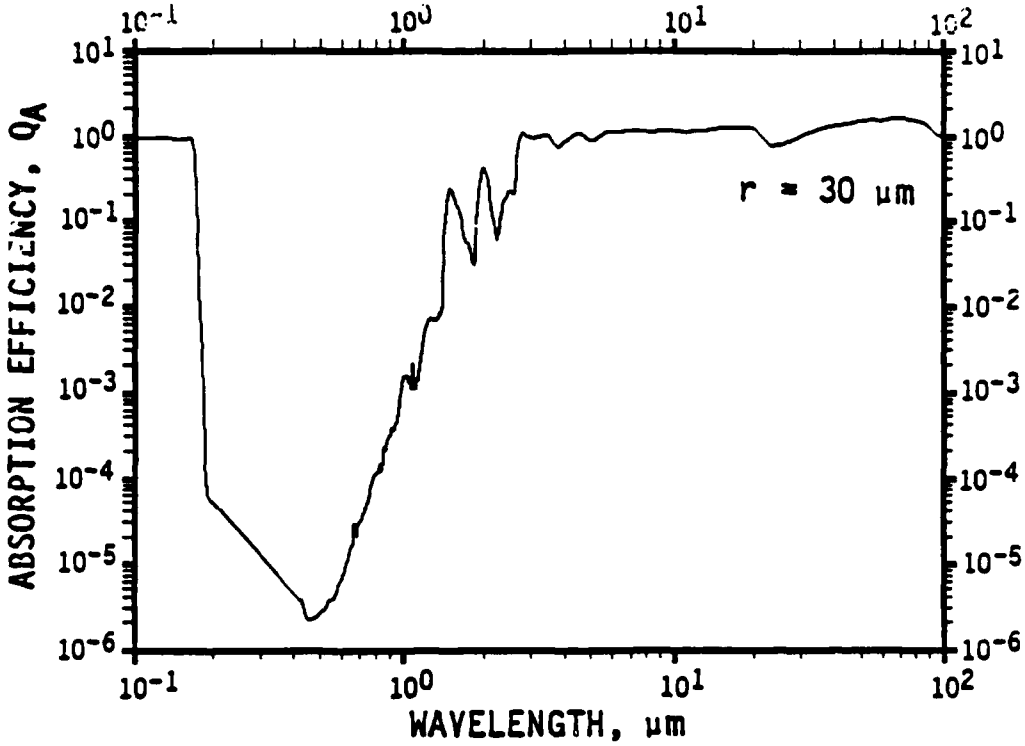
ABSORPTION EFFICIENCY, Q_A
r = 30 μm
WAVELENGTH, μm

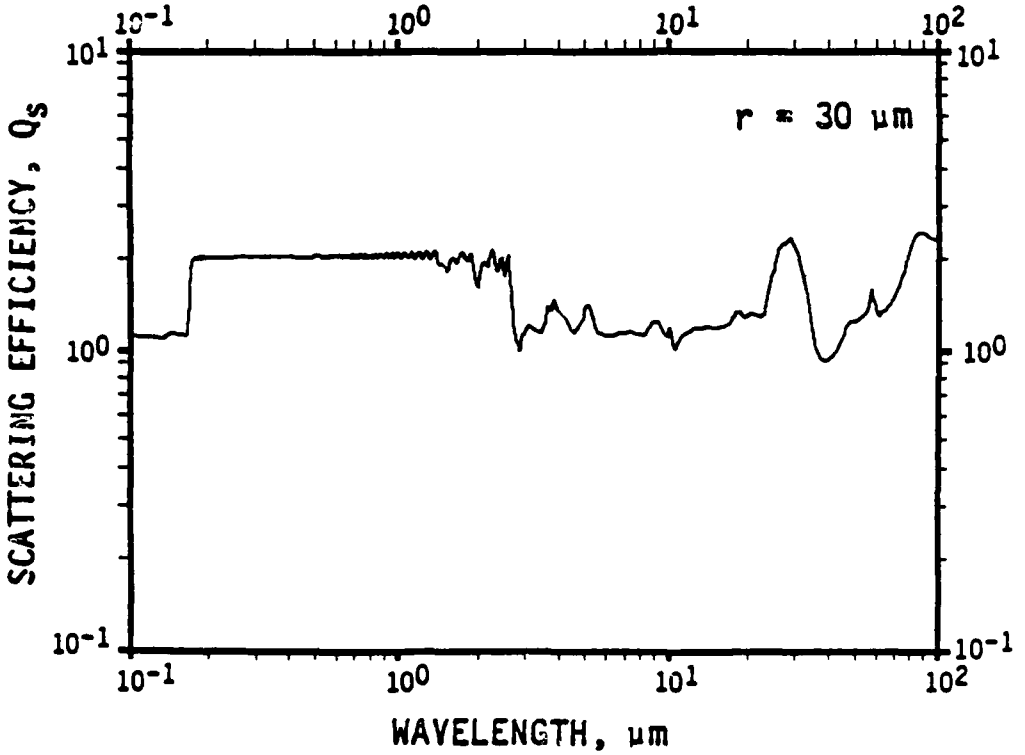
SCATTERING EFFICIENCY, Q_S
r = 30 μm
WAVELENGTH, μm

A-2078

ANGULAR DEPENDENCE OF LIGHT SCATTERING

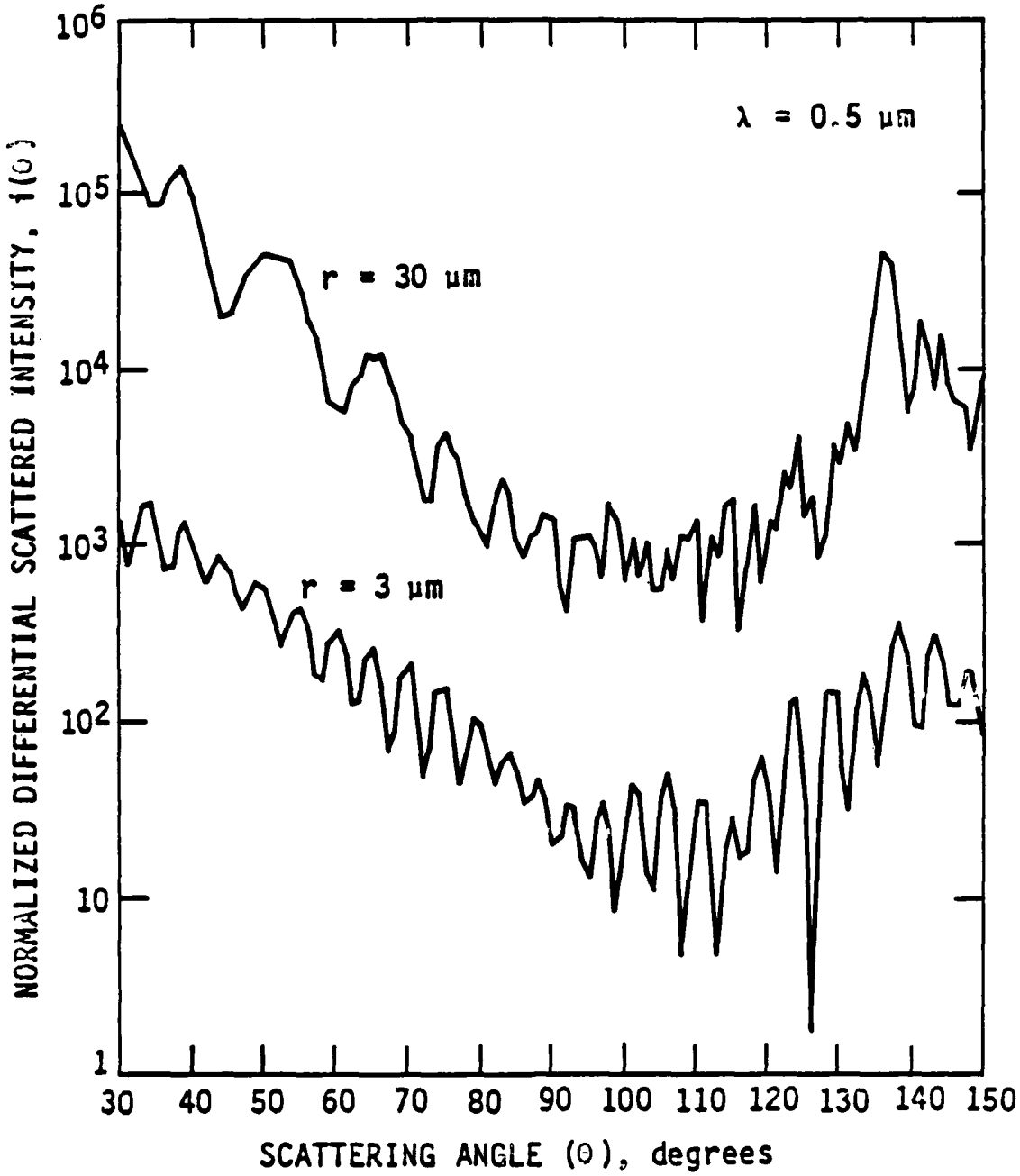

A-2081

SUN AND EARTH RADIANT FLUX

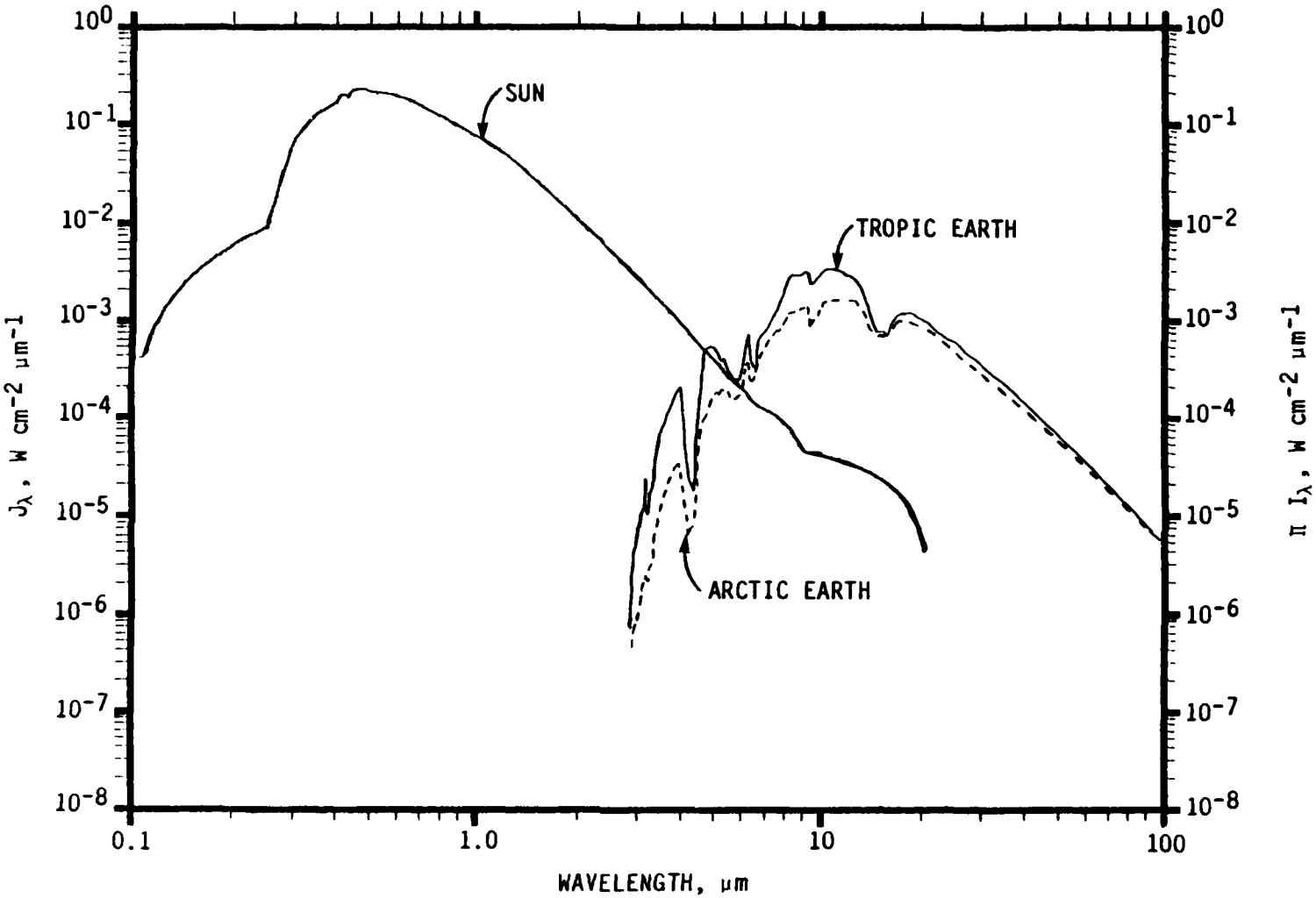

A-2084

STEADY-STATE ICE PARTICLE TEMPERATURES

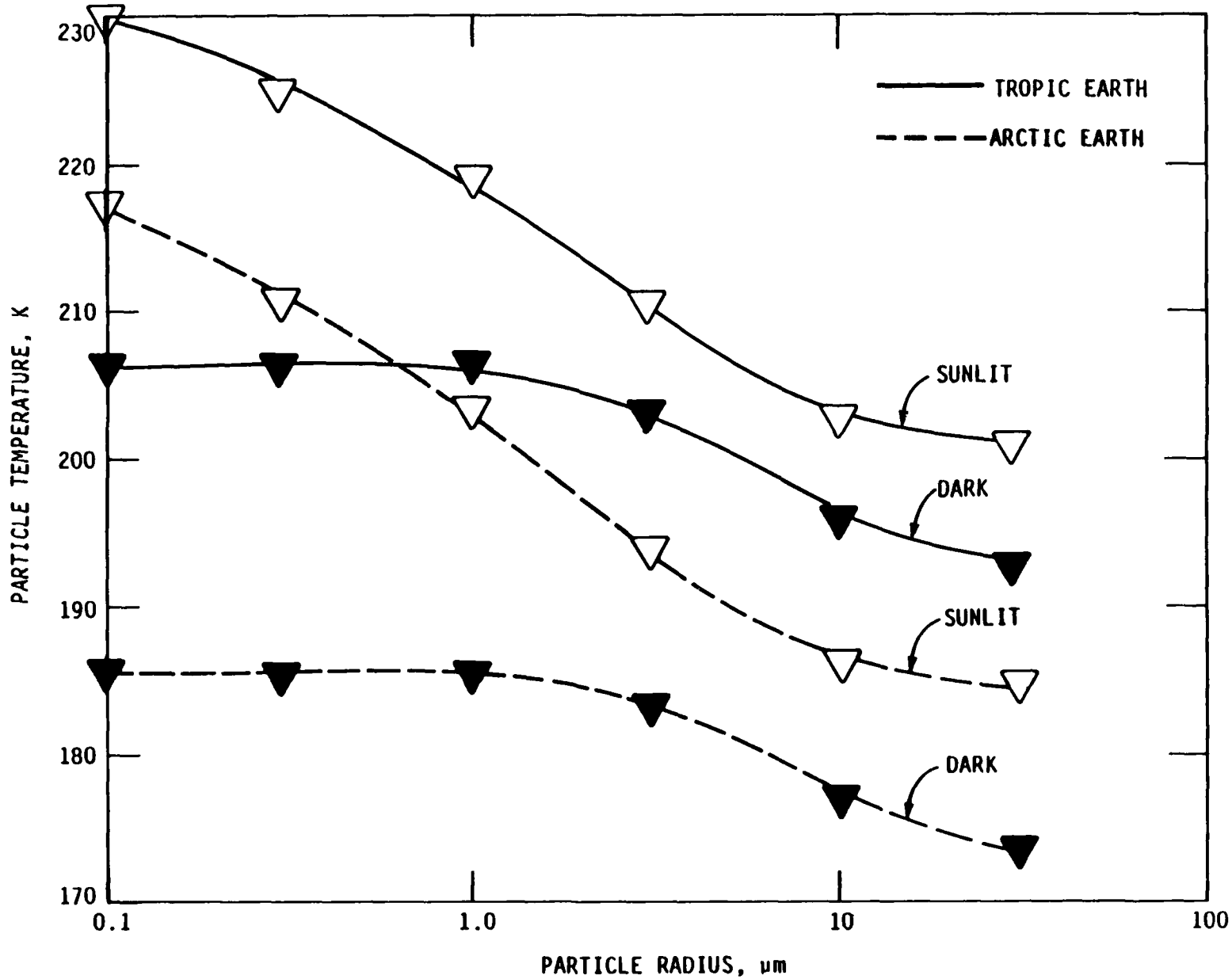

SINGLE PARTICLE, TROPIC EARTH, FORWARD SOLAR SCATTERING (Θ = 30°)

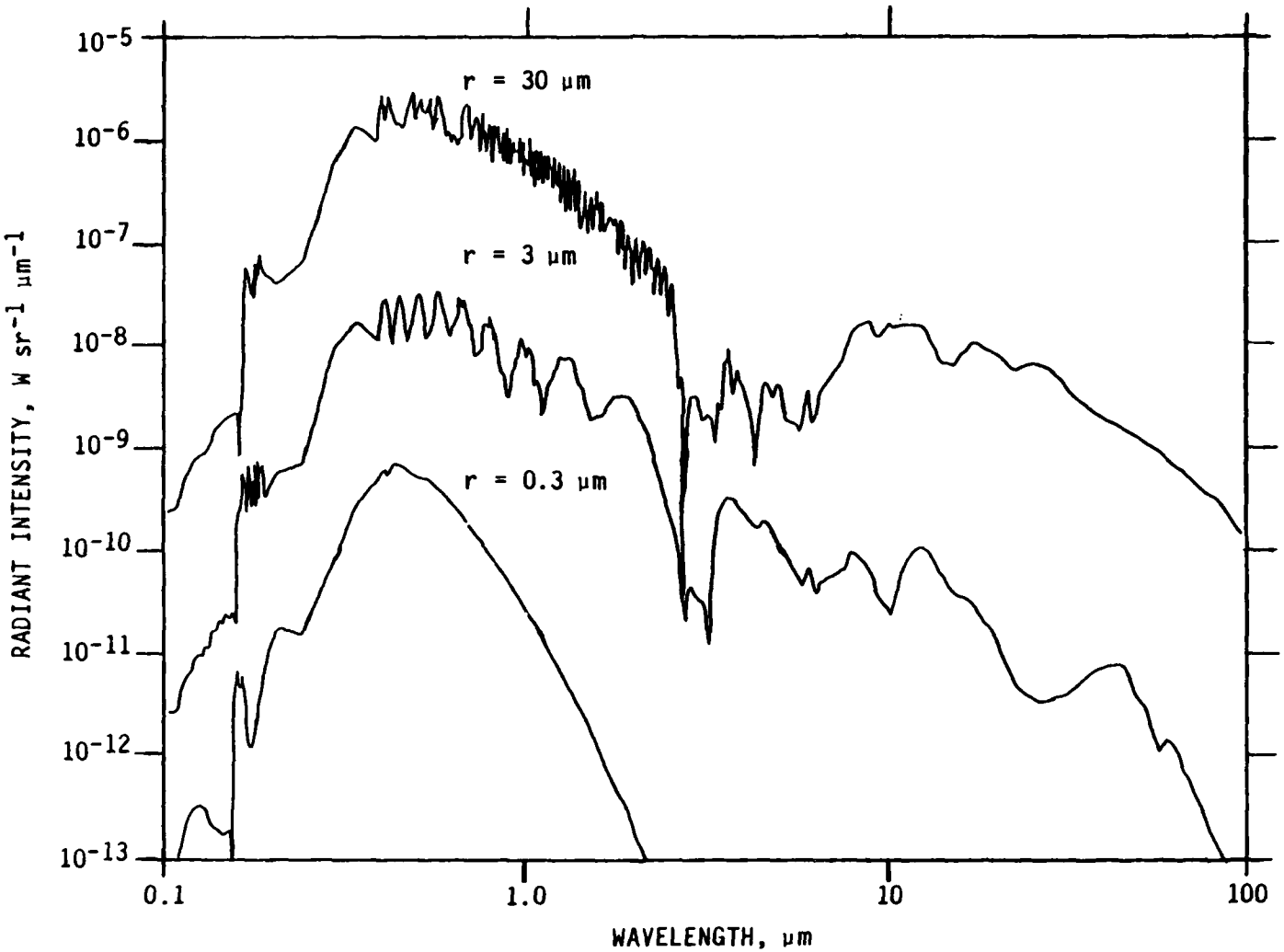

A-2082

INFRARED PARTICLE BRIGHTNESS

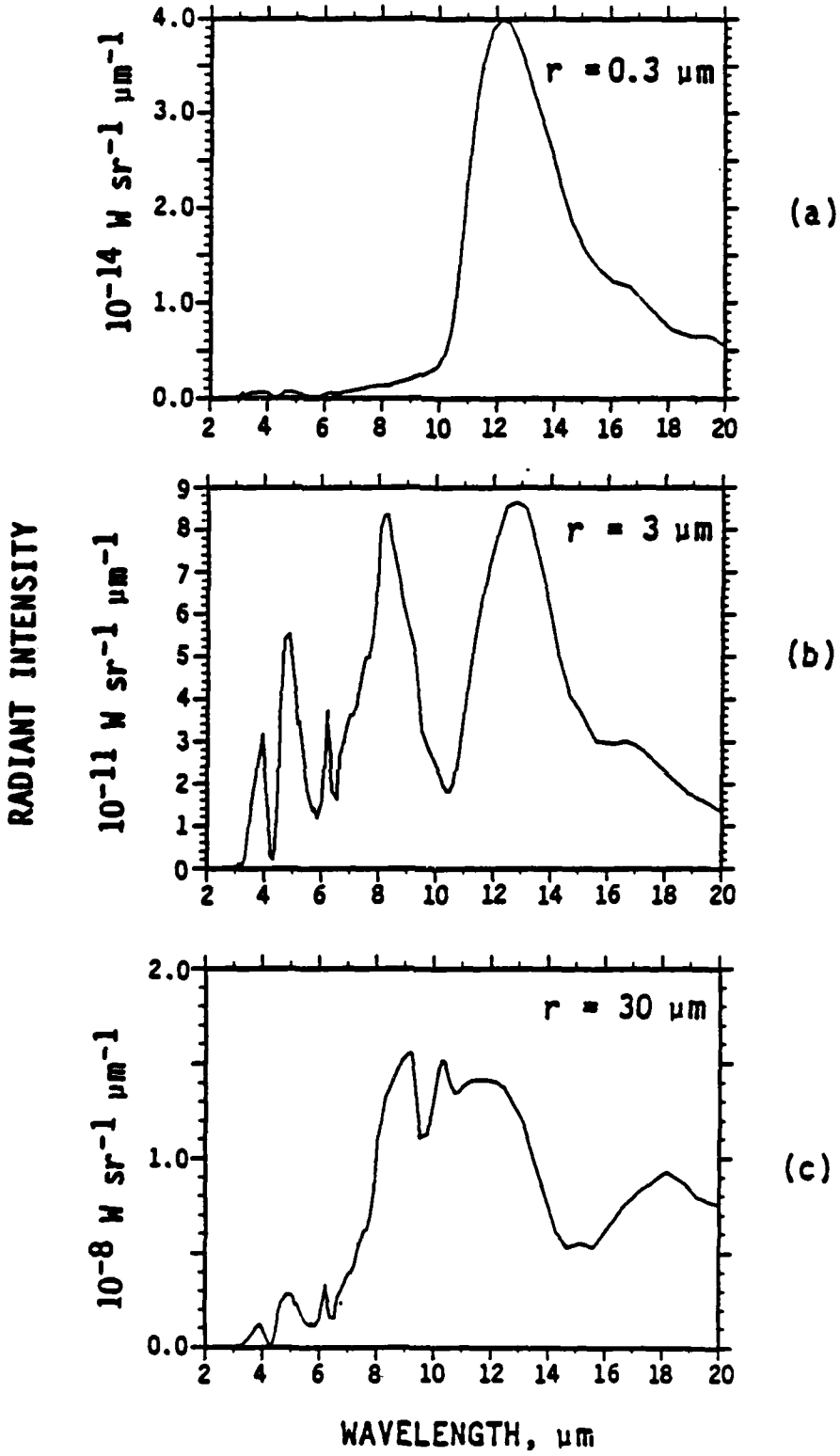

A-2087

SINGLE PARTICLE RADIANCE, W cm^{-2} sr^{-1} μm
(APERTURE AREA 100 cm^2)
NIGHT, TROPICAL EARTH

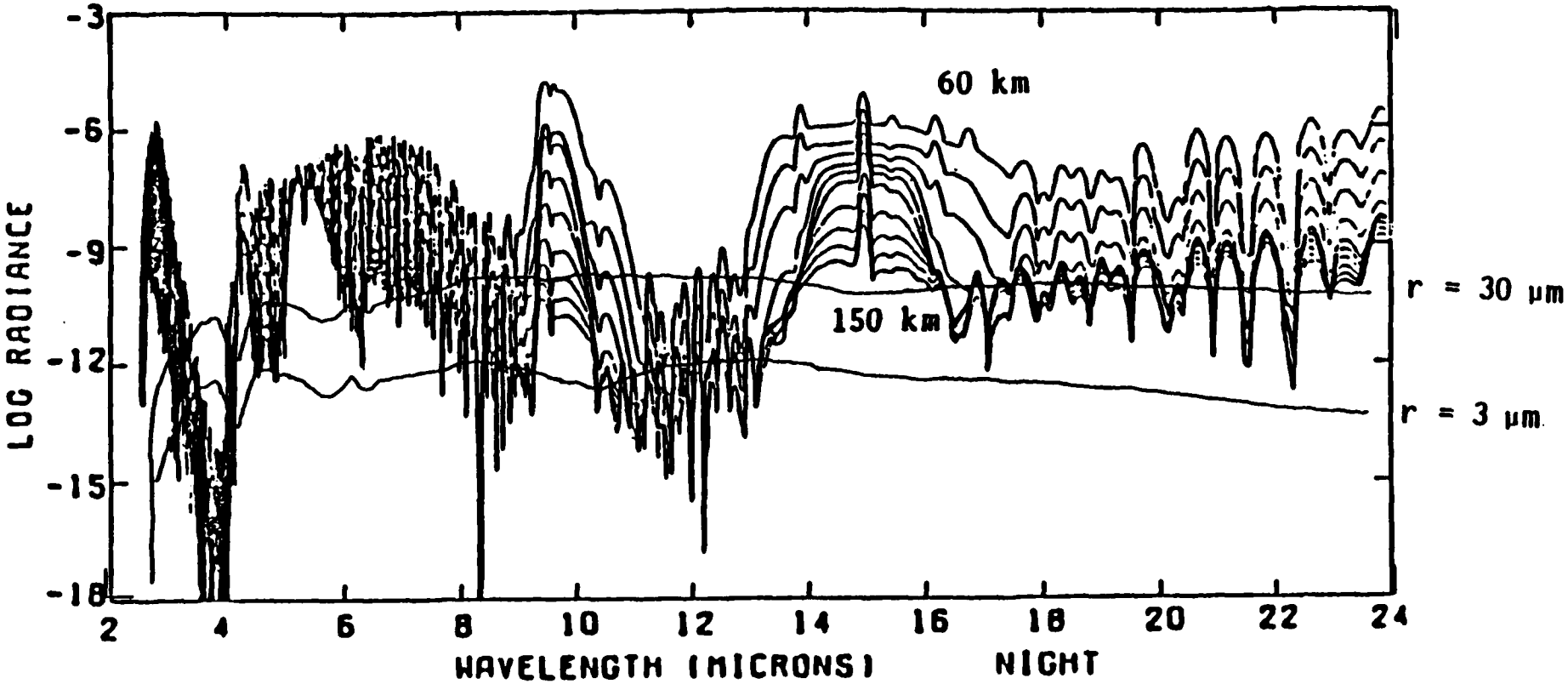

AFGL LIMB RADIANCE MODEL
W cm^{-2} sr^{-1} $μm^{-1}$

A-2089

SINGLE PARTICLE RADIANCE, W cm^{-2} sr^{-1} μm
(APERTURE AREA 100 cm^2)
SUNLIT, θ = 90°, TROPICAL EARTH

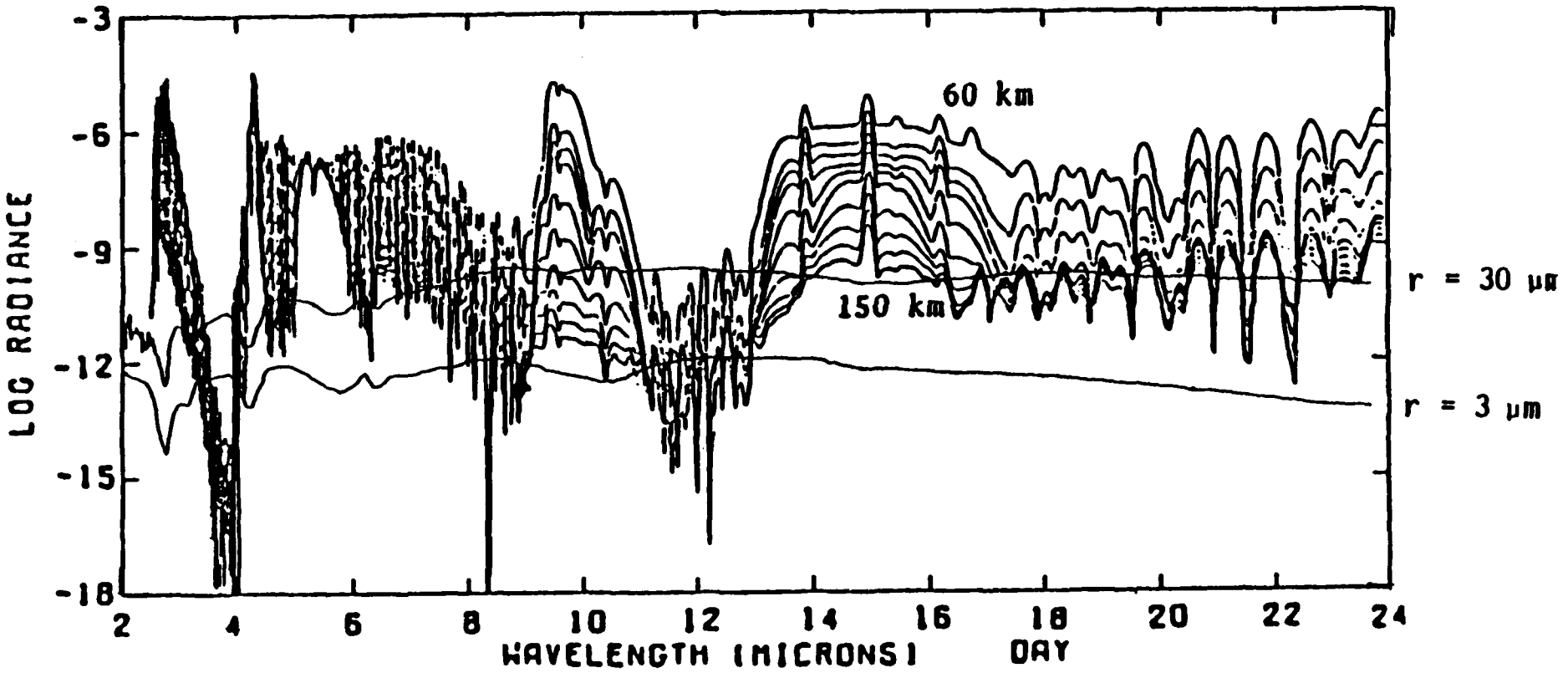

AFGL LIMB RADIANCE MODEL
W cm^{-2} sr^{-1} $μm^{-1}$

A-2088

EXTREMELY CRUDE CALCULATION

- TYPICAL PARTICLE 100 μm, MOVING 10°/s ACROSS FIELD OF VIEW
- TYPICALLY 3 PARTICLES OBSERVABLE IN PACS FOV UNDER PROPER ILLUMINATION CONDITIONS
- THUS EXPECT A 100 μm PARTICLE TO CROSS CIRRIS FOV AT LEAST ONCE EVERY 30 SECONDS DURING DATA ACQUISITION
  - 10^{-9} W/cm^{2}srμm AT 10 μm
- PARTICLE SIZE DISTRIBUTION UNKNOWN
  - CIRRIS PARTICLE THRESHOLD < 20 μm
  - INTRIGUING EFFECTS ON INTERFEROGRAMS

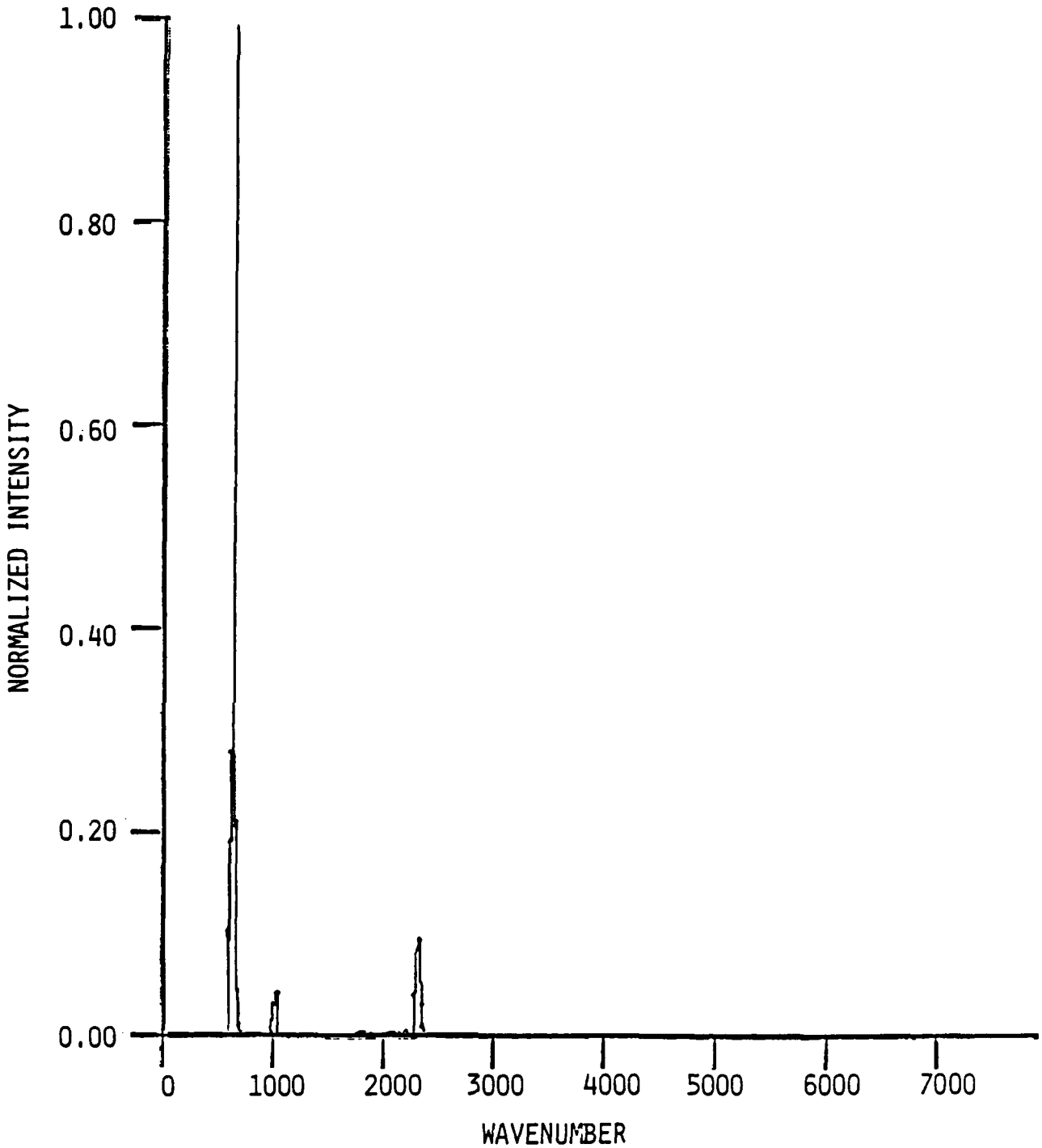

Fig. 3.1 Data from HIRIS mission - scan 23, payload altitude 97 km. Interferometer was sensitive only in the 400-2500 cm^{-1} region. Entire spectrum 0-7901 cm^{-1} is plotted to demonstrate particulate effects. Maximum intensity 1.12×10^{-8} W/cm^2 sr cm^{-1}.

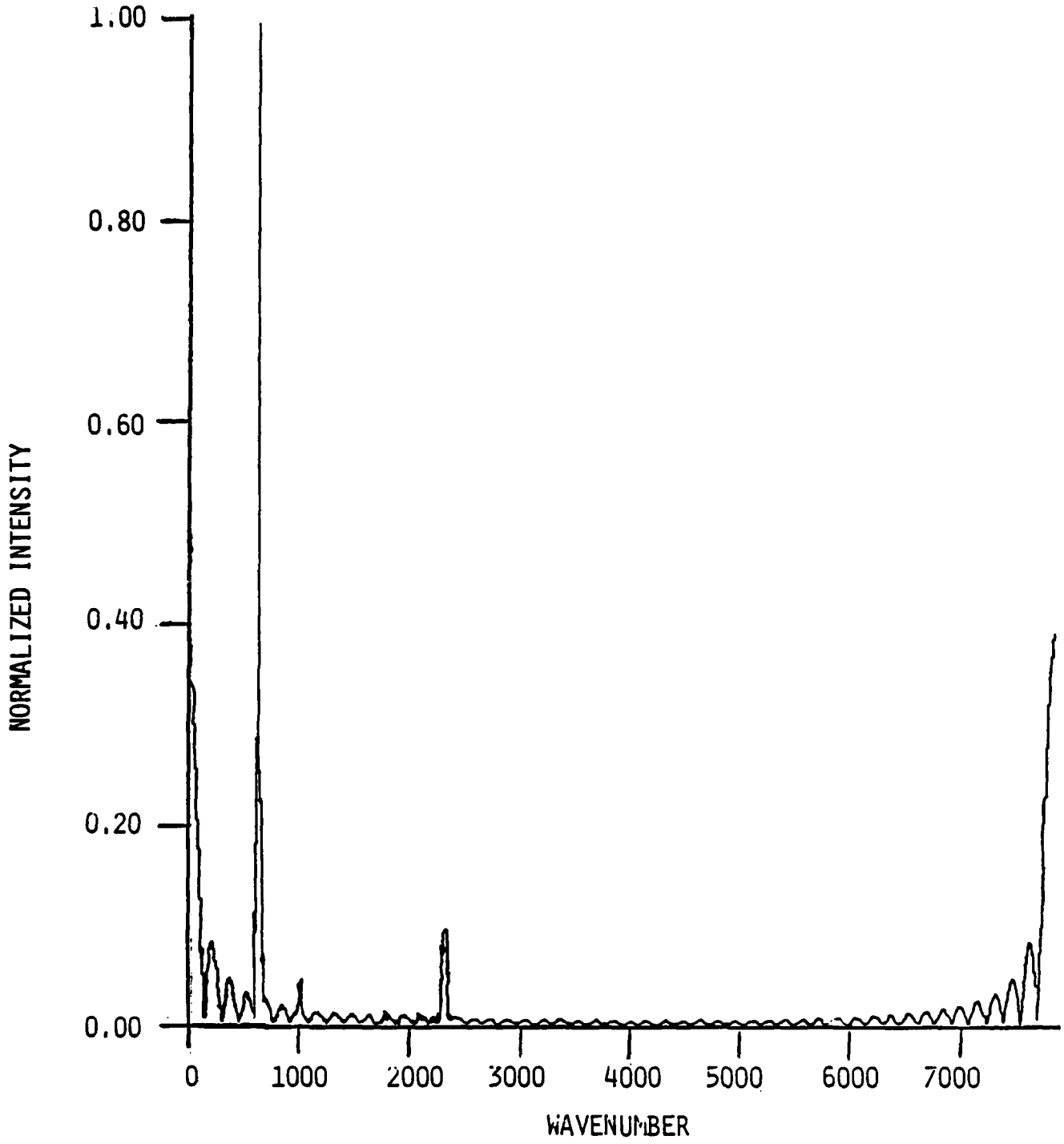

Fig. 3.3 Spectrum from sum of HIRIS scan 23 interferogram and standard additional radiance in first 50 points. $(\sin x/x)^2$ ringing is observed. Maximum intensity is 1.14×10^{-8} W/cm^2 sr cm^{-1}.

PACS - SUMMARY AND PRELIMINARY CONCLUSIONS

- FILM ANNOTATED WITH ATTITUDES AND EVENTS
  PARTICLE HISTOGRAMS } 3 MOS. AFTER DATA RECEIVED
- SOLAR ILLUMINATION ANGLE IS KEY PARAMETER
  - PARTICLES ALWAYS PRESENT; OBSERVABLE UNDER PROPER CONDITIONS
  - OBSERVED ON 1/3 OF TERMINATOR CROSSINGS
  - SELF EMISSION DOMINATE IR
- PACS THRESHOLD FOR PARTICLE DETECTION COMPARABLE TO CIRRIS 1A
- PARTICLES OBSERVED
  - ALL ACTIVITY SUPPRESSED
  - AFTER MANEUVERING (?)
  - AFTER PAYLOAD BAY DOORS OPERATED
  - DURING SATELLITE LAUNCH
  - DURING/AFTER WATER DUMPS (DECAY DEPENDS ON ATTITUDE?)
  - AFTER SUNRISE (THERMAL STRESSES?)

PACS - SUMMARY AND PRELIMINARY CONCLUSIONS (CONT.)

- FEW PARTICLES OBSERVED BY STROBE - MOSTLY BEYOND 6 FEET FROM PACS
- OBSERVED PARTICLES SHOULD HAVE RADIANCES COMPARABLE TO LIMB
- PARTICLES WILL HAVE INTERESTING EFFECTS ON INTERFEROGRAMS
  - ROTATIONS
  - CROSS FOV
  - SOME HAVE VERY LOW RELATIVE VELOCITY - PERSIST FOR MINUTES

APPENDIX N

The Particle Environment On-Orbit: Observations, Calculations, and Implications

Advances in Space Research, 7, 161-168 (1987), COSPAR XXVI (1986)

SR-274 is reproduced in its entirely.

THE PARTICLE ENVIRONMENT ON-ORBIT: OBSERVATIONS, CALCULATIONS, AND IMPLICATIONS

Byron David Green

Physical Sciences Inc.
Research Park, P.O. Box 3100
Andover, MA 01810, U.S.A.

ABSTRACT

The full potential for making remote observations from space free from atmospheric attenuations and distortions may not be realized due to the residual environment surrounding orbital experiments: particulates could overwhelm or severely complicate remote astronomical or atmospheric sounding observations. Small particles are lifted into space by the observatory and its carrier and take considerable time to evolve from surfaces. Single near-field particles have been observed which produce irradiance levels larger than the brightest stars and brighter than the emission from the entire earth limb airglow layer.

The existing data bases are reviewed including: 1) the low light level camera videotape data of STS-3 in which large persistent particles were observed; 2) the data from the stereo cameras which were part of the Induced Environmental Contamination Monitor pallet assembled by NASA Marshall - which is being analyzed to obtain particle number densities, trajectories, and decay times; and 3) data from the Particle Analysis Camera for Shuttle which was part of the HITCHHIKER pallet on a January 1986 Mission is current being analyzed to obtain decay rates and correlations with orbital activities. The implications for several other data bases such as the Infrared Telescope is also described.

The analysis of these spectrally broad band observations is further complicated by the nature of the particle's scattering of light. Depending on wavelength and particle size, the scattering of solar radiation or earth radiation, or particle self emission will dominate the optical signature. The scattering and emission from particulates will likely be highly structured as a function of wavelength. We present Mie scattering calculations for particle size distributions observed on-orbit. Finally, we assess the consequences of the observations and calculations on future space-based observations.

INTRODUCTION

The other articles in this issue have presented many facets of the on-orbit environment which will have deleterious effects on our ability to perform sensitive remote observations from orbital platforms. This paper deals with the particulate environment which is perhaps the most severe for astronomical observations. Since the first manned missions, particles have been observed under the proper illumination conditions. During Skylab, coronographic techniques were used to quantify the particulate environment./1/ A rough size distribution scaling as $r^{-3/2}$ was determined for particles down to micron sizes. Particles were observed even after the vehicle had been on-orbit for months.

There have also been many observations of particulates from the Shuttle. NASA, recognizing the potentially serious nature of the earlier observations, set design guidelines (CRDG) for the normal Shuttle operational environment as an average of less than one particle per orbit entering a 1.5×10^{-5} sr field of view along any line within 60 degrees of the -Z axis (out of bay), and this field-of-view should contain no discernible particles for 90 percent of the operational period. A discernable particle is a particle with diameter of 5 μm within a range of 10 km./2/ In order to determine their responsiveness to these self-imposed guidelines NASA included a pair of sensitive film cameras as part of the Induced Environment Contamination Monitor (IECM) payload assembled at Marshall Space Flight Center. The IECM pallet was manifested on the STS-2,-3,-4 and -9 (Spacelab 1) missions./2,3/ Their findings are discussed in the Observations sections. There are low light level television cameras mounted in the bay. On Mission STS-3, the Shuttle was oriented tail-to-sun so that particles in the bay could be very sensitively observed./4/ These results are also discussed in the Observations section. The Shuttle Induced

Atmosphere experiment was also on mission STS-3. J. Weinberg in another paper in this issue /5/ reports clear evidence of a blizzard of particles in his non-imaged radiometric data early in the mission. The polarization of the detected light indicated that the source was local scattering from particles and not galactic. The effects of this scatter are greatest in the red portion of the spectrum. He observed that the number of particles decreases as mission elapsed time passes. This latter finding is supported by the IECM camera data. The Infrared Telescope (IRT) was part of the Spacelab 2 mission in the summer of 1985. D. Koch and G. Fazio report their findings in another paper in this issue./6/ Their observations indicate the presence of a large number of particles (and even indicate particle rotations). Unfortunately the IECM pallet originally manifested to be aboard the Spacelab 2 mission was removed from the manifest only months before the flight and thus photographic data is not available to corroborate the IRT radiances. Another camera experiment was on STS-61C in January 1986. The Particle Analysis Cameras for Shuttle (PACS) acquired data throughout the mission. Their preliminary findings are described in the Observations section. In addition to the optical observations, other data exists regarding the particulate environment. Several other experiments on the IECM were sensitive to particles. These included the Passive Sample Array, the Optical Effects Module, the Temperature controlled Quartz Crystal Microbalances (TQCM), and an air sampling system. These experiments sample the particle environment during ascent, descent, and to some degree on orbit. Their results have been reported previously/2,3/. In addition JPL has flown a contamination monitoring package and TCQM's have been aboard several other missions. The Spacelab 1 mission TCQM results are discussed in the Observations section.

SOURCES OF PARTICLES

The particles observed on-orbit are believed to arise primarily from ground based processing. The orbiter processing facilities have been improved significantly with particulate counts being carefully monitored by passive techniques, such as witness arrays, at every stage of processing. The improvements have resulted in substantially less particulate loading (area coverage) on the arrays. In spite of these improvements it is still recommended that most sensitive payloads adopt protective measures against particles until safely on-orbit. Another major contamination period is during ascent when the payload bay venting could move particles around and down onto sensitive surfaces. Simultaneously, vibrations from the Solid Rocket Boosters and when the Shuttle goes transonic will act to redistribute particles. It has long been known that activites such as water dumps generate copious ice particles, but in the next section we report that a whole range of events such as crew activities and engine firings can shake loose or produce particles detectible to sensitive astronomical instruments. While on-orbit micrometeorites spall off substantial material as modeled by Barengoltz./7/ He predicted that formation of smaller particles down to 2 μm is favored. The reader interested in data from the passive collection techniques and ground processing facilities is referred to the detailed discussions and references in the Particulate Environment Section of ENVIRONET which has been compiled by Barengoltz./8/ A general review has also recently appeared./9/ One clear objective of the acquiring of a prelaunch and orbital observations database should be the development of a predictive model based on these data. This model may then be exercised to predict optimum observational periods or suggest key ameliorative procedures to be undertaken.

PARTICULATE OBSERVATIONS

The low light level television cameras observed large particles during STS-3 as previously reported by Maag, Barengoltz and Kuykendall./4/ They analyzed videotape data from the camera located in the forward part of the bay looking aft with a four degree field-of-view. With the tail blocking the sun, any particles in the bay or near the tail were observed from their forward scattering lobe. This configuration provides the most sensitive detection of particles. Particle distances from the camera were not known, but atmospheric drag was used to size/range particles. Because of the relative insensitivity of the camera only large particles could be detected even in the forward scattering configuration. Nevertheless, a large number of particles were detected. They were estimated to be in the mm-cm radius size range. Over 60 particles larger than 5 mm were observed.

Stu Clifton, Carl Benson, Edgar Miller, and Jerry Owens from NASA/Marshall have been analyzing the Camera/Photometer data from the IECM pallet /2,3/ which was on missions STS-2,-3,-4, and -9 (Spacelab 1). This experiment involved a pair of 16 mm cameras with 32 degree fields-of-view. Overlapping fields of view provided the stereo coverage necessary to determine particle position in three dimensions relative to the camera. From exposure time each particle's velocity vector can be determined and by assuming a emissivity/scattering efficiency, each particle's size can be determined from film exposure level and distance. The particle velocity vector determination was aided by use of a chopping shutter. An integrating photometer terminated the frame's exposure when sufficient radiance levels were achieved. Exposures up to 15s were achieved under the lowest light conditions. The experiment and their findings are described more fully in References /2,3/. The IECM was positioned in the rear of the bay near the centerline just below the sidewall rails

looking directly out of the bay (-Z axis). The cameras gathered data for the duration of the missions taking an exposure every 150s. Consequently there is over 300 hours of data on the particulate environment surrounding the Shuttle. Those researchers found that a number of orbital events give rise to particles including water dumps, engine firings occasionally, and payload bay door operations. In general the particle concentration drops with time on-orbit. This trend is shown in Figure 1 (from Reference /2/). The figure displays the results for the combined observations of STS-2, -3,-4, the early checkout missions. The percentage of frames having 10 or more particles drops below 10 percent of the time by the end of the first day on-orbit, while over two-thirds of the frames have no visible particles after the first day. On STS-9 a different behavior was observed, however, as shown in Figure 2 (from Reference /3/). After an initial decrease, greater than 50 percent of the frames have detectible particles for the duration of the mission. The persistance of particulates has been attributed to the presence of the complex Spacelab 1 payload and crew activities. Recently, Scialdone /10/ has noted a strong correlation of the bay thermal profile with observed particles loadings suggesting that thermal processes play a large role. The distribution of IECM camera frames showing various levels of particulates during Spacelab 1 is summarized in Table 1 (from Reference /3/). Frames around the time of obvious orbital activities have been excluded from the table and Figures 1 and 2.

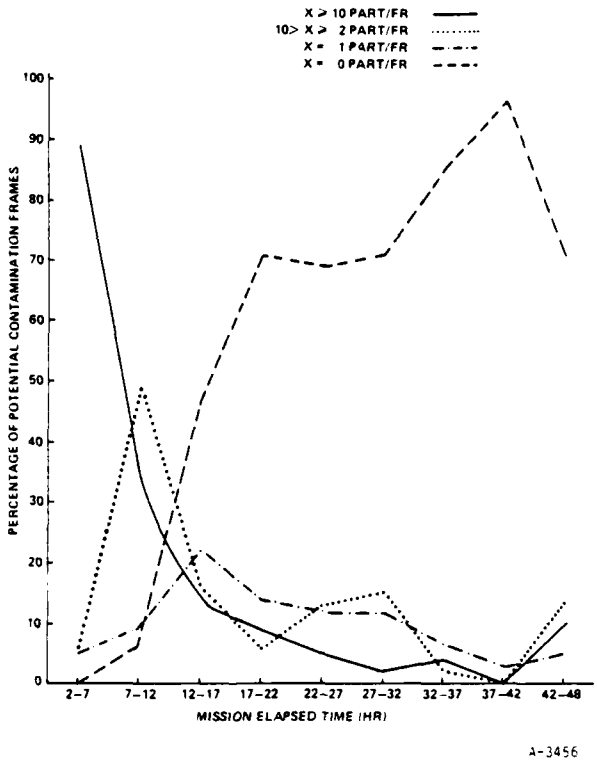

Fig. 1. IECM - STS-2,3,4 combined observations taken from NASA TM-82524, E.R. Miller, Ed. (Ref. /2/).

The clearing time of the local environment after a serious perturbation such as a water dump is of prime interest for astronomical observations. The sequential frames of IECM data after water dumps have been analyzed to provide the data of Figure 3. The number of particles in a 1s exposure is seen to decay expontentially after the dump with a characteristic e-folding time of about 5 min. The visible particle count drops to the pre-dump levels well within a half-hour of termination of the dump.

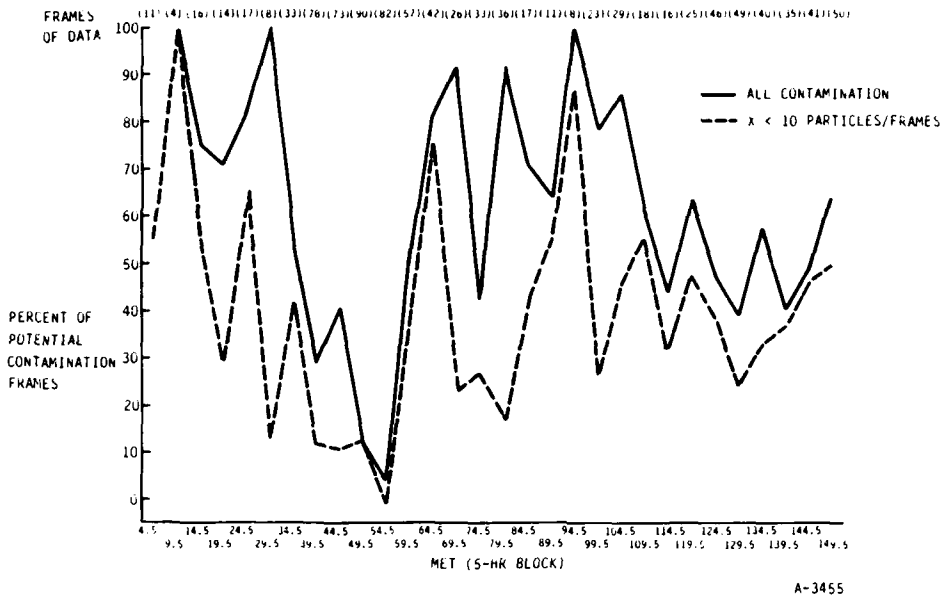

Fig. 2. IECM - Spacelab 1 observed contamination taken from NASA TM-86451, E.R. Miller, Ed. (Ref. /3/).

TABLE 1 STS-9 observed particle concentrations

Number of Particles per Frame	Number of Frames	Percentage of Potential Contamination Frames
X > 10	192	19 percent
10 > X > 2	179	17 percent
X = 1	142	14 percent
X = 0	515	50 percent
Total Contamination	513	50 percent

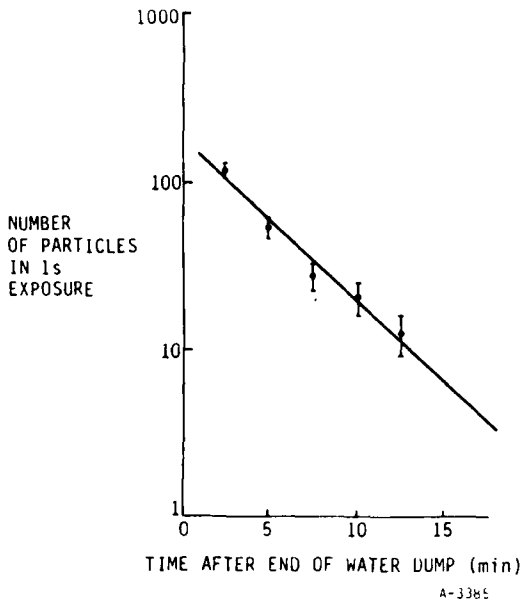

Fig. 3. NASA-IECM data for water dump decay

The IECM cameras have seen stars as faint as tenth visual magnitude; background levels of 10^{-13} solar brightness were achieved. Smaller particles which were undetectible, but were found by the TQCM (discussed below), could still interfere with sensitive astronomical observations looking for objects fainter than tenth magnitude. Computer-based algorithms for film analysis are now operational at NASA/MSFC. The film has been digitized. Particle positions, velocities and radii have been determined. Particles up to 300 μm have been observed.

Another interesting set of observations were acquired by the temperature controlled quartz crystal microbalances (TQCM) flown on the Spacelab 1 mission by McKeown (Faraday), Fountain and Cox (NASA/MSFC) and Peterson (Aerospace)./11/ Sensors were pointed along five directions (±X, ±Y, -Z). The sensor facing out of the bay (-Z) acquired the least mass indicating that collisional backscattering of particulates does not appear to be a significant process. The sensor facing Spacelab 1 gained the most

mass. Post-flight analysis of particulates found that most particles were in the 1-20 μm range, a size which is below the camera data threshold. This indicates that the cameras see only a small portion of the particles in the environment. The sources of the TQCM particulates were estimated via elemental analysis to be from ascent redistribution and solid rocket motor firings on-orbit. However, crew activity-generated particles must be substantial to explain the large accretion on the sensor facing Spacelab 1.

The Particle Analysis Cameras for Shuttle (PACS) experiment was on the recent STS-61-C mission in January of 1986. M. Ahmadjian of the Air Force Geophysics Laboratory was the principal investigator and K. Yates (also of AFGL) is responsible for data analysis. They have been assisted by B.D. Green of Physical Sciences Inc. H. Miranda of Epsilon Laboratories assembled the camera package, and D. Bunnell of Utah State University was responsible for payload integration into the HITCHHIKER pallet. The PACS experiment also consisted of a pair of cameras configured in stereo viewing geometry. The aim of this experiment was to quantify the particle environment throughout the mission, to use the particle trajectories to identify sources and to characterize particle generating events. PACS differed from the IECM cameras in that the exposure sequence was of fixed duration. There were four exposures in a sequence, each on a different frame of film. Exposure times were 0.3, 0.3, 1.0 and 2.5s during a 6.5s period. This sequence was repeated every 120s. Fast film (ASA2000) was used to compensate for shorter exposure durations. In addition a strobe light was incorporated into the package so that solar illumination would not entirely dominate viewing time -- permitting particles to be observed during orbital night.

PACS was part of the HITCHHIKER G-1 pallet (under the direction of T. Goldsmith of NASA/Goddard) which provided power, time keeping and telemetry. The flexibility and smooth operation of the HITCHHIKER pallet contributed greatly to the success of PACS. The STS 61-C mission was an excellent candidate mission for heavy particle loadings. The Columbia had been just refurbished and this represented its first flight in two years. Also the orbiter was exposed to several weeks of heavy rains while on the pad prior to launch. One of the cameras operated successfully throughout the six day mission. Data was acquired during 80 orbits and nearly 15,000 film frames were exposed.

We are currently in the process of correlating observations with events and attitudes. Preliminary results indicate that many frames exhibit no detectible particles and should provide clear fields for remote observations. However, particles have been observed on many frames. At present only stars as faint as sixth visible magnitude have been identified, but we are in the process of using digital image enhancement techniques to increase our sensitivity. Particles above 25-30 μm should be detectible. Again both water dumps and thruster events have been observed to cause particle generation. The PACS experiment observed the decay in particles after a water dump to have two components: a very prompt non-exponential decay followed by a slower return to baseline levels. Particles were observed whose intensities periodically varied during an exposure suggesting rapid rotation of non-spherical particles. Additionally there appears to be a correlation of number of detectible particulates with orbital sunrise. This may be due to thermal stresses. These observations are only preliminary and are being carefully verified by a more thorough analysis at present.

RADIANCE CALCULATIONS

From the above observations it is clear that particles are visually very significant and could hamper the observation of faint astronomical objects. In order to quantify this statement, Mie scattering calculations were undertaken by W.T. Rawlins of PSI to systematically assess the impact of radiance and scattering of smaller particles on more sensitive instruments and on measurements in other spectral bandpasses. The total radiant intensity from a particle has three major components: emission, solar scattering and earthshine scattering as governed by the complex index of refraction and viewing geometry. For these calculations we assumed that ice would be the major scattering constituent and that the particles were spherical. The TQCM and camera data indicate that these assumptions are certainly not always valid. However these simplifying assumptions make the problem more tractable and permit first pass scoping calculations. Ice has highly structured indices of refraction across the wavelength region of interest as shown in Figure 4 (from /12/). The assumption of blackbody or grey body behavior would cause for larger errors than the assumptions above. In addition solar scattering is highly angle dependent as shown in Figure 5 (from /13/). The forward lobe ($\theta < 40°$) permits the most sensitive particle detection as employed in the "snowflake" study./4/ For example a 3 μm radius particle at 30° solar scattering angle will be as detectible as a 30 μm particle for a 90° scattering angle. The structure with scattering angle is mathematically rigorous and is not "noise." Infrared astronomical observations such as the IRT discussed in this issue /6/, will see particles dominantly from their self-emission, although there will still be day/night, particle size, and latitude variations as shown in Figure 6. In that figure (from /13/)

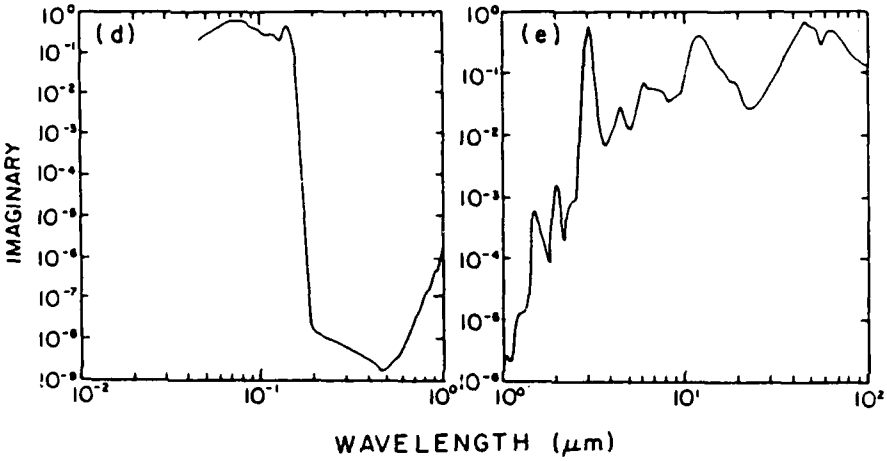

Fig. 4. Highly-structured imaginary component of index of refraction for ice for wavelengths between the vacuum ultraviolet and far infrared (from /12/).

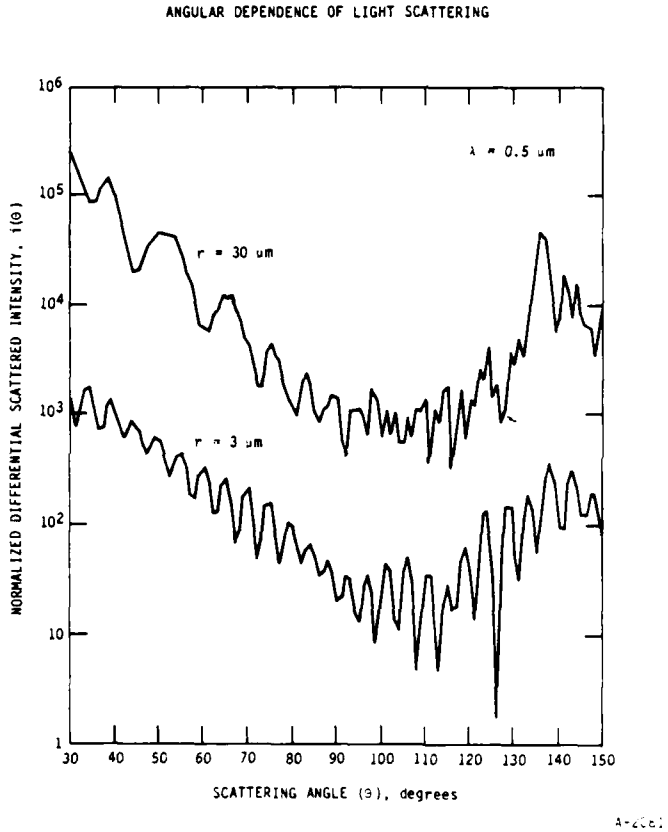

Fig. 5. Angular dependence of light scattering for two different size spherical particles of ice (from /13/).

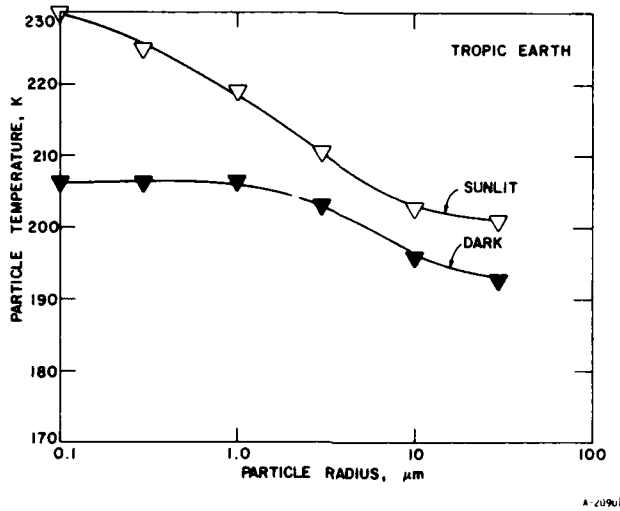

Fig. 6. Steady-state ice particle temperatures (from /13/).

the steady state temperature achieved by ice particles is plotted as a function of size and illumination (solar, earth) conditions. Due to the structured nature of the complex index of refraction, the infrared emission spectrum will be highly structured and also varying with particle size as shown in Figure 7. This should present an interesting challenge for analysis of infrared data.

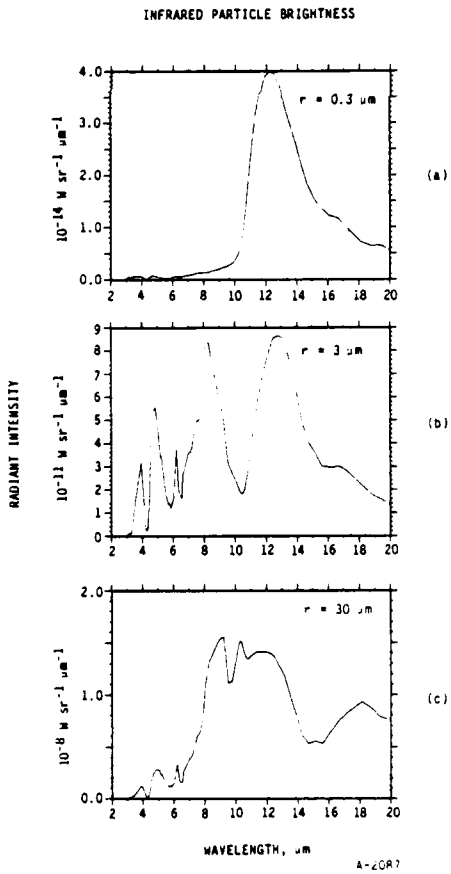

Fig. 7. Infrared particle brightness calculated for three different size particles. Note exponents of intensity (from /13/).

SUMMARY

For visible particulate observations, solar illumination angle is the key parameter. Particles appear to *be often present*, but are observable only under proper illumination conditions. Infrared observations will provide a clearer test of the shuttle particulate environment. Particles have been observed after orbital maneuvers and payload bay door operations, during and after water dumps, after sunrise and even occasionally during quiescent "observational" periods. The observed particle environment is highly variable. Particles have been observed which are brighter than any star in the visible.

Accurate diagnosis of the optical environment surrounding the shuttle will occur as existing databases are analyzed and the insight gained is used to plan future experiments. The next generation of experiments already planned include: the Interim Operational Contamination Monitor (from Jet Propulsion Laboratory) which utilizes compartments to capture particles during ascent, orbital trimming, and even on-orbit; the Ascent Particle Monitor (from Martin Marietta); and a reflight of the PACS experiment with minor improvements to gain sensitivity. Only with an increased understanding of the particulate sources on-orbit can remedial actions be suggested so that future astronomical observation payloads are not constrained to be particulate detection experiments.

ACKNOWLEDGEMENTS

The author gratefully acknowledges many useful discussions with Stu Clifton and Edgar Miller of NASA/Marshall and with Jack Barengoltz of JPL. Terry Rawlins and Catherine White of PSI also assisted with data reduction and modeling.

This review and the meeting presentation were supported by Physical Sciences Inc. internal research funds.

REFERENCES

1. D.W. Scheurman, D.E. Beeson, and F. Giovane, Coronagraphic technique to infer the nature of the Skylab particulate environment, Appl. Optics 16, 1591-1597 (1977)

2. E.R. Miller, ed., STS-2,-3,-4 induced environmental contamination monitor (IECM) summary report, NASA Tech. Memo. 82524, NASA/Marshall Space Flight Center, Alabama (Feb. 1983)

3. E.R. Miller, ed., induced environment contamination monitor - preliminary results for the Spacelab 1 flight, NASA Tech. Memo. 86461, NASA/MSFC, Alabama (Aug. 1984)

4. C. Maag, J. Barengoltz, and F. Kuykendall, STS-3 "snow flake" study, A291-A294 in The Shuttle Environment Workshop, J. Lehmann, org. (Feb. 1983)

5. J. Weinberg, Optical observations from the Space Shuttle, this issue

6. D.G. Koch, Infrared observations from the Space Shuttle flight 51-F, this issue

7. J. Barengoltz, Particulate release rates from Shuttle orbiter surfaces due to meteoroid impact, J. Spacecraft 17, #1, 58-62 (1980)

8. J. Barengoltz, ed., The particulate environment around Shuttle, panel report (Section 10) located on ENVIRONET computerized database operated by NASA/Goddard Space Flight Center

9. B.D. Green, G.E. Caledonia, and T.D. Wilkerson, The Shuttle environment: gases, particles and glow, J. Spacecraft 22, #5, 500-511 (1985)

10. J.J. Scialdone, Particulate contaminant relocation during shuttle ascent, NASA Tech. Memo. 87794, NASA/Goddard Space Flight Center, Maryland (June 1986)

11. D. McKeown, J.A. Fountain, V.H. Cox, and R.V. Peterson, Analysis of TQCM surface contamination adsorbed during the Spacelab 1 mission, AIAA paper 85-7008, 108-115 in AIAA Shuttle Environment and Operations II Conference Proceedings, Houston, TX (Nov. 1985)

12. S.G. Warren, Optical constants of ice from the ultraviolet to the microwave, Appl. Optics 23, #8, 1206-1225 (1984)

13. W.T. Rawlins and B.D. Green, Spectral signatures of micron-sized particles in the Shuttle optical environment, submitted to Appl. Optics (1986)

APPENDIX O

The Particulate Environment Around the Shuttle as Determined by the PACS Experiment

Paper 777 01 SPIE Contamination Effects Conference (1987)

PSI-139/SR-298 reproduced in its entirety.

The particulate environment around the shuttle as determined by the PACS experiment

B. David Green

Physical Sciences Inc., Research Park, P.O. Box 3100, Andover, MA 01810

G. Kenneth Yates and Mark Ahmadjian Air Force Geophysics Laboratory, Hanscom AFB, MA 01731

Henry Miranda, Miranda Laboratories, 1 DeAngelo Drive, Bedford, MA 01730

Abstract

The Particle Analysis Cameras for Shuttle (PACS) Experiment was flown on Mission STS61C (Columbia) in January 1986. This experiment involved a pair of cameras in a stereo viewing configuration and an associated strobe light flash to permit particle observation during the entire orbit. Although only one camera functioned properly, significant trends and particle counts were still obtained from the film data. We report here the preliminary analysis and conclusions from that mission.

Introduction and background

Ever since the first manned missions in earth orbit, there have been visual reports of activity-induced particles surrounding the spacecraft. During the Mercury through Apollo missions many unusual particle observations were reported. The sensitivity to particle detection however strongly depends upon illumination geometry, and quantification of the observations required more controlled observations. Both video and coronagraphic investigations were undertaken on Skylab in 1973.[1-3] Particles with radii as small as 5 μm were detected. Our analysis of their data has revealed that the numerous particles observed had a size distribution which followed a rough $r^{-1.5}$ dependence, i.e., on average there would be 30 times as many 5 μm radius particles as 50 μm radius particles. Moreover the particle velocities observed were in the 0.1 to 20 m/s range with the larger particles generally moving more slowly. These particles were observed after Skylab had been on-orbit for several months. Because the Shuttle Orbiter was to act as an orbital observation platform carrying astronomical and aeronomical experiments into orbit for week long observation missions, both NASA and the Air Force realized that the local particulate environment could seriously compromise the ability to make remote observations.

From the inception of the Shuttle program, environmental optical quality goals were set by a NASA Panel. The Contamination Requirement Design Group (CRDG) guidelines[4] specified an acceptable particulate contamination level on-orbit for the normal Shuttle operational environment as an average of less than one particle per orbit entering a 1.5×10^{-5} sr field of view along any line within 60 deg of the -Z axis (out of bay), and this field-of-view should contain no discernible particles for 90 percent of the operational period. A discernible particle is a particle with diameter of 5 μm within a range of 10 km.

Contamination below this level was generally deemed as undetectable or as an acceptable nuisance level Recent advances in detector technology (especially in the infrared) may require more stringent future guidelines for Space Station or drive the most sensitive experiments off large space structures onto free flying platforms. The particles observed on-orbit are believed to arise primarily from ground based processing. The orbiter processing facilities have been improved significantly with particulate counts being carefully monitored by passive techniques, such as witness arrays, at every stage of processing. The improvements have resulted in substantially less particulate loading (area coverage) on the arrays. In spite of these improvements it is still recommended that most sensitive payloads adopt protective measures against particles until safely on-orbit. Another major contamination period is during ascent when the payload bay venting could move particles around and down onto sensitive surfaces. Simultaneously, vibrations from the Solid Rocket Boosters and when the Shuttle goes transonic will act to redistribute particles. It has long been known that activities such as water dumps generate copious ice particles, but in this paper we report that a whole range of events such as crew activities and engine firings can shake loose or produce particles detectible to sensitive astronomical instruments. While on-orbit, micrometeorites may spall off material as modeled by Barengoltz.[5] He predicted that formation of smaller particles down to 2 μm is favored. Data from the passive collection techniques and ground processing facilities is carefully reviewed in the Particulate Environment Section of ENVIRONET which has been compiled by Barengoltz.[6] A general review of this environment has also recently appeared.[7] One clear objective of the acquiring of a prelaunch and orbital observations database should be the development of a predictive model.

based on these data. This model may then be exercised to predict optimum observational periods or suggest key ameliorative procedures to be undertaken.

In order to verify that CRDG Guidelines were met a pair of cameras in a stereo viewing geometry were included as part of the Induced Environment Contamination Monitor (IECM) diagnostic pallet which was manifested on the earliest missions (STS2,3,4) and on the Spacelab 1 Mission (STS9). This pallet was assembled under the guidance of Edgar Miller of NASA/ Marshall Space Flight Center. The pallet and its results have been reported elsewhere[4,8] and will only be briefly described here. This experiment involved a pair of 16 mm cameras with 32 deg fields-of-view. Overlapping fields of view provided the stereo coverage necessary to determine particle position in three dimensions relative to the camera. From exposure time each particle's velocity vector can be determined and by assuming an emissivity/ scattering efficiency, each particle's size can be determined from film exposure level and distance. The particle velocity vector determination was aided by use of a chopping shutter. An integrating photometer terminated the frame's exposure when sufficient radiance levels were achieved. Exposures up to 15s were achieved under the lowest light conditions. The IECM was positioned in the rear of the bay near the centerline just below the sidewall rails looking directly out of the bay. Based on the film exposure curves and intensity of stars observed (10th magnitude visual) they have estimated a particle detection threshold for their Spacelab 1 experiment as 28 μm and slightly better for the early STS2,3,4 observations. This compares with a preflight estimate that a 25 μm ice particle within a range of 30m traveling at 3 m/s (observed at 60° to 90° solar illumination angle) would produce an image density 5 percent above the fog level.[9]

In addition to film camera data there have been other observations of particles in the shuttle environment. The low light level television cameras observed large particles during STS-3 as previously reported by Maag, Barengoltz and Kuykendall.[10] They analyzed videotape data from the camera located in the forward part of the bay looking aft with a four degree field-of-view. With the tail blocking the sun, any particles in the bay or near the tail were observed from their forward scattering lobe. This configuration provides the most sensitive detection of particles. Particle distances from the camera were not known, but atmospheric drag was used to size/range particles. Because of the relative insensitivity of the camera only large particles could be detected even in the forward scattering configuration. Nevertheless, a large number of particles were detected. They were estimated to be in the mm-cm radius size range. Over 60 particles larger than 5 mm were observed.

Another interesting set of observations were acquired by the temperature controlled quartz crystal microbalances (TQCM) flown on the Spacelab 1 mission by McKeown, Fountain and Cox, and Peterson.[11] Sensors were pointed along five directions (±X, ±Y, -Z). The sensor facing out of the bay (-Z) acquired the least mass indicating that collisional backscattering of particulates does not appear to be a significant process. The sensor facing Spacelab 1 gained the most mass. Post-flight analysis of particulates found that most particles were in the 1 to 20 μm range, a size which is below the camera data threshold. This indicates that the cameras see only a small portion of the particles in the environment. The sources of the TQCM particulates were estimated via elemental analysis to be from ascent redistribution and solid rocket motor firings on-orbit. However, crew activity-generated particles must be substantial to explain the large accretion on the sensor facing Spacelab 1.

The Air Force realized that particulates could interfere with remote atmospheric observations of the chemical processes occurring in the thermosphere and mesosphere which are planned from the Shuttle. In order to assess the magnitude and time scales for this interference the Particle Analysis Cameras for Shuttle (PACS) experiment was developed. As for the IECM cameras, the PACS cameras were oriented so that their fields-of-view overlapped. Analysis of the film images from the cameras would have permitted position and velocity determination. An error analysis of the digitization and correlation procedure performed by EKTRON indicated accurate determinations of position and velocity components at the few percent level were attainable from film data.[12] More importantly the particle's scattered intensity and persistence after orbital events could be accurately monitored from the film data.

The PACS cameras differed from the IECM cameras in several aspects, however. Film exposures were taken in sets of four. This exposure sequence was repeated every 120s. In order to detect small particles, ASA2000 negative film was used and the cameras were focused at 25m rather than infinity. This distance represents a compromise between enhanced near field sensitivity to particles and loss of the far field stars which allowed for orientiation and in-flight calibration. (For the 25m focal distance stars were observed as small, well-defined circles. Because the stellar irradiance was spread over several film resolution elements, only stars brighter than seventh magnitude have been observed in the PACS data.) A major new feature of the PACS experiments was the use of a strobed flashlamp to illuminate the closest particles throughout the entire orbit. Because scattered solar illumination (not thermal emission or earthshine) permits particle detection in the visible, previous observations were limited to the sunlit part of the orbit.

The objectives of the PACS experiment were to: 1) quantify the particulate sizes and trajectories so as to identify source locations; 2) determine the severity of events such as dumps, purges, maneuvers, and various operations and measure their decay (clearing) times. In the next section we describe the PACS experimental design and mission performance. In the following section we discuss post flight data reduction and analysis and present observed trends in particulate populations and interesting observations. We also compare our findings with the other orbital observations. Conclusions, recommendations and future plans are presented in the last section.

Experiment design and mission performance

The components of the PACS experiment were designed and assembled at Epsilon Laboratories. The film cameras used were manufactured by Photo-Sonics, Inc. These 16 mm motion picture cameras were modified to operate in a stepping mode where film was advanced a single frame after each shuttered exposure. An electronic controller unit was used to synchronize shutter, film advance, and strobe unit operation. The timing sequence for the exposure and strobe sequence is as follows: 0.0 to 0.3s, first frame exposure; 0.3 to 1.0s shutter closed, film is advanced one frame; 1.0 to 1.3s, second frame exposure; film advances; 2.0 to 3.0s, third frame exposure with strobe light pulses at beginning and end of exposure; film advances; 3.7 to 6.4s, long fourth frame exposure followed by film advance. This sequence was chosen so that smaller particles could be detected during longer exposures, while velocity information would be obtained by correlating particles observed on sequential frames. The cameras were mounted in sealed enclosures which maintained nearly atmospheric pressure for the entire week-long mission. The cameras and strobe were mounted on a frame in a stereoscopic configuration - with all elements coplanar as shown in Figure 1. Each camera has a 17° x 24° field of view and is canted 2.5° toward the strobe unit optical axis. In this geometry, the stereo overlapping zone begins within a meter of the cameras. The fields of view are shown schematically in Figure 2. The lenses are 25 mm, f/0.95 and were carefully focused at 25m distance and locked into position.

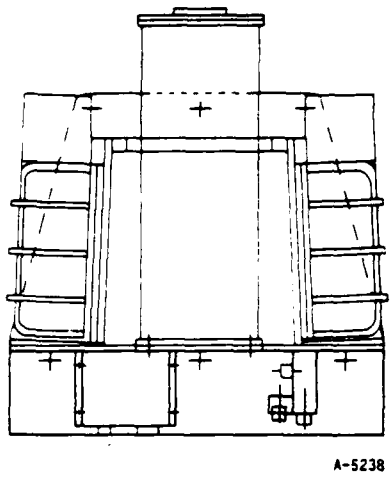

Figure 1. Two Cameras and Strobe Assembled to Form PACS Experiment

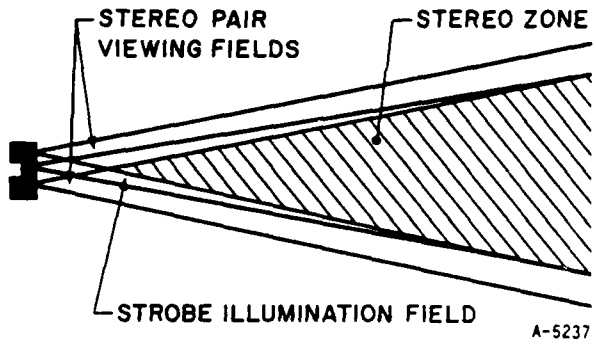

Figure 2. Diagram of PACS Fields of View

This focusing permitted factor of two more sensitive detection of the particles in the near field. Thresholds in the 25 μm range were calculated. The focus at 25m also resulted in a blurring of the stars. The data was adequate to permit constellations to be observed and thus the orientation to be determined. The film magazine for each camera contained 450 ft of Kodak 2484 PAN film. This extremely high speed (ASA2000) negative film is well suited to low light level photography. Due to its already grainy nature, further push processing to ASA6000 was not performed. Elements in the optical train and film responsivity limit the bandpass of these observations to the spectral region 400 to 550 nm.

The 25W Xenon EG&G strobe (approximately a 12,000 K blackbody) was located in a high efficiency optical configuration using a parabolic reflector to refocus the strobe 6 in. beyond the vacuum enclosure glass window. During the one second film exposure, the strobe is pulsed twice. Each pulse has about 50 $\mu J/cm^2$ of visible light which is delivered on axis 2m from the face of the cameras. The pulses are about 200 μs in duration. The illumination

pattern is peaked on axis and falls off linearly from the optical axis (half intensity points at 6 deg half angle). This means that even if a particle is moving faster than 3 m/s the reflected strobe illumination reaching a film grain will exceed the reflected solar illumination for particles within 2m of the cameras. Final testing and integration of the PACS experiment were performed by Dave Bunnell of Utah State University.[13]

PACS was configured to be a Hitchhiker-type payload of opportunity, and participated in the first Hitchhiker-G mission (HHG-1). Coordinated by NASA/Goddard, Hitchhiker payloads are provided with power by the orbiter and have downlink telemetry. A timing signal is also provided to the payload. The Mission Elapsed Time (MET) was optically encoded on the film margins facilitating analysis. The PACS experiment was largely self-contained, with the PACS microprocessor-controlling exposure and other routine operations. The Shuttle payload specialist had the ability to disable the strobe during observational periods of other experiments.

The extremely fast film restricted the desired operating temperature range. The Hitchhiker structural plate is maintained in the operational range of 0° to 30°C by means of resistance heaters. The cameras were thermally coupled to this plate. To further ensure thermal stability the PACS experiment was enclosed in a multi-layer insulation blanket to minimize responses to thermal cycling during bay-to-sun and bay-to-space periods.

During mid-1985 the PACS experiment was integrated onto the HHG-1 pallet which was placed on-board the Columbia along the starboard side wall of the bay, forward in bay position two, 2m behind the rear cabin wall, high in the bay - above the side wall. The PACS experiment is shown mounted on the orbiter Columbia in Figure 3. The Columbia had just undergone a substantial refurbishment taking two years. Unfortunately the launch was delayed for several weeks due to inclement weather including heavy rains while on the launch pad. Thus this mission was likely to have a larger than representative contamination environment. Liftoff occurred at 6:55 a.m. (EST) on 12 January 1986. A nearly circular orbit of 290 km altitude was achieved at 28° inclination. After orbit stabilization and opening the payload bay doors, PACS was turned on at 3 hours 30 min mission elapsed time (day 0/3:30 MET). Initial indications were that temperature and power consumption and strobe power transients were as expected. Shortly however the shutter monitor located on camera 1 stopped indicating movement. With the assistance of NASA personnel at the Hitchhiker command center several tests were performed and diagnostic information retrieved from the Orbiter downlinked housekeeping data file. The experiment was turned off and restarted with no marked improvement in performance. Rather than discontinue operation of the experiment we elected to ignore the shutter monitor. Consequently during the rest of the mission careful notes were taken on Shuttle operations and attitudes. These proved invaluable in the post-flight analysis, highlighting critical data to be examined more carefully once the Orbiter Operations Ancilliary Data Tape containing positions and attitudes became available several months later. During the last days of the mission three attempts were made to land in Florida rather than California. Each time the PACS Experiment was turned off and the payload bay doors were closed. The weather remained perverse and the Columbia landed at Edwards Air Force Base at 5:59 a.m. PST on 18 January 1986.

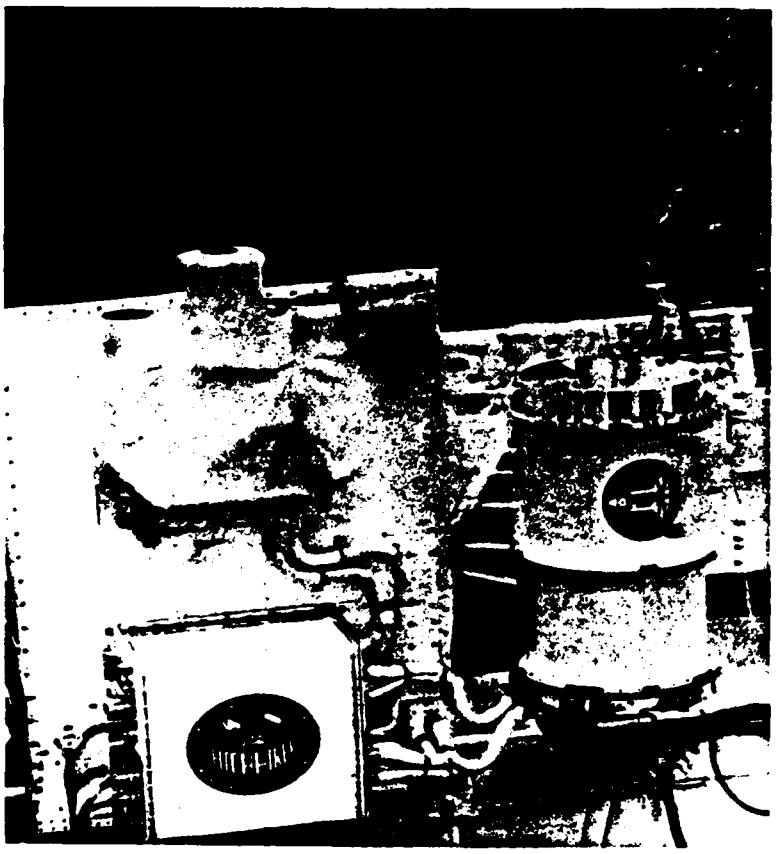

Figure 3. PACS Camera Experiment Mounted on Hitchhiker Pallet During Mission STS 61-C

Several significant events occurred during the six day mission. A 12,000 lb RCA TV satellite was launched at 0/9:32 MET (the first day of the mission at 9 hours 32 min). There were five water dumps, and a variety of attitudes were used including passive thermal control and several different inertial attitudes for comet Halley and astronomical missions. The measurement period of greatest interest to PACS occurred on the third day of the mission. Columbia traveled an entire orbit with the bay facing deep space with all activities suppressed (including thruster firings) then traveled another orbit in the gravity gradient attitude (nose to earth) with the bay facing the wake direction again with all activities suppressed. These periods should be representative of the best observational conditions achievable in the bay of the orbiter.

Access to the film canisters was provided 10 days after landing. Inspection revealed that the film in camera 1 had jammed from the start. Camera 2 recorded data during the entire mission exposuring over 400 ft of film. The film was developed by the Aerospace Corporation. Several copies were made and analysis began 16 days after touchdown. In total 14,788 frames of film data were acquired, covering parts of 83 orbits during every day of the mission.

Data analysis

While we were at Hitchhiker Control Center during the mission we gathered a great amount of available data on Shuttle attitude, sun angles, velocity vector, earth coordinates and the mission timeline. We did this in response to previous reports of difficulty in obtaining such information after the mission. The staff at the Control Center (NASA and its associated contractors) were extremely helpful, providing a wealth of information and assistance We made extensive use of the Shuttle Ground System Attitude display which provided Shuttle position and orientation updates several times a minute. This data permitted us to begin understanding the PACS data as soon as the film reached PSI. The detailed Orbiter Ancilliary Data Tape became available approximately six months later and proved useful in verifying the preliminary analysis.

Confronted with a massive film data base, after assigning orbital periods, we categorized the frames into earth viewing, sky viewing, overexposed, and those containing obvious particles. Overexposure resulted both from having the sun too near the field-of-view of the cameras and from viewing the sunlit earth. Using the binary encoded mission elapsed time (MET) display and the mission timeline we quickly reconciled the film display with the attitude information. Figure 4 shows a typical frame of the negative film data with a 2.7s exposure taken during the first day of the mission at 22:45 MET. The camera is looking back into the wake and observes the pre-dawn city lights of Florida, the earth limb, the tenuous hydroxyl airglow layer at ~90 km, and stars in the constellation Orion. By the time the next exposure sequence had started two minutes later, the orbiter had crossed the terminator and was in sunlight while the earth below remained in darkness. Figure 5 shows data in this sequence. Solar-illuminated particles have appeared in the near field environment and rival the rest of the scene in brightness. The particles are being observed in the backscattering lobe.

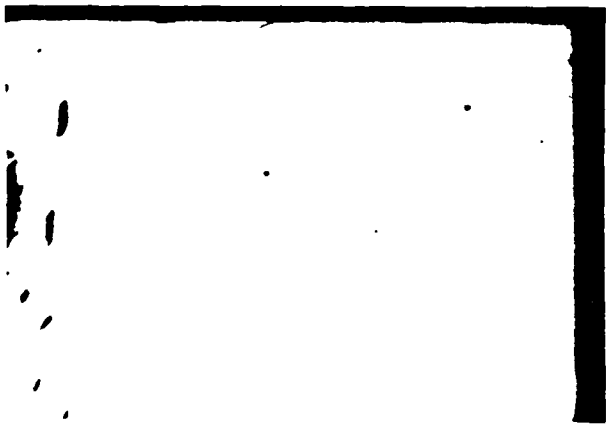

Figure 4. Exposure Taken at 0/22:45 MET Just Before Sunrise

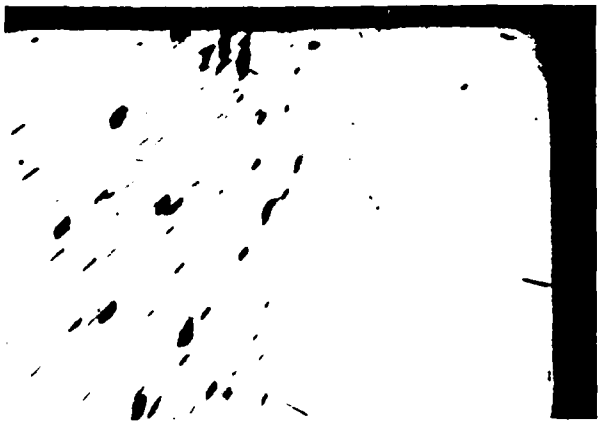

Figure 5. Frame Taken Two Minutes After Figure 4. Shuttle has moved into sunlight and particles are observed.

Terminator crossings (sunrises, sunsets) provide optimal detection conditions for particulates. The fraction of film frames at terminator crossings in which particles were detected is plotted in Figure 6. Although particles were observed very often during the first day on-orbit, there appears to be a marked decrease in their occurrence with time on-orbit. By the end of the six day mission less than 25 percent of the terminator crossings have any detectable particles in any frame. The anomalously large value on day three may be due in part to the orbit attitude. The Shuttle spent most of day three in Passive Thermal Control (rotisserie) attitude which sequentially exposes most surfaces to the sun. We believe this generates particles due to local thermal expansions and flexing. This phenomenon will be discussed more fully below.

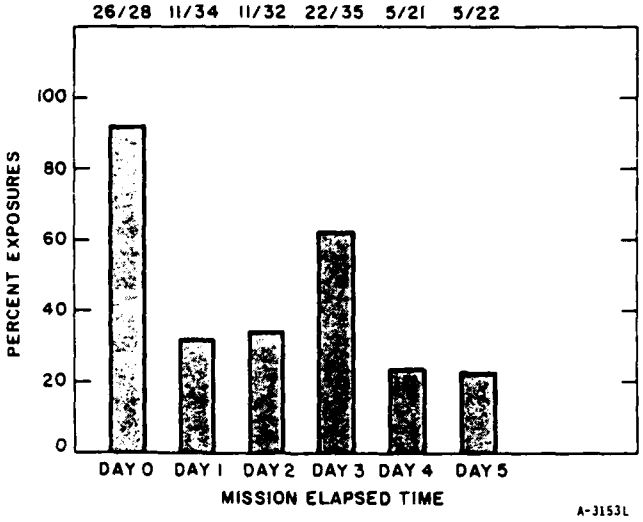

Figure 6. Fraction of Film Exposures Having Particles at Sunrise/Sunset

The scattered intensity of each particle is an extremely sensitive function of scattering angle and also depends on particle shape, particle composition and particle size.[14] Quantitative understanding of particulate concentrations is hampered by the constantly varying illumination angles and attitudes. During the first orbital sleep period the orbiter was placed in a sun inertial attitude with the starboard (+Y axis) wing pointed at the sun. In this attitude when the space above the cameras is illuminated, particles are observed at constant solar-scattering angles of 90° ± 10°. Each orbit the Shuttle crosses the terminator and is illuminated for a few minutes before the earth below is lit overexposing the film. The sunlit earth is observed for 1/4 orbit. Then the sunlit shuttle observes deep space for ~20 min before crossing the night terminator. The average number of particles observed during the two periods "*sunrise*" and "*afternoon*" are displayed for each orbit during the sun inertial period. Again there appears to be a décrease in particles with time on-orbit. In addition there are clearly more particles per frame at sunrise than later in the orbital day. Again we feel this is a result of thermal stresses generated at sunrise.

One of the goals of PACS was to determine the time required to return to a clean optical environment after a water dump. Although several dumps occurred during the mission and particles associated with those dumps were observed, only one happened under proper illumination conditions so that a temporal decay could be observed. Particles were observed promptly in the first frame taken about 1 min after the start of the dump. The optical environment is severely degraded during the dump. Figure 7 shows the 0.3s exposure taken just after the end of the water dump at 21:51 MET. More than a hundred particles are observed in the 0.13 sr field-of-view. Because this dump occurred at the end of the first sleep period the Shuttle was still in sun inertial attitude. For fixed solar angle the observed temporal decay of the particles reflects a real drop in concentration, since detection sensitivity is a constant. The number of visual particles in each 2.7s exposure is plotted in Figure 8 from the end of the dump until orbital sunset 19 min later. There is a rapid (nearly two orders of magnitude) decrease in the first 6 min followed by a much slower decay. The water ejection occurs from a jet on the opposite (port) side of the Shuttle well below the opened bay doors. Ice particles formed in the expansion will undergo complex trajectories due to plume collision effects and atmospheric drag. Although particles were observed with many different trajectories, the usual direction observed was across the bay -- the direction from the water dump jet outlet to the PACS field of view. During the period after the dump, the shuttle orientation with respect to the velocity vector changed. During the dump the bay was in the ram direction (+ZVV) so that atmospheric drag would tend to force the particles behind the shuttle. By the end of the dump, a component of the atmospheric drag was across the bay so that some of the particles would be forced across the bay. This component changed with time so that just before sunset (22:07) the velocity vector had rotated so that the water jet side of the shuttle squarely faced the ram direction (-YVV). During the decay after the dump there was no obvious change in particle direction or brightness (size/distance). However, this change in attitude may have affected the temporal decay of the particles. For comparison, the decay in particles was observed after a dump by the NASA IECM Cameras. They agree in magnitude with the particle counts observed by PACS. The decay in that data seems to more closely follow a single exponential decay with an e-fold time of less than 5 min. The PACS data shows a more rapid early time decay. However,

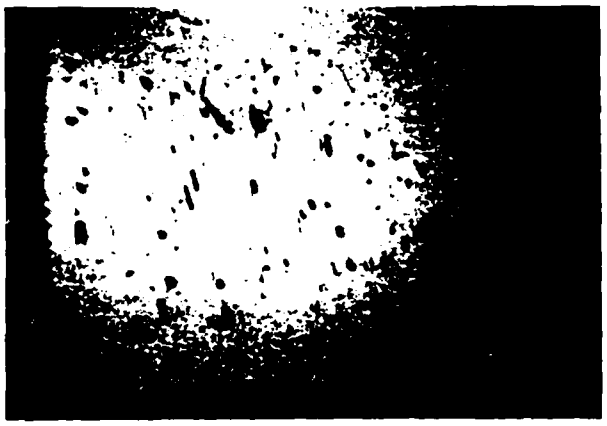

Figure 7. Exposure Taken Just After the End of the Water Dump

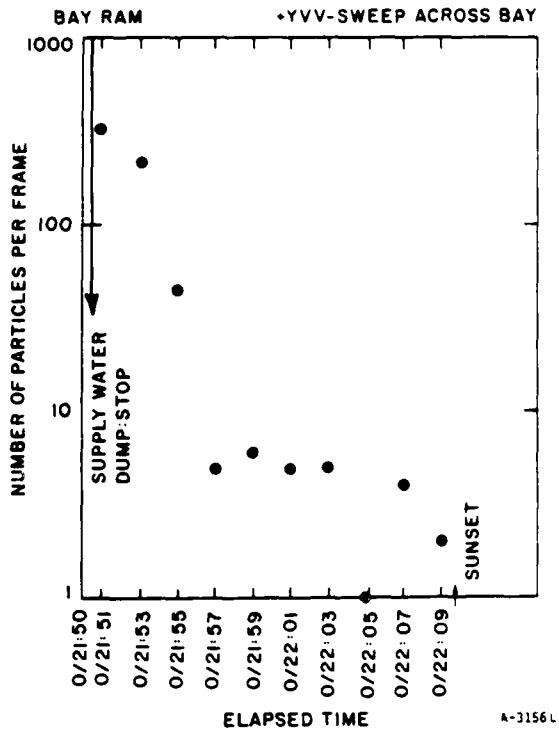

Figure 8. Particle Decay After Supply Water Dump (Visual Particle Count)

we feel the details of the decay are dependent on the atmospheric drag velocity vector. There were eleven fuel cell purges during PACS observational periods. We detected no obvious particulates associated with these events.

The other mission event that dramatically increased the detectible particles was the TV satellite deployment at 0/9:32 MET. This satellite was located in the rear of the bay in a retractable clamshell container. Starting with the opening of the container particles were observed moving across the camera field of view away from the rear of the bay. As the satellite was spun up to its 50 rpm rotation period copious particles were continuously observed. They first moved rapidly, then more slowly as if the particles were released early in the spin-up but with a distribution of velocities. Thus the fast moving particles reached the field of view first, followed by the slower moving portion of the distribution. For all particles the direction of motion was mainly away from the rear of the bay. During the 15 min prior to satellite launch the optical environment was the worst during the entire mission. The 0.3s exposure frame taken 11 min before deployment is shown in Figure 9.

During this period the shuttle was in a sun-inertial attitude. Illumination conditions remained nearly constant with a 80° angle between the sun, the particles, and the camera. At the start of deployment the velocity vector was across the bay, later the bay was in the wake. Atmospheric drag may have altered the particle trajectories somewhat in Figure 9 giving rise to a crossbay velocity component. We have attempted to assess the magnitude of this component. The acceleration due to atmospheric drag, a, can be written[15]

$$a = 3 \frac{\rho_A}{\rho_P} \frac{V^2}{d} \quad .$$

This assumes elastic scattering of the atmosphere by the particle. The atmospheric density, ρ_A, at 280 km is 3×10^{-14} g/cm^3 (Ref. 16) and the shuttle velocity is 8×10^5 cm/s. For a particle density, ρ_P, of 2 g/cm^3 then ad = 0.03 cm^2/s^2. If the scattering is very inelastic the acceleration could be nearly half this value. During the early part of the deployment particles from the rear of the bay that were displaced by drag by more than 5m would not be detectable in the PACS field of view traveling in a mostly forward (to the nose) direction. Thus for 100 μm particles, the drag acceleration will be 3 cm/s^2. In order to satisfy the above criteria the particle would have to be traveling faster than 1/2 m/s making the trip from satellite to PACS field of view in less than 1/2 min. Larger particles could be moving

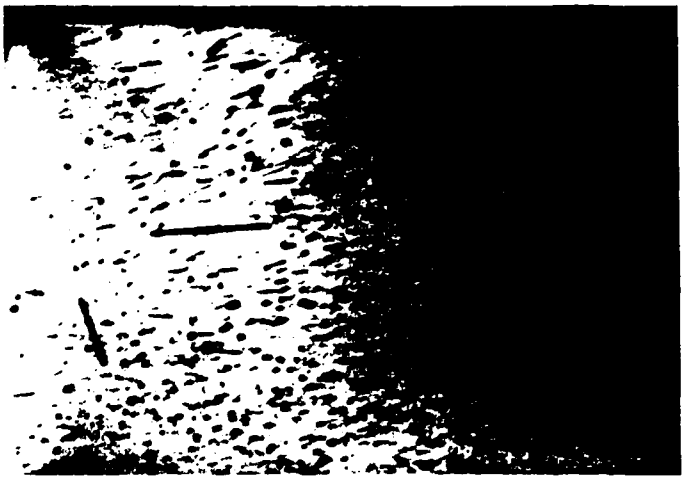

Figure 9. Exposure Taken During Preparation for Satellite Launch

slower and still reach the field of view. Obviously atmospheric drag can significantly alter particle trajectories. We are in the process of modeling this process more accurately.

The slowly moving particles seen at the end of the deployment sequence could easily have taken several minutes to arrive in the camera field of view. Because the bay was in the wake during this time the particles did not undergo acceleration by atmospheric photo drag.

At several times during the mission groups of particles were observed within the field of view for several sets of exposures. Groups of ~75 particles were observed to be in the same relative positions in frames taken two minutes apart. One particle took eight minutes to traverse the field of view. These nearly immobile particles were observed in several different attitudes including the velocity vector across the bay (so that the entire column in the field of view was subjected to atmospheric drag) and even when the bay was in ram. Because several of these particles had clear disks they were not on the camera lens but rather quite remote, >10m. Based on drag calculations they must have been quite large (larger than cm diameters) in order to persist with negligible motion in the field of view. We can offer no better explanation at this time.

Particles were often observed with rapidly oscillating radiance levels as if they were presenting different geometric aspects to the camera. We believe they were non-spherical particles rotating. One particle exhibited 47 periodic oscillations during a 2.5s exposure. We are unable to postulate a source mechanism which would give rise to such rapidly rotating particles. Drag would tend to damp these rotations.

Besides the events which obviously degrade the optical environment around shuttle, there were two key observational periods during which all activities were suppressed. On mission day 2, after 50 hours on-orbit, the shuttle maneuvered into a deep space viewing attitude (nose into the velocity vector, earth below the port wing). No further thruster firings were used to maintain this attitude. Data was acquired for 105 minutes in this mode (>1 orbit), then the shuttle maneuvered into gravity gradient attitude (nose to earth, bay facing wake). Again thrusters were disabled. The shuttle attitude varied only slightly (<5°) during this orbit. The numbers of particles observed within the field of view during the two sequences is shown in Figures 10 and 11.

The frames taken in deep space viewing attitude have near optimum viewing geometry - the sun is nearly perpendicular to the bay so that even near field particles are solar illuminated and observed at a 90° scattering angle. In Figure 10 there are two clear periods when particles were observed: just after the maneuvering was completed and just after orbital sunrise. Note there is no corresponding feature at sunset. Due to slight attitude precession during the orbit, the solar angle changes slowly. The film data is overexposed whenever the sun illuminates the cameras directly. Better rejection baffles will be needed on future missions. However during the period 2/03:39 to 03:59 the cabin shadows the bay so that particles are observed in the region beyond 1.75m from the cameras. Orbital sunrise occurred at 2/03:37. The illumination conditions are quite constant so that the fluctuations in the particle counts after sunrise should be real. Several very different trajectories were observed. (A nose-to-tail direction of motion should have been favored due to drag.) Because the bay was not illuminated during this period (shadowed by cabin) the observed particles may have arisen from very different parts of the orbiter.

In Figure 11 the gravity gradient data is presented. The film is most often overexposed in this attitude. The earth is in the field of view so that the sunlit earth overexposes the film. The best viewing conditions are when the shuttle bottom is illuminated and the earth is still dark as occurred from 2/05:10 to 05:18. Here again a flurry of particles are observed just after orbital sunrise. They are observed with a solar illumination angle of ~100 deg. This is a very sensitive configuration.[14] The bay is shadowed, but the field of view begins to be illuminated about 3.5m from the cameras. The particle trajectories seem

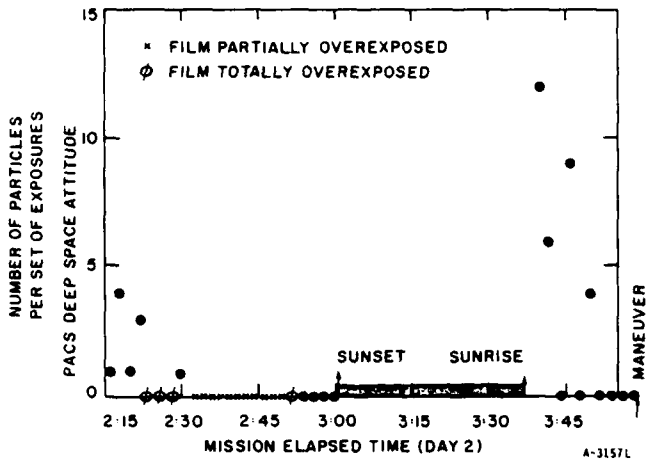

Figure 10. Particles in Field of View During PACS Prime Measurement Sequence (Deep Space Viewing - All Disabled)

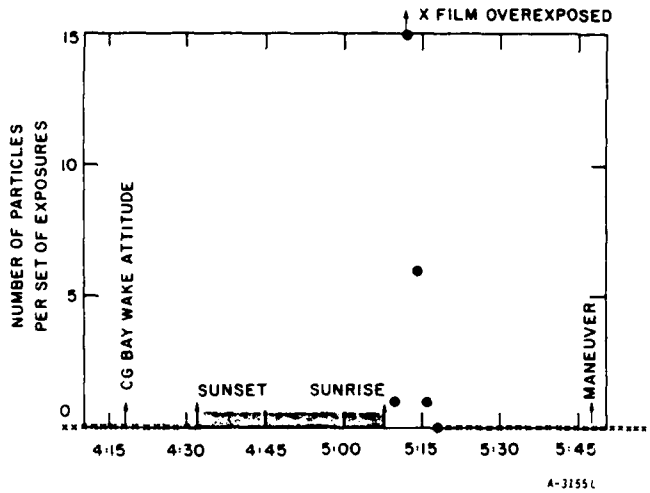

Figure 11. Particles in Field of View When Gravity Gradient Attitude Bay in Wake (All Disabled)

to be mainly rear to forward. The bay is in wake and not solar illuminated, thus any particles observed most probably are swept into the field of view by drag.

Scialdone[15] has recently suggested that several thermal processes could drive particles off surfaces. We feel that the current data shows clear evidence that sunrise related thermal stresses induce particle generation.

Summary and future plans

The PACS camera successfully gathered data on the orbital particulate contamination environment during mission STS-61C. The film data clearly indicate that the solar illumination angle is the key parameter. We suspect particles were often present but we were able to observe them only under proper illumination conditions. At terminator crossings (when illumination conditions were reasonably good) particles were observed about 1/3 of the time within the 17 x 24 deg field of view of the PACS cameras. Particles were observed: when all activity was suppressed, after maneuvering, after payload bay door operations, during the preparations for a satellite launch, during and after water dumps, and after sunrise. During active events such as dumps and the satellite launch the particle trajectories observed extrapolated back to the vicinity of the source. Atmospheric drag accelerations only slightly perturb the trajectories of detected particles during these events. Only a few particles were detected by the strobe-illumination. This indicates that the particles were nearly always beyond 2m from the cameras. It also appears that particles are often very asymmetric offering different geometrical areas to the cameras at an angular rate of up to 20 per second. Particles with trajectories from every direction were observed.

We can attempt to compare the PACS observations with the CRDG guideline standards. Roughly particle occurrence is on average 1/3 particle per 0.3s exposure (~1 particle per second) late in the mission within the 0.126 sr field of view of PACS. This corresponds to approximately 2/3 particle per orbit within a 1.5×10^{-5} sr field of view. The PACS observations would satisfy the CRDG guidelines except that PACS is unable to sense particles down to 5 μm diameters and certainly is not sensitive enough to see one at 5 km. However, the PACS results are encouraging in that there may be quiescent times when the optical environment is quite clean. Unfortunately there are many times when it is not.

We are currently examining in more detail the particle trajectories and angular velocities associated with particular events. By correlating these with exact attitudes we hope to extract drag and hence size information. Unfortunately with data from only a single camera, details of size and velocity determinations are not possible. Radiance levels can be used to estimate particle sizes for those cases when the particle has a visible disk rather than a blurred disk. Thus film calibration is being performed. By relating the illumination variations to cross sectional areas, particle asymmetry can be estimated for rotating particles.

In addition, image enhancement techniques are being applied to the film data including histogram manipulations, edge operations, and contrast segmenting to determine the presence of smaller particles. This work is being performed by Ben Gold at EKTRON Applied Imaging. This processing destroys the ability to measure absolute radiance levels but may push the detection threshold to the 20 μm diameter particle level. To date sensitivity has been increased by another factor of 2.5 so that about five times as many stars and particles are detectable in a frame.

Thus in spite of certain limitations the PACS data has been very useful in identifying timescales of various processes and ranking the severity of contamination sources for the shuttle environment. We are currently planning to refurbish and upgrade the cameras for reflight on a future mission.

Acknowledgements

The authors appreciate many useful discussions with Ed Murad and Charlie Pike (AFGL), Terry Rawlins and Catherine White (PSI), and Stu Clifton and Edgar Miller (NASA/MSFC). We also acknowledge the help of all the personnel associated with the Hitchhiker G program at NASA/Goddard, but especially Ted Goldsmith, Jim Kunst and Rich Day.

References

1. D.W. Schuerman, D.E. Beeson, and F. Giovane, Coronagraphic technique to infer the nature of the Skylab particulate environment, Appl. Optics 16, 1591-1597 (1977).

2. D.W. Schuerman and J.L. Weinberg, Preliminary study of contaminant particulates around Skylab, NASA CR-2759 (1976).

3. F. Giovane, D.W. Schuerman, and J.M. Greenberg, Photographic coronagraph, Skylab particulate experiment T025, Appl. Optics 16, #4, 993-998 (1977).

4. E.R. Miller, ed., STS-2,-3,-4 induced environmental contamination monitor (IECM) summary report, NASA Tech. Memo. 82524, NASA/Marshall Space Flight Center, Alabama (Feb. 1983).

5. J. Barengoltz, Particulate release rates from Shuttle orbiter surfaces due to meteoroid impact, J. Spacecraft 17, #1, 58-62 (1980).

6. J. Barengoltz, ed., The particulate environment around Shuttle, panel report (Section 10) located on ENVIRONET computerized database operated by NASA/Goddard Space Flight Center.

7. B.D. Green, G.E. Caledonia, and T.D. Wilkerson, The Shuttle environment: gases, particles and glow, J. Spacecraft 22, #5, 500-511 (1985).

8. E.R. Miller, ed., Induced environment contamination monitor - preliminary results for the Spacelab 1 flight, NASA Tech. Memo. 86461, NASA/MSFC, Alabama (Aug. 1984).

9. H.A. Miranda, Jr., Camera/Photometer Final Report Contract NAS-8-32235 (July 1979).

10. C. Maag, J. Barengoltz, and F. Kuykendall, STS-3 "snow flake" study, A291-A294 in The Shuttle Environment Workshop, J. Lehmann, org. (Feb. 1983).

11. D. McKeown, J.A. Fountain, V.H. Cox, and R.V. Peterson, Analysis of TQCM surface contamination adsorbed during the Spacelab 1 mission, AIAA paper 85-7008, 108-115 in AIAA Shuttle Environment and Operations II Conference Proceedings, Houston, TX (Nov. 1985).

12. B. Gold and W. Jumper, PACS image processing, Ektron Applied Imaging Final Report, (Nov. 1986).

13. F.J. Redd, D.R. Bunnell, M. Ahmadjian, Particle analysis camera for Shuttle (PACS): the first Hitchhiker (HHG-1), AIAA paper 85-7005, 104-107 in AIAA Shuttle Environment and Operations II Conference Proceedings, Houston, TX (Nov. 1985).

14. W.T. Rawlins and B.D. Green, Spectral signatures of micron-sized particles in the Shuttle optical environment, Accepted by Appl. Optics (1987).

15. J.J. Scialdone, Particulate contaminant relocation during Shuttle ascent, NASA Tech. Memo. 87794, NASA/GSFC, Greenbelt, MD (June 1986).

16. U.S. Standard Atmosphere (Washington, DC, 1976).

☆U.S. GOVERNMENT PRINTING OFFICE: 1988-500-000/60009